T. R.
VAN YÜZÜNCÜ YIL UNIVERSITY
INSTITUTE OF NATURAL AND APPLIED SCIENCES
DEPARTMENT OF GEOLOGICAL ENGINEERING

COMPARISON OF STRAIN ELLIPSOID SHAPE BASED ON THE RESULTS OF THE MAGNETIC SUSCEPTIBILITY ANISOTROPY AND PALEOSTRESS METHODS: CASE STUDY OF AKSU BASIN (ANTALYA, SW TURKEY)

M.Sc. THESIS

PREPARED BY: Muhammad Harbi WASOO
SUPERVISOR: Asst. Prof. Dr. Ayten KOÇ

VAN-2019

T. R.
VAN YÜZÜNCÜ YIL UNIVERSITY
INSTITUTE OF NATURAL AND APPLIED SCIENCES
DEPARTMENT OF GEOLOGICAL ENGINEERING

COMPARISON OF STRAIN ELLIPSOID SHAPE BASED ON THE RESULTS OF THE MAGNETIC SUSCEPTIBILITY ANISOTROPY AND PALEOSTRESS METHODS: CASE STUDY OF AKSU BASIN (ANTALYA, SW TURKEY)

M.Sc. THESIS

PREPARED BY: Muhammad Harbi WASOO

VAN-2019

ACCEPTANCE and APPROVAL PAGE

This thesis entitled "Comparison Of Strain Ellipsoid Shape Based On The Results Of The Magnetic Susceptibility Anisotropy And Paleostress Methods: Case Study Of Aksu Basın (SW Turkey) presented by Muhammad Harbi Wasoo under supervision of Asst. Prof Ayten KOÇ in the department of Geological Engineering has been accepted as a M. Sc. thesis according to Legislations of Graduate Higher Education on 24/06/2019 with unanimity / majority of votes members of jury.

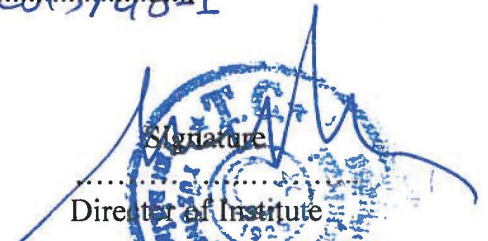Chair: Prof Dr. Erdin BOZKURT   Signature:

Member:Doç. Dr. Serkan ÜNER   Signature:

Member: Asst. Prof. Ayten KOÇ (Supervisor)   Signature:

This thesis has been approved by the committee of The Institute of Natural and Applied Science on .26.07.2019 with decision number .2019/40-1

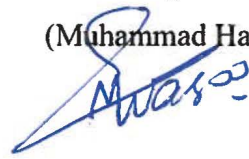Signature:
....
Director of Institute

THESIS STATEMENT

All information presented in the thesis obtained in the frame of ethical behavior and academic rules. In addition all kinds of information that does not belong to me have been cited appropriately in the thesis prepared by the thesis writing rules.

Signature
(Muhammad Harbi Wasoo)

ABSTRACT

COMPARISON OF STRAIN ELLIPSOID SHAPE BASED ON THE RESULTS OF THE MAGNETIC SUSCEPTIBILITY ANISOTROPY AND PALEOSTRESS METHODS: CASE STUDY OF AKSU BASIN (SW TURKEY)

WASOO, Muhammad Harbi
M.Sc. Thesis Geological Engineering
Supervisor: Asst. Prof. Dr. Ayten KOÇ
June 2019, 195 pages

Aksu Basin is the marine sedimentary basin located in the center of the Isparta Angle (SW Turkey). Its structures and geometry may provide very useful information about Miocene crust deformation and stress field in the region.

In this study, it is aimed to determine main paleostress directions (σ_1, σ_2, σ_3) that have been effective in the Aksu Basin. For this purpose, more than 1000 fault-slip measurements from the mesoscopic faults were collected at the 83 different sites. The results demonstrate that the Aksu Basin developed under four different tectonic phases; 1) ~E-W extensional phase, 2) ~N-S compressional (Lycian) phase, 3) ~E-W compressional (Aksu) phase and 4) N-S extensional Neotectonic phase. In order to test fault-slip data independently, ~490 oriented samples for Anisotropy of Magnetic Susceptibility (AMS) measurements were collected and analyzed. The results of the AMS data show that two different magnetic lineations (Kmax) directions are present. These are 1) N-S magnetic lineation in Pliocene and 2) from N-S to NW-SE magnetic lineation in the Miocene.

This study shows that AMS data are consistent with kinematic observations and provide independent information for understanding of the deformation pattern in the Aksu Basin. Based on the AMS data, Recent phase can be differentiated from the rest of the data. AMS data can be evidently used help to construct the paleostress stratigraphy.

Key words: Aksu Basin, Anisotropy of Magnetic Susceptibility (AMS), Paleostress inversion.

ii

ÖZET

MANYETİK DUYARLILIK ANİZOTROPİSİ YÖNTEMİ İLE ELDE EDİLEN DEFORMASYON ELİPSOİDİNİN PALEOGERİLİM SONUÇLARI İLE KARŞILAŞTIRILMASI: AKSU HAVZASI ÖRNEĞİ (GB TÜRKİYE)

WASOO, Muhammad Harbi
Yüksek Lisans Tezi, Jeoloji Mühendisliği Anabilim Dalı
Tez Danışmanı: Dr. Öğr. Üyesi Ayten KOÇ
Haziran 2019, 195 sayfa

Aksu Havzası, Isparta Açısının (GB Türkiye) tam merkezinde bulunan denizel tortul bir havzadır. Havzanın yapısı ve geometrisi, Isparta Açısı olarak tanımlanan bölgenin Miyosen kabuk deformasyonu ve stress kurulumu hakkında çok önemli bilgiler sağlamaktadır.

Bu çalışmada, Aksu havza çökellerinde gözlemlenen faylardan 83 farklı lokasyondan 1000'den fazla kinematik veri toplanmış, ters çözüm metodu kullanılarak ana gerilim yönlerinin (σ1, σ2, σ3) belirlenmesine çalışılmıştır. Elde edilen sonuçlar, Aksu Havzası'nın dört farklı tektonik safha etkisinde geliştiğini göstermektedir. Bunlar; 1) D-B genişleme fazı, 2) ~ K-G sıkışma (Likya) fazı, 3) ~ D-B sıkışma (Aksu) fazı ve 4) K-G genişlemeli Neotektonik fazıdır. Hata-kayma verilerini bağımsız olarak test edebilmek amacı ile, Manyetik Duyarlılık Anizotropisi (MDA) ölçümleri için ~ 490 adet yönlü örnek toplandı ve analiz edildi. Elde edilen MDA sonuçları, iki farklı maximum uzama ekseninin (Kmax) varlığına işaret etmektedir. Bunlar; 1) Pliyosen'de görülen K-G yönlü manyetik uzama ekseni ve 2) Miosen'de var olan ve K-G ila KB-GD arasında değişim gösteren manyetik uzama eksenidir.

Yapılan çalışmalar göstermiştir ki, MDA verileri ile kinematic veriler birbirleri ile tutarlıdır ve Aksu Havzası'nda görülen deformasyon modelinin anlaşılmasında bağımsız bilgi sağlamıştır. Bu çalışma, AMS verilerinin, havzada etkin olan güncel tektonik fazın, diğer geri kalan fazlardan ayrılması ve paleostress stratigrafisinin oluşturulmasında etkin olarak kullanılabileceğini göstermiştir.

Anahtar kelimeler: Aksu Havzası, Magnetik duyarlılık analizi (MDA), Paleogerilim dönüşümü.

ACKNOWLEDGEMENTS

"goodness can never be defined
and
good human beings can never be denied"

2019

Muhammad Harbi Wasoo

TABLE OF CONTENTS

LIST OF TABLES

LIST OF FIGURES

Figure **Page**

xv

xx

Figure   **Page**

SYMBOLS AND ABBREVIATIONS

Some symbols and abbreviations used in this study are presented below, along with descriptions.

Symbols	Description
F	Magnetic foliation
k	Principal susceptibility magnetic susceptibility
L	Magnetic lineation
pj	Corrected anisotropy degree
R (Φ)	Stress ratio
T	Shape parameter
σ	Principal stress
τ	Stress tensor

Abbrevations	Description
AMS	Anisotropy of magnetic susceptibility
ATFZ	The Aksu Thrust Zone
INVD	Direct Inverse Method
KTF	Kapıkaya Thrust Fault
MTA	The Mineral Research and Exploration Directorate of Turkey

1. INTRODUCTION

1.1. General

The Alpine-Himalayan orogeny in the Eastern Mediterranean region has been created by ongoing plate tectonics, as a result of Mesozoic-to-Cenozoic-to-recent closure of the Tethys ocean and collision process between the northward-moving Arabian and African plates (Şengör and Yılmaz, 1981; Storetvedt, 1990; Barrier and Vrielynck, 2008) The geology of Turkey therefore consists of a number of suture zones that demarcate the former position of the now subducted oceans (Şengör and Yılmaz,1981; Robertson and Dixon, 1984; Okay, 1986; Yılmaz, 1993; Göncüoğlu et al., 1996–1997, Okay and Tüysüz, 1999; Robertson, 2002; Stampfli and Borel, 2002; Robertson and Ustaömer, 2004; Robertson et al., 2006, 2007, 2009; Oberhänsli et al., 2010; Pourteau et al., 2010), The most important of these is the İzmir-Ankara Erzincan suture zone (Figure 1.1), where the Pontides, to the north, belonging to Eurasia since the early Mesozoic (Torsvik and Cocks, 2009), and Tauride and Anatolide Platform to the south, rifted away from the Gondwana in the Triassic, collided after the complete consumption of the Northern Branch of the Neotethys. The collision between Pontide and Taurid platform started at the late Cretaceous and maybe it lasted to the end late Eocene (Okay and Özgül, 1984; Meijers et al., 2010; van Hinsbergen et al., 2010; Gülyüz et al., 2012). The second subduction zone existed to the south of the İzmir-Ankara Suture Zone, between the Taurides and Kırsehir Block in the central part of the Turkey (the Inner Tauride Suture, e.g. Görür et al. 1984; Okay et al., 1996; Dilek et al., 1999; Clark and Robertson, 2002, Parlak and Robertson, 2004; Pourteau et al. 2010). This oceanic basin was consumed during latest Cretaceous to early Cenozoic time, which led to the formation of the Tauride fold and thrust belt in the southern Turkey.
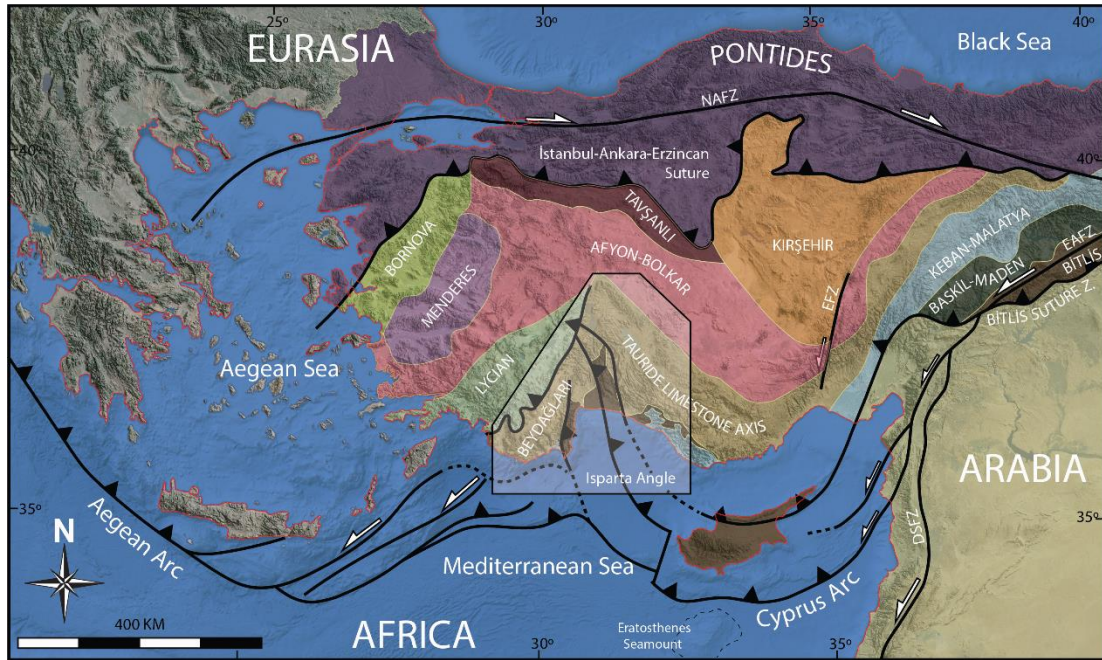
Figure 1. 1. Major tectonic zones of Turkey where NAFZ: North Anatolian Fault Zone, EAFZ: East Anatolian Fault Zone, EFZ: Ecemiş Fault Zone, BZSZ: Bitlis Zagros Suture Zone, DSFZ: Death sea Fault System and IAESZ: İzmir-Ankara-Erzincan suture zone (Okay et al., (1996) and Kaymakçi et al. (2010). The highlighted area shows the location of the Isparta Angle and the study area. See Figure 1.2 for detailed geological map of the Isparta Angle.

The southern branch of the Neotethys still subducts today along the Cyprus subduction zone on the south of the Taurides (Khair and Tsokas, 1999; Papazachos and Papaioannou, 1999; Biryol et al., 2011) (Figure 1.1). In the eastern continuation of the zone, this branch has been entirely subducted where continuing convergence of the African (Arabian) and Anatolian accommodated across Bitlis suture zone, with the arrest of subduction at the end of the Middle Miocene (Şengör and Yılmaz, 1981; Şengör et al., 2003; Keskin, 2003; Faccenna et al., 2006; Hüsing et al., 2009; Okay et al., 2010). The subduction under the Taurides at great mantle depth suggests that continuous unbroken subduction was succeeded by successive slab detachments, and consequent tears, as continental collision proceeded from east to west since the Middle Miocene (Facenna et al., 2006; Gans et al., 2009; van Hinsbergen et al., 2010; Biryol et al., 2011).
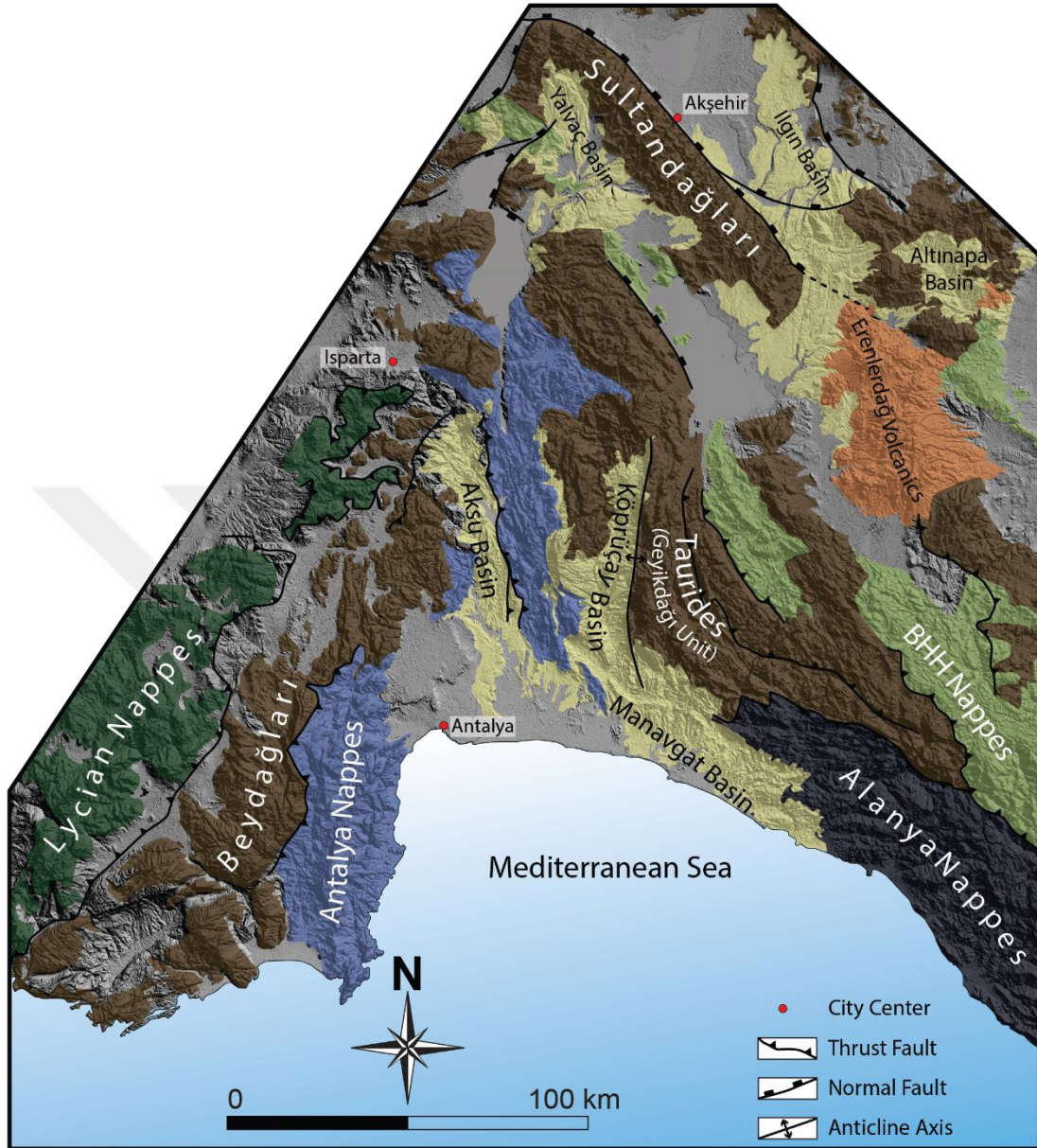
Figure 1. 2. Major tectonic structures and units in the Isparta Angle (from 1/500000 scale geological map (Konya map) produced by The Mineral Research and Exploration Directorate of Turkey (MTA)).

Due to the intense deformation of the Anatolia in the context of long-lived and still ongoing convergence between Africa and Eurasia, a complex subduction system with bow-like trenches are formed, namely Aegean-west Anatolia, and Cyprus 'arcs' (Figure 1.1). At the intersection of these arcs, a triangular-shaped morphotectonic structure called Isparta Angle (IA) (Blumenthal, 1963) separates the western and central Tauride

mountains and extends offshore into Antalya Bay. The Isparta Angle contains shortened Mesozoic units and ophiolites that were thrust and stacked during Late Cretaceous to Miocene times, with opposing thrust vergences (Figure 1.2). The deepest tectonostratigrafic unit in the western limb of the Isparta Angle is the Beydağları platform that is composed of shallow-marine limestone, dolomites and neritic limestone of late Triassic to the Eocene time (Robertson and Woodcock, 1982, 1984) and is overthrusted from the NW by the Lycian Nappes, a composite nappe system of ophiolites and Mesozoic sediments that underwent its final emplacement over the Beydağları foreland in the Early Miocene (Hayward 1984; Okay 1989; Collins and Robertson 1997, 1998, 2003; van Hinsbergen 2010). The thin-skinned Central Tauride fold and thrust belt forms the eastern limb of the Isparta Angle and overthrust the Beydağları platform to the southeast (Figure 1.2). Thrusting occurred continuously or intermittently from the Late Cretaceous to Neogene times (Şengör and Yılmaz, 1981; Hayward, 1984; Collins and Robertson, 2003; Poisson et al., 2003a; van Hinsbergen, 2010). The youngest thrusting at the contact between Beydağları and western Taurides occurred in the Early Miocene (Hayward, 1984).

After long and intense thrusting and folding history, the Central Taurides became overprinted by multi-directional extension (Koç et al., 2012, 2016 and 2017) since Miocene times. Interestingly, this extension occurred contemporaneously with E-W shortening accommodated by N-S striking folds and thrusts in the center of the Isparta Angle (Dumont and Kerey 1975; Glover and Robertson 1998a; Poisson et al. 2003; Deynoux et al. 2005; Flecker et al. 2005; Çiner et al. 2008; Schildgen et al. 2012a). Here, marine sediments that were accumulated in the Aksu, Köprüçay and Manavgat basins unconformably abovethe Tauride carbonates are exposed (Figure 1.2). Thrusting in the Isparta Angle is dominated by the Aksu Thrust which delimits the eastern margin of the Aksu Basin. It exemplifies Miocene to Pliocene E-W to NE-SW directed thrusting in the core of the Isparta Angle and together with its offshore equivalents in the Bay of Antalya indicates that the youngest compressional tectonic event in the heart of the Isparta Angle lasted until the Pliocene (Poisson et al., 2003) or even into the Quaternary (Hall et al. 2014).

1.2. Purpose and Scope

Miocene E-W thrusting is restricted to the heart of the Isparta Angle and is not prominent elsewhere in the south Anatolia. Thrusting in the center of the Isparta Angle did not stop in the Eocene, but either continued or was reactivated in the Middle Miocene to Pliocene times. In this thesis, on Aksu basin, which is located at the center of the Isparta Angle, is chosen for detailed study because it contains marine sediments with strong folding and thrusting of the lower to uppermost Miocene stratigraphy (Figure 1.3). In this regard, structural, sedimentological and kinematic characteristics of the Aksu Basin are very crucial to improve geological understanding of the region within the context of deep and crustal processes, which create unusual deformational patterns in the study area and its surroundings (Biryol et al., 2011; Koç et al., 2016b; Kaymakçı et al., 2018).

The deformational pattern in the study area is not straightforwardly explained in the context of ~N-S Africa-Eurasia convergence. In addition to this regional complexity, type of deformation may change due to local stress re-distributions near major faults. The orientations and relative magnitudes of the principal stress axes using fault slip data that are attained from the basin infill and basin bounding faults can be estimated by the method of stereographic plot (Angelier, 1979). One of the purposes of this study is to apply paleostress inversion techniques to unravel the paleostress history of the Aksu Basin by constraining the timing of each deformation phase.

The anisotropy of magnetic susceptibility (AMS) has proven as a very useful tool to establish the sedimentary and tectonic history in weakly deformed sedimentary rocks due to its relationship with the regional stress field (Tarling and Hrouda, 1993). In young, weakly deformed sedimentary rocks or the case that paleostress indicators are usually missing, the AMS analysis can represent the tool for extracting the deformation history, particularly when it is combined with other kinematic observations from the structural studies. In other words, the AMS analysis can be used as time indicators for the recent tectonic evolution. So far extended work has been done in Southern Turkey (Flecker, 1995; Karabıyıkoğlu et al., 2004; 2005; Kelling et al., 2005; Çiner et al., 2008; Üner et al., 2015; Koç et al., 2016; 2017), however no AMS work was carried out in the Antalya Basin including Aksu, Köprüçay and Manavgat basins. Aksu Basin is a good candidate

for AMS study since it preserves its original position since the Middle Miocene time (Koç et al., 2016). This thesis, presents the first AMS results from the Middle Miocene-Pliocene sedimentary succession of the Aksu Basin. It is also attemptedto distinguish between the tectonic phases through Middle Miocene to Pliocene by using AMS campaign as an independent method to test the paleostress results.
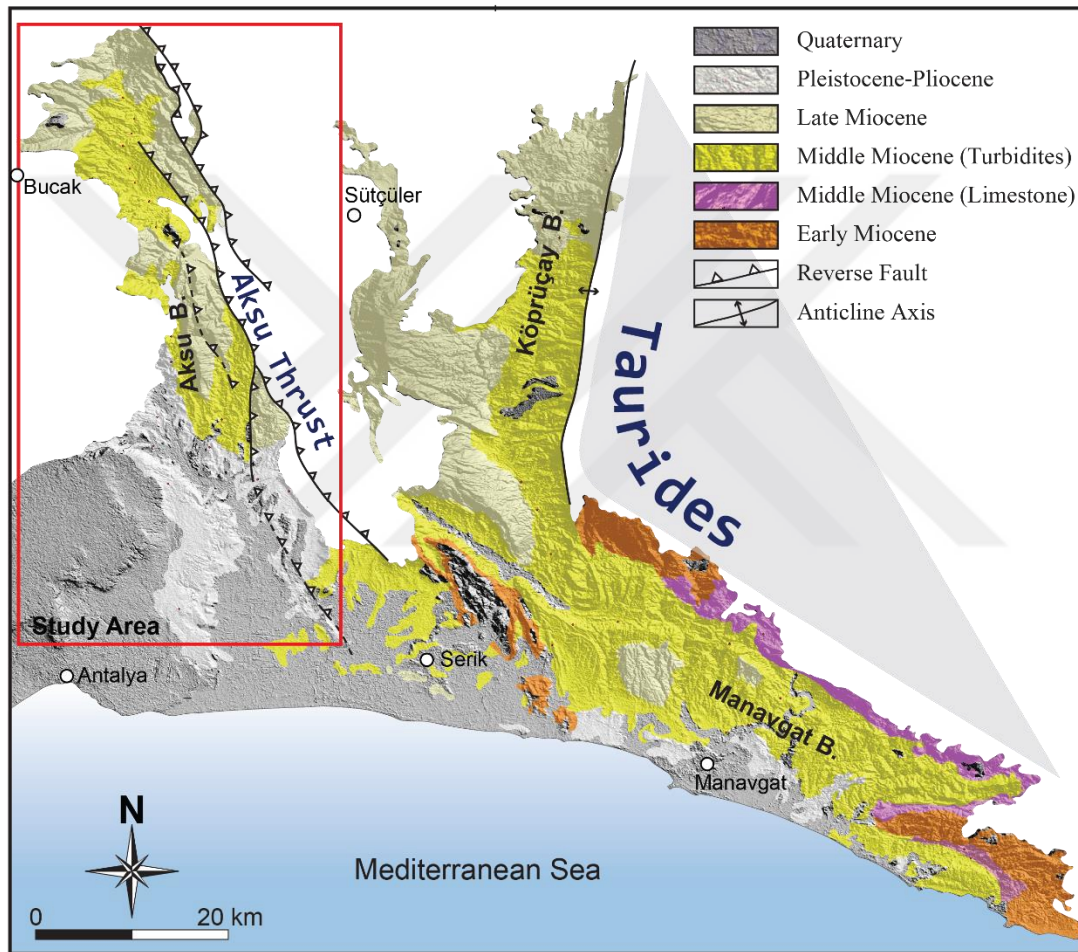
Figure 1. 3. Simplified geological map of the Miocene marine basins located at the center of the Isparta Angle. Study area is indicated as red rectangle (1/100000 scale geological map produced by The Mineral Research and Exploration Directorate of Turkey (MTA) (from Koç et al., (2016b)).

.

In order to reach these objectives, following specific questions required to be answered;

1. What is the stratigraphy of the infill successions in the Aksu Basin?
2. What are the sedimentological characteristics, depositional environments and paleogeography of their infills?
3. What are the tectonic regimes during its formation and how it has evolved in time?
4. What are the major tectonic structures that control and3D geometry of the basin?
5. What are the temporal and spatial relationships of these structures, their kinematics during the Neogene?
6. What is the relationship between the stress directions obtained from fault slip data and the anisotropy of magnetic susceptibility (AMS)?

1.3. Study Area

The area under investigation –Aksu Basin– is a north–south-extending basin in south-central Anatolia in a very strategic position at the western edge of the Central Tauride Mountains. It is located between Bucak-Sütçüler-Antalya provinces in the central part of the Isparta Angle which separates two important continental blocks –Beydağları to the west, and Central Tauride to the east (Figure as 1.2 and 1.3). It has an area of 2000 km^2 between 37° 40' 02" N to 37° 39' 43" N latitude in the north and 30° 59' 55" E to 31° 00' 02" E longitude in the east and lies obliquely in front of the NE–SW-trending Lycian Nappes.

The sedimentary infill of the basin is mainly characterized by thick delta to marine deposits with coarse conglomerates, sandstone, mudstone and reefal carbonatees deposited since the Early Miocene (Çiner et al., 2008; Karabıyıkoğlu et al., 1997 and 2005; Üner et al., 2018). It unconformably overlies the basement units of the Beydağları carbonate platform, Alanya Metamorphics, Antalya Nappes and Lycian Nappes (Figure 1.2).

The Aksu thrust delimiting the eastern margin of the Aksu Basin exemplifies Miocene to Pliocene E–W-to-NE–SW directed thrusting. Aksu Thrust was evaluated the

last major tectonic event (Poisson et al., 2003) that shaped the present-day configuration of the Isparta Angle (Blumenthal 1963).

Study area and its vicinity are covered by the Konya sheet of the 1/500.000 scale map of Turkey prepared by Directorate of Mineral Research and Exploration (Ankara, Turkey). Additionally, the study area is located within J11, K11 and L11 1/100 000 scale topographic map sheets.

1.4. Previous Studies

Previous studies related to this study are classified into four groups. First group includes the studies related to regional geology; the second group, related to the geology of the Aksu Basin. Third and the forth groups are focused on the methodology and consist of studies on paleostress and AMS, respectively. These groups will be described in detail below.

1.4.1. Regional Studies

This review focuses on the works about the Isparta angle and Antalya Basin. Penck (1918), was the first to describethe Isparta Angle apex and his work is focused on the main tectonic lines on the region, such as Burdur-Fethiye, Dinar, Kırkavak and Beyşehir faultsand Paleogene stratigraphy.

The main lithostratigraphic series on the Isparta Angle has been studied by Parejas (1943), who was concentrated on distinguishing and dating of the Palaeozoic basement units and Mesozoic (Upper Cretaceous to Tertiary) transgressive sequences. Altınlı (1944; 1945), recognized the thrust front of the Antalya Nappes and Lycian Nappes from the east and west side of the Beydağları unit, respectively.

The geomorphological description of the area between the Mediterranean Sea coast and the region of the Burdur–Isparta lakes has been made by Planhol (1956; 1958) and he pointed out one of the most important problems in this region, the origin of the Antalya Basin. Later this led to an extensive discussion among geologists for a long time.

The major research in the area was the first tentative synthesis of "Isparta bend" (Blumenthal, 1963), which was focused on the stratigraphic data. In this study, it is tried to describe several zones within the Isparta bend: an ophiolitic zone from Beyşehir to Dinar, Elmalı-Burdur zone following the Serik-Isparta zone (the zones containing allochthonous carbonate slices of the Aksu thrust) and the 'schisto-radiolaritic formations (with basically belongs to Antalya nappes). Blumenthal (1963) poorly understood the complexity of the Isparta area and did not interpret these zones as far travelled nappes thrust onto the Tauride platform.

The Isparta region has been mapped by a French team that was led by Brunn in 1964, in which southern and south-western part of the Isparta Angle between Korkuteli, Antalya and Isparta (A. Poisson) and south-east and east side of the region between Beyşehir and Akseki studied by (O. Monod) and the north side of Isparta was by (M. Gutnic). After these pioneering studies, more detailed studies were made by Brunn et al. (1970, 1971). In these studies, the main structural units were defined as autochthonous carbonate platforms including Beydağları carbonate platform to the SW and Beyşehir-Akseki platform to the NE), the three allochthonous systems of (Lycian Nappes to the NW, Antalya Nappes in the south-central part and the Hoyran–Beyşehir–Hadim Nappes to the NE) (Uysal et al., 1980; Piper et al., 2002).

Özgül and Arpat (1973) studied Upper Triassic to Quaternary the stratigraphic section in the western Taurus, and defined two distinctstratigraphic sequences as autochthonous Beydağları units and Antalya Nappes. In this study, they also described the structural geology of the Taurides.

The central part of the Isparta Angle was studied by Dumont (1976) and Akbulut (1977). Dumont (1976) mapped an area at the eastern side of the Eğirdir Lake which is located on the NE side of the Isparta Angle. Akbulut (1977), worked on the Isparta Angle and suggested that the Angle has experiencedan important phase of Late Miocene thrusting, known as the Aksu phase.

The Isparta angle has formed the subject of many French (Juteau 1975; Monod 1977; Poisson 1977; Marcoux 1987) and Turkish (Tuzcu 1972; Özlü 1978) theses during seventies. In addition to the thesis, there are thematic projects focused on the Mesozoic carbonate platforms by Dumont et al. (1980) and Lheureux (1983). These studies

provided new results on the southern part of the Beydağları platform and the Anamas Mountain on the northeastern side of the Isparta Angle.

The Antalya Neogene basins on top of the Tauride platform were also studied by several researchers, such as Dupoux (1983), Poisson et al. (1983), Akay et al. (1985), Akay and Uysal (1985, unpublished MTA report). These studies projects were concentrated onlithology, biostratigraphy and structural features of the region. Detailed geological mapping (1:100 000 scale) of the Manavgat, Köprüçay and Aksu basins were also produced during these projects. The main results confirm the existence of the Late Miocene Aksu thrust phase throughout the Isparta Angle and the pre-Oligocene age for the initialemplacement of the Antalya Nappes (Poisson et al. 1984; Akay et al. 1985). Poisson et al. (1984) proposed the first model that incorporated all the data from the Mesozoic-Neogene sequencefor the Isparta Angle.

Waldron (1984a; 1984b) reported Jurassic and Cretaceous ages from radiolarian cherts in the east of Isparta Angle. In this study, Isparta Angle was interpreted as a mosaic of small carbonate platforms separated by several oceanic basins. This model was previously proposed by Robertson and Woodcock (1984) for SW of Antalya, and then it was extended to the whole Isparta Angle (Robertson, 1993; 2000).

Flecker et al. (1995; 1998) worked on the Miocene Antalya Basin in detail and then the Plio-Quaternary units studied by Glover (1995), Glover and Robertson (1998a, 1998b; 2003). Robertson (1990; 1993; 1998; 2000) renewed the discussion about the general organization of the Antalya area. Synthesis was made at the scale of the Isparta Angle and then they enlarged it at the scale of the Eastern Mediterranean.

The regular geological maps at the 1:100 000 scale was finally published by the Turkish Geological Survey (MTA, Ankara, Şenel, 1997). Facies analysis and paleoenvironmental reconstructions have been completed more recently by Karabıyıkoğlu et al., 1997, 2000, 2005; Tuzcu and Karabıyıkoğlu, 2001; Deynoux et al., 2005; İşler et al., 2005; Çiner et al., 2008; Poisson et al., 2011).

Although numerous studies are related to pure geology, some geophysical studies were also carried out. Kissel et al. (1993) reported the first rotational data in the eastern part of the Isparta Angle. Paleomagnetic results in this study are consistent with40° clockwise rotation in the eastern limb since Eocene times. After this pioneering study,

Kissel and Poisson (1987), Morris and Robertson (1993), van Hinsbergen et al. (2010) suggested 20-30° counterclockwise rotation in the western limb of the Isparta Angle. Recently, Koç et al. (2016) studied vertical axis rotations in Antalya Basin and reported 20-30° clockwise rotation in the Köprüçay Basin and approximately 25-35° counterclockwise rotation in the Manavgat Basin since the Middle Miocene. On the other hand, the Aksu Basin preserves its original position since the Middle Miocene.

1.4.2. Studies on the Aksu Basin

The Aksu Aasin is an important basin to understand the regional tectonic configuration, located at the center of the Isparta Angle, therefore, many researchers have studied on this basin since 1944.

Altınlı (1944), studied the stratigraphy of the Aksu Basin and identified the Tortonian Aksu conglomerates and the Pliocene rocks in the southern part of the basin. Blumenthal (1951) studied on the Belkis conglomerate and age of this formation is interpreted as Pleistocene. Also, Tintant (1952; 1953) and Chaput and Darkot (1953) dated molluscs and foraminifera from the south of the basin and suggestedPliocene age. After these pioneering studies, some researchers (Akbulut, 1977; Poisson, 1977; Monod, 1977; Gutnic et al., 1979; Dumont, 1976; Poisson et al., 1983; 1984; 2003; Akay et al., 1985; Akay; Uysal, 1985) studiedthe lithostratigrafic and biostratigrafic characteristics of the Antalya Basin and partly the Aksu Basin.

Akay et al. (1985) studied the stratigraphy of the Aksu basin. They distinguished the Aksu conglomerate as a member of the Aksu formation, the age of the member, based on the fossil content is assigned as Serravallian to Tortonian (Şenel et al., 1992; 1996). According to this study, timing of the Aksu thrust must be sometime between Post-Tortonian and Pre-Messinian since Gebiz limestone is in Messinian age.

Flecker et al. (1995; 1998) mainly focused on the Aksu, Manavgat and Köprüçay basins showing contrasting orientations and stratigraphies. They proposed that Early Miocene basin initiation is related to coeval southeastward thrusting of the Mesozoic Lycian Nappes. Depocentre development of all three basins is explained by flexurally

induced block faulting of the foreland in front of the Lycian Nappes along pre-existing structural weaknesses.

Glover and Robertson (1998) studied the Plio-Pleistocene evolution of the Aksu basin. They suggested two-stages of evolutionary history for the Aksu Basin: Late Miocene–Early Pliocene transtension and subsidence; Late Pliocene–Early Pleistocene rifting and marginal uplift.

Poisson et al. (2003), proposed new data concerning the age of the Aksu Thrust. They defined that the dominant facies in the southern part of the Aksu Basin are marls and silts, which contain an abundant fauna of molluscs, foraminifera, and nannoplankton of Early to Late Pliocene age. They also noticed that this sequence was affected by intense compression, which resulted in duplication of the succession along several flat thrust faults. They concluded that this event is contemporaneous with the Levant fault system and with the thrusting in the Kyrenia Range, north Cyprus.

Çiner et al. (2008) studied late Cenozoic sedimentary evolution of the Antalya Basin including Aksu, Köprüçay and Manavgat basins. They noticed that the stratigraphic organization, the time and space relationships of facies in these basins indicate contrasting styles of sedimentation as characterized by several facies associations. According to these facies represent deposition in colluvial and alluvial fan/fan delta with coralgal reefs, reefal shallow carbonate shelf, base of fault-controlled fore reef slope and clastic open marine shelf environments in tectonically active sub-basins.

Poisson et al. (2011) studied the Late Cenozoic evolution of the Aksu Basin which initiated as an elongated N-S graben. They proposed that the Aksu Basin migrated towards the south due to the uplift of its northern margin. During Messinian time, Aksu Basin was reduced to a narrow gulf along the eastern margin of which the Gebiz limestones were deposited as fringing coral reefs. In this study, deformation of the Aksu Basin is attributed towest-directed Aksu compressional event during Zanclean times.

Üner et al. (2015; 2018) has studied on the tectonic and sedimentological evolution of the Aksu Basin. They provided new kinematic and sedimentological data, which indicate that the Aksu Basin has evolved by four alternating compressional and extensional tectonic phases since its formation. They also explained the development of alluvial fan and four formations of fan deltas in the basin.

During this literature survey, we noticed that there is a long-lasting discussions and debate about the age of the Gebiz limestone (Bizon et al., 1974; Poisson, 1977; Akay et al., 1985; Akay and Uysal, 1985; Glover, 1995; Glover and Robertson, 1998; Tuzcu and Karabıyıkoglu, 2001; Karabıyıkoglu et al., 2005; Poisson et al., 2003; Poisson et al., 2011).

1.4.3. Studies on Paleostress Analysis

Methods of kinematic analysis from the fault-slip data are mainly divided into two groups based on the graphical and analytical means. Main idea behind both methods is the same and based upon the theoretical relationships between stress and shear as described by Wallace (1951) for the first time. Bott (1959) revealed the mathematical relationship of the principal stress magnitudes and orientations to the resulting directions of maximum shear stress within the fault planes.

One simplest graphical method of the paleostress analysis using is fault-slip data to plot the fault planes with slip direction on Schmidt stereographic projection. The drawback of this method is that it only works on the simplest of conjugate fault sets (Suppe, 1985; Marshak and Mitra, 1988). Arthaud (1969) developed another graphical method from a postulated direct relationship between the regional strain ellipsoid and the regional stress ellipsoid associated with fault population. A serious limitation in this method is that it can be successfully applied only to fault populations originating in uniaxial stress field (Carey, 1976; Aleksandrowski, 1985). Aleksandrowski (1985) modified Arthaud's method in order to make it applicable to a general triaxial stress field.

The Right Dihedral Method is another graphical method of paleostress analysis and has been developed by adapting the construction techniques of fault-plane solutions from seismic data to striated fault population (McKenzie, 1969; Angelier and Mechler, 1977; Lisle, 1987 and 1988). Lisle (1987) proposed another constraint upon the orientations of σ_1 and σ_3 by considering how the orientation of the slip vector S changes as the stress ratio Φ changes. These methods gave satisfactory results for asymmetrical fault populations, however, it did not perform very well when dealing with certain types of symmetrical fault populations. such as conjugate fault sets.

The inverse problem is consisting of determining the stress tensor knowing the direction and sense of the slip-on numerous faults of different orientations. In 1974, Carey and Brunier made the first attempt at formulating and solving the mathematics defining the inverse problem. Two years later, Carey (1976) developed the first paleostress analysis program which sought to minimize the angular deviations between measured fault striations and the calculated shear stress directions on each fault plane for a chosen paleostress tensor σ. Angelier (1975) also developed a similar method at approximately the same time. Since then, various successive methods were developed by Angelier (1979; 1984; 1989; 1994) and serious improvements in the mathematical algorithms have been proposed to perform the analysis (Etchecopar et al., 1981; Armijo et al., 1982; Will and Powell, 1991; Nemcok and Lisle, 1995; Nemcok et al., 1999; Arlegui-Crespo and Simon-Gomez, 1998; Fry, 1999; 2001; Yamaji, 2000; Shan et al., 2003; 2006; Tobore and Lisle, 2003; Liesa and Lisle, 2004; Orife and Lisle, 2006; Sato and Yamaji, 2006; Žalohar and Vrabec, 2007).

Those methods were succeeded in analyzing the homogenous fault systems, but it may represent a highly problematic strategy for dealing with heterogeneous data sets (Katsushi and Yamaji, 2006; Yamaji, 2006). Numerical algorithms have been proposed which separate faults into different faulting phases (Simon-Gomez, 1986; Fry, 1992; Nemcok and Lisle, 1995; Nemcok et al., 1999; Yamaji, 2003; Žalohar and Vrabec, 2007). This type of analysis is allowed faults to be assigned into homogeneous subsets prior to stress inversion.

Žalohar and Vrabec (2007) represented the new method (the Gauss method) for separation of heterogeneous fault systems into the homogeneous fault subsystems. The method is based on the traditional concept of fault-slip data inversion, which is the best-fit stress tensor. This tensor is generally produced by minimizing or maximizing the object function.

1.4.4. Studies on Anisotropy of Magnetic Susceptibility (AMS)

The first study and theory about anisotropy of magnetic susceptibility (AMS) goes back to a century. Itwas performed by Voight and Kinoshita (1907). After this pioneering study, AMS theory was used as a petrofabric marker by Ising (1942) and Graham (1954) and they first proposed its application to geology. Those authors were first realized that magnetic methods could be used to characterize the preferred orientation of minerals within the rock samples. Ising (1942), studied the varved clay in the Geophysical Laboratory at Djursholm (Sweden) and noticed that the magnetic susceptibility was higher on the bedding plane than orthogonally to it. Graham (1954) used the anisotropy of magnetic susceptibility (AMS) in rocky materials and referred to as an "*unexploited petrofabric element*". Since then, AMS has successfully been used to investigate the spatial and geometrical configurations of the rock components for quantitative estimation of fabric development.

For historical convenience, one of the key landmarks in progress of the magnetic petrofabrics was carried out by Fuller (1963). Fuller has notedthat AMS is due to the frequency distribution of minerals and he also recognized the importance of the spatial distribution of the ferromagnets. A remarkable development after this study is the concept of magnetic carriers that contribute to the magnetic anisotropy. Over the years it became clear that both ferromagnetism and paramagnetism contribute to the total magnetic anisotropy (Daly, 1967; Parry, 1971; Owens and Bamford, 1976; Henry, 1983; Henry and Daly, 1983; Rochette and Vialon, 1984; Borradaile et al.,1986; Lamarche and Rochette, 1987; Borradaile, 1988).

AMS is nowadays an indispensable tool in a wide range of disciplines in Earth Sciences. 12 years later, Graham (1966) focused on the application of AMS to deformed sedimentary rocks and noticed that the flat-lying sediments have an oblate magnetic susceptibility ellipsoid. He also examined folded Paleozoic sandstones from the Valley and Ridge of the Appalachian fold and thrust belt. The results led Graham (1966) to speculate on the development of a magnetic fabric during folding. After a while of Graham's work, AMS studies proved that the sedimentary rocks gain a magnetic fabric

during deposition and also at the highest stage of deformations (Granar, 1958; Fuller, 1960; 1963; Rees, 1961; 1965; Hamilton and Rees, 1971; Kent and Lowrie, 1975).

In addition to sedimentary rocks, many scientists used AMS in the investigation of volcanic or igneous (Girdler, 1961; Khan, 1962; King, 1966; Heller, 1973) and metamorphic rocks (Atkinson, 1977; Borradaile et al., 1982; Hrouda, 1982). Several scientists become interested in developing the methods aiming at fabric separation (Owens and Bamford, 1976; Henry, 1983; Rochette and Fillion, 1988). The main idea behind such separation of magnetic anisotropies is the variation of susceptibility with either temperature or applied field.

Tensor-statistics are essential for the characterization of fabric orientation-distributions. Characterizing the mean orientations of principal directions (k_{MAX}, k_{INT}, k_{MIN}) from numerous samples is more complicated and requires the tensor-statistical approach. Jelinek (1978) has a fundamental contribution to the correct statistical characterization of a sample of tensors.

Scribaand Heller (1978) and Schmidt et al. (1988) proposed a method aiming the fabric separation. They determined the anisotropy tensors by using the 100 µT radial field in a SQUID magnetometer and rotated the sample about each of three mutually perpendicular axes in steps of 45° and for a total of 24 positions.

Borradaile and Tarling (1981), showed that the Kmax axes in AMS ellipsoid is not always parallel to maximum extension of the strain ellipsoid by studing the AMS data that collected from mud rocks.

Ramsay and Huber (1983) showed that the AMS may record preferred grain orientation in sedimentary rocks with no macroscopic strain indicators, even before the appearance of embryonic cleavage.

Stephenson et al. (1986) studied very fine particles specifically single-domain magnetite and determined the magnetic anisotropy of magnetite by examining the magnetic grain size.

The work by kissel et al. (1986), in weakly deformed rocks is possibly the first to demonstratethe great potential of the AMS, as these authors have employeda technique that is possible to detect very weak deformation in rocks otherwise considered to be undeformed. More recent studies tacke advantage of the AMS sensitivity to define the

orientation of the weak tectonic magnetic fabrics (e.g., Aubourg et al., 1991; Averbuch et al., 1992; Owens 1993; Parés and Dinarès 1993; Sagnotti and Speranza 1993; Collombat et al., 1995; Parés et al., 1999; Sagnotti et al., 1999).

Rochette and Fillion (1988), termed the inverse magnetic fabrics and he proposed two causative models: (1) maximum susceptibility of ferroan calcite grains is parallel to the c-axis and (2) single domains are elongated grains. Rochette and Fillion (1988) also determined the susceptibility anisotropy of both ferromagnetic and paramagnetic fractions, by using a new method, they used a vertical-access SQUID magnetometer and trapped a DC field. By rotating the sample about a horizontal axis at a frequency of (0.01 Hz) and analyzing the generated signal.

Hrouda and Jelinek (1990) presented a mathematical method for separating the components by measuring a sample in two different fields above the saturation magnetization of the ferromagnetic contribution.

Jackson (1991) studied on the magnetic minerals and proposed that bulk magnetic fabric of multidomain (MD) particles mimics grain orientation because the maximum/minimum susceptibility coincides with the long/short axes of the grains. In SD particles, the minimum axis of susceptibility is parallel to the long axes of the grain and produce inverse magnetic anisotropy.

Hrouda and Tarling (1993) presented the basics of the AMS and studied the anisotropy of low and high field anisotropy of magnetic susceptibility by applying it on magnetic minerals in rock or unconsolidated sediments.

Pares et al. (1999) suggested a new model for advanced stages in AMS evolution within the strained mud rocks and the model includes four types of magnetic fabrics that develop in weakly deformed mud rocks undergoing progressive deformation. After that similar studies have been made on similar rock types by several researchers (Frizon de Lamotte et al., 2002; Saint-Bezar et al., 2002; Souqué et al., 2002; Sans et al., 2003; Larrasoaña et al., 2004; Parés, 2004; Robionetal., 2007; Cifellietal., 2009; Debacker et al., 2009; Olivaetal., 2009; Sotoetal., 2009; Weil and Yonkee, 2009; Mochales et al., 2010; Pueyo-Anchuela et al., 2010).

Although numerous studies were made to build the theoretical background of the AMS, some geological application studies of the AMS were also carried out in order to

understand the evolutionof the deformation. Recently, Vasiliev et al. (2009) have performed one of these types of studies. They studied the syn- and post-collisional evolution of the Romanian Carpathian foredeep by comparing the AMS with paleostress data collected from upper Miocene and Pliocene sedimentary successions in this area. The study is quite successful in interpreting the collisional evolution since the Kmax of the AMS data and shortening direction of paleostress data are compatible with each other.

2. METHODOLOGY

This study integrates several data sets obtained from various geological disciplines in order to to fulfill the stated objectives of the thesis. The methods can be classified into two groups as Paleostress inversion and Magnetic Susceptibility Anisotropy (AMS) studies.

In this study, paleostress inversion technique is performed by using T-Tecto Software (Zalohar and Vrabec, 2007) to resolve the kinematics of the local and regional faults. At the same time, Magnetic Susceptibility Anisotropy (AMS) is applied as an independent method with the purpose of testing the stress directions from the fault slip data.

2.1. Paleostress Analysis

Paleostress is a paleo (historical) stress that affected the rock; the method is based on the principle which states that the past tectonic stress should leave a trace in the rocks and that we can find the stress history acted on this rock (Hancock, 1985). Paleostress analysis refers to various methods, which attempt to determine a regional stress tensor consistent with existing geological structures. Principal stress directions and relative magnitudes have been determined from fault population, earthquake focal mechanism, joint sets, dike sets, calcite e-twins, microstructural features, folds, stylolites and kink bands.

Fault-slip analysis is the topic of this study and attempts to estimate the relative magnitudes and orientations of the three principal stresses σ_1, σ_2, and σ_3 from fault populations and their slip directions (Angelier, 1990, 1994; Carey and Burinier, 1974). The theoretical relationships between stress and shear was described by Wallace (1951) for the first time. And then Bott (1959) formulated the relationship of the principal stress magnitudes and orientations to the resulting directions of maximum shear stress within the fault planes.

The aim is to use fault-slip data to determine the stress tensor; therefore, some hypothesis must be made about the failure mechanisms involved. Study of Anderson (1951) on faulting (Figure 2.1a) and Coulomb's failure criterion (Coulomb, 1776; Handin, 1969) (Figure 2.1b) were used to predict the orientations of the three principal stress axes in three common types of conjugate fault systems, namely thrust, normal and strike-slip (Figure 2.1).
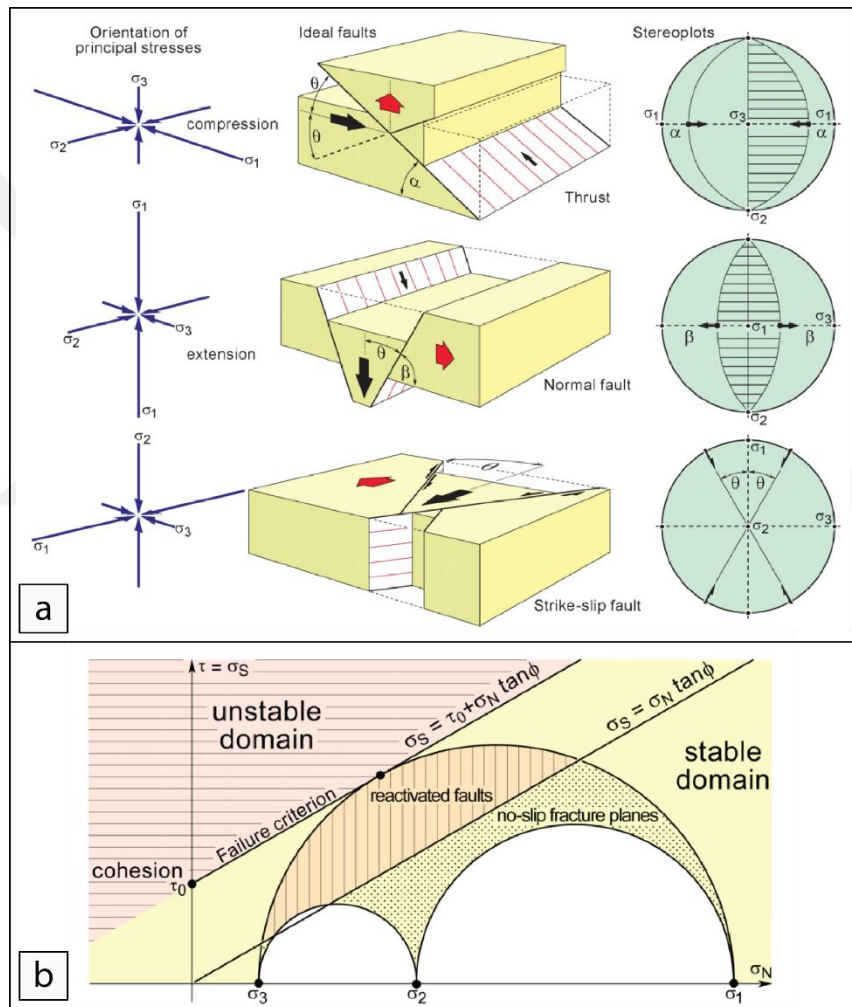
Figure 2. 1. (a) Anderson's theory of orientation of principal stress and its block diagram and stereoplots and (b) Domain of intact rock, reactivated or inherited fractures in a Morh diagram with the three principal stresses (from Jean-Pierre Burg (2018).

The next principle in paleostress analysis is the determination of the relationship of shear stresses to the orientation of fault planes and their associated slip direction

(Wallace, 1951) and the relationship of the principal stress magnitudes and orientations to the resulting directions of maximum shear stress within fault planes (Bott, 1959).

Based on the basic principles, several techniques are used to analyze fault-slip data and to estimate the components of the local stress tensor. One of the simplest graphical methods of paleostress analysis using fault-slip data is P-T method that includes a single fault in isotropic rock with a determined sense and direction of displacement. Another graphical method of paleostress analysis is the Right-Dihedra method that has been developed by adapting the construction techniques of fault-plane solution from earthquake focal mechanism. The inverse method is an analytical or computational method which is based on the finding a stress tensor satisfying known slip directions and orientations for a faults population. Brief information about these methods is given below.

2.2.1. Methods of paleostress analysis

2.2.2.1. Single fault: P-T method

This is a very simple method to determine paleostress directions. This method can be applied to a situation of a single fault in isotopic rock with determining the direction and sense of the displacement. The basis for this method is the assumption, that movement plane (the movement plane is the plane that is perpendicular to the fault plane and contains the slip direction) includes maximum stress σ_1 and minimum stress σ_3 of principal stresses directions and the line normal to the slickenline within the fault plane represents the intermediate stress σ_2. And fractures generate with an angle of about 30° to σ_1. This assumption is only valid in ideal homogenous media with no preexisting fractures, therefore can be directly applied to focal mechanism of earthquakes. Nevertheless, sometimes this method still yields meaningful results. In order to determine paleostress directions, fault plane with displacement vector pairs must be entered to calculate P (compression) and T (tension) directions. Obviously, the bigger the number of striated planes orientation has been measured, the best it is to find approximate positions of the stress axes.

2.2.2.2. The right-dihedra method

Since the 1970s a variety of methods have been proposed for estimating paleostress phases from field data of striations on fault plane (Carey and Brunier, 1974; Angelier and Mechler, 1977; Nemčok and Lisle, 1995; Yamaji, 2000; Žalohar and Vrabec, 2007). One of the best known and a widely used graphical method to perform paleostress analysis is the Right Dihedral Method developed by Angelier and Mechler (1977). The method displays paleostress analysis in a form resembling earthquake focal mechanisms.

The right dihedra method can be applied to two or more fault slips which occurred in the same stress regime (the same orientations of principal stress axes and the same ratio Φ). It takes advantage of this by assuming, in a population of faults, the geographic orientation that falls in the compressional dihedral (P-quadrants) is most likely to coincide with the orientation of σ_1 and the orientation of the σ_3 axis should belong to the extensional dihedral (T-quadrants). However, the orientation of the σ_2 axis and ratio Φ is not taken into account in this method. Spatial orientation and position of the P and T quadrants are defined by orientation of the fault plane and the slip direction along it. The accuracy of the results is obviously dependent on the variety of geometrical orientations of fault slip data: the more diversified the fault-slip orientations, the tighter the constraints on compatibility directions for compression and tension.

2.2.2.3. Inversion method

The inverse problem consists of determining the stress tensor by knowing the direction and sense of the slip-on numerous faults of different orientations. In 1974, Carey and Brunier made the first attempt at formulating and solving the mathematics defining the inverse problem. After this pioneering study, many researchers studied the fault-slip analysis and proposed the mathematical algorithms to perform the analysis (Angelier 1979, 1984, 1989, 1994; Armijo et al., 1982; Etchecopar et al., 1981; Will and Powell, 1991; Nemcok and Lisle, 1995; Nemcok et al., 1999; Arlegui-Crespo and Simon-Gomez, 1998; Fry, 1999, 2001; Yamaji, 2000a, 2000b; Shan et al., 2003; Tobore and Lisle, 2003;

Liesa and Lisle, 2004; Shan et al., 2006; Orife and Lisle, 2006; Sato and Yamaji, 2006; Žalohar and Vrabec, 2007). The methods proposed by those researchers are all based on the same assumption: 1) the direction of movement on the faults parallels the shear stress on those faults, 2) the faults do not interact (the movement along one fault is independent of the movement on the other faults), 3) the blocks bounded by the fault planes do not rotate, 4) the stress field activating the faults is time-independent and homogeneous. The paleostress inversion problem can be most easily formulated mathematically when analyzing homogeneous fault systems, where all faults have been active at the same time and in the same stress regime (Angelier, 1989; 1994). Mostly, the fault systems are affected by more than one stress regimes corresponding to deferent tectonic regimes. In this case, the fault systems are referred to as being heterogeneous and are composed of homogeneous subsystems (Angelier 1989).

The inversion method minimizes the difference between measured and computed slip directions on the fault planes, with the requirement that for each fault plane the striation is parallel to the resolved shear stress. The goal of this method is to find stress model with three stress directions (σ_1, σ_2, and σ_3) and a value of shape parameter that is represented by R or Φ ratio (Eq. 2.1). The shape parameter is used to convey, in a single quantity, information about the relative magnitudes of the three principal axes of the tensor. $\sigma_1 > \sigma_2 > \sigma_3$ are the magnitudes of maximum, intermediate, and least principal stress, respectively, with compression being positive. The definition given below essentially compares the magnitude of the intermediate axis σ_2 to the others.

$$R = \frac{\sigma_2 - \sigma_3}{\sigma_1 - \sigma_3} \cdots\cdots\cdots\cdots\cdots (note\ that\ 0 \leq R \leq 1) \cdots\cdots\cdots\cdots\cdots\cdots (Eq.\,2.1)$$

Stress Tensor Type	EXTENSIVE		STRIKE-SLIP		COMPRESSIVE	
Stress Symbols						
Stress Ratio (R)	0.00 0.25 0.5 0.75 1.00		0.75 0.5 0.25 0.00		0.25 0.5 0.75 1.00	
Stress Symbols						
Stress Regime	RADIAL EXTENSİVE	PURE EXTENSİVE	TRANS-TENSİVE	PURE STRIKE-SLIP	TRANS-PRESSIVE	PURE COMPRESSIVE	RADIAL COMPRESSIVE
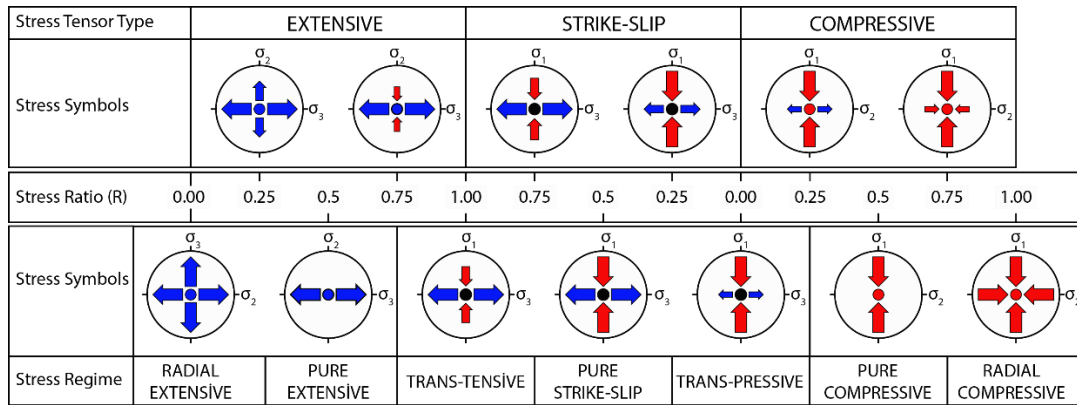
Figure 2. 2. Illustration of the relation between stress regime and orientation of the stress ellipsoid (modified from Delvaux et al., 1997). Stress symbol with horizontal stress axes as a function of the stress ratio R. Their length and color symbolized the horizontal deviatoric stress magnitude, relative to the isotropic stress. Blue outward arrows: extensional deviatoric stress, red inward arrow: compressional deviatoric stress. The vertical stress is represented by blue, black and red solid circle for extensional (σ_1), strike-slip (σ_2) and compressional regime (σ_3), respectively.

There are three main tectonic regimes, which they are differentiated according to the vertical principal stress. Faults will be normal, strike-slip, or reverse depending on whether the maximum (σ_1), intermediate (σ_2) or minimum compressive (σ_3) principal axis, respectively, is most nearly vertical (Figure 2.1a). For analyzing paleostress data, the R and nature of the vertical or sub-vertical stress axis were taken into account (Angelier 1994). According to stress field ratio R with comparison with Anderson's theory, if σ_1 is vertical and stress ratio between ($0<R<0.25$) will form radial extension regime and ($0.25<R<0.75$) form pure extension and ($0.75<R<1$) will form transpersion region, and if σ_2 vertical and stress ratio be between ($0<R<0.25$) will form transpression region and between ($0.25<R<0.75$) form pure strike slip region and between ($0.75<R<1$) transtension region and for σ_3 vertical and stress ratio between ($0<R<0.25$) transpression, ($0.25<R<0.75$) pure compression, and ($0.75<R<1$) radial compression (Delvaux et al. 1997) (Figure 2.2).

In order to measure or estimate paleostress tensor, more than one inverse method have been proposed such as Direct Inverse Method (INVD) (Angelier, 1984; 1990; 1994) and Gauss Method (Zalohar and Vrabec, 2007). Brief information about these methods are given below.

Direct inversion method

This method was developed by J. Angelier (1984; 1990; 1994) for homogenous fault systems. The principal stress directions (σ_1, σ_2, σ_3) and stress ratio (R) can be calculated by applying the direct inverse method (INVD) to the fault-slip data measurements observed in the field (Angelier, 1994). The INVD is referred to determine the mean stress tensor τ, of a known orientations and sense of the slip-on numerous faults. Practically, it is a least-square minimization of the angle between measured stretch marks and the direction of the maximum shear stress that act along the fault planes (Angelier and Goguel 1979). The procedure is searching for the best fit between all fault-slip data that belong to a given tectonic event and a mean stress tensor τ (one computes for each fault the angle, β, between the calculated directions of maximum shear stress acting along the individual fault planes and the measured slip directions) (Figure 2.3).

This procedure allows for the rapid calculation of the big amount of data sets but has limitations. The assumption that all faults, which moved during the same tectonic event, were moving independently but consistently within a single stress tensor is an obvious limitation (Angelier, 1994). In this case, a least-square analysis is appropriate since the misfits are normally distributed. If there are erratic data with very large misfits, as empirically is often the case in fault-slip data analysis, then too much constraint placed on these and they tend to dominate a least-squares inversion (Allmendinger et al., 1989). Angelier (1984) has solved this problem by rejecting anomalous data.
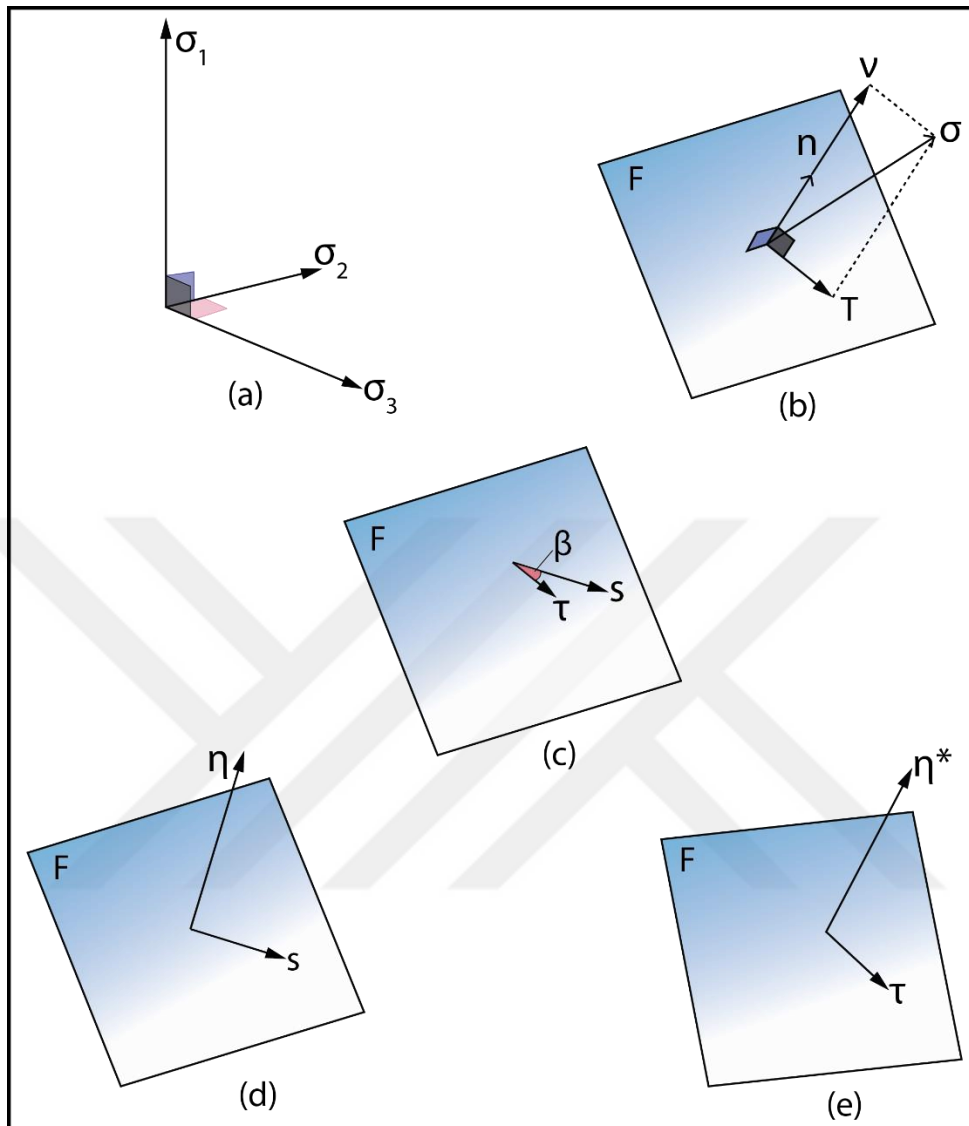
Figure 2. 3. (a) Stress state (σ_1, σ_2 and σ_3 principle stress axes). (b) Weakness plane activated as a fault. F, fault plane; n, unit vector perpendicular to fault plane; σ, stress vector acting perpendicular to fault plane; v, normal stress (acting perpendicular to F); T, shear stress (parallel to F). And note that the stress vector σ depends on both n and σ_1, σ_2 and σ_3. (c) Actual slip,s, and theoretical shear stress, τ, on F. (d) Real and (e) theoretical fault slip, s, unit slip vector and, τ, computed shear stress; n*, normal to best-fitting fault plane in which τ is computed. From Angelier (1994).

During the application of this method, it is necessary to be aware of the theoretical and practical (data collection) limitations. The INVD method is a statistical method. A statistic treatment dealing with a large number of data is necessary to approach the state

of stress; therefore, number of collected data is also important to increase the reliability of the stress state.

Gauss method

Paleostress inversion problem can be most easily formulated mathematically for homogeneous fault systems, where all faults have been active at the same time and under the same stress regime. However, fault systems in the nature are seldom homogeneous since they have been influenced by several different stress regimes. Zalohar and Vrabec (2007) describe the Gauss Method for separation of heterogeneous fault systems into the homogeneous sub-systems. The method is based on the traditional philosophy of fault-slip data inversion and analyzing the fault-slip data based on the best-fit stress tensor.

In the Gauss Method, the compatibility function is defined as Gaussian function. The compatibility function depends on compatibility measure which consists on both the angular misfit between the resolved shear stress and the actual direction of movement on the fault plane, and the ratio between the normal and shear stress on the fault plane on Mohr diagram assuming that the results of paleostress inversion should be in agreement with the Amoton's frictional law. The physical meaning of this law is that the fault plane is activated only when shear stress exceeds some critical value (Eq. 2.2) which represents the frictional strength.

$$\tau \geq \mu \sigma_n \cdots\cdots\cdots\cdots\cdots\cdots (Eq.\,2.2)$$

where τ is shear stress, σ_n is the normal stress on the fault and μ is the coefficient of residual friction for sliding on pre-existing fault. In the Mohr diagram (Figure 2.4), Mohr points representing the values of normal and shear stress on the faults lie between two straight lines defined by equations $\tau = \sigma_n.\tan \phi_1$ (which represents the tangent of the largest of the largest Mohr circle) and $\tau = \sigma_n.\tan \phi_2$ (which represents the Amoton's frictional law respectively). The parameter ϕ_1 roughly approximates the value of the internal friction angle constraining the shear strength of an intact rock, therefore the

equation can approach to the Coulomb-Navier failure criterion (Eq. 2.3) (Jaeger and Cook, 1969; Ranalli and Yin, 1990; Zalohar and Vrabec 2007).

$$\tau = S + \sigma_n \cdot \tan \phi_i \cdots\cdots\cdots\cdots\cdots\cdots (Eq.\,2.3)$$

The Gauss Method uses four parameters (s, Δ, ϕ_1, and ϕ_2) to analyze the paleostress data. S is dispersion parameter (dispersion of the angular misfit), Δ is threshold value for the compatibility measure, the parameter ϕ_1 represents the highest possible case for the friction angle on the pre-existing fault and the parameter ϕ_2 constrains the lowest possible case for the friction angle along pre-existing fault. All these parameters can significantly influence the topography of the object function F and therefore the obtained solutions Zalohar and Vrabec (2007). These parameters need to be specified prior to calculation.

This procedure allows that the Gauss Method is a highly effective and simple way of separating heterogeneous fault systems into homogeneous sub-systems and calculating reliable stress tensor for each stress phase. This method has limitations only when the difference in orientation of stress axes between the separate stress states becomes too small. In this case, the object function may have only one prominent maximum or maxima of the object function may be misplaced with respect to the real solution Zalohar and Vrabec (2007).
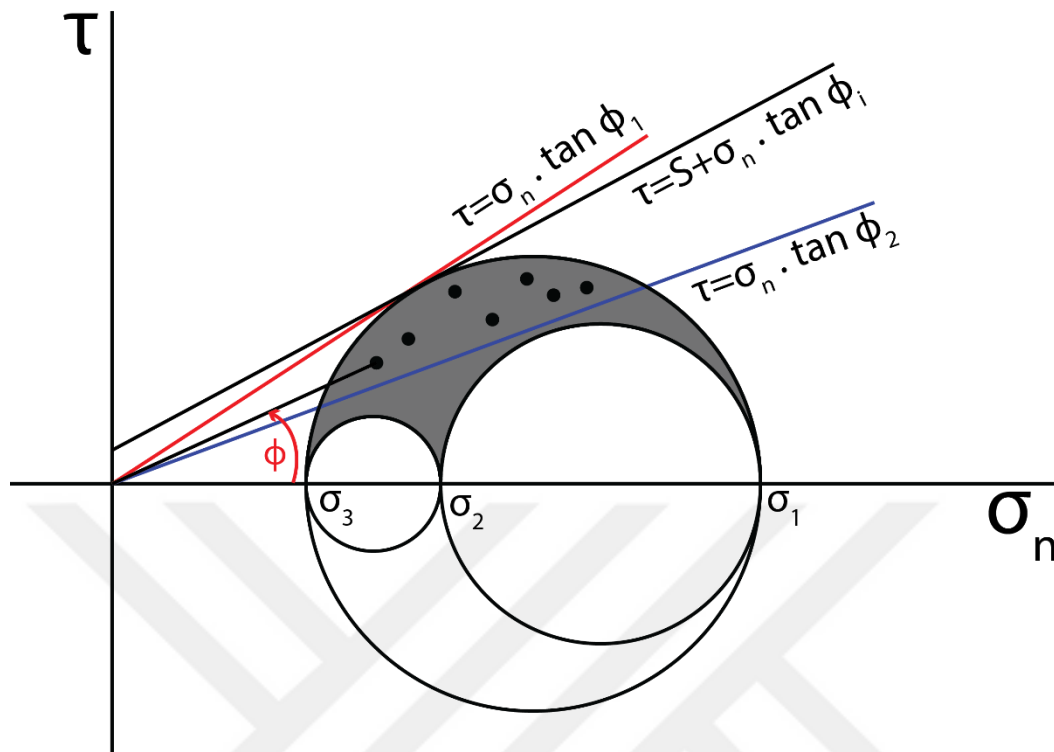
Figure 2. 4. Mohr diagram illustrating normal σ_n and shear stress τ on the faults (black points are Mohr points). σ_1, σ_2 and σ_3 represent principal stress magnitudes and S is the cohesion. The position of the Mohr points for all possible orientations of the faults is restricted to the gray area. However, for mechanically acceptable solutions the position of Mohr points is additionally restricted to the area between the two straight lines with equations $\tau = \sigma_n.\tan \phi_1$ and $\tau = \sigma_n.\tan \phi_2$. The first represents the tangent of the largest Mohr circle and roughly approximates the angle of internal friction angle ϕ_i for intact rock and the second represents the Amoton's frictional law (Zalohar and Vrabec, 2007)

2.2.3. Field measurements: kinematic indicators

The deduction of the sense of motion on the fault surface from the slickensides has been a usual, but also complicated procedure in the structural geology. These kinematic criteria are key elements for paleostress reconstructions (Angelier, 1994). The detail analyses of these indicators are undertaken by some researchers (Petit, 1983, 1987; Doblas, 1985, 1987, 1997; Mercier and Vergerly, 1992). This section of the thesis intends to describe some of these criteria.

Different types of indicators may be observed on a fault surface. The mostly used (Figure 2.5) are explained briefly below:

1. *Accretionary mineral steps* that develop due to fibrous crystal growth or crystallized grains during fault slip. Fibrous minerals that develop along slickenside lineation and form steps indicate the sense of the motion (Durney and Ramsay, 1973; Doblas, 1998). Most are made of quartz or calcite. The criterion is reliable (Angelier, 1994).

2. *Tectonic tool marks* occur as asymmetrical grooves or as a relief on the fault surface (Angelier, 1994). These figures arise from the sheltering effect of protuberances acting as hard objects. These may be a small quartz grain or large boulder. It is reliable criteria for determination of the sense of movement.

3. *Riedel shears*, generally discontinuity surfaces that intersect the fault surfaces. This surface makes a 5-25° angle with the fault plane. Their intersection with fault surface is nearly perpendicular to slickenside lineation (Angelier, 1994).

4. *Stylolite's peaks* are zigzag surfaces within the rock mass. they are special and extensive structures that result from water-assisted pressure dissolution in rocks such as limestones and dolomites (Rutter, 1983; Angelier, 1994; Passchier and Trouw, 1996). During this process, volume of rock decreases. The trend of the structure is perpendicular to the σ_1 direction, which make it reliable paleostress indicators (Stel and De Ruig, 1989; Angelier, 1994; Koehn et al., 2007).

5. *Tension gashes* are among the best criteria to infer the sense of shear on slickensides (Doblas, 1985; Petit, 1987). It is intersecting and make 30-50° acute angle with fault surface. It is approximately perpendicular to a slickenside lineation (Angelier, 1994).

6. *Conjugate shear fractures* or small faults that make 40-70° angle to the main fault plane and perpendicular to slickenside lineation of main fault surface (Angelier, 1994).

7. *Polished (smooth surface) and rough surface*, these criteria is extremely common in all rock types and especially useful in non-calcitic rocks and they are widely used in basalt and sandstone. They have various shapes and are perpendicular to the slip direction (Angelier, 1994).
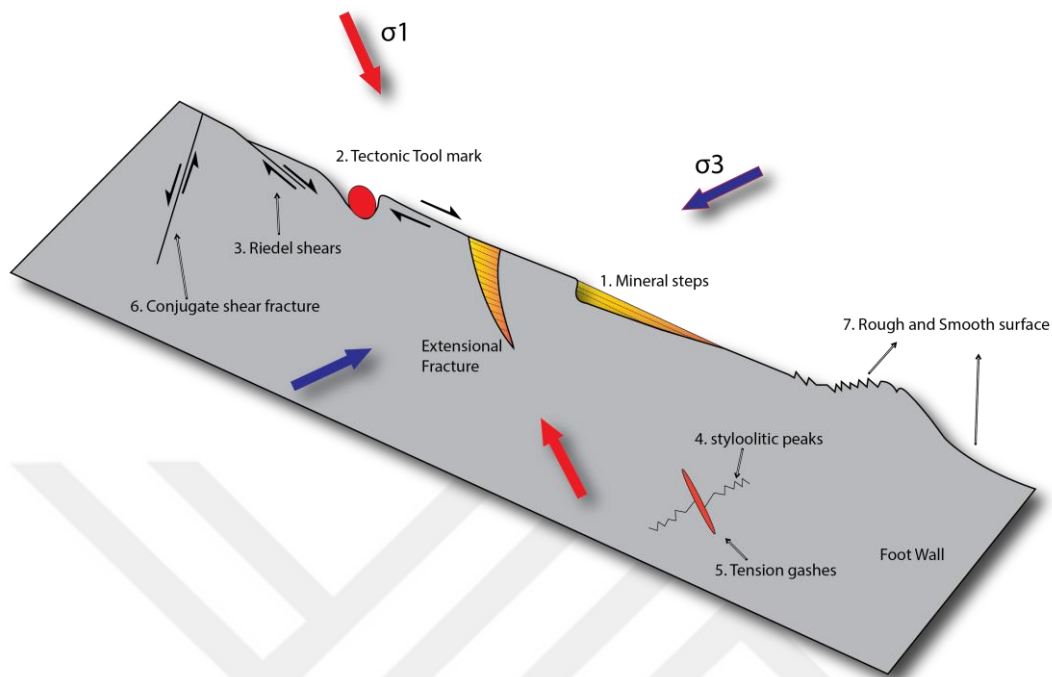
Figure 2. 5. Illustration of the kinematic indicators observed on the fault surfaces 1. Accretionary mineral steps, 2. Tectonic tool mark, 3. Riedel shears, 4. stylolite's peak, 5. Tension gashes, 6. Conjugate shear fracture, 7. Polished (smooth surface and rough) surface.

Other criteria that are rarely used since some may be ambiguous such as shear lenses or rotating blocks along the fault plane (Angelier, 1994).

2.2. Anisotropy of Magnetic Susceptibility (AMS)

The anisotropy of magnetic susceptibility (AMS) can be defined as the dependency of induced magnetization on orientation of the applied magnetic field in the rock and it depicts the preferred orientation of magnetic minerals in a rock or unconsolidated sediment (Hrouda, 1982; Tarling and Hrouda, 1993). The basic systematic background was first introduced by Voight and Kinoshita (1907), and then used as a routine tool to investigate petro-fabric texture of the rock units (e.g. Ising, 1942; Graham, 1954). Studies on magnetic anisotropy progressively developed the following decades and Hrouda (1982) published first comprehensive review on magnetic anisotropy and its application in geology. Later, the studies on the magnetic anisotropy gained

widespread use and application in the geology and the method was extended to examine the fabric in a variety of sedimentary, igneous and metamorphic rocks (Lanza and Meloni, 2006; Hrouda, 2007).

The principle of using the method is to determine the intensity of magnetization within a rock unit in certain directions under a specific magnetic field. The different magnetic susceptibility values can be obtained where each measurement in different directions may be related to both a magnetic mineral structure in the rock and/or an external factor(s) (compaction and/or tectonic deformation, alteration, etc.). Therefore, two principle mechanism control the magnetic anisotropy of rocks; 1) Lattice alignment of crystals with magnetocrystalline anisotropy and 2) shape alignment of ferromagnetic grains.

The AMS of rocks contains information about both the grains susceptibilities and distribution of their orientation. The distribution of preferential orientation distribution of mineral grains is, in fact, typical of almost all rock types and it develops during various geological processes, such as water flow in sediments, magma flow in igneous rocks, ductile deformation in metamorphic rocks, and even incipient strain in the paramagnetic clay matrix of apparently undeformed fine-grained sediments. In addition to rock forming processes, a preferred orientation distribution of mineral grains is closely related to an orientation of structural features (e.g. fold, fault, foliation, and lineation) that were formed under dominant deformation (Hrouda and Janak 1976; Borradaile 1988; Averbuch et al. 1992; Robion et al. 2007; Borradaile and Jackson 2010).

Comparing the AMS with other methods of fabric analysis (such as U-stage, X-ray, texture goniometry and neutron texture goniometry), AMS is fast, cheap, high resolution and non-destructive technique (Tarling and Hrouda, 1993). AMS is non-destructive technique and it is applicable to rock samples that do not show certain strain markers, such as deformed fossils and ooid etc. It can be useful in all type of rocks that are weakly deformed (Tarling and Hrouda 1993; Borradaile and Henry 1997; Evans et al. 2003). Further detailed information about the technique was described in Tarling and Hrouda (1993).

2.2.1. Theoretical background

Magnetic properties arise from the motion of electrically charged particles. This means that all the materials have magnetic properties at temperature above absolute zero (0 K) and are susceptible to become magnetized in the presence of an applied magnetic field (Taring and Hrouda, 1993). If the magnetic field is relatively weak, the magnetization of a rock is a linear function of the intensity of this field. The low field magnetic susceptibility (k) is defined as the ratio of the induced magnetization (M, dipole moment per unit volume or J, dipole moment per unit mass) to the applied low intensity magnetic field (H) (Eq. 2.4). The magnetic susceptibility is a dimensionless proportionality module. Only for isotropic substances the induced magnetization is strictly parallel to the applied field, and the magnetic susceptibility is a scalar. In the general case of anisotropic media, like minerals and rocks, the induced magnetization is not parallel to the applied field.

$$M = \text{k. H} \cdots\cdots\cdots\cdots\cdots\cdots\cdots\cdots\cdots (Eq. 2.4)$$

A natural rock contains a variety of minerals – paramagnetic, diamagnetic or ferromagnetic – each grain of which makes its own contribution to the total (bulk) susceptibility and, hence, to the anisotropy of susceptibility (Tarling and Hrouda, 1993).

The magnetization of a rock induced weak magnetic field is a linear function of the intensity of field and the variation of susceptibility with orientation can be described mathematically in terms of asymmetric second-rank tensor as:

$$\begin{bmatrix} M_x \\ M_y \\ M_z \end{bmatrix} = \begin{bmatrix} k_{xx} & k_{xy} & k_{xz} \\ k_{yx} & k_{yy} & k_{yz} \\ k_{zx} & k_{zy} & k_{zz} \end{bmatrix} \begin{bmatrix} H_x \\ H_y \\ H_z \end{bmatrix} \cdots\cdots\cdots\cdots\cdots\cdots (Eq. 2.5)$$

where, M_i (i=x, y, z) are the components of the magnetization vector (in the Cartesian coordinate system), H_j (j=x, y, z) the component of the vector of the intensity of the magnetic field and the set of the constant k_{ij} ($k_{ij}=k_{ji}$) represents the component of the

symmetric tensor second rank, called susceptibility tensor. Generally, a non-diagonal component of the susceptibility tensors is not zero, but there exists such a Cartesian coordinate system in which the non-diagonal components of the susceptibility tensor are zero and the equation that is given above (Eq. 2.5) will change into equation 2.6;

$$\begin{bmatrix} M_x \\ M_y \\ M_z \end{bmatrix} = \begin{bmatrix} k_{xx} \\ k_{yy} \\ k_{zz} \end{bmatrix} \begin{bmatrix} H_x \\ H_y \\ H_z \end{bmatrix} \dots\dots\dots\dots\dots\dots\dots\dots\dots (Eq.\,2.6)$$

The components k_{xx}, k_{yy} and k_{zz} represent the principal susceptibilities and their directions are called as principal directions (eigenvectors). The principal susceptibilities (k_{xx}, k_{yy} and k_{zz}) are usually referred to as the maximum (k_{max}), intermediate (k_{int}) and minimum (k_{min}) susceptibilities, respectively. The orientation of principal susceptibilities indicates distribution of magnetic minerals fabric in rock sample; however, the composition of the rock sample and metamorphic grade may influence the anisotropy of magnetic susceptibility and bulk susceptibility of rock sample (Borradaile and Henry, 1997, Nakamura and Borradaile, 2004).
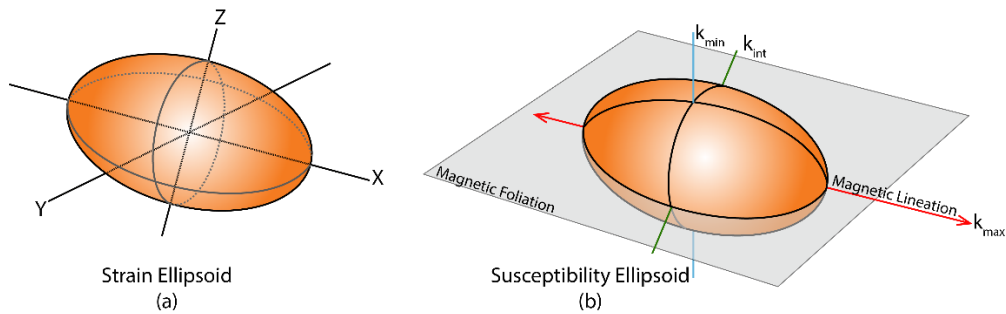
Figure 2. 6. Schematic illustration of the relation between (a) strain axes (X, Y, and Z, X≥Y≥Z) and (b) susceptibility principal axes (kmax ≥ kint ≥ kmin). The reference system is cartesian coordinates (x, y, and z correspond to X, Y and Z in strain ellipsoid, and k_{max}, k_{int} and k_{min} in susceptibility ellipsoid, respectively) (from Taring and Hrouda, 1993).

Table 2. 1. The most used magnetic anisotropy parameters in AMS studies (Winkler et al., 1997).

Name of Parameter	Parameter Symbol	Parameter Formula	Refrences
Degree of anisotropy	P	k_{max}/k_{min}	Nagata (1961)
Corrected degree of anisotropy	P'	$exp\sqrt{\{2[(n1-n)2 + (n2-n)2 + (n3-n)2]\}}$	Jelinek (1981)
Magnetic Lineation	L	kmax/kint	Balsley and Buddington (1960)
Magnetic Foliation	F	kint/kmin	Stacey et al. (1960)
Shape of Ellipsoid	T	$2(n2-n3)/(n1-n3)-1$	Jelinek (1981)
Mean Susceptibility	Km	$(k1+k2+k3)/3$	Nagata (1961)
n1= lnk1, n2 = lnk2, n3 = lnk3, n = (n1+n2+n3)/3			

Therefore, the bulk susceptibility (Km) and anisotropy of the susceptibility are used to determine the state of strain and petro-fabric. The AMS is represented by magnitude ellipsoids, geometrically shaped by three magnetic principal axes ($K_{max} \geq K_{int} \geq K_{min}$ or $K_1 \geq K_2 \geq K_3$), and those are closely related to the strain axes (X>Y>Z) (Figure 2.6). Numerous parameters have been defined both for the quantification of the magnitude of anisotropy and for determination of the shape of the ellipsoid (Table 2.1). These are described under five parameters: 1) Degree of anisotropy (indicated by P, P' or Pj), 2) magnetic lineation (L), 3) magnetic foliation, 4) shape of an ellipsoid (T) and 5) mean susceptibility (Table 2.1).

Tabulated data are rarely comprehensive without considerable study. In this context, graphical representation of anisotropy should be similar to those conventionally used by structural geologist. For this reason, it is adopted in the structural studies as its advantages for illustrating the AMS apply equally in studies of strain (Figure 2.7). Conceptually, plotting of the susceptibility ellipsoid shapes and their magnitudes is not much different from the Flinn plot.
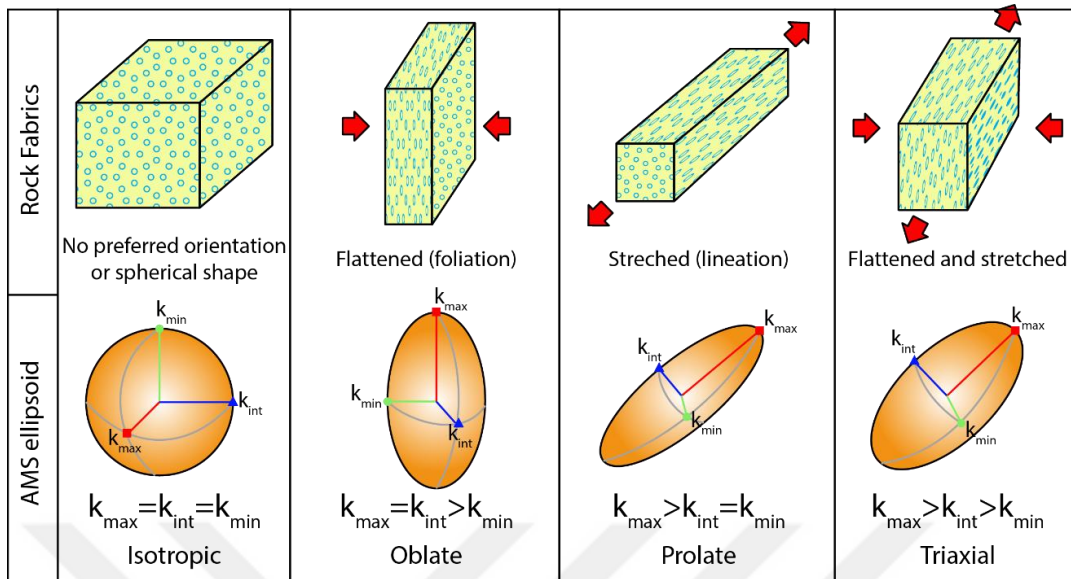
Figure 2. 7. Illustration shows that the relation between rock fabric and magnetic susceptibility ellipsoids. Note that based on the magnitude of the AMS axes, the shape of the AMS ellipsoid changes from spherical to triaxial (from Winkler et al., 1997).

Shape of the AMS and strain ellipsoids are described in the same way as follows:

a)   kmax ≈ kint ≈ kmin (X ≈ Y ≈ Z in strain ellipsoids); the AMS ellipsoid is a sphere (isotropic susceptibility).

b)   kmax ≈ kint > kmin (X ≈ Y > Z in strain ellipsoids) ; the AMS ellipsoid has an oblate shape (i.e. the magnetic fabric is planar).

c)   kmax > kint ≈ kmin (X > Y ≈ Z in strain ellipsoids); the AMS ellipsoid has a prolate shape (i.e. the magnetic fabric is linear).

d)   kmax > kint > kmin (X > Y > Z in strain ellipsoids); the AMS ellipsoid is triaxial.

2.2.2. Field sampling and laboratory procedures

AMS can be determined for a very wide variety of rock materials, but AMS studies require carefully chosen oriented rock samples. We have to emphasize that most directional errors in AMS studies occur during field sampling and orientation. Hence,

particular care is essential in undertaking all parts of these procedures. In this part of the thesis, collection of the samples in the field and measurement procedure of the prepared samples in the laboratory will be presented.

2.2.2.1. Field sampling

The field sampling methods in the field are exactly the same as those used to collect orientated rock samples for paleomagnetic purposes (Cox and Doell, 1960; Collinson, 1983; Taring, 1983; Taring and Hrouda, 1993). However, magnetic anisotropy is more sensitive to the shape of the specimen than paleomagnetic.

The sampling procedure can be done in two ways in ; (1) by drilling cores using a gasoline power motor (or portative electrical) driller with a water pump, or (2) by collecting hand specimens that are oriented in situ and later drilled to provide cores using an air driller in the laboratory. The samples should be taken from the fresh surface to avoid secondary magnetization effects on the rock samples, such as present magnetic field effect, chemical alterations or volcanic activity, etc.

During the field sampling, strike orientation and dip amount of the bedding must be measured and if exists, other geological structures, such as lineation, flow direction, foliation and minor faults should be measured as well. Since AMS measurements possibly affected by these factor(s), all these factors should therefore be taken into account during interpretation. The samples should be preserved properly by wrapping with the allium-foil, and placed in the plastic bag for transportation. The plastic bag will protect the samples from drying and preserving its property.

The most common standard shape for the core is 2.5 cm in diameter and 2.1 cm in height (Tarling and Hrouda, 1993). Since the specimen holder of measurement equipment has a standard size for both AMS and the other paleomagnetic studies, drilled rock samples need to be taken in a certain size. In order to obtain statistically significant AMS result, 5-10 core samples per site must be collected (Dubey, 2014). In this study, approximately 10-15 core samples per site were sampled for AMS study.

Location of sample sites is also important since the strain values can vary along or across the geological structures, in different fold geometries, and even in two limbs of

the fold. Hence, it is suggested that study area should be carefully mapped for geological structures and their geometries.

2.2.2.2. Laboratory equipment and measurement

AMS is known as direction dependent rock magnetic susceptibility and is generally measured by low magnetic field along at least six (more directions are desired) directions so that the susceptibility ellipsoid can be drawn (Tarling and Hrouda, 1993). Two methods are commonly used to measure AMS. The first method, called static technique, consists of determining the full susceptibility tensor, whereas the second method, spinning specimen method, measures the deviatoric susceptibility tensor. The full tensor can be obtained by measuring the susceptibility in specified directions (6 to 15) relative to sample coordinates (Jelinek, 1981). The measurement procedure needs the determination of at least 6 directional susceptibilities to compute the 6 independent elements of the symmetric (3×3) susceptibility tensor. The AMS ellipsoid is estimated by a least-squares fit to the directional data. If more than the minimum numbers of measurements are carried out, the ellipsoid is over-defined and the error of fitting can be determined (Jelinek, 1977). The spinning specimen method is generally done by rotating the sample in the low magnetic field successively in three mutually orthogonal planes (Figure 2.8) and also bulk susceptibility is measured. The specimen is rotated around three perpendicular axes and generates a harmonic signal composed from *sine* and *cosine* components. Shape of magnetic anisotropy is produced from this signal and the mathematical background is more complicated with respect to the static specimen method. One of the primary importance of spinning specimen method is sensitivity, as well as the accuracy of the measured main axes, are substantially higher than those of static specimen method.
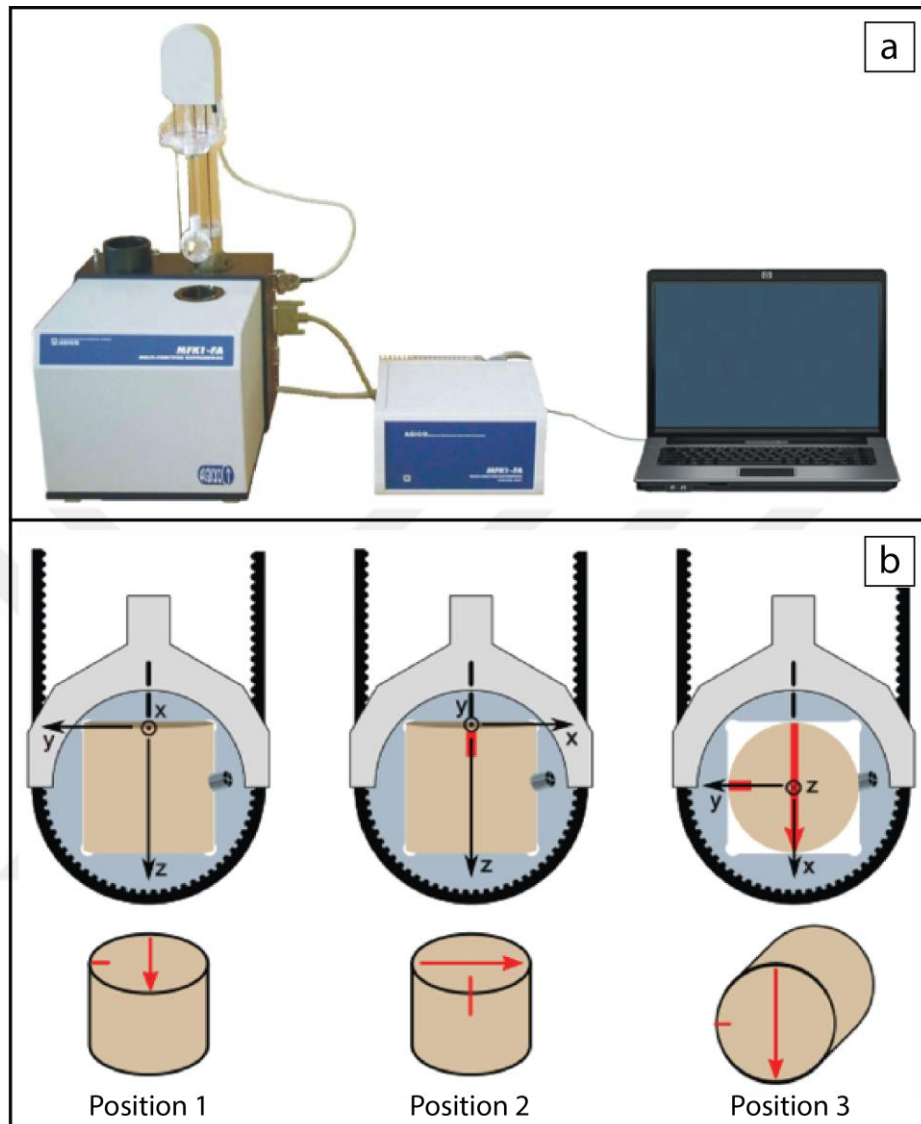
Figure 2. 8. a. Kappabridge (MFK1-A) measurement system, and b. mesurement position of a rock sample for three measuring axes (in x, y and z) *www.agico.com*.

Generally, if a sample has a high susceptibility and strong anisotropy; measurements carried out by one of the above methods are reproducible within small measurement errors. However, for samples having low susceptibility or weak anisotropy, the noise level of the measurement may exceed the order of the anisotropy of the sample. Therefore, subsequent measurements for the same specimen may give strongly different results in terms of the degree, shape and principal directions of the anisotropy ellipsoid.

In this study, AMS measurements were carried out with AGICO MFK1-FA (Multi Function Kappabridge) in spinning mode at Fort Hoofddijk Paleomagnetic Laboratory in Utrecht University (The Netherlands). The MFK1 susceptibility bridges have a sensitivity level of 2×10^{-8} SI at a frequency of 976 Hz and in a field of 400 A/m.

2.2.2.3. Plotting of magnitude and shape of susceptibility ellipsoid

The AMS ellipsoid is a fabric ellipsoid that represents the orientation distribution of all deformed magnetic minerals in the specimen. Magnitudes of the ellipsoid axes are properties of the state matter and different specimens have different mean susceptibility (Km). Therefore, they can be different in magnitude and shape (Dubey and Ashok; 2014).

Plotting of the susceptibility ellipsoid shapes and magnitudes is not much different from strain ellipsoid plot that is represented by two-dimensional Flinn diagram. The axial ratios of a magnetic ellipsoid are plotted in the susceptibility plot with foliation that is defined as F=Kint/Kmin in the horizontal axis and, with lineation that is stated as L=Kmax/Kint in the vertical axis (Figure 2.9). L/F ratio is equal to 1.0, which corresponds to the 45° slope in the graph. It represents the plane strain (triaxial) ellipsoids and divides the area of prolate strain in the upper part and oblate strain in the lower part. Anisotropy degree abbreviated as "Pj" increases starting from the origin of the diagram for all the AMS ellipsoids (Figure 2.9).

The diagram that is given in Figure 2.9 can provide means to understand the fabrics developed during litho-genesis or subsequent tectonic event and may help to correlate magnetic and tectonic strain.

The shape parameter (T) (Eq. 2.7) contains information of lineation (L) and foliation (F) parameters. Therefore, all three principal susceptibility information hidden in these parameters (L and F) have been represented in a single measure. If the shape parameter T lies between $0 < T \leq 1$, then the AMS ellipsoid is the oblate shape, whereas negative values, $-1 \leq T < 0$, corresponds to prolate shape (Figure 2.10). Plane strain ellipsoid is represented when the shape parameter T is equal to 1.

$$T = (\ln L - \ln F)/(\ln L + \ln F) \cdots\cdots\cdots\cdots\cdots\cdots (Eq.\ 2.7)$$
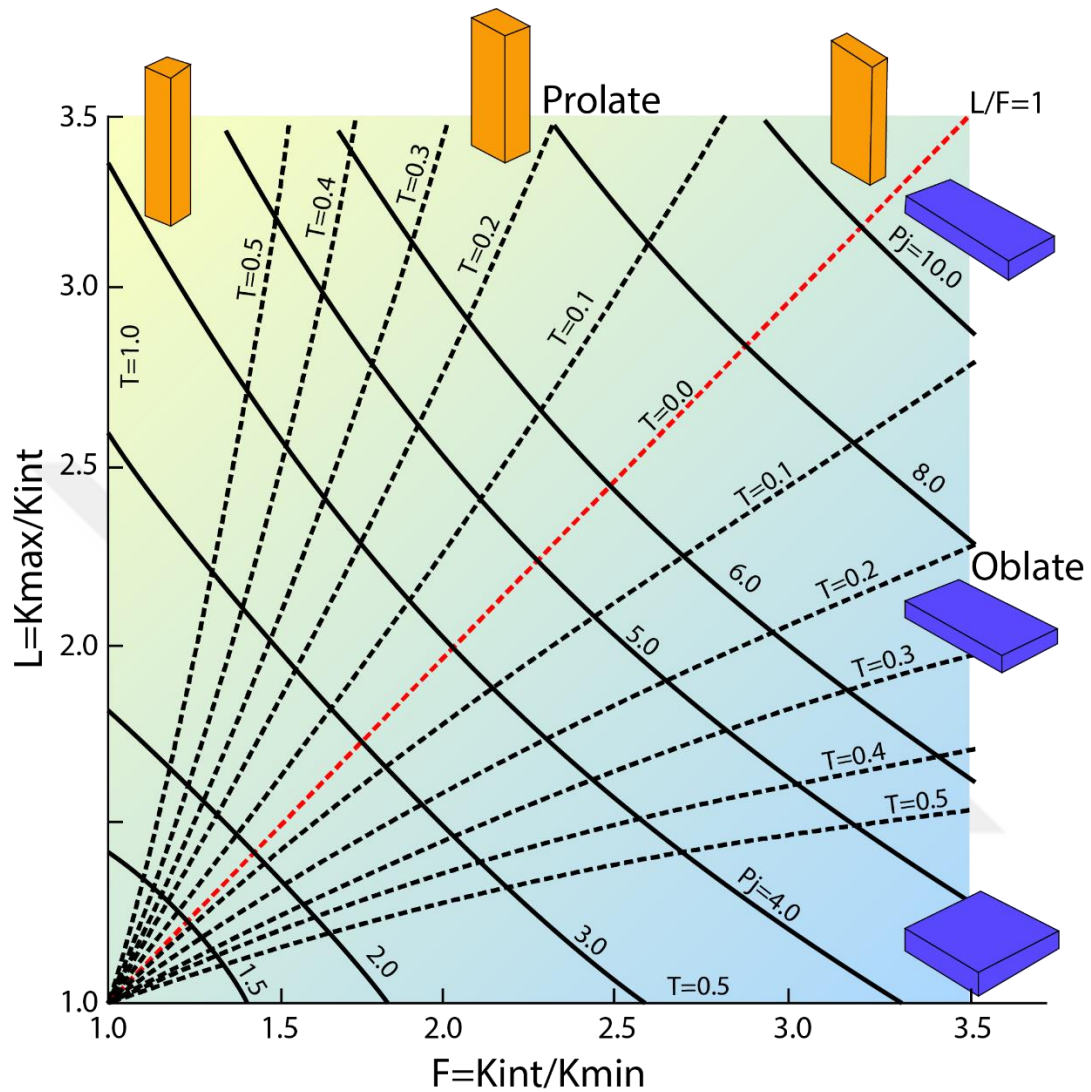
Figure 2. 9. Flinn-type plot of the degree of lineation and foliation. It has been conventional to plot a measure of foliation against a measure of lineation as this is anagolous to the plots of strain and shape ratios commonly used in structural geology (Flinn, 1962; 1965a, b). Oblate fabrics plot below the slope of unit gradient and prolate fabrics plot above (from Tarling and Hrouda (1993)).
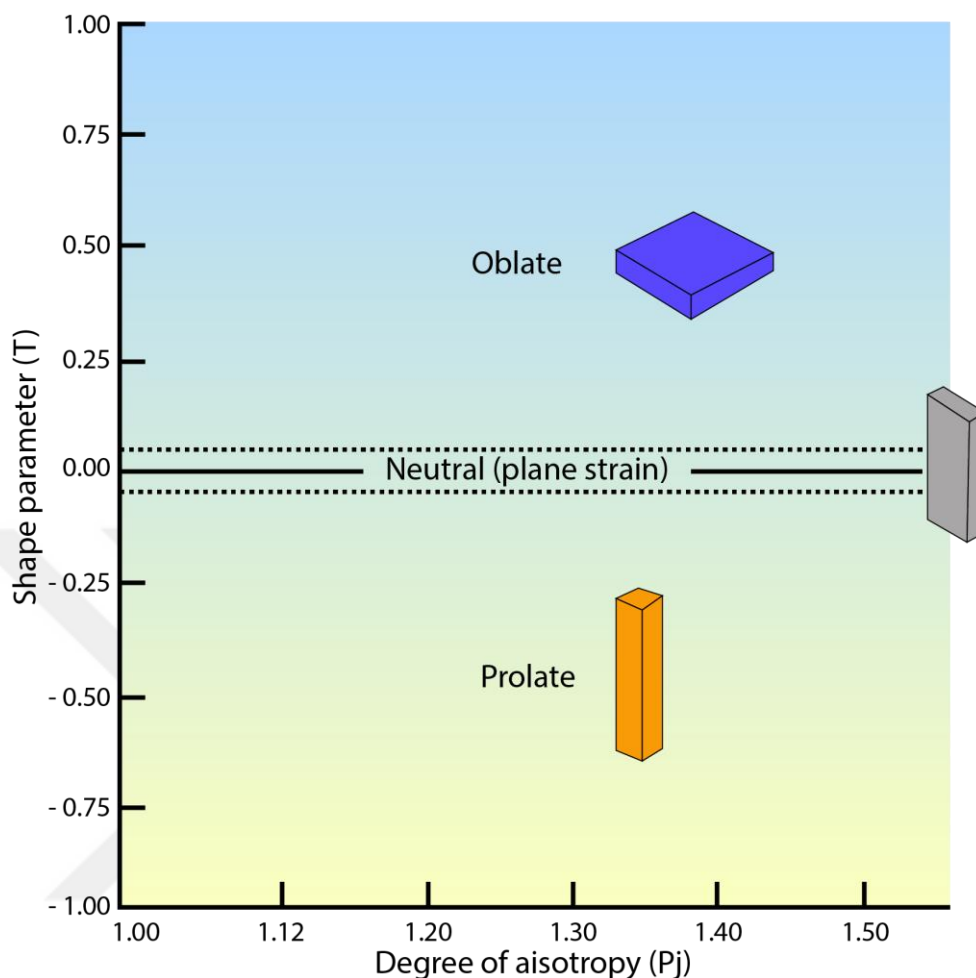
Figure 2. 10. The Jelinek plot illustrates the relationship between degree of anisotropy (Pj) and shape parameter (T). Note that oblate shapes have positive T values approaching to 1, whereas the prolate shapes have negative values approaching -1. Triaxial shapes plot close to T=0.0 (from Tarling and Hrouda (1993)).

The parameter "Pj" is '*corrected anisotropy degree*' that is proposed by Jelinek (1981). It corresponds to the degree of alignment of minerals as a function of strain intensity or magnetic mineralogy that is linear to the bulk susceptibility (Borradaile, 1988; Pares and van der Pluijm, 2002). By definition, the parameter Pj incorporates both the intermediate and mean susceptibilities, which make this parameter more informative previously defined parameters. In this circumstance, Jelinek (1981) suggested that another two-dimensional plot (Figure 2.10) for depicting the magnitude and shape of susceptibility ellipsoid where the parameters Pj and T are used. In this graph, Pj is plotted

along the horizontal axis (1 < Pj) while T is plotted along the vertical axis (−1 < T < 1). In the diagram, all prolate shapes have negative values and oblate shapes have a positive value, while the triaxial (plane strain ellipsoid) shapes have zero value. The plot of Jelinek is really practical since the both magnitudes and shapes are displayed as the values together with the ellipsoid pattern of the study area.

2.2.2.4. Plotting of the AMS principal axes

Magnetic fabrics of a rock samples are represented by three axial directions (k_{max}, k_{int} and k_{min}), which is explained in detail in the previous sections.
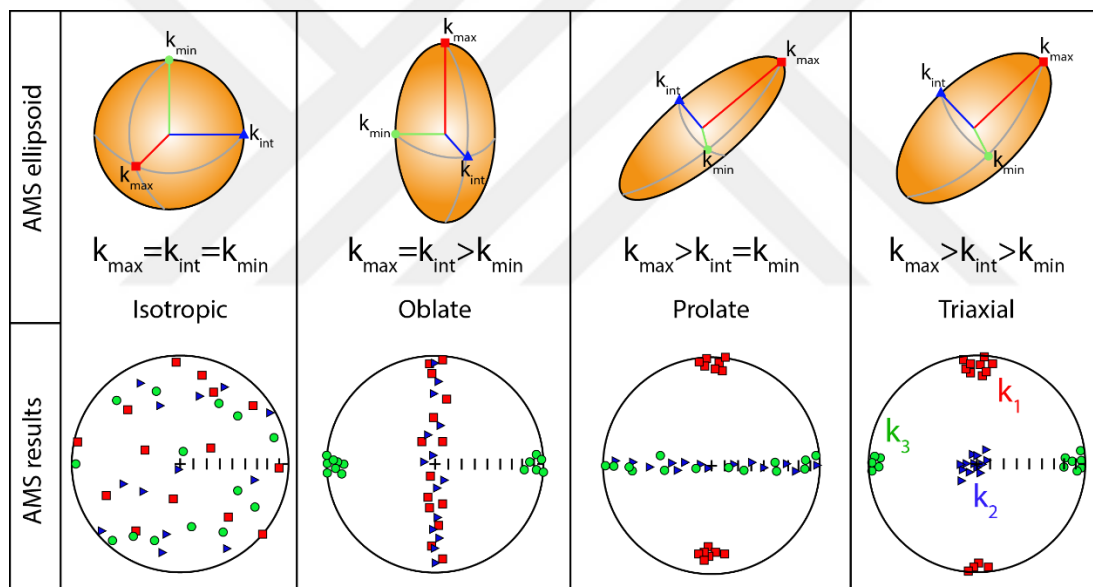
Figure 2. 11. Ploting of the anisotropy directional data on a stereographic projection. The projection shown here the lower hemisphere-equal-area type. The directions of maximum principal axes, k_{max} are plotted as squares, of intermediate axes, k_{int} as trianges, and of minimum principle axes, k_{min}, as circle (from Borradaile (1988)).

The directions of the principle axes of AMS are commonly plotted on lower hemisphere, equal-area stereographic projections in order to keep the uniformity of structural plots of field data such as bedding, field lineations, and field foliations. The axes of K_{max}, K_{int} and K_{min} are plotted as squares, triangles and circle, respectively (Figure

2.11). Generally, plotting of the maximum and minimum axes alone is adequate for visualization of the distribution since the position of these axes defines the intermediate axes since the three axes are orthogonal (Figure 2.11).
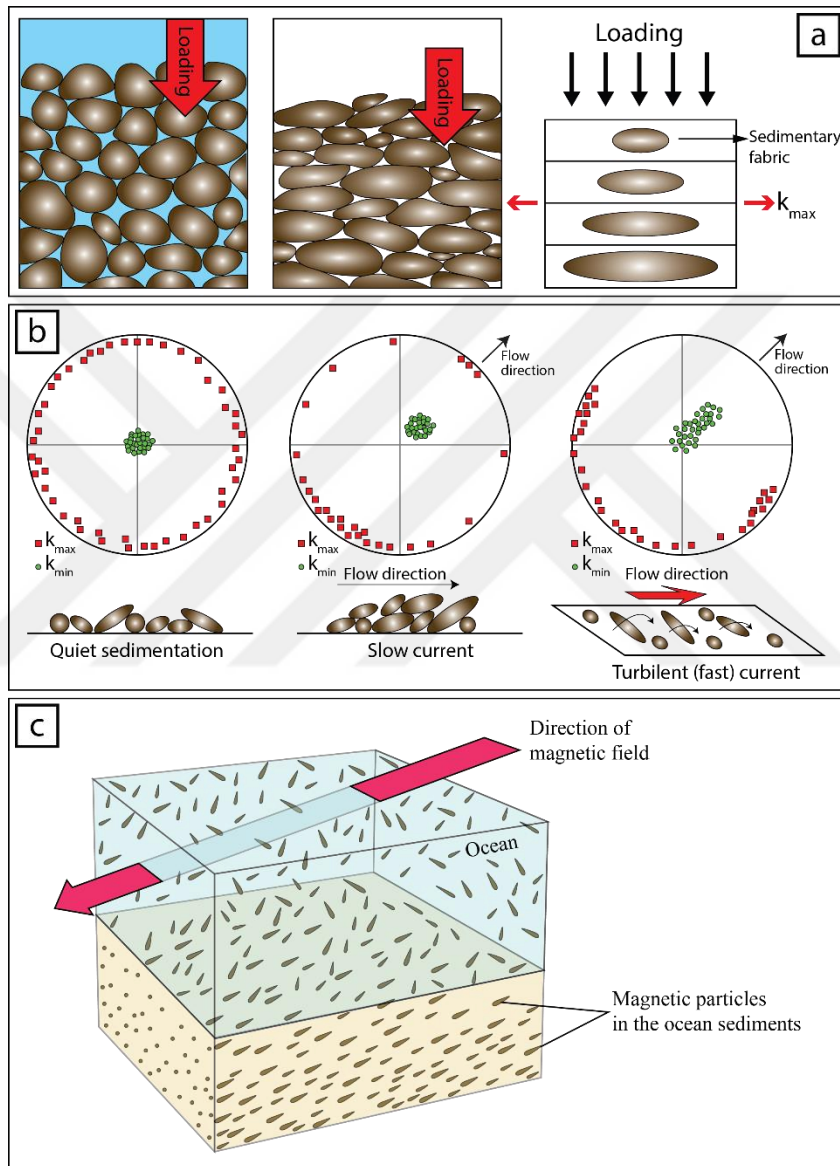
Figure 2. 12. Processes effecting on the petro-fabric and magneto-fabric design in the sedimentary rocks, which are Earth's gravitational effect (a), water current effect. (b) and, geomagnetic field effect (c) (after Tarling and Hrouda (1993), modified).

2.2.2.5. AMS settings on sedimentary rocks

This study is an attempt to apply magnetic properties (AMS) to tectono-sedimentology. The AMS measurements in sedimentary rocks provide information on the deposition and compaction processes. The petro-fabric and magneto-fabric organization in the sedimentary rocks have been affected by three processes: these are 1) Earth's gravity, 2) water current, and 3) geomagnetic field.

When the deposition occurs in still water (in the absence of any current) gravitational setting is the only significant force and causes all platy grains to lie in the plane of the depositional surface or bedding plane (Tarling and Hrouda, 1993) (Figure 2.12a). This gives rise to a simple, strongly oblate fabric (magnetic foliation) resulting from a combination of depositional processes and diagenetic compaction in the sedimentary rock (Figure 2.12a). In this case, k_{max} is parallel to the depositional surface (bedding plane) while the k_{min} axis is perpendicular to bedding plane.

If water currents are present during the deposition, transport mechanism forces grains to align parallel or perpendicular to the transportation direction dependent on velocity of the current and the slope of the depositional surface (Tarling and Hrouda, 1993). When the current velocity is weak or moderate, it aligns the long axes of prolate grains and producing a lineation parallel to the direction of flow. Whereas, strong current (>1cm/s) increase the angle of imbrication so that plane of magnetic foliation is tilted by 5-20°away from the bedding plane. In this case, prolate grains are now more stable and their long axes align themselves perpendicular to the flow direction (Granar, 1958) (Figure 2.12b).

During the sedimentation phase, Earth magnetic field force suspended ferromagnetic grains in the water to align its long axes parallel to the local magnetic field vector (Figure 2.12c). After depositional phase, sedimentary rocks can be exposed to a continuous deformation so that the grains which contain magnetic minerals will transform into the tectonic fabrics and those tectonic fabrics are very important indicators to determine tectonic deformation process (Hrouda, 1982, 1993; Borradaile, 1988, 1991; Lowrie, 1989; Borradaile and Henry, 1997; Borradaile and Jackson, 2004).

AMS studies in different tectonic settings described three major categories of AMS fabric (Sagnotti et al. 1998; Pares et al. 1999; Saint-Bezar et al. 2002; Pares 2004). Depending on the distribution of k_{max}, k_{int} and k_{min}, three fundamental fabric are identified as: (1) the planar uniaxial fabric (Figure 2.13a) characterized by a k_{min} axis clustered and dispersion of k_{max} and k_{int} in a plane which is normal to the k_{min}; (2) the linear uniaxial fabric (Figure 2.13b) characterized by k_{max} axis clustered and a dispersion of k_{int} and k_{min} axes; (3) the triaxial fabric (Figure 2.13c) characterized by three distinct clusters of anisotropy axes. Later, Robion et al. (2007) have suggested six type of fabric patterns (Figure 2.13d) in progressily deformed rocks and tectonic fabrics by the angle between the mean of the k_{min} axes and pole to the bedding plane. These six different phases (Figure 2.13d) are given in detail below;

Type 1: In this stage, the sedimentary fabric is at the initial stage and they are only affected by depositional loading (compaction). This phase is characterized by tectonically undeformed state. The sedimentary fabrics develop parallel to the bedding plane. In this case, k_{min} axes are parallel to the gravity force and perpendicular to the sedimentation plane. k_{int} and k_{max} axes are scattered in the bedding plane. The angle between K_{min} and the bedding pole varies from 0° to 15°.

Type 2: This pattern is essentially sedimentary where the bedding and magnetic foliation are parallel with weak development of magnetic lineation (intermediate phase). In the sedimentary fabric, k_{min} axes stay to remain in an initial position, which is perpendicular to the bedding plane, but k_{max} will be perpendicular to the maximum compressional direction in the bedding plane. The angle between K_{min} and the bedding pole varies from 0° to 15°.

Type 3: This phase corresponds to an intermediate fabric in which the compressional force on the sedimentary fabric is more effective. The AMS ellipsoid has more prolate shape and k_{max} stays perpendicular to the compressional axis. The sedimentary fabric is classified according to angle between k_{min} and bedding. k_{min} has to be parallel or oblique to bedding with an angle varying from 0° to 15°. This phase is called pencil structure.
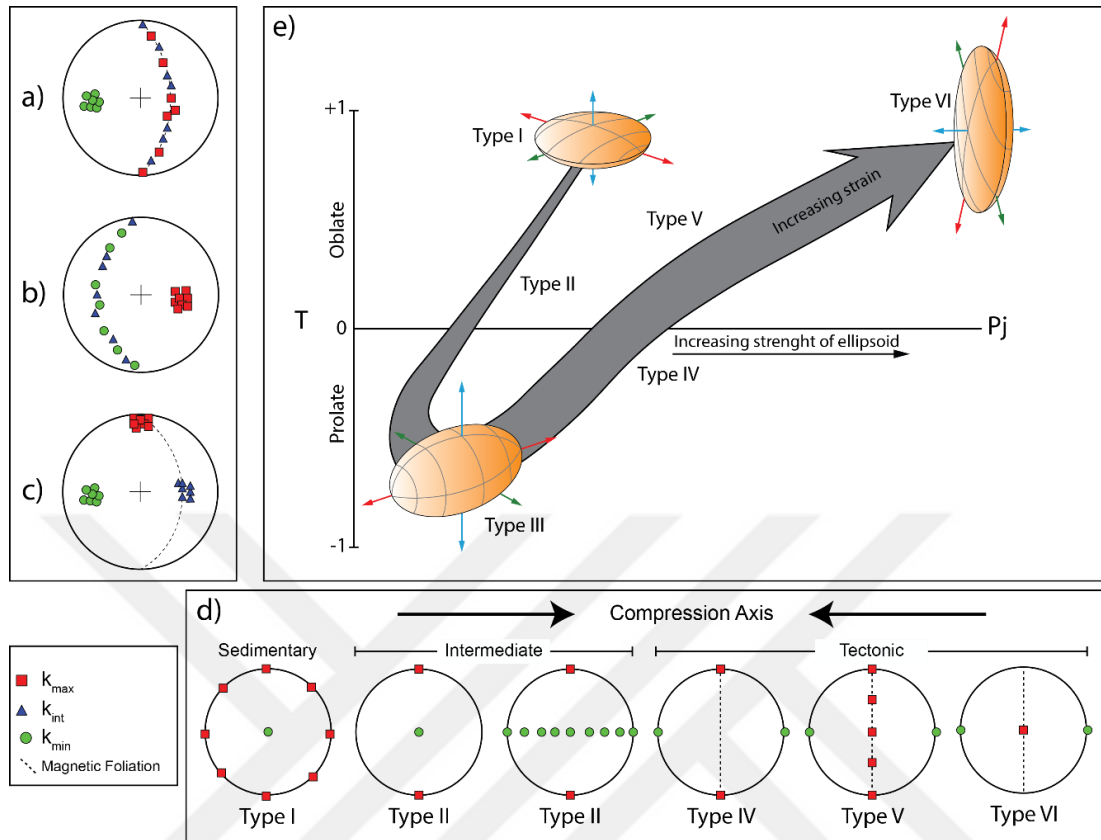
Figure 2. 13. AMS susceptibility ellipsoids under the progressive deformation on a sedimentary rock units. a. oblate fabric (or planar uniaxial fabric), b. prolate fabric (or linear uniaxial fabric), c. triaxial fabric with both magnetic foliation and lineation, d. major phases of magnetic fabric in progressily deformed rocks. Bedding plane is horizontal and maximum shortening axis is oriented right /left. Type I is assumed to be the initial sedimentary fabric with isotropy in the bedding plane, e. Plot of the shape parameter T vs degree of anisotropy parameter P for progressively deformed rocks (from Borradaileand and Henry (1997), Parés (2004) and Robion et al. (2007)).

Type 4: In the increasing deformation condition, when k_{min} lies within the beding plane, and an angle between k_{min} and bedding pole is grater than 75°, the fabric is identified as type IV or cleavage fabric (Pares, 2004). k_{max} is perpendicular to shortening direction while k_{min} starts to be parallel to compressional direction. In this phase, cleavage is in embryonic form.

Type 5: This phase represents the last stage of the prolate form of AMS ellipsoid. Magnetic anisotropy ellipse starts changing into oblate form with creating foliation

surface. In this deformation phase, k_{min} axis is perpendicular to this new forming foliation surfaces and kmax axis lies along the expansion direction in the cleavage plane.

Type 6: This is the final stage of the deformation where AMS ellipsoid will be more triaxial in shape. Increasing deformation results in stronger lineation and foliation setting. Axes of k_{min} approximately are parallel to the compression direction. The sedimentary fabric pattern progressively changes into tectonic fabric.

3. LITHOSTRATIGRAPHY

In this chapter, stratigraphic units of the Aksu Basin are described and evaluated in detail. Their lithology, age, contact relationships and an interpretation of their depositional environments are provided.

The Aksu Basin is N-S trending basin and has approximately 2000 km^2 area (Figure 3.1). It is one of the sub-basins of Antalya basin within the Isparta angle in the south of Turkey (Blumenthal, 1963). It has more than 1 km thick clastic-dominated Miocene infill resting nonconformably on the Beydağları carbonate platform in the west, as well as on the Lycian Nappes (Hayward, 1984) in the north. Aksu Basin is separated from the Köprüçay sub-basin by a basement high associated with Aksu thrust that over thrusting the Antalya Nappes on to the Miocene sediments of the basin in the east (Akay et al. 1985).

The Aksu Basin was first defined as an Aksu valley by Poisson (1977). After this pioneering study, the researchers were concentrated mainly on Neogene stratigraphy (Akay et al., 1985; Glover and Robertson, 1998; Poisson et al., 2003, 2011; Çiner et al., 2008). The age of formations is defined based on macro- and microfossils (Akay et al., 1985; Glover and Robertson, 1998). The Late Cenezoic infill of the basin is represented by non-marine to marine, clastic dominated Miocene sediments with subordinate coralgal reefs and reefal shelf carbonates, and Pliocene to Recent marine and terrestrial clastics, and travertines (Çiner et al., 2008)

The Aksu Basin consists of Oymapınar Limestone, Aksu Formation (including Karadağ and Kapıkaya members), Karpuzçay Formation, Gebiz Limestone, Kurşunlu Formation, Yenimahalle Formation, Eskikoy Formation, Belkis Conglomerate, Antalya Travertine and Çamlık Travertine of Miocene, Pliocene and Quaternary ages, respectively (Blumenthal, 1951; Eroskay, 1968; Poisson, 1977; Gutnic et al., 1979; Akay et al., 1985; Akay and Uysal, 1985; Şenel, 1997).

Below, their lithology, age and contact relationships are described and a first-order interpretation of their depositional environments is provided (Figure 3.1).
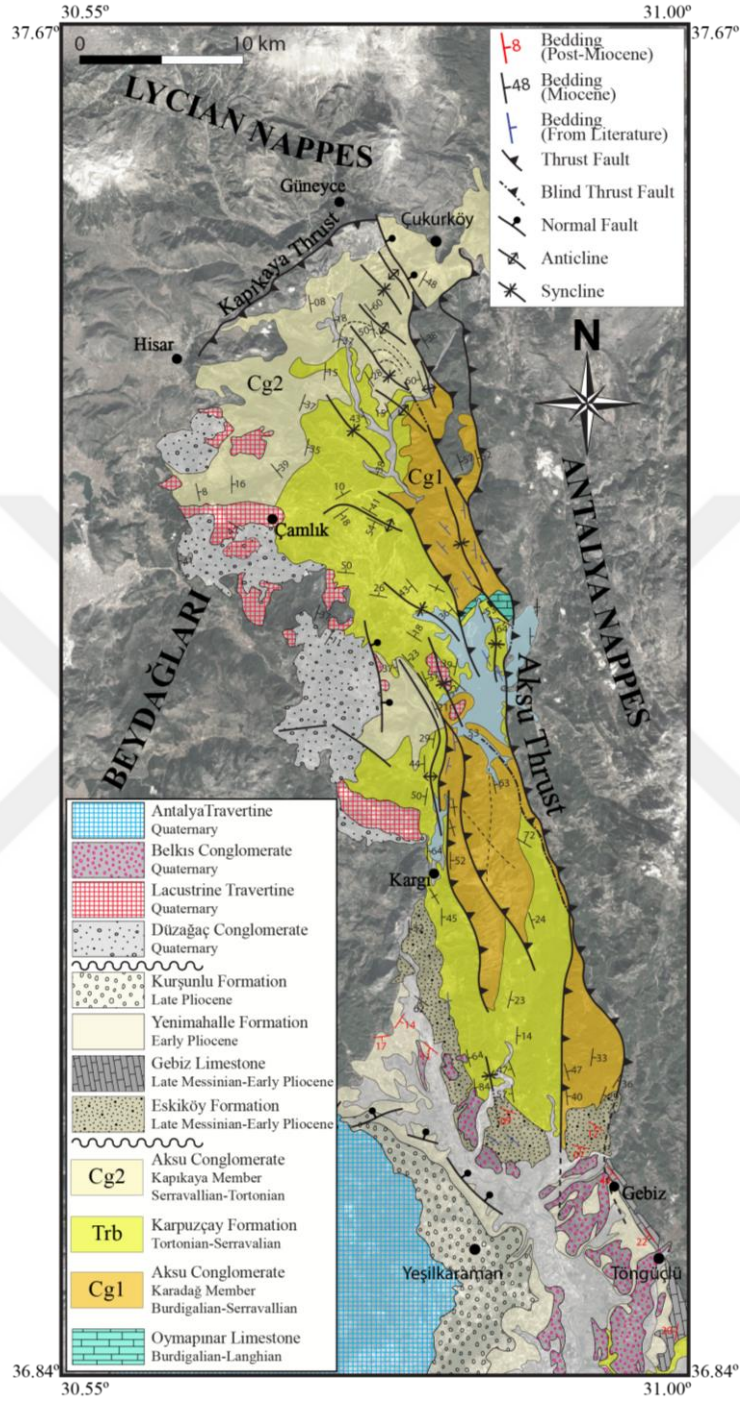
Figure 3. 1. Revised geological map of the study area (modified from 1/100000 scale geological map produced by General Directorate of Mineral Research and Exploration-MTA).

51
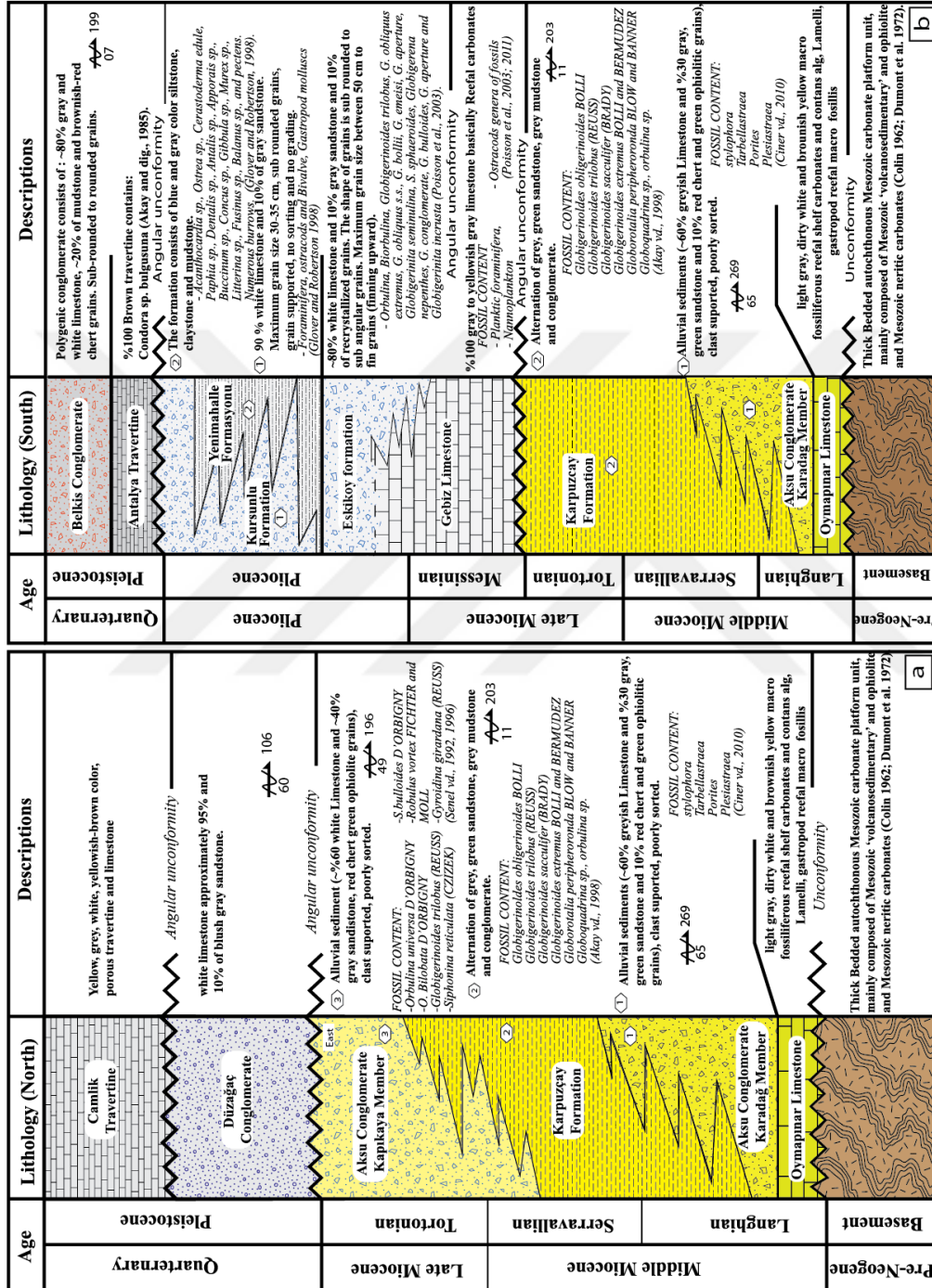
Figure 3. 2. Generalized stratigraphic column for the northern (a) and southern (b) part of the Aksu Basin.

3.1. Oymapınar Limestone

Oymapınar Limestone first described by Monod (1977). This formation is exposed at the east side of the basin. The contact relationship between Oymapınar Limestone and Aksu Conglomerate (Karadağ member) is well exposed near Melikler village where the Oymapınar formation display transitional relationship with the Aksu Conglomerate (Karadağ member) (Figure 3.3a).
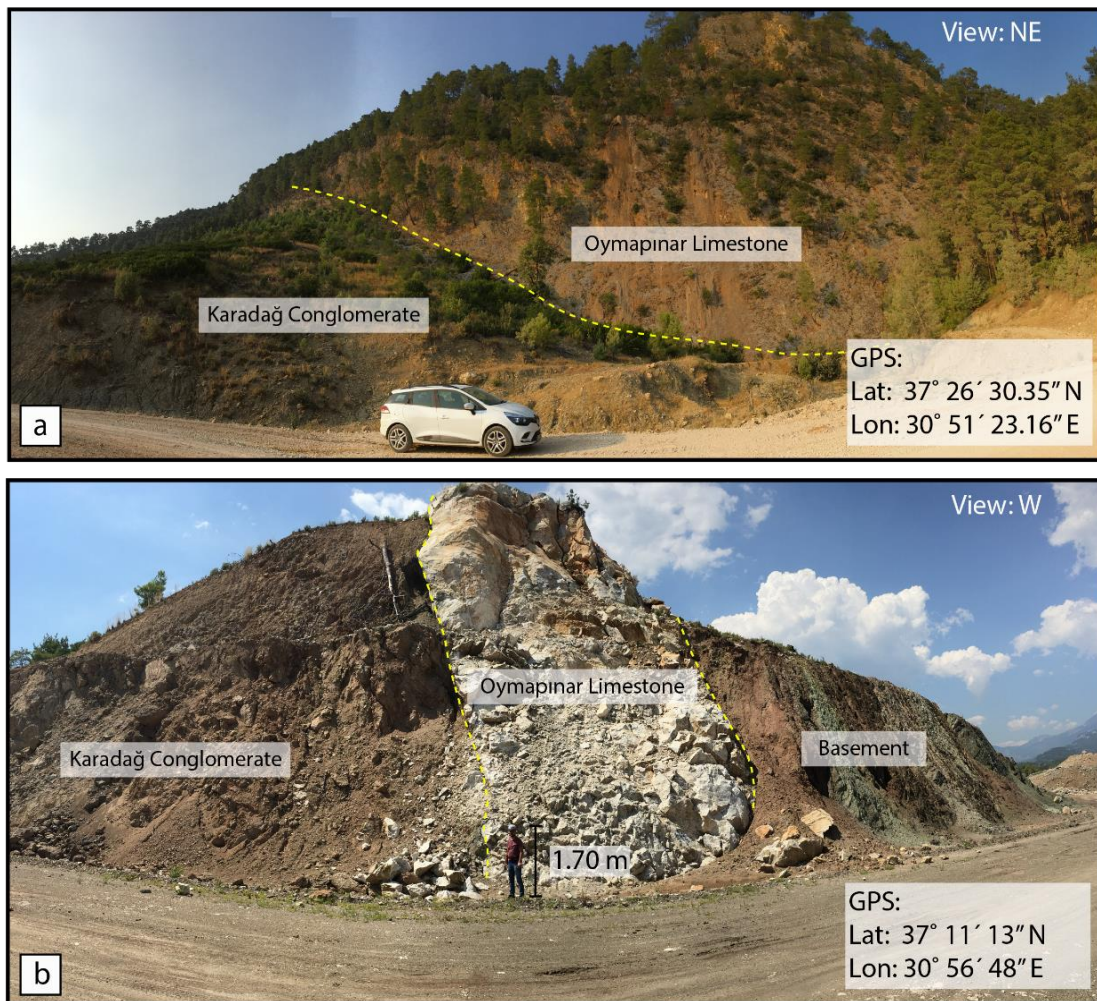
Figure 3. 3. a. Oymapınar Limestone is observed at the north of the Karacaören dam lake where the Oymapınar formation display transitional relationship with the Aksu Conglomerate, b. another observation of the Oymapınar Limestone was made at the south of the basin which is near by Hacıosmanlar village where is Oymapınar Limestone unconformably overlies the Antalya Nappes.

The contact relationship between Oymapınar Limestone Antalya Nappes is well exposed 4 km south of Kozan whereas the Oymapınar Limestone unconformably overlies the Antalya Nappes near Hacıosmanlar village (Figure 3.3b).

Oymapınar Limestone is composed of medium bedded, light grey, dirty white and brownish yellow macro fossiliferous reefal shelf carbonates (Figure 3.1). The thickness of the formation is approximately 200 m with medium bedding thickness. The formation contains *Borelis cf. melo (FICHTEL & MOLL), Amphistegina sp., Operculina sp., Orbulina sp., Gypsina sp., Lithothamnium sp., Miogypsina sp., Orbulina universa D'ORBIGNY, Orbulina suturalis BRONNIMAN, Globoquadrina cf. altispira (Monod, 1977) (CUSHMANJARVIS)* (ŞenelŞenel and diğ, 1992; 1998). According to the fossils content, the authors assigned Late Burdigalian–Langhian age to the formation. The unit is deposited in a shallow carbonate shelf.

3.2. Aksu Formation

Aksu Formation covers a large area in the study area (Figure 3.1). The first study that incorporated the Aksu Formation was performed by Poisson (1977), which defined Aksu Formation as Aksu Conglomerate based on the lithological characteristics. The Neogene stratigraphy of the study area was firstly constructed by Akay and Uysal (1985) who classified all the conglomerate-dominated succession in both Upper and Lower Miocene as Aksu Formation. Çiner et al. (2008) provided the most recent study focused on Late Neogene stratigraphy and identified Aksuçay Conglomerate comprising two members: 1) Karadağ Conglomerate and 2) Kapıkaya Conglomerate (Figure 3.2). The formation nomenclature of Çiner et al. (2008) is adopted for this study.

3.2.1. Karadağ conglomerate member

Karadağ conglomerate is exposed only in the eastern margin of the Aksu Basin, and morphologically recognized by the conspicuous conglomeratic cliffs, over 500 m high, facing to the Kargı Dam Lake (Figure 3.4a and b).

In the previous study (Akay et al., 1985) Karadağ conglomerate (Figure 3.4c) is considered as Aksu Conglomerate without a determination of its stratigraphic position. For this reason, it is redefined and mapped as separate member namely Karadağ Conglomerate (Monod et al. 2006; Çiner et al. 2008;Üner et al. 2018). Upwards, the conglomerates alternate with coarse to fine sandstone and silty-mudstone and it grades vertically and laterally into Karpuzçay Formation.
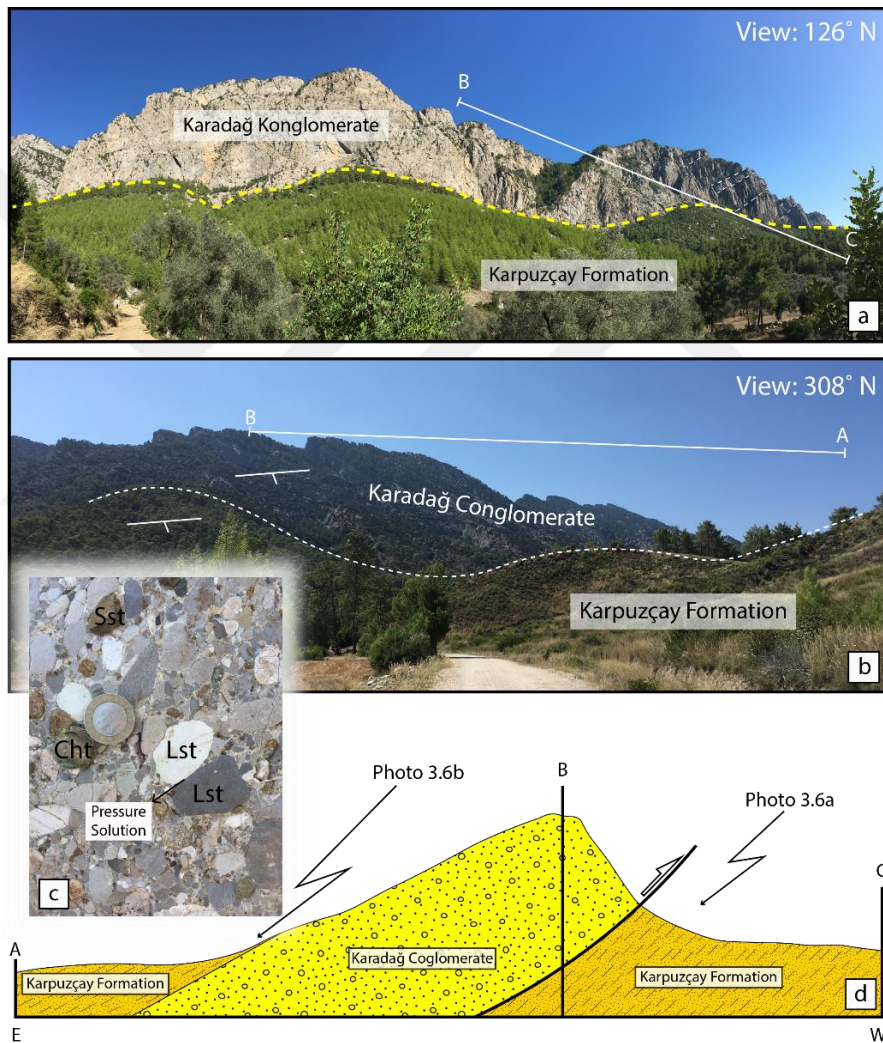
Figure 3. 4. Field views from the Karadağ conglomerate member, a. the thrust contact between the Karadağ conglomerate above and the Karpuzçay Formation. b. Conformable contact between the Karpuzçay Formation above and the Karadağ conglomerate below, c. Close-up view of the Karadağ conglomerate. Note pressure solution and the type of the clasts, d. Cross section ilustrating the contact relationship between Karadağ conglomerate and Karpuzçay Formation.

The contact relation between Karadağ Conglomerate and Karpuzçay Formation is conformable (Figure 3.4b and d). The lower boundary of the Karadağ conglomerate is marked by creamy-white limestone, but this limestone is exposed only in very limited areas (Figure 3.1 and 3.3a, b) along the eastern margin of the basin and it is attributed to probably over thrusting by Aksu Fault (Figure 3.3a and b).

The Karadağ conglomerate member is composed of fragments from ~%60 white to grey limestone and ~30% grey and green sandstone. The rest consists of red and green chert pebbles (Figure 3.4c). The conglomerate is generally polygenic, clast and matrix-supported (depends on the stratigraphic level) (Figure 3.4c), well-cemented and thick-bedded (Figure 3.4a). Clasts are angular to sub-rounded, poorly sorted and range from gravel to boulder in size (occasionally up to 70 cm along the long axis). Sedimentary structures such as pebble imbrication is rare at this level of the formation. Bottom bedding surfaces are remarkably irregular indicating erosional processes such as scour-and-fill structures. Pressure solution pits at pebble contacts are occasional and suggest significant compaction (Figure 3.4c).

Çiner et al. (2008), reported *Stylophora, Tarbellastraea, Porites and Plesiastraea* within the Karadağ Conglomerate coral reefs exposed about 5 km south of the Aşağı Gökdere area. These fossil assemblages are not diagnostic for precise dating. While the base of the Karadağ unit is conformable with the Burdigalian-Langhian Oymapınar Limestone (Figure 3.3), upper part of the Serravallian-Tortonian Karadağ Conglomerate grades vertically and laterally into Karpuzçay Formation (Çiner et al., 2008). Therefore, Langhian-Serravalian age is adopted, in this study, for the Karadağ Conglomerate based on its stratigraphic relationships with other units.

In order to understand the provenance of the clasts in the Karadağ Conglomerate, paleocurrent directions are measured from the imbricated pebbles (Figure 3.5b and c), and then analysed using rose diagrams (Figure 3.5a). It is found that dominant paleocurrent directions are range between 207°-245° N. Çiner et al. (2008) reported that the metamorphic pebbles are abundant and consists of white marble, quartzite, green schist and amphibolite. Moreover, HP-LT blueschist fragments, with angular shapes, suggested short distance transportation. And they (Çiner et al., 2008) claimed that the probable origin of the metamorphic detritus is Alanya Massif, as previously suggested by

Akay et al. (1985). The present outcrop of the Alanya Massif is located in the southeastern part of the basin. During the formation of the Karadağ Conglomerate (Miocene), the Alanya Massif was located very close to the eastern margin of the Aksu Basin. On the other hand, Üner et al. (2018) claimed that the NE-SE oriented paleocurrents (opposite direction that we observed) in the Karadağ Conglomerate, are similar to paleocurrent directions published by Flecker (1995).
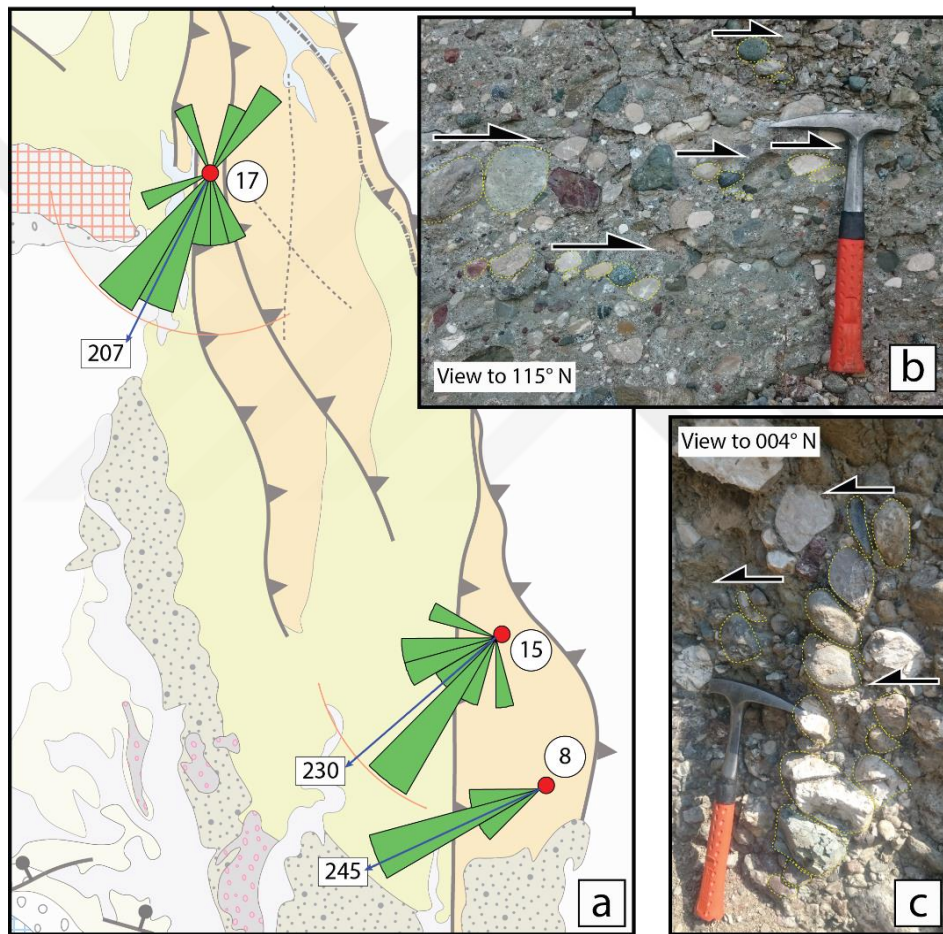
Figure 3. 5. a. Paleocurrent directions obtained from the Karadağ Conglomerate in the study area. b; c. close-up views frompebble imbrications from which paleocurrent data is acquired.

Unsorted, angular and boulder to block size, polymict, thick-bedded conglomerate in the lower level of the unit indicates close proximity to the source area. Sandy, matrix-supported conglomerate suggests sub-aqueous debris flows (Üner et al., 2018).

Intermittently, the clast-supported conglomeratic levels indicate energetic aqueous transport that deposited gravel beds, while sand is still carried in suspension (Colby, 1963). Erosional base of the conglomerate units also demonstrates a high-energy environment. Imbricated pebbles are occasionally observed at this level. The facies characteristics of the Karadağ Conglomerate indicate alluvial fan-fan delta complex.

3.2.2. Kapıkaya Conglomerate Member

Kapıkaya Conglomerate is observed only in the north of the Aksu Basin, and is characterized by reddish clastics including conglomerates and intercalating coarse sandstone. This unit is first defined by (Gutnic et al., 1979) and later modified by Flecker (1995), who determined the maximum observable thickness of these coarsed-grained deposits as >50 m. The member unconformably overlies the pre-Neogene units that include creamy-white carbonates (Figure 3.6) and it grades vertically and laterally into the Karpuzçay Formation.

The sequence starts at the bottom with angular, unsorted, well-cemented, and thick-bedded (1.5-2 m) reddish conglomerate (Figure 3.7a). Clasts within this conglomerate range from gravel (Figure 3.7b) to block-size (Figure 3.7c) and are derived from Mesozoic white-creamy limestones (60%) and light to dark grey sandstones, red cherts and green ophiolites (40%). The fabric is typically clast-supported and dramatically poorly sorted suggesting rapid and chaotic sedimentation at lower part. In some levels of the sequence, the matrix-supported conglomeratic units are also present. Sedimentary structures, such as pebble imbrications, cut and fill structures (channel deposits) are occasionally observed.

Figure 3. 6. Field view of the unconformity between Kapıkaya conglomerate member and basement limestone. View towards the 323° N.

These conglomerate levels are intercalated with medium to thick bedded sandstone (50- 100 cm) (Figure 3.7a). The overall sequence shows basin- ward grading (from N to S) into sandstone and mudstone units of the Karpuzçay Formation (Figure 3.8). On the other hand, to the south of the basin it is not possible to make correlation of the Kapıkaya Conglomerate since there are several isolated conglomeratic forms and tectonic imbrications.

Şenel et al. (1992 and 1996) reported marine organisms (forams), including *Orbulina universa D'ORBIGNY, O. Bilobata D'ORBIGNY, Globigerinoides trilobus (REUSS), Siphonina reticulata (CZIZEK), S.bulloides D'ORBIGNY, Robulus vortex FICHTER and MOLL and Gyroidina girardana (REUSS)* from the Kapıkaya Conglomerate member suggesting Serravallian to Tortonian age. In addition to this, Çiner et al. (2008) found intercalated patch reefs at the top of the conglomerates and reported only a limited variety of coral genera including *Porites, Tarbellastraea, Siderastrea*. This

restricted faunal assemblage that suggested Late Miocene (?Tortonien) age and this age may be attributed to upper age limit for the age of Kapıkaya Conglomerates.
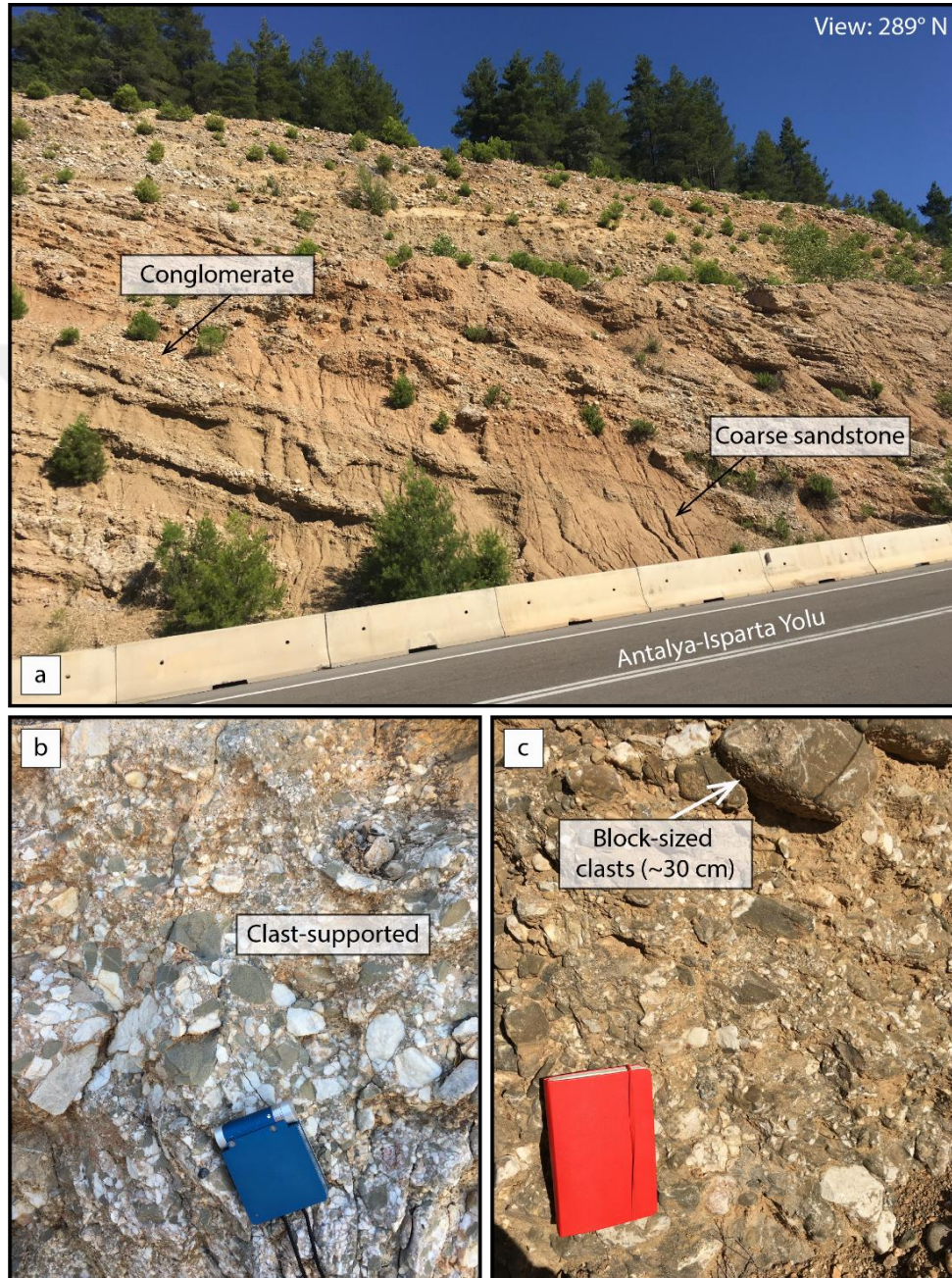
Figure 3. 7. a. Field view of the Kapıkaya Conglomerate Member along the Antalya-Isparta highway, note that channelized conglomeratic units are intercalating coarse sandstone levels. Close-up views from (b) clast-supported, c. block-sized, angular, poorly sorted (chaotic) and conglomerates.
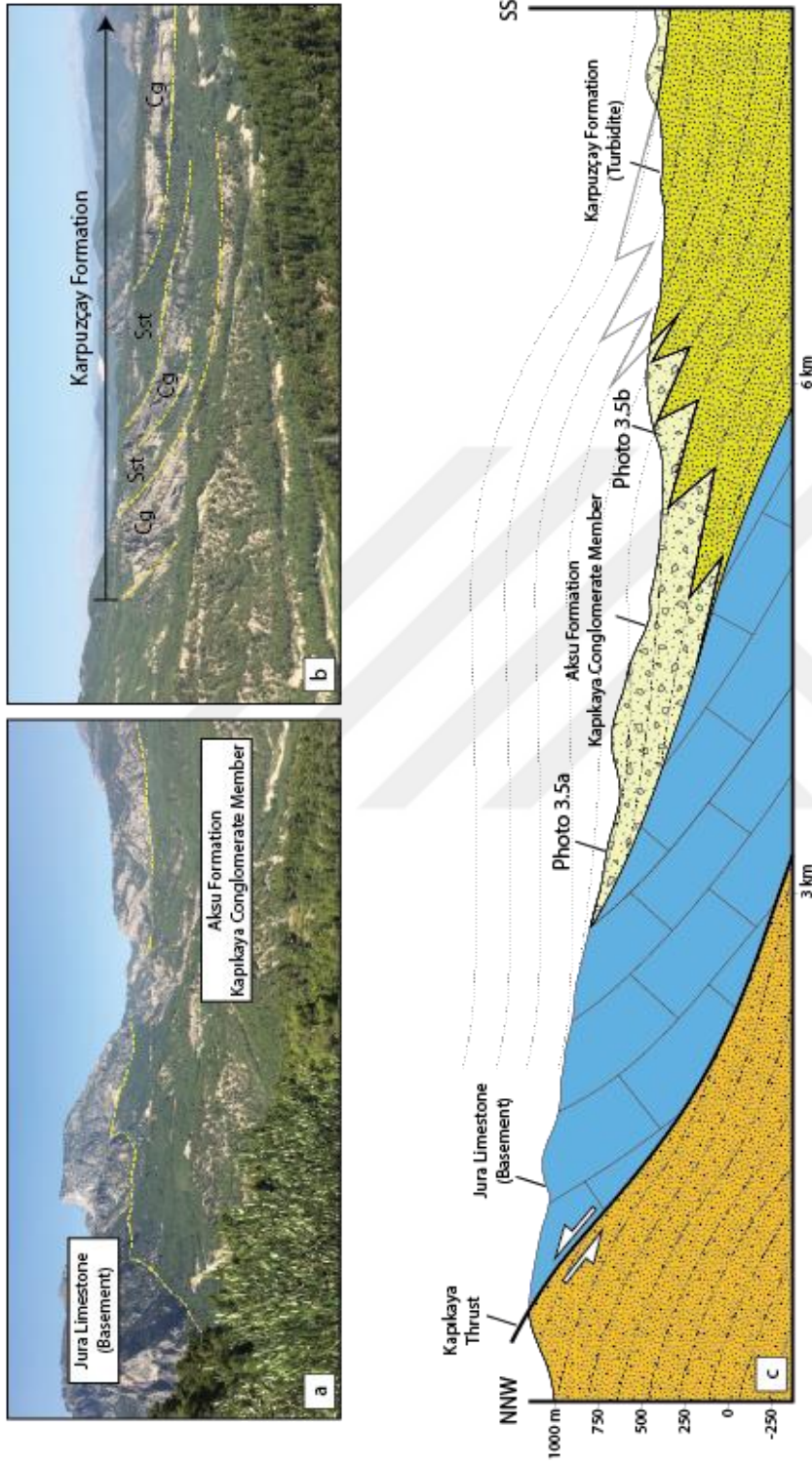
Figure 3. 8. Field views from the Kapıkaya Conglomerate Member of the Aksu Formation. Note that the formation is characterized by consolidated angular conglomerates (a) in the north of the basin and conglomerate - sandstone/mudstone alternation (b) in the south. Cross-section interprets the relationships between Aksu and Karpuzçay formations it also shows grain size variation from north to south of the Aksu Basin (c).

Unsorted, angular, clast- and matrix-supported and block-to-pebble sized conglomerates indicate that the Kapıkaya Conglomerate member has molass character and was probably deposited in an alluvial fan environment. Additionally, presence of patch reefs suggests that depositional environment is a shallow shelf. Therefore, the Kapıkaya Conglomerate is interpreted as coastal alluvial fan that evolved into a fan delta (Çiner et al., 2008; Üner et al., 2015 and 2018).

3.3. Karpuzçay Formation

Karpuzçay Formation is the most extensive unit in the basin (Figure 3.1). it is characteristically composed of turbiditic sandstone-siltstone-mudstone alternations at the lower level of the sequence. Commonly it incluesclast-or matrix-supported conglomeratic horizons at the relatively upper part of the formation (Figure 3.9b) and the conglomerate horizons are marked by erosive lower contacts.

Karpuzçay Formation is defined by Akay et al., (1985) in the Aksu Basin and interpreted asequivalent of Karpuzçay Formation in the Köprüçay and Manavgat basins, therefore the same nomenclature is adopted in the literature (Akay et al., 1985; Flecker, 1995; Karabıyıkoğlu et al., 2000; İslamoğlu, 2002; Deynoux et al., 2005; Çiner et al., 2008) and also in this study.

In general, the sequence consists of thin to laminated-parallel bedded mudstone and decimeter thick intercalations of normally graded sandstone with sharp-flat bases. This part refers to stratigraphically lower level of the Karpuzçay Formation (Figure 3.9a) and it is well-exposed near Yenice and Çamlık village along the Antalya-Isparta main road. Frequency of the sandy levels increases in the upper part of the formation and the finally a few to several meters thick conglomeratic levels (50-70 cm) are involved in the system (Figure 3.9b). Conglomeratic levels are clast-supported with normal grading. Clasts are mainly (90-95%) made up of boulder to pebble size (up to 35 cm), sub-rounded to rounded, grey to milky-white limestones (90-95 %). Sedimentary structures such as pebble imbrication, channel deposits and ripple marks, are occasionally observed (Figure 3.9c).
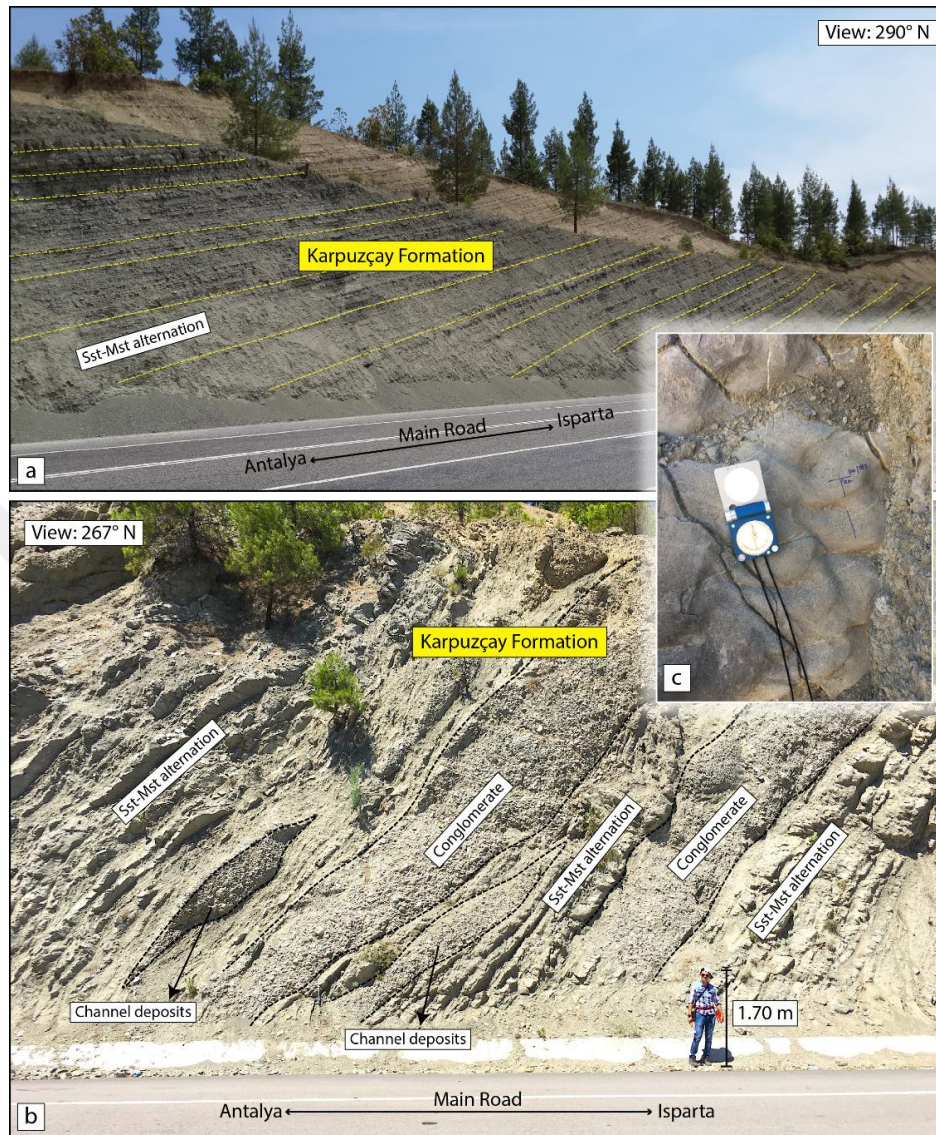
Figure 3. 9. Field views from (a) Turbiditic sandstone-siltstone-mudstone alternations at the lower level of the Karpuzçay Formation, (b) conglomeratic horizons in the upper part of the formation; and (c) ripple marks at the bottom of the sandstone bedding.
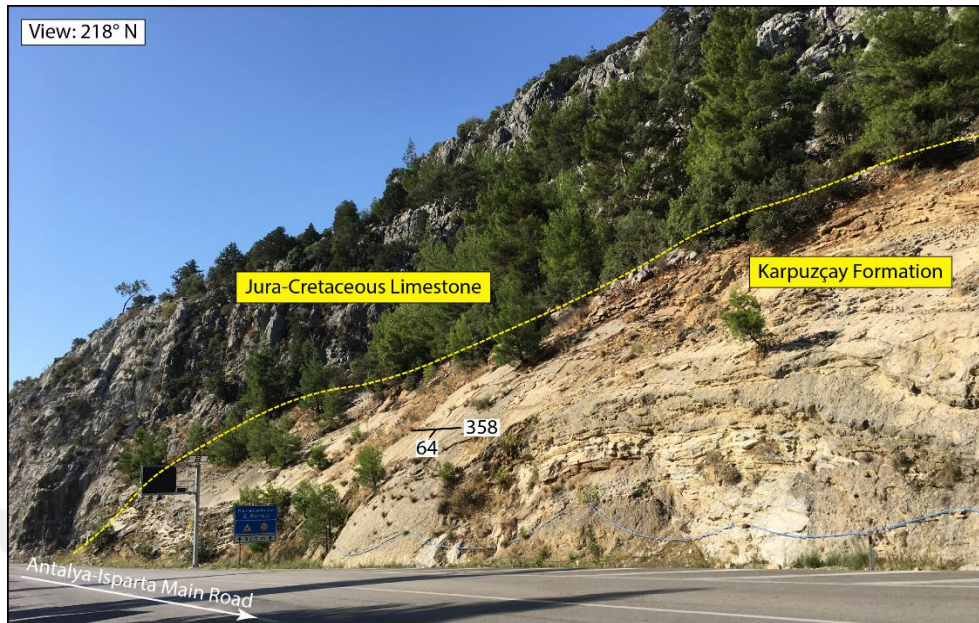
Figure 3. 10. Field view of the contact relationships between Karpuzçay Formation and Jurassic-Cretaceous limestone (basement). Note that the dip of the bedding towards to the east and the Karpuzçay Formation onlaps the basement rock.

The contact relationship between the Karpuzçay Formation and the basement is well-exposed near Karacaören Dam along the Antalya-Isparta main road. In this location, the Karpuzçay Formation dips to the east and onlaps the basement rocks which delimits the western boundary of the Aksu Basin (Figure 3.10). The lithology and facies characteristics of the Karpuzçay Formation gradually changs from west (which refers to roughly center of the basin) to east (which is delimited by the tectonically active boundary). In the east, the contact relation between the Karpuzçay and the Karadağ Conglomerate is clearly observed at the backside of the thrust sheet and it is a conformable contact (Figure 3.4b).
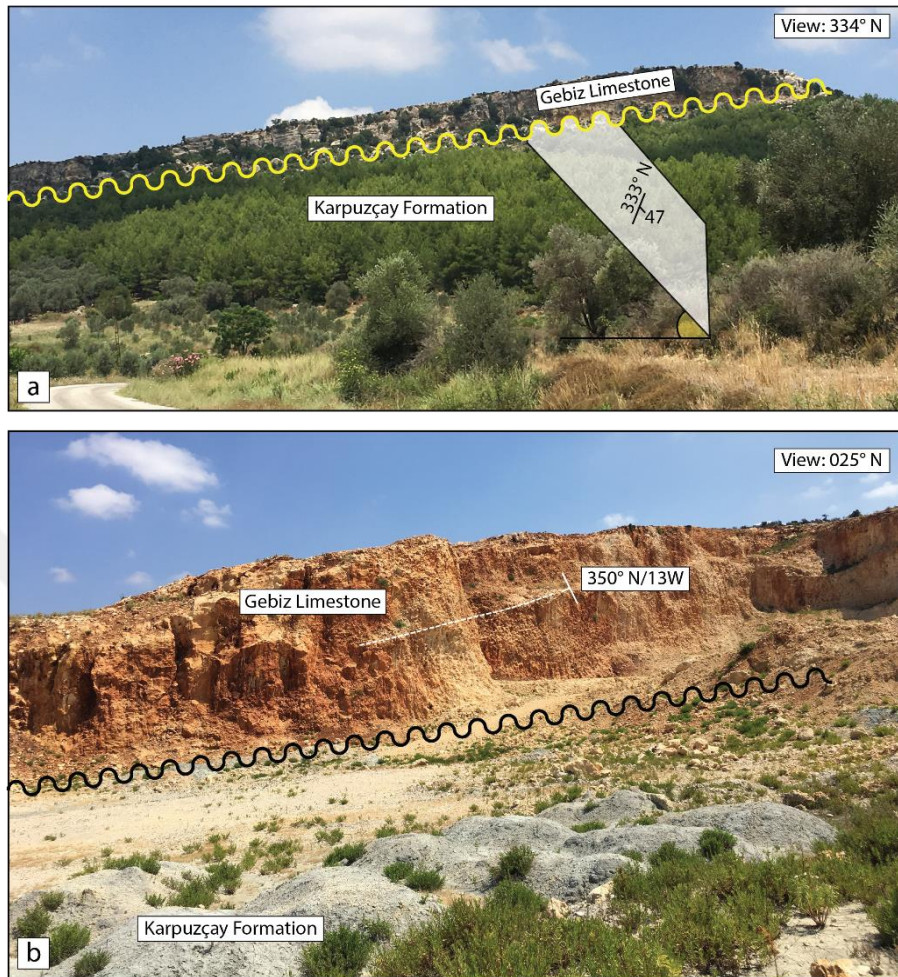
Figure 3. 11. a. Field view of the contact relationship between the Karpuzçay Formation and the Gebiz Limestone, b. Close-up viewfrom the Gebiz Limestone.

The Karpuzçay Formation grades horizontally and vertically into Kapıkaya Conglomerates in the north (Figure 3.8). The Gebiz Limestone (in the southeast) (Figure 3.11) and Eskiköy Formation (in the central east) (Figure 3.12) unconformably delimit the upper boundary of the Karpuzçay Formation. During this study, measured stratigraphic section of the Karpuzkaya Formation is produced in order to understand characteristics of the sequence. The starting point of the section, which is the core of the anticline, is located east of the Çamlık village and it is measured at the northern limb of the anticline along the Antalya-Isparta main road (Figure 3.1). The starting point of the measured section represents relatively center of the basin and mainly consists of mudstone-sandstone alternation (Figure 3.13). In upper part of the sequence, the

conglomeratic levels, which probably belong to the Aksu Conglomerate, start to involve the system. It is clearly observed that the Karpuzçay Formation is composed of a coarsening upward sequence.
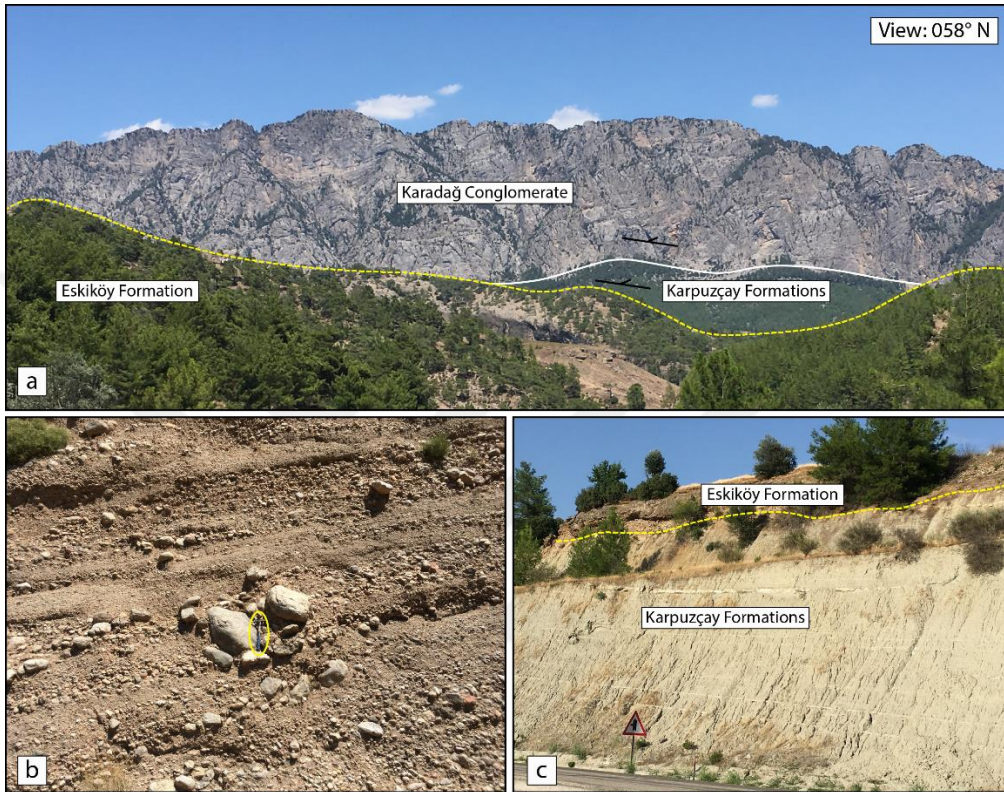
Figure 3. 12. a. Field view illustrating the upper (Eskiköy Formation) and lower boundary (thrust delimited) of the Karpuzçay Formation, b. close-up view of the Eskiköy Formation, the formation is characterized by conglomerates with boulder size clasts. Note that the yellow circle marks the geological hammer, c. Field view of the contact relation between Eskiköy and Karpuzçay Formations where Eskiköy Formation unconformably Karpuzçay Formation.
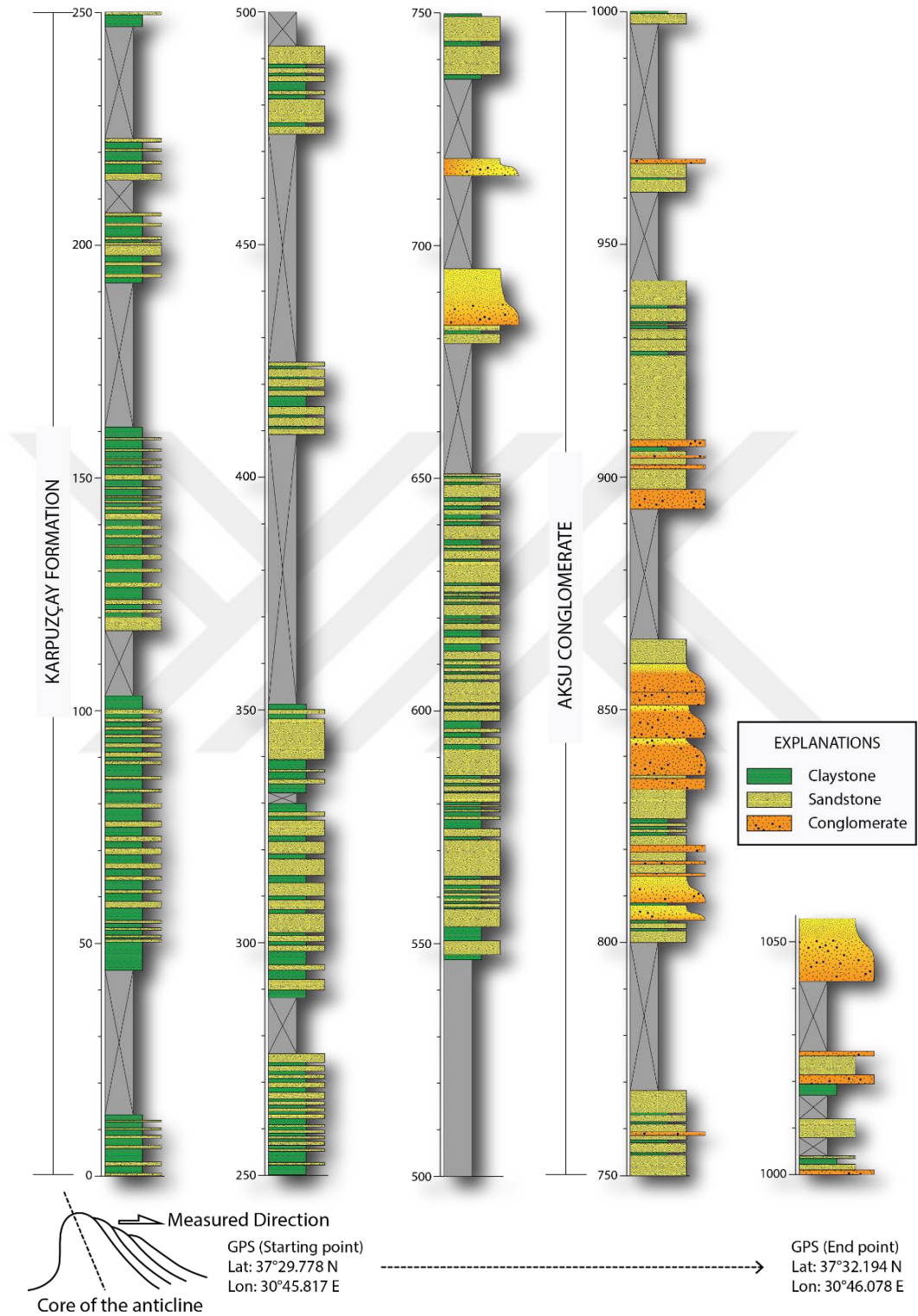
Figure 3. 13. Measured stratigrafic section of the Karpuzçay Formation.

Poisson (1977) studied planktic foraminifera population to date the Karpuzçay Formation in the Aksu Basin near the Kargı Dam and proposed a Serravalian to Lower Tortonian age for this unit. Akay et al. (1985) documented marine organisms (forams), including *Globigerinoides obliquus BOLLI, Globigerinoides trilobus (REUSS), Globigerinoides sacculifer (BRADY), Globigerinoides extremus BOLLI and BERMUDEZ Globorotalia peripheroronda BLOW and BANNER, Globquadrina sp., Orbulina sp.* in the Karpuzçay Formation. The upper contact of the Karpuzçay Formation appears to be gradational into Tortonian conglomerates with interbedded small patch reef (Flecker, 1995). Based on fossil contents and stratigraphic relations, Langhian-Tortonian age is adopted for Karpuzçay Formation in this study.

Alternation of the mudstone-sandstone with parallel based bed-shapes, normally graded laterally continuous beds with sharp lower and upper contacts are common sedimentary features in the lower levels of the Karpuzçay Formation, these are attributed to low energy turbiditic deposition in off-shore marine environment. In the upper part of the sequence, the Karpuzçay Formation is significantly richer in conglomerate than the lower levels. Grain size, erosional base of the bedding, channel formations and the asymmetric rippled surfaces are interpreted as high-energy environment. The conglomerate rich Karpuzçay Formation may indicate proximal (high energy) to distal (low energy) relationship within the basin basically from north to south. Therefore, the Karpuzçay Formation is interpreted as fan-delta environment in the north, and towards to the south it evolved into a deep marine environment.

In total, 71 paleocurrent directions are collected from the asymmetric ripples (Location 1 in Figure 3.14a and b) and also from the imbricated pebbles (Location 2, 3,4 and 5 in Figure 3.14a and c) at 5 sites from the Karpuzçay Formation. Four of them (1,2,3 and 5) are from the upper part of the Karpuzçay Formation (from transition to Kapıkaya Conglomerate) in the northern part, while one from relatively lower part of the formation (from transition to Karadağ Conglomerate) in the eastern part of the Aksu Basin. Rose diagrams are used to analyze the collected data (Figure 3.14a). Current directions obtained from the first three sites are consistent in indicating 192-206° N paleocurrent direction (approximately towards north), but mean direction of the site five (206° N) does

not fit this data where mean paleocurrent direction is 256° N. It is consistent with the paleocurrent direction collected from the Karadağ Conglomerate (Figure 3.5a).
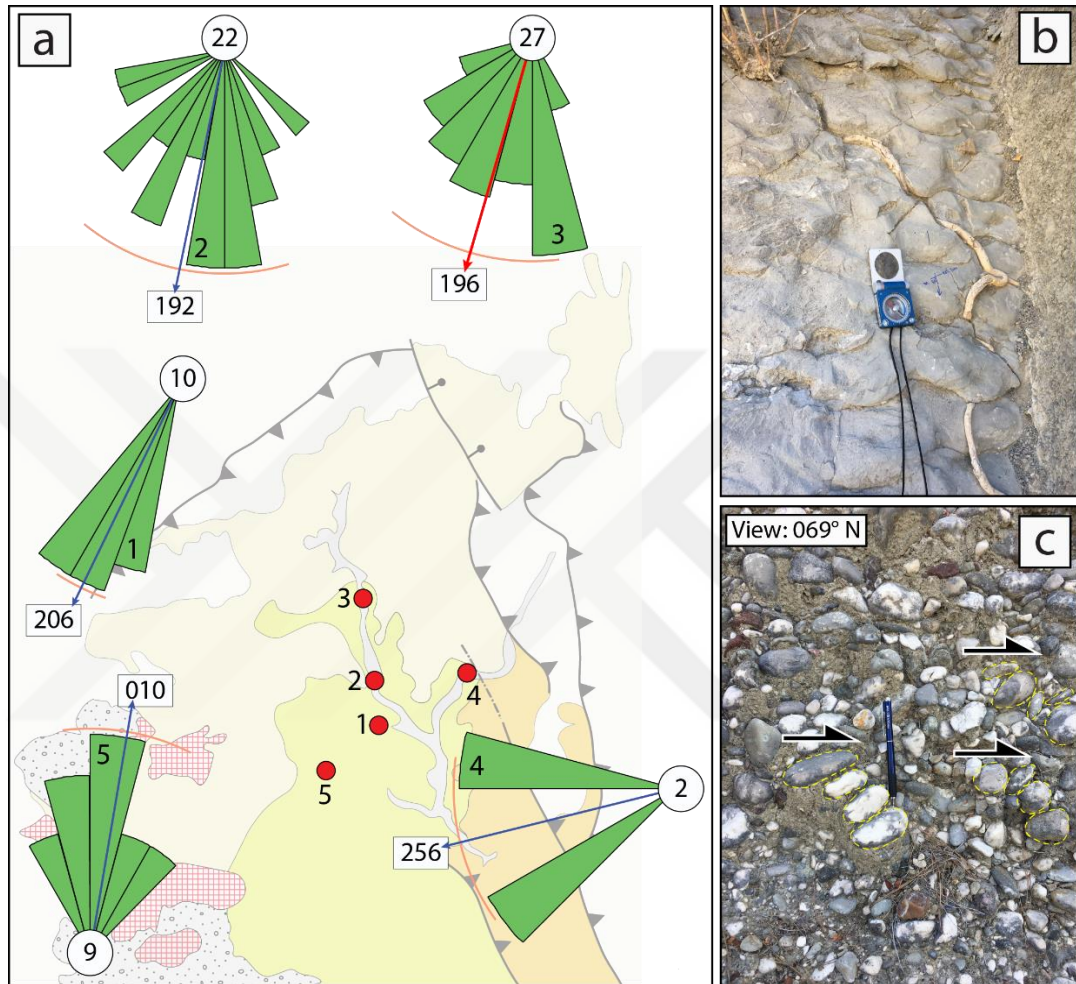
Figure 3. 14. a. Paleocurrent directions obtained from the Karpuzçay Formation in the study area, b. Collected data were collected from ripple marks (from site 1), c. pebble imbrications (from site 2).

It is documented that dominant paleocurrent directions are ranging between 207-245° N. Çiner et al. (2008) reported that the metamorphic pebbles are abundant and consists of white marble, quartzite, green schist and amphibolite. Moreover, the presence of angular HP-LT blueschist rock fragments suggest a rather distance transportation. And they (Çiner et al., 2008) claimed the probable origin of the metamorphic detritus is Alanya Massif, as previously suggested by Akay et al. (1985). The present outcrop of the Alanya

Massif is located southeastern part of the basin and during the formation of the Karadağ Conglomerate (Miocene), the Alanya Massif extended very close to the eastern margin of the Aksu Basin. On the other hand, Üner et al. (2018) claimed that NE-SE oriented paleocurrents (opposite direction that we observed) are determined in the Karadağ conglomerate and this is similar to paleocurrent directions published by Flecker (1995).

3.4. Gebiz Limestone

Gebiz Limestone is located the east of Gebiz town in the southeastern part of the Aksu Basin. It is described firstly by Poisson (1977) (Figure 3.1).

The contact relationship between the Gebiz Limestone and Yenimahalle Formation is well exposed near Gebiz town where Yenimahalle formation on laps the Gebiz Limestone (Figure 3.15a). The contact relationship between the Gebiz Limestone and the underlying basement (Antalya Nappes) is well exposed near Gebiz Towne, in this location, the Gebiz Limestone steeply dips to the south-east and unconformably overlies the basement (Figure 3.15b). Farther south at the south side of the Tonguclu village the contact relationship between Karpuzçay Formation and Gebiz Limestone is well exposed where limestones dip gentlyto the south-east and unconformably overlies the Karpuzçay Formation (Akay et al., 1985 and Poisson et al., 2003) (Figure 3.11b). The variation of the dip amounts and presence of slickensides (with striations) within the Gebiz Limestone unit is attributed possibly to the deformation associated with the Aksu Fault.

Gebiz limestone consists of gray to yellowish gray reefal carbonates (3.15c). Many researchers studied the fossil content (Tuzcu and Karabıyıkoglu 2001, Karabıyıkoglu et al., 2005; Poisson et al., 2003; 2011), and reported different species of Planktic foraminifera, Nannoplankton and Ostracods.
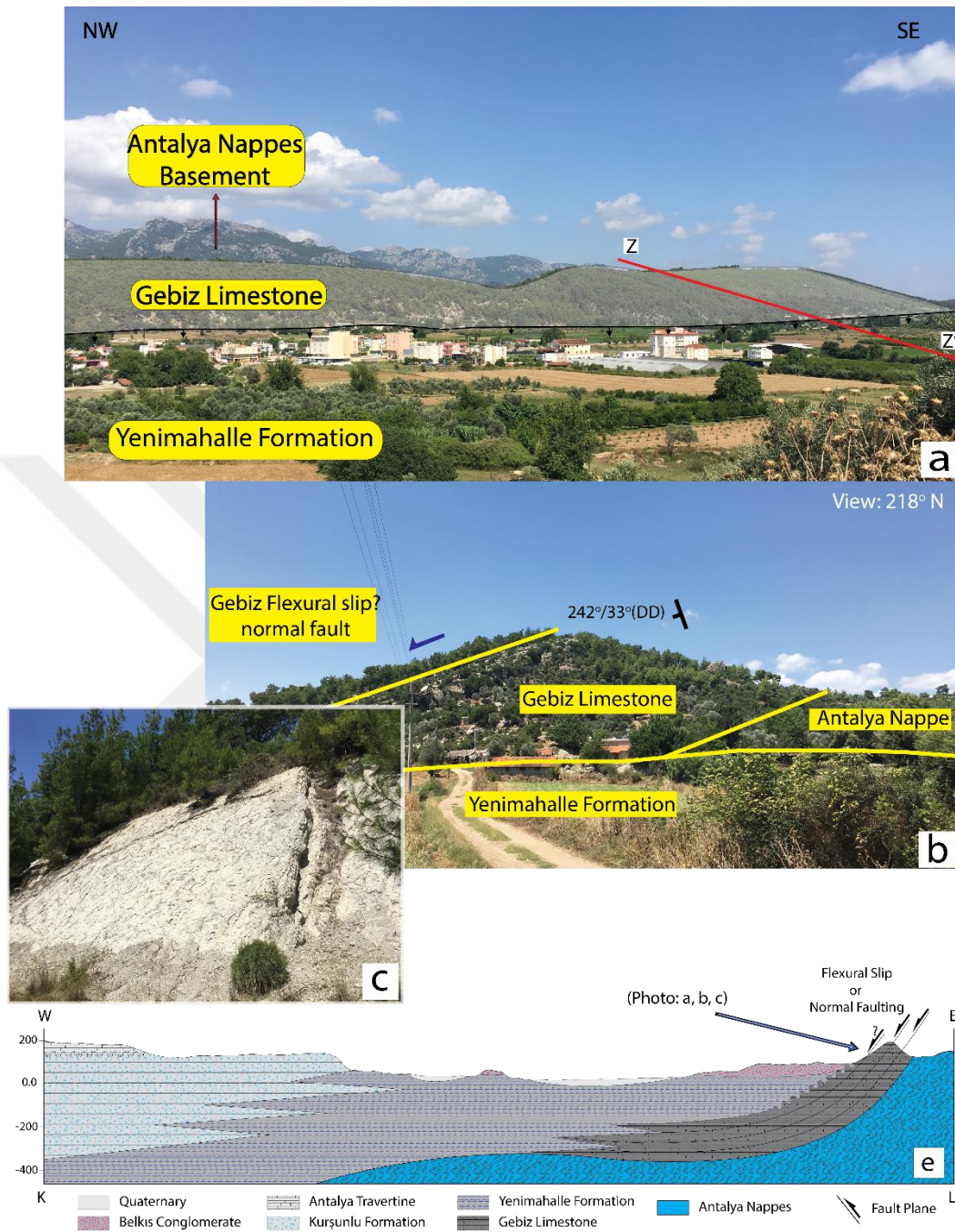
Figure 3. 15. a. Field view from theGebiz Limestone in the south-west side of the Aksu Basin, b. Field view of the contact relationships between the Gebiz limestone, Antalya Nappes and Yenimahalle Formation, c. Close view of Gebiz Limestone, d. Cross-section between z and z' showing the Gebiz Limestone unconformably overly the Antalya nappes and Yenimahalle formation onlapping Gebiz Limestone.

The age of the Gebiz Limestone subjected to an argument. Initially Poisson (1997), assigned the Lower Pliocene age to the Gebiz limestone. Later, based on bio-stratigraphic data, Akay et al. (1985) estimated the Messinian age, whereas Glover & Robertson (1998) deduced the Tortonian age and Poisson et al. (2003) proposed Early Pliocene age. Poisson et al. (2011) gave a Messinian age to the Gebiz Limestone based on planktic foraminifera.

The Gebiz Limestone formed within open to restricted marine environment based on fossil content (Poisson et al., 2003; 2011).

3.5. Eskiköy Formation

The Eskikoy Formation crops out in the south part of the Aksu Basin and is well exposed along Antalya Isparta road (Figure 3.1b). It is introduced by Akay et al (1985) who reported a maximum thickness of about 300 m.

The unconformable contact relationship between the Eskiköy Formation above and Antalya Nappes (basement) below is well exposed near Kızılseki village (Figure 3.16c). The contact relationship with the Karpuzçay Formation is well exposed near Karaöz Mahallesi/ Antalya where Eskiköy Formation unconformably overlies the Karpuzçay Formation (Figure 3.16d). Akay et al. (1985), has interpreted the formation as lateral equivalent of the Gebiz Limestone this contact not exposed on the surface.

It is laterally transitional with the Yenimahalle Formation (Poisson 1977; Gutnic et al. 1979; Glover and Robertson 1998a); this contact is also not exposed. The conglomerate is composed of ~80% white limestone and 10% grey sandstone and 10% of recrystallized grains. The shape of grains is subrounded to subangular grains. The conglomerate is matrix-supported conglomerate and Maximum grain size is between 50cm and clasts are finning upward, with very thick bedding between 1m to 3m. Farther to the south of the basin, bedding becomes thinner, ca. 30-60 cm (Figure 3.16a, b).
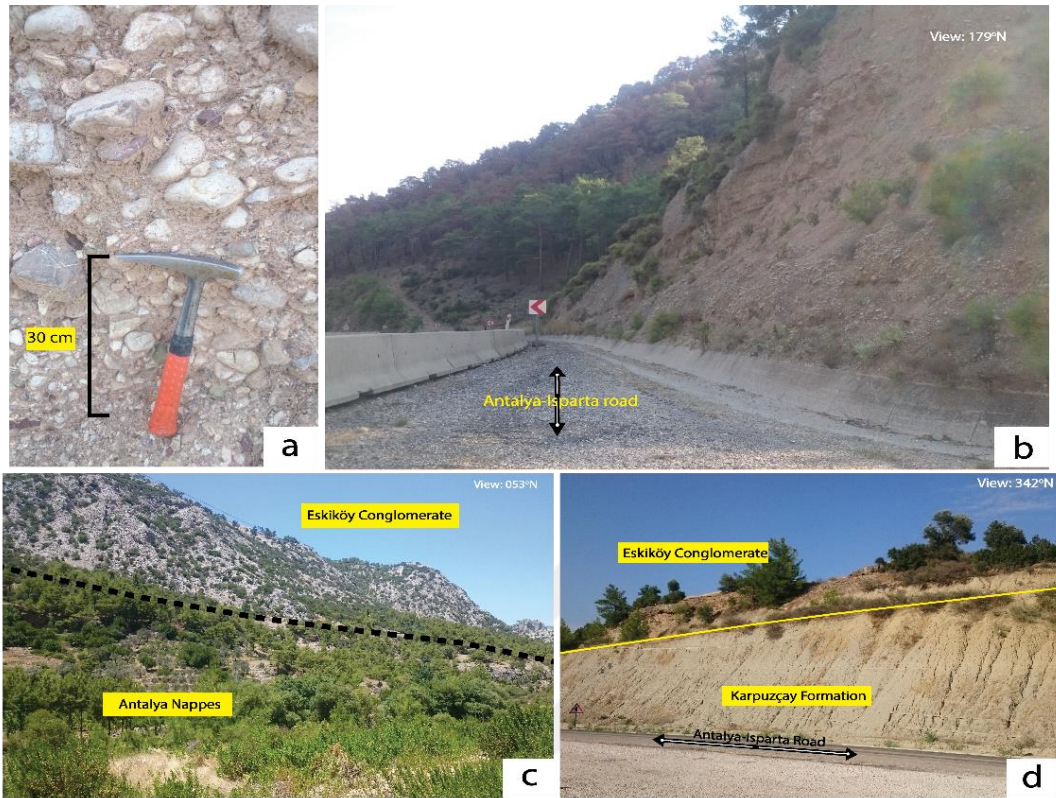
Figure 3. 16. Field views from (a, b) the Eskiköy Formation; note in (a) that the clast-supported conglomerate contains sub-rounded grains; (c, d) unconformable contact relationship of the Eskiköy Formation above and the Antalya Nappes (c) and Karpuzcay Formation (d).

Poisson et al. (2003), studied the fossil content of the formation and reported that the formation contains *Orbulina, Biorbulina, Globigerinoides trilobus, G. obliquus extremus, G. obliquus s.s., G. bollii, G. emeisi, G. aperture, Globigerinita seminulina, S. sphaeroides, Globigerena nepenthes, G. conglomerate, G. bulloides, G. aperture and Globigerinita* incrusta. Poisson et al. (2003), based on this fossil content the suggested an age of Late Miocene to Early-Pliocene for the formation. Akay et al. (1985), has interpreted the formation as a lateral equivalent of the Gebiz Limestone and considered the age as the Messinian. Pliocene age is also suggested for the Eskiköy Formation because it unconformably overlies the Langhian-Tortonian Karpuzçay Formation and laterally transitional with the Yenimahalle Formation (Poisson 1977; Gutnic et al. 1979; Glover and Robertson 1998a). The Eskikoy Formation is represented as an alluvial fan.

3.6. Quaternary Units

3.6.1. North of the Basin

3.6.1.1. Düzağaç conglomerate formation

The Düzağaç Formation is named by Eroskay (1968) and, Akay and Uysal (1985). It is well exposed in the northeastern side of the Aksu Basin. The formation is represented mainly by conglomerates (~40 cm thick) and thin sandstone interbeds (Figure 3.17d). The clast-support conglomerate consists of sub-rounded to sub-angular white limestone (~95%) and few grey sandstone grains with maximum size reaching up to 50-60 cm. The conglomerate is aquatic, which means there is no sorting or grading.

The unconformable contact with the underlying Jurassic calciturbidites of the Antalya Nappes (basement) or the Karpuzçay Formation and overlying Çamlık Travertines are well exposed at the east side of the Kargı Dam (Figure 3.17a-c).

The age of the formation is interpreted late Pliocene-Pleistocene by MTA (Geological Map Series of Turkey 1:100000 scale, Antalya J 11 sheet; publications of General Directorate of Mineral Research and Exploration, Ankara).

view: 044° N

Düzağaç Conglomerate

Jurassic- Calciturbidite

136°/17°(DD)

a

view: 072° N

Çamlık Travertine

136°/17°(DD)   Düzağaç Conglomerate

b
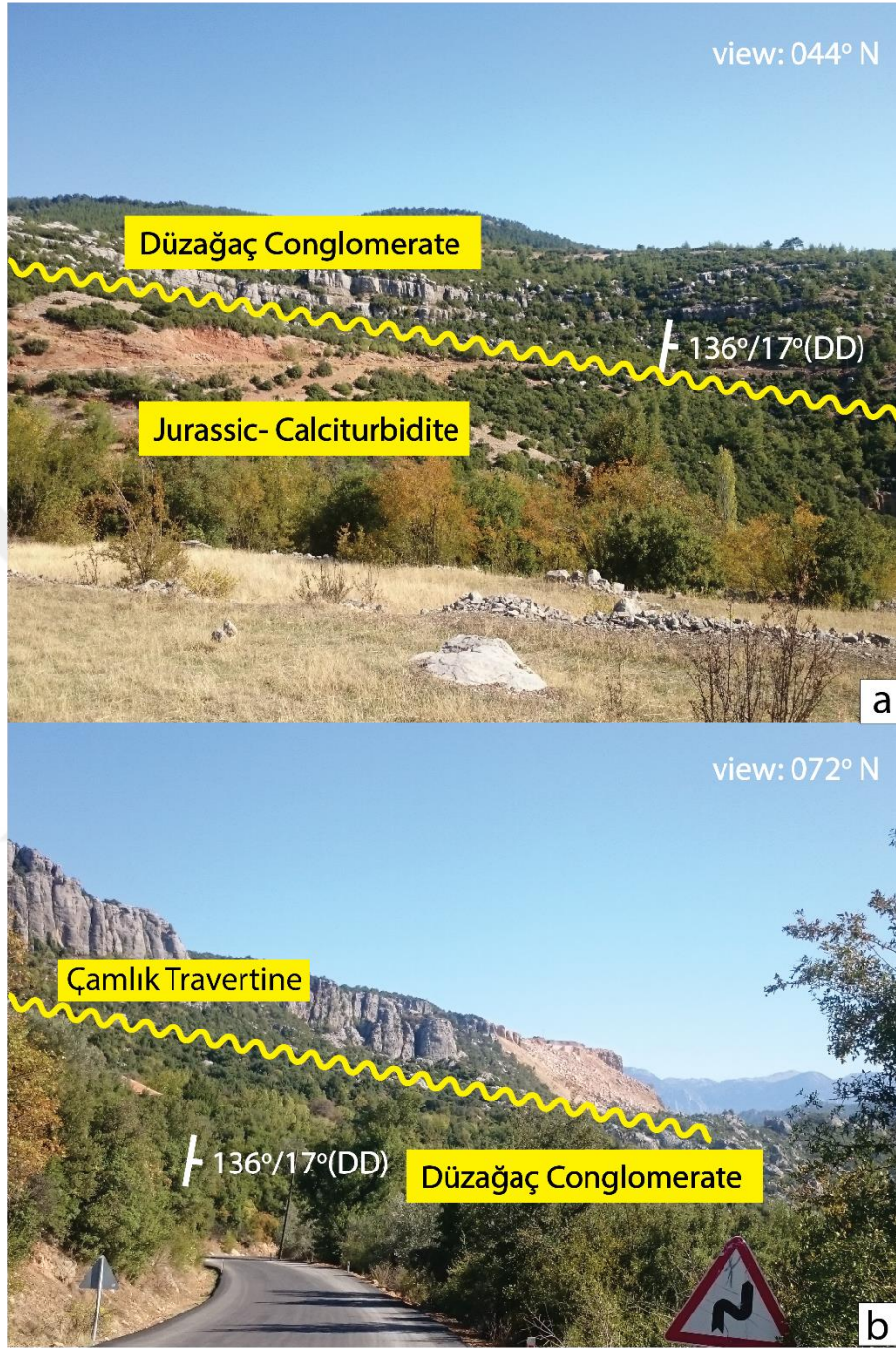
Figure 3. 17. Field views showing unconformable contact relationship between the Düzagaç Conglomerate where overlying Jurassic calciturbidites (a), overlined by Çamlık Travertine (b), and overlying Karpuzçay Formation (c), d. Close-up views from the Düzağaç Conglomerate.

Figure 3.17. Figure 3. 18. Field views showing unconformable contact relationship between the Düzagaç Conglomerate where overlying Jurassic calciturbidites (a), overlined by Çamlık Travertine (b), and overlying Karpuzçay Formation (c), d. Close-up views from the Düzağaç Conglomerate. (Continued).

3.6.1.2. Çamlık travertine

Çamlık Travertine is first reported by (Şenel, 1997). The unit outcrops out in different locations within the western side of the Aksu Basin (Figure 3.1). The unconformable contact with the Düzagaç Conglomerate is well exposed at the west side of the Kargı Dam (Figure 3.18a).
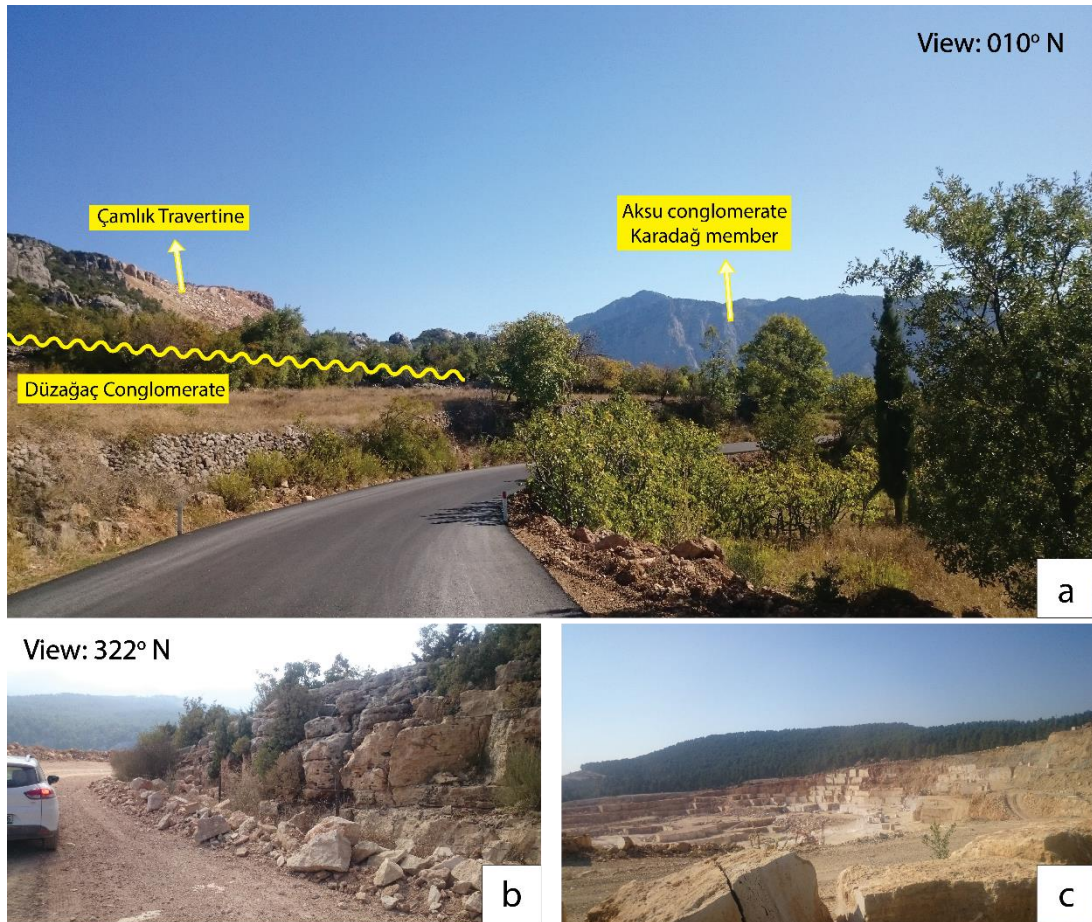
Figure 3. 19. Field views of the Çamlık Travertine. The unconformable contact with the underlying Düzağaç Conglomerate is well exposed in the western side of the Aksu Basin (a). Close views from the travertines (b, c). There are quarries in the travertine occurrences.

The unit is consisting of %100 gray, milky and brownish yellow colour travertines (Figure 3.18b, c). It is attributed to deposition by carbonate supersaturated waters that comes from springs (Glover and Robertson, 1998). The formation contains pisolic and

oolitic carbonates. According to gastropod fossils Pleistocene age is assigned (Geological Mmap Series of Turkey, 1:100000 scale, Antalya J 11 sheet. Publications of General Directorate of Mineral Research and Exploration, Ankara).

3.6.2. South of the Basin

3.6.2.1. Yenimahalle formation

Yenimahalle Formation first reported by (Akay and diğ., 1985). The formation is exposed at the southern part of the Aksu Basin (Figure 3.1). The contact relationships with the Gebiz Limestone and Belkıs Conglomerate are well exposed near Gebiz Town where it onlaps the Gebiz Limestone and is overlapped by the Belkıs Conglomerate (Figure 3.15a, d). It shows lateral transition with the Yenimahalle Formation (Poisson, 1977; Gutnic et al., 1979; Glover and Robertson, 1998a) but the contact is not well exposed. The formation grades upward into the Kurşunlu Formation and it is well exposed near Yeşilkaraman village (Poisson, 2003) (Figure 3.19 and 3.20c).

The formation consists of blue and grey colour siltstone, claystone and mudstone. Glover and Robertson, (1998), reported marine organisms as *Acanthocardia sp., Ostrea sp., Cerastoderma edule, Paphia sp., Dentalis sp., Antalis sp., Apporais sp., Buccinum sp., Concus sp., Gibbula sp., Murex sp., Litterina sp., Fusinus sp., Balanus sp., and pectens*. Numerous burrows include concentrations of Skolithos, Chondrites, Thalassanoides, Scoyenia and Planolites and Rind burrows.

Based on fossil content, Glover and Robertson (1998), interpreted the Yenimahalle formation as a product of a shallow-marine environment. The Yenimahalle formation contains the Margaritae and Puncticulata zones in the Gebiz area, indicating an Early Pliocene age (Poission et al., 2003).
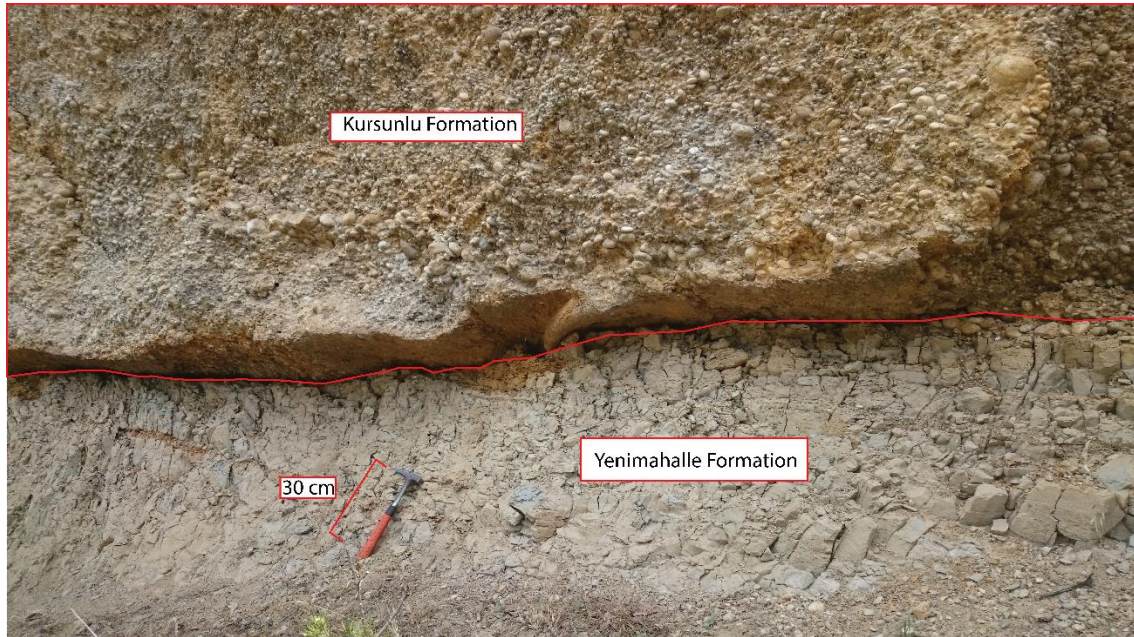
Figure 3. 20. Field view that shows Kurşunlu Formation overlying the Yenimahalle Formation.

3.6.2.2. Kurşunlu formation

It is first named by Akay et al., (1985). The formation is located in the south part of the Aksu Basin and is restricted to the southwest of the Aksu valley. The Kurşunlu Conglomerate consists of white limestone (~90%) and some gray sandstone sub-rounded clasts with maximum size reaching up to 30-35 cm. The grain-supported aquatic conglomerate shows no sorting and no grading. This conglomerated are marked by very thick beds between ~4 m to ~6 m (Figure 3.20a, b). The Kurşunlu Formation transitionally overlies the Yenimahalle Formation near Yeşilkaraman village (Poisson, 2003) (Figure 3.17). The Antalya Travertine is conformable above the Kurşunlu Formation (Figure 3.20c) whereas it unconformably overlies the Antalya Nappes (basement) near Eksili village (Figure 3.20d).

The formation contains Foraminifera, ostracods, Bivalve, Gastropod molluscs (Glover and Robertson, 1998). Upper Pliocene age is suggested by (Akay et al., 1985; Glover and Robertson, 1998). Glover and Robertson (1998), based on the occurrence of pebbles bored by sponges and marine bivalves, interpreted the formation as marine in origin. . Poisson et al. (2003) suggested a deltaic environment. Based on our field

observations the Kurşunlu formation is deposited in a delta environment because the Formation grades downward into Yenimahalle Formation.
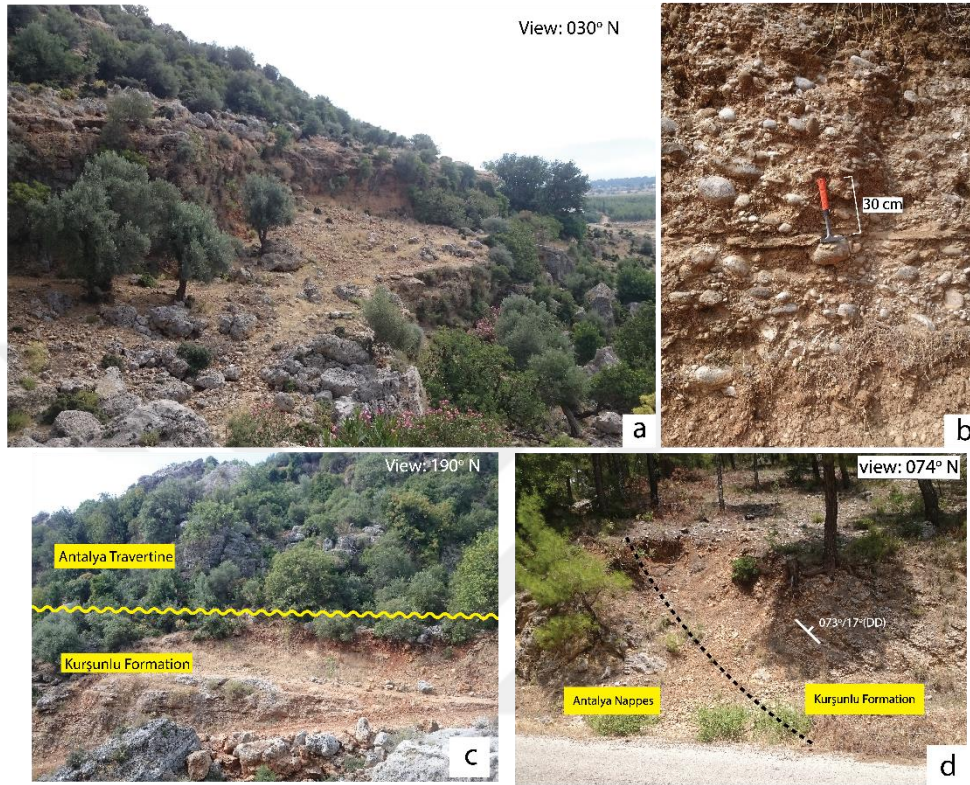
Figure 3. 21. Field views from the Kurşunlu Formation. (a) General appearance of the formation; (b) close-up view showing grain-supported conglomerates and sub-rounded clasts; (c) the contact relationships with the onlapping Antalya travertines; (d) whereas the Kurşunlu Formation onlaps Antalya Nappes.

3.6.2.3. Antalya travertine

The Quaternary Antalya Travertine occurs inthe south side of the Aksu Basin and covers a large area. First reported by Poisson (1977) and then studied by Akay and diğ. (1985) and latter researchers have reported a thickness of about 300 meters for the travertines. The unit is characterized by brown travertines. (Figure 3.21).

Figure 3. 22. Field view of Antalya Travertine at the southern side of the Aksu Basin.

The travertines conformably overlie the Kurşunlu Formation and the contact is well exposed near Yeşilkaraman village (Figure 3.1 and 3.20e). The fossil content, Condora sp. Bulgusuna, suggests a deep marine environment and a late Pliocene-Quaternary age (Akay et al., 1985). Koşun (2012) suggested, based $\delta 13C$, $\delta 18O$ and $14C$ isotopes, a Quaternary age for the travertines.

3.6.2.4. Belkıs conglomerate

Blumenthal (1951) first described the Pleistocene Belkis conglomerate. It occursat the south side of the Aksu Basin and conformably overlies the Yenimahalle and Eskikoy formations (Figures 3.1 and 4.2). The unit consists of sub rounded to rounded clasts derived from gray and white limestones (~80%) and brown and red mudstone-cherts (~20%). Clast-supported conglomerates show no sorting and display finning upward in grain size. The clast size ranges between 2 mm to 20 cm. Bedding thickness may reach up to ~1.5 m; cross-bedding is common (Figure 3.22) and is considered as good indicator for flowing depositional Environments, such as a stream environment. Pleistocene age is assigned to the formation (Geological Map Series of Turkey 1:100 000 scale, Antalya J

11 sheet; Publications of the General Directorate of Mineral Research and Exploration, Ankara).

Figure 3. 23. Field view of Belkis conglomerate that shows cross-stratification in the conglomerate. note that the conglomerate consists of rounded grains and grain supported.

4. STRUCTURAL GEOLOGY

This section concentrates on the detailed description of geological structures that shaped the Aksu Basin. The major structures in the Aksu basin basically include large scale thrust-fault system, numerous mesoscopic faults commonly with no more than a few meters offset, and generally tight-asymmetrical fold systems. Most structures are mapped using remote sensing techniques and subsequently verified in the field. Analysis of lineaments, fault patterns, and geomorphologic characteristics based on remote sensing data are given in the following sections.

4.1. Lineament Analysis from Remotely Sensed Data

Lineaments originate from two types of sources. Firstly, they may form due to tectonic activity and this type of lineaments generally corresponds to faults, joints and/or lithological boundaries. The other type of lineaments is due to man-made features including roads, railroads, crop field boundaries or any kind of variations in land use patterns. First type of lineaments, occurred by the tectonic activity, is the main concern of geologic studies.

In this study, Terra-ASTER (Advanced Spaceborne Thermal Emission and Reflection Radiometer) (Figure 4.1) and Quickbird images obtained from Google Earth are used to improve delineation and characterizing the lineaments. Detail information about the ASTER images used during this study is given in Table 4.1.
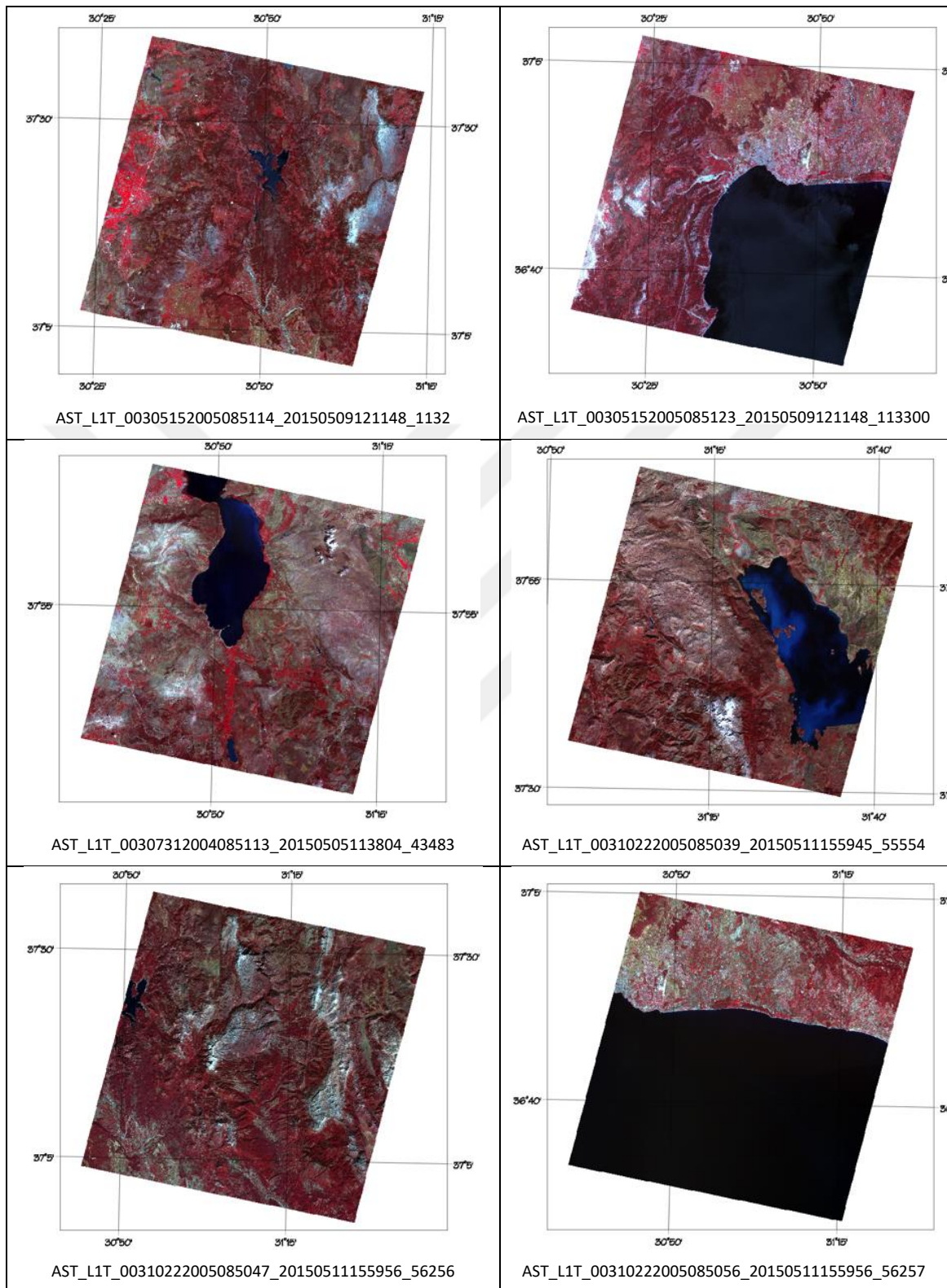
Figure 4. 1. Quick look of the ASTER images used during the lineament extraction
process.

Table 4. 1. Catalog information of the ASTER images used in the study

Image No	Image Type	Image Code	Aquired Date
1	ASTER Level 1T	AST_L1T_00305152005085114_20150509121148_113296	2005/05/15
2	ASTER Level 1T	AST_L1T_00305152005085123_20150509121148_113300	2005/05/15
3	ASTER Level 1T	AST_L1T_00307312004085113_20150505113804_43483	2004/07/31
4	ASTER Level 1T	AST_L1T_00310222005085039_20150511155945_55554	2005/10/22
5	ASTER Level 1T	AST_L1T_00310222005085039_20150511155945_55554	2005/10/22
6	ASTER Level 1T	AST_L1T_00310222005085056_20150511155956_56257	2005/10/22

Delineation of the lineament from the remotely sensed data is a complex process and includes some uncertainties related to spatial resolution and spectral characteristics of the images. Various enhancement and image-processing techniques are used in order to improve the spectral and spatial resolution of the images. Among these techniques, contrast enhancement, color composite, principal component analysis (PCA) and decorrelation stretching (DS) techniques are applied to improve the visual interpretability of an image. The processed images are later draped on high-resolution digital elevation models (DEM's) obtained from Google Earth to improve 3D visualization in different directions.

Lineament extraction process is performed manually on the images since expert perception can easily interpret geospatial signatures and discriminate them from the artificial linear features (roads, rail roads etc.). Resultant lineament map of the Aksu Basin length weighted rose diagram of the extracted lineaments are given in Figure (4.2).

The resultant map includes both discriminated faults, based on field observations and literature data (1:100000 scale MTA geological map) and also lineaments extracted from remotely sensed data. The rose diagram (Figure 4.2) including both faults and lineaments shows NW-SE dominant directions. This direction is approximately parallel to strike of the Aksu Thrust. This may imply that the tectonics of the study area has been mainly controlled by the Aksu Thrust.
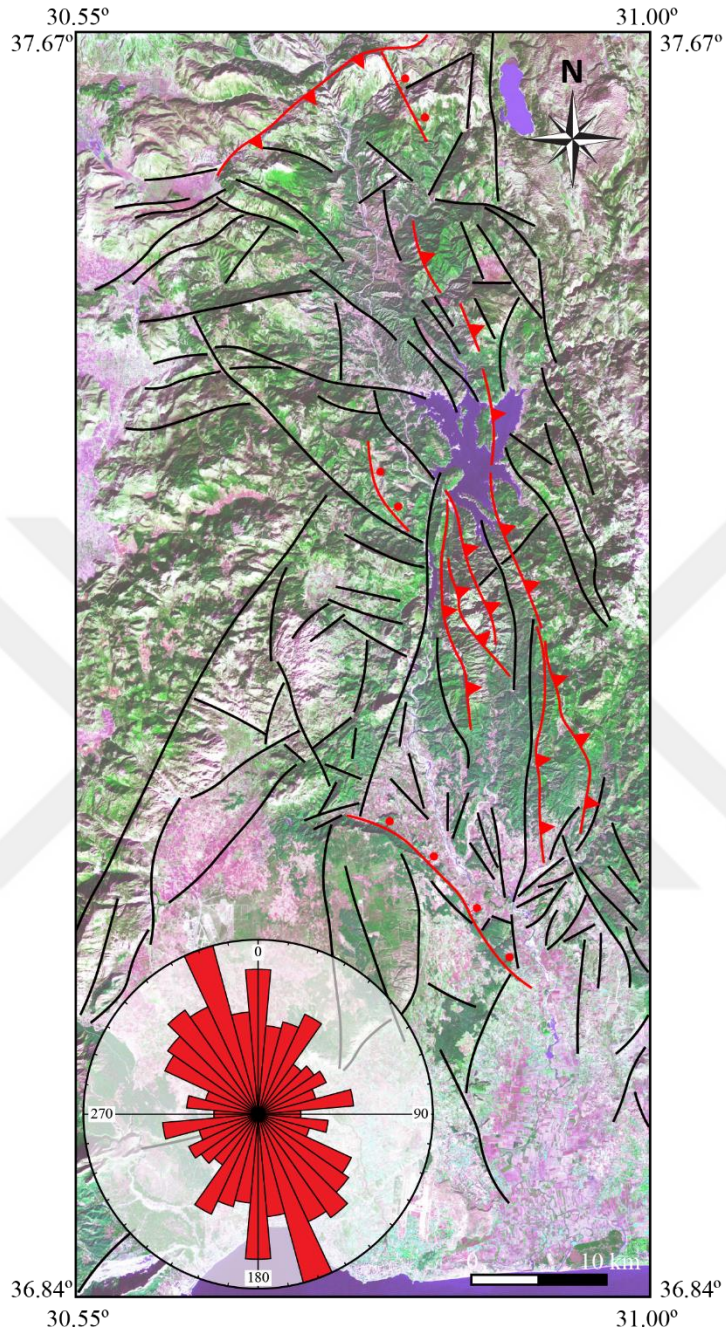
Figure 4. 2. Lineament map of the Aksu Basin. Rose diagram (length-weighted) is prepared from delineated lineaments. Band combination of the background image is 742 in RGB with shaded relief of Digital Elevation Model (DEM) obtained from Google Earth 'courtesy of Dr. Ayten Koç'.
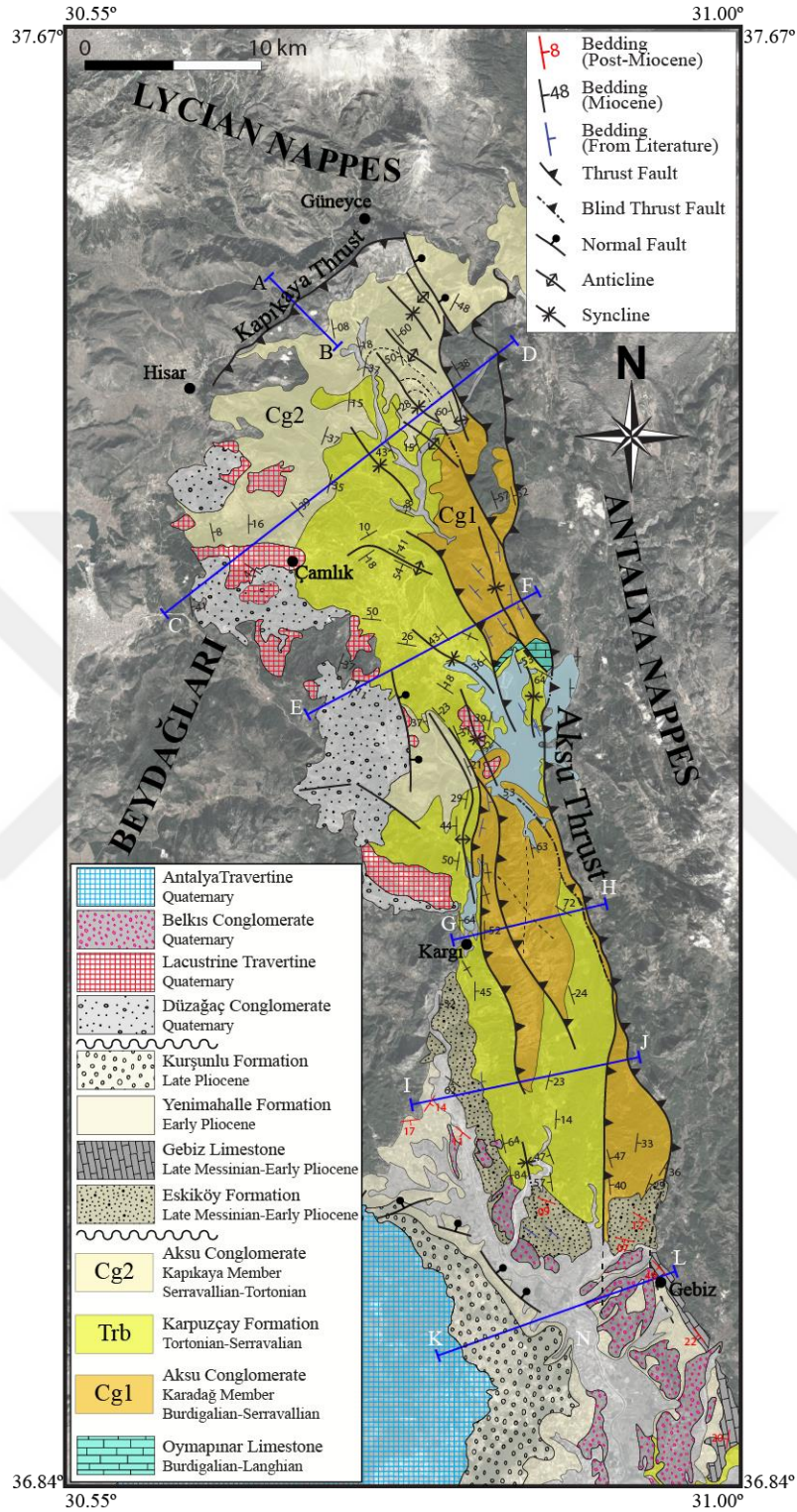
Figure 4. 3. Geology map of the study area from revised 1/100.000 scale geological map by MTA.

4.2. Field Observations

The Aksu Basin is an approximately 90 km long and N-S trending basin (Figure 4.3). The major structures that formed the Aksu Basin are thrust faults (Figure 4.3). Morphologically, the most prominent structures controlling the eastern and northern boundary of the study area are thrust faults, namely Aksu and Kapıkaya thrust faults. They are generally recognized by a sharp and curvilinear boundary between the basement and basin infill. Those two major thrust fault systems generating numerous mesoscopic faults, which developed after and during the sedimentation, have controlled the evolution of the Aksu Basin. In addition to those fault systems, the basin-fill is also deformed by numerous tight-asymmetric fold structures (Figure 4.3).

4.2.1. Faults

Morphologically, two major structural trends are identified in the study area (Figure 4.3). These trends include approximately ENE-WSW and N-S striking faults within the Miocene infill of the basin. All of these faults are characterized as thrust faults. In addition to the thrust faults, also the normal faults with ~NW-SE trending are recorded in the younger basin infill (mainly Pliocene-Pleistocene age). The basic characteristics of the major faults will be described in the following sub-sections.

4.2.1.1. Kapıkaya Thrust Fault (KTF)

Kapıkaya Thrust Fault (KTF) is a well-exposed structure comprising approximately 15 km long, ENE-WSW trending thrust fault (Figure 3.8a). It controls the northern boundary of the Aksu Basin (Figure 4.3). Miocene infill (Kapıkaya Conglomerate) of the Aksu Basin occurs at the top of the Kapıkaya Thrust sheet that is a high angle the Lycian remnant Jurassic-Cretaceous limestone (Figure 3.8b and c). An abrupt change in topography provides morphological evidence for the presence of the faulting.

The main fault plane dips southwards where dip amount is more than 45° (high-angle) (Figure 3.8a and b). The western continuation of the KTF is clearly traceable to the southeast of the Hisar village, and then it dies out within the low Quaternary topography. The trace of the KTF in the east can be followed easily until where it is cut by ~N-S trending normal fault in the south of the Güneyce Village.

Antalya-Isparta road crosses the main fault scarp. This fault scarp juxtaposes Jurassic-Cretaceous basement unit and Eocene-Miocene turbiditic sandstones (Figure 3.8a). KTF does not directly create the displacements on the Miocene sediments of the Aksu Basin since they were formed at the back side of the Kapıkaya Thrust. Fortunately, it is possible to observe discontinuous fault sets (synsedimentary movement) within the Kapıkaya conglomerate member (Figure 4.4).
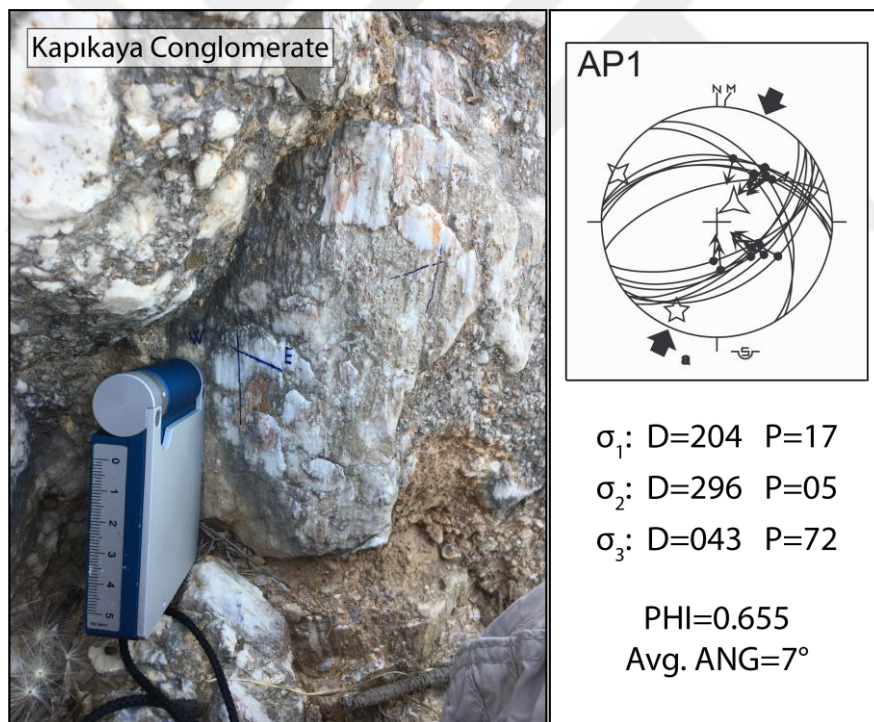
Figure 4. 4. Fault surface that is observed in the Kapıkaya Conglomerate and constructed paleostress configuration based on the collected fault-slip data (equal area, lower hemisphere projection).

Therefore, a sudden break in slope, juxtaposition of different lithologies, and well-developed slickensides are used as criteria for the recognition of the KTF. The

stereographic plot of fault-slip data shows that the KTF is a thrust fault. The orientation of the inferred principal stresses and the stress ratio are: $\sigma1= 204°$ N/17°, $\sigma2= 296°$ N/05°, $\sigma3= 043°$N/72° and indicate compressive deformation. The stress ratio is $\Phi=0.655$, which represents a well-developed tri-axial stress conditions (Figure 4.4).

4.2.1.2. Aksu Thrust Fault Zone (ATFZ)

The Aksu Thrust (ATFZ) is approximately 60 km long and 50 km wide structure that is composed several parallel fault segments (Poisson et al., 2003). Approximately N-S trending Aksu Thrust is morphologically easily recognized as a linear mountain front rising steeply in the eastern margin of the Aksu Basin (Figure 4.5). The ATFZ comprises several parallel fault planes that create complex tectonic slices in the basin (Figure 4.5a). It is the most prominent structure that deforms the infill of the Aksu Basin. The well-expressed fault surface is approximately 13 km long and exposed nearby by the Kargı Dam Lake (Figure 4.5b).

The master fault of the ATFZ displays easterly dipping thrust fault (Figure 4.6d), and dip of the fault surfaces ranges between 31° and 88° (Figure 4.6c). The main branch of the Aksu Thrust extends between Gebiz town in the south and Çukurköy village in the north of the basin (Figure 4.3). Morphologically, the northern continuation of the Aksu Thrust is clearly traceable on satellite images; however, the southern continuation near Gebiz town can not be traced easily because of the more gradual change in elevation (Figure 4.3 and 4.5a). Along the main branch of the Aksu Fault, the Miocene infill of the Aksu Basin (including Karpuzçay and Aksu Conglomerate) is juxtaposed with the basement units that are composed mainly of Antalya Nappes' Triassic Carbonates. In addition to morphological evidence, field observations provide that the well-developed slickensides are also present within the fault zone (Figure 4.6a and b). Slickenlines on the fault plane are used as criteria for the recognition of the ATFZ. The stereographic plot of fault-slip data on the Schmidt's lower hemisphere net shows that the characteristic of Aksu master Fault is a thrust fault with average dip of 60° (from 31° to 88°) E with a minor amount of dextral or sinistral strike-slip component (Figure 4.6b and c).
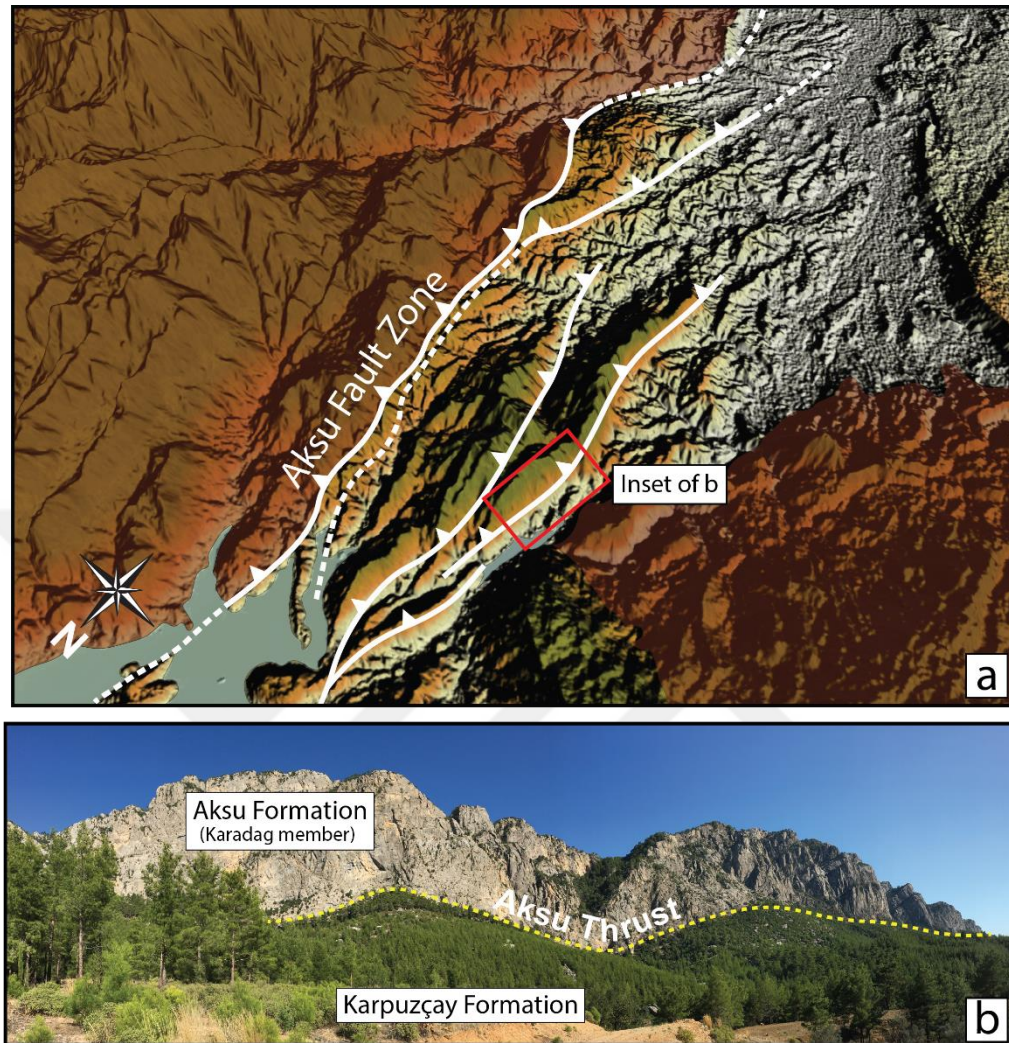
Figure 4. 5. a. Digital elevation model (DEM) with 60*60 m spatial resolution shows 3D view of the E dipping Aksu Thrust Fault Zone (ATFZ) at the eastern margin of the Alsu Basin, b. Field view of Aksu Thrust Fault (Kargı set) in the central part of the Aksu basin. Note that Karadağ Conglomerate show steeply rising mountain front at the hanging wall of the fault.

At the northeastern side of the basin, fault-slip data (site AP4) is collected from the Tortonian Kapıkaya Conglomerate (Frizon de Lamotte et al., 1995; Poisson et al., 2003). The orientation of the inferred principal stresses and the stress ratio of this data are as follows: (σ_1= 211ºN/02º, σ_2=121ºN/12º, σ_3= 310ºN/78º) and indicate compressive deformation. The stress ratio is R= 0.5, which represents a well-developed tri-axial compressional stress conditions (Figures 4.6c; 2.2).

From north to south, several cross-sections are produced to determine the geometry and the characteristics of the Aksu Fault (Figures 4.6d and 4.7d). Fault-slip data (site AP12) from the Langhian-Serravallian Karadağ Conglomerate (Figure 4.7a and b) shows the inferred orientation of the principal stress and the stress ratio (Figure 4.7c) as: σ1= 044°N/13°, σ2=314°N/02°, σ3= 215°N/77°); the data indicates compressive deformation. The stress ratio is R= 0.4, which represents a well-developed tri-axial compressional stress conditions (Figures 2.2 and 4.7c).

 Aksu Fault Zone is characterized by of several duplications of the succession along several thrust faults. The well- developed parallel fault planes are observed in the central part of the Aksu Basin, namely Kargı Fault Set (Figure 4.8a, d). Karpuzçay Formation and Karadağ Conglomerate are intensely affected by thrusting. Additionally, conglomeratic unit covering a very small area with respect to the whole basin and stratigraphically upper part of the Karpuzçay Formation, which is namely Kargı Conglomerate in the literature (Çiner et al., 2008), also show deformation associated with this thrusting. The age of this conglomeratic unit is probably Tortonian.

Similarly, fault-slip data (site AP32) from the Kargı Fault set (Figure 4.8d) which is located within the Karpuzçay Formation (Langhian-Tortonian) and Karadağ Conglomerate (Langhian-Serravalian), indicates that principal stress orientations (Figure 4.8c) and the stress ratio are: σ1= 267oN/13o, σ2=172oN/23o, σ3= 023oN/63o . The data is consistent with compressive deformation since the σ3 direction is close to vertical. The stress ratio is R= 0.3 and represents a well-developed tri-axial compressional stress conditions (Figures 4.8c; 2.2).
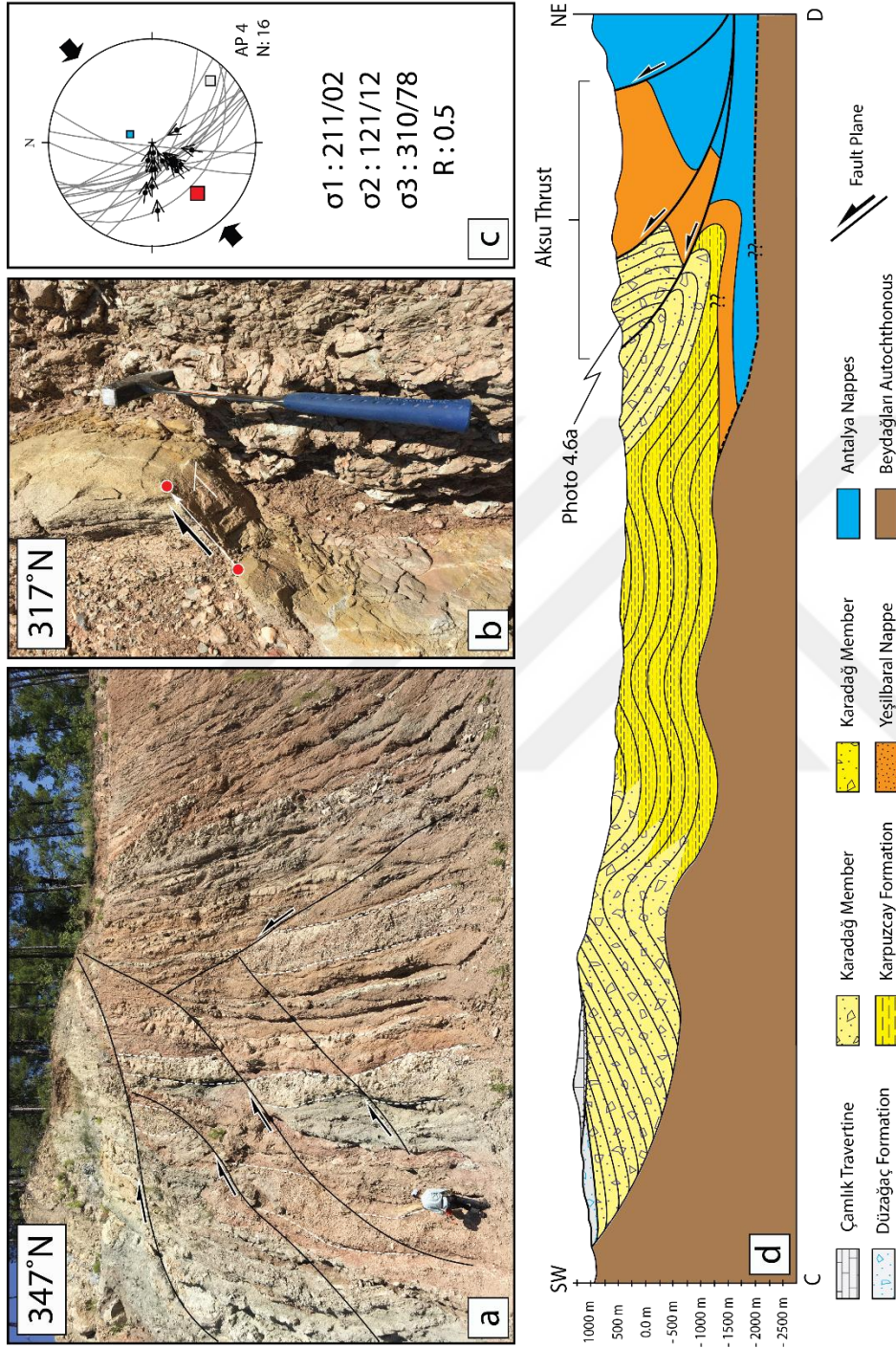
Figure 4. 6. (a) Field view of the reverse fault within the Aksu Fault Zone in the southeastern part of the Aksu Basin; (b) close-up view of the fault surface with slickenlines and (c) constructed paleostress configuration of the fault-slip data (equal area, lower hemisphere projection), (d) cross-section interprets the Aksu Fault zone in the northeastern part of the Aksu Basin (see the Figure 4.3 for the location of the cross-section line).
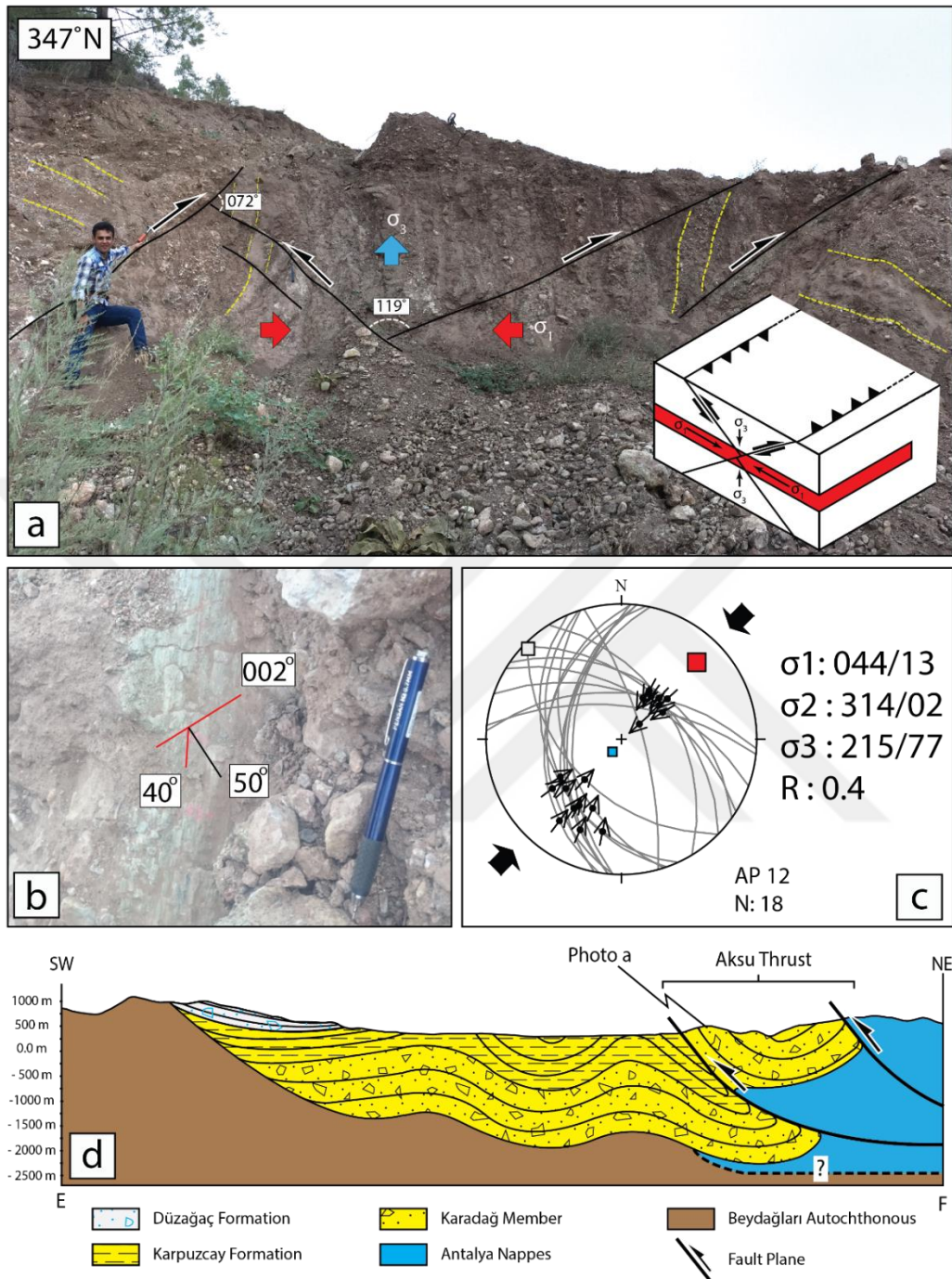
Figure 4. 7. (a) Field view of the Aksu Fault Zone at the north of the Karacaören Dam Lake, (b) close-up view of the fault surface with slickenlines and (c) constructed paleostress configuration of the fault-slip data (equal area, lower hemisphere projection), (d) cross-section along the E-F line (in Figure 4.3) interprets the Aksu Fault zone at the north of the Karacaören Dam Lake.
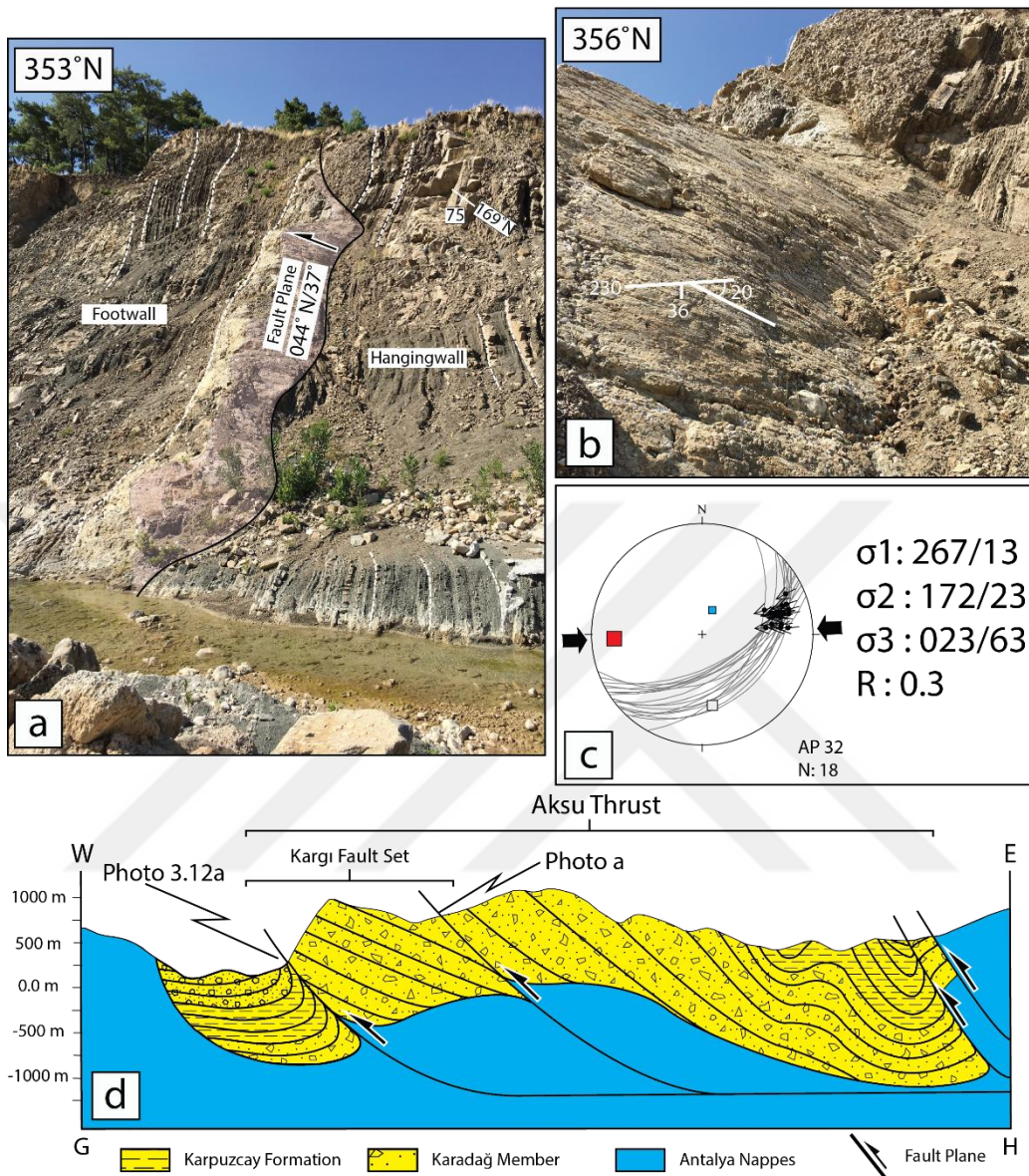
Figure 4. 8. a. Field view of the Kargı Fault Set of the Aksu Fault Zone at the north central part of the Aksu Basin, b. close-up view of the fault surface with slickenline, c. constructed paleostress configuration of the fault-slip data (equal area, lower hemisphere projection), d. Cross-section along the G-H line (see Figure 4.3) interprets the Aksu Fault zone at the central part of the Aksu Basin.
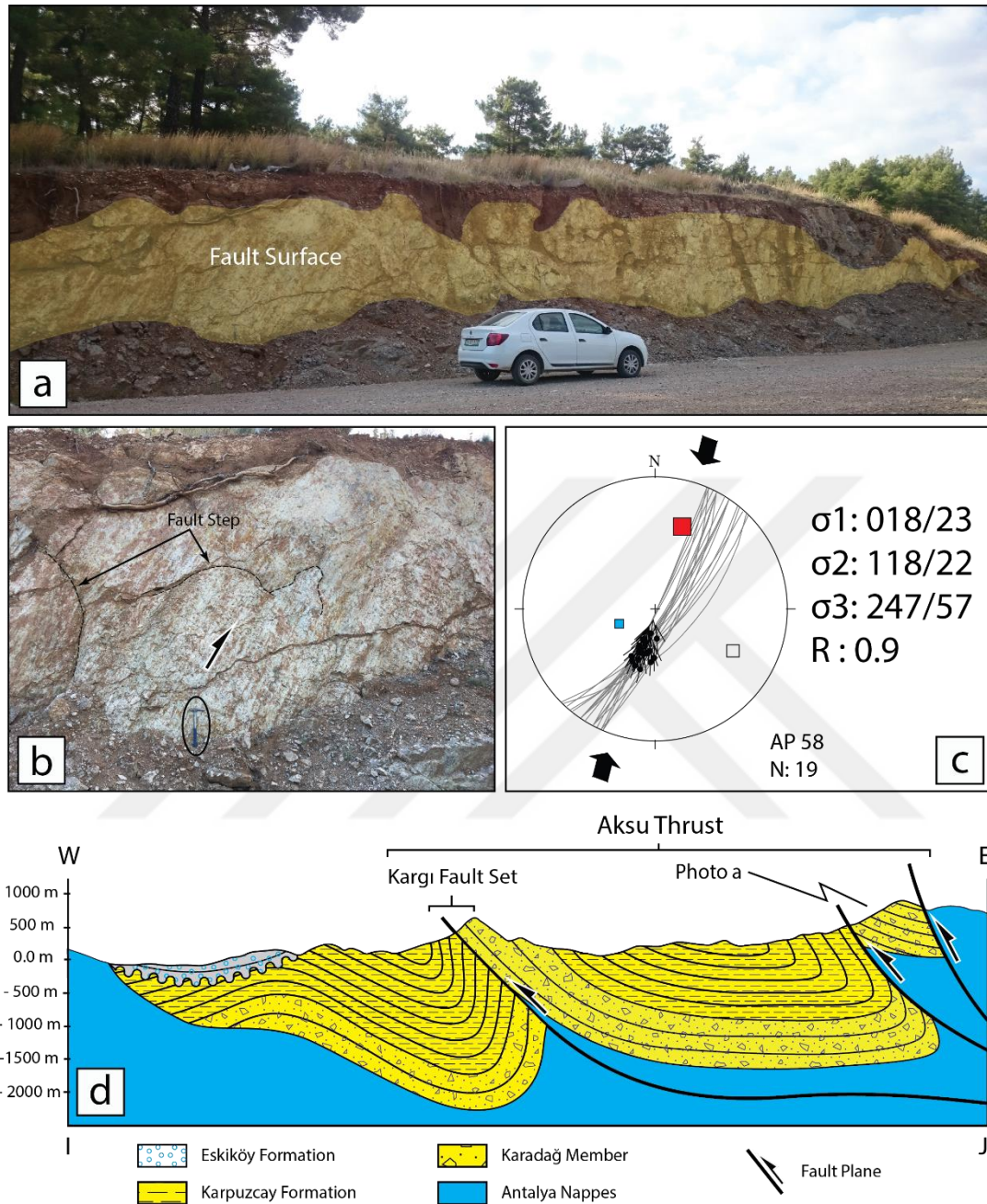
Figure 4. 9. a.Well-developed fault surface of the Aksu Thrust in the southern part of the Aksu Basin, b. close-up view of the fault surface, note that well-developed fault step and slickenline on the surface, c. constructed paleostress configuration based on the collected fault-slip data (equal area, lower hemisphere projection), d. Cross-section along the I-J line (see Figure 4.3) interprets the Aksu Fault zone at the southern part of the Aksu Basin.

In the south of the Aksu Basin, Karadağ Conglomerate and Karpuzçay formations show evidence for intense deformation associated with the Aksu Thrust Fault Zone, whereas Eskiköy Formation is slightly tilted (Figure 4.9d). Paleostress data (site AP58) (Figure 4.9a, b) indicates principal stress orientations as: $\sigma1= 018°N/23°$, $\sigma2=118°N/22°$, $\sigma3= 247°N/57°$). The data is consistent with NE-SW compressive deformation in this part of the Aksu Thrust. The stress ration is R=0.9 and represents radial compressive stress since $\sigma1$ and $\sigma2$ are very close to each other (Figure 4.9c).

A sudden break in slope, juxtaposition of different lithologies, and formation of well-developed slickensides are used therefore as criteria for the recognition of the Aksu Thrust Fault Zone. The overall east-west shortening is probably substantial, but precise evaluation must be done based on the detail stratigraphic information.

4.2.1.3. Normal Faults (Post-Miocene)

The major structures controlling the Aksu Basin are generally thrust/reverse faults. On the other hand, there are small-scale normal faults (max. 5 km long) deforming relatively young basin infill in the southern part of the Aksu Basin. The well-exposed ~E-W-trending normal faults are located in the north of the Hatipler (Figure 4.10a-d). This normal fault cuts Pliocene Yenimahalle and Kurşunlu formations. Unfortunately, it is not possible to collect fault-slip data from this fault since we could not found well-preserved slickensided surfaces.

The Gebiz Limestone dips to the west and faulted (Figure 4.11a, b). The dips of the Gebiz Limestone are higher (~65-70°) in the northern tip than in the southern tip (15-20°) of the fault. The sudden break in slope follows the bedding surfaces (Figure 4.11a).
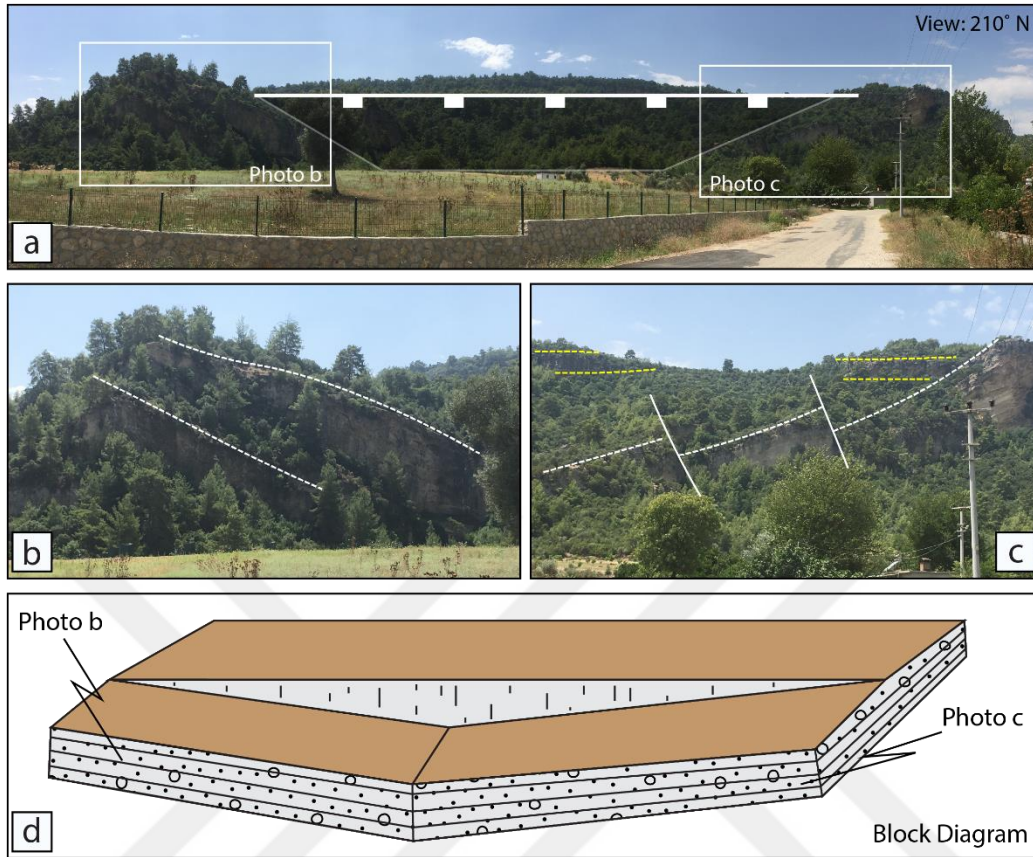
Figure 4. 10. (a) Field view of the normal fault in the Yenimahalle and Kurşunlu Formations in south of the Aksu Basin, close-up views from the southern (b), and northern (c), tips of the fault (d). Block-model of the faulting.

Juxtaposition of Gebiz Limestone and Yenimahalle Formation with differing bedding attitudes may be attributed to faulting (Figure 4.11b). From the poorly-developed slickensided surfaces (Site 57) (Figure 4.11d) indicates principal stress axes as $\sigma_1=270^oN/86^o$, $\sigma_2=098^oN/04^o$, $\sigma_3=008^oN/01^o$, the data is consistent with extensional deformation since the orientation of the σ1 is vertical. The stress ration is R=0.3, which represents pure stress conditions (Figure 4.11c).

On the other hand, the bedding attitude of the Gebiz Limestone (142°N/66W) is very close to attidutes of the fault surfaces (136°N/58W). It may be an indication of the flexural slip (Figure 4.11e) which is developed due to the uplift of the thrust front.

In the south of the Aksu Basin, another cross-section was carried out along the K-L line, which is given in Figure 4.11e. Line of the cross-section is indicated on the map given in Figure 4.3. The Cross-section line cut through the Gebiz Limestone, Yenimahalle

and Kurşunlu Formations, Antalya Travertine and Belkıs Conglomerate. The northern edge of the Gebiz Limestone (Messinian-Early Pliocene in age) have been affected by the Aksu Thrust Fault Zone (Figure 4.11a), however, Yenimahalle and Kurşunlu Formations (Early Pliocene) are mainly deformed by normal faulting (Figure 4.10).

Another mesoscopic scale normal fault with well- developed slickenline occurwithin the Yenimahalle Formations along the Antalya-Isparta main Road (Figure 4.12a). The stereographic plot of fault-slip data (Figure 4.12b) collected from Site 81 show the orientation of the inferred principal stresses as σ_1= 131°N/65°, σ_2= 233°N/05° and σ_3= 325°N/24°. The stress ration is found as R=0.2, which represents radial extension stress conditions since $\sigma2$ and $\sigma3$ are very close to each other (Figure 4.12c).

Field view of the normal fault in Figure 4.12c is also observed within the Yenimahalle Formation. The strike orientation of the faults is 104°N (approximately E-W) with listric character. Unfortunately, it is not possible to collect fault-slip data since it has unsuitable material property.

Hence, a sudden break in slope, juxtaposition of different lithologies, and formation of well-developed slickensides and direct observation of the mesoscopic scale normal faults are used as criteria for the recognition of the normal faults in the younger basin infill including Yenimahalle and Kurşunlu formations. The overall observations show that it is substantial to mention the approximately north-south trending extensional tectonic regime.
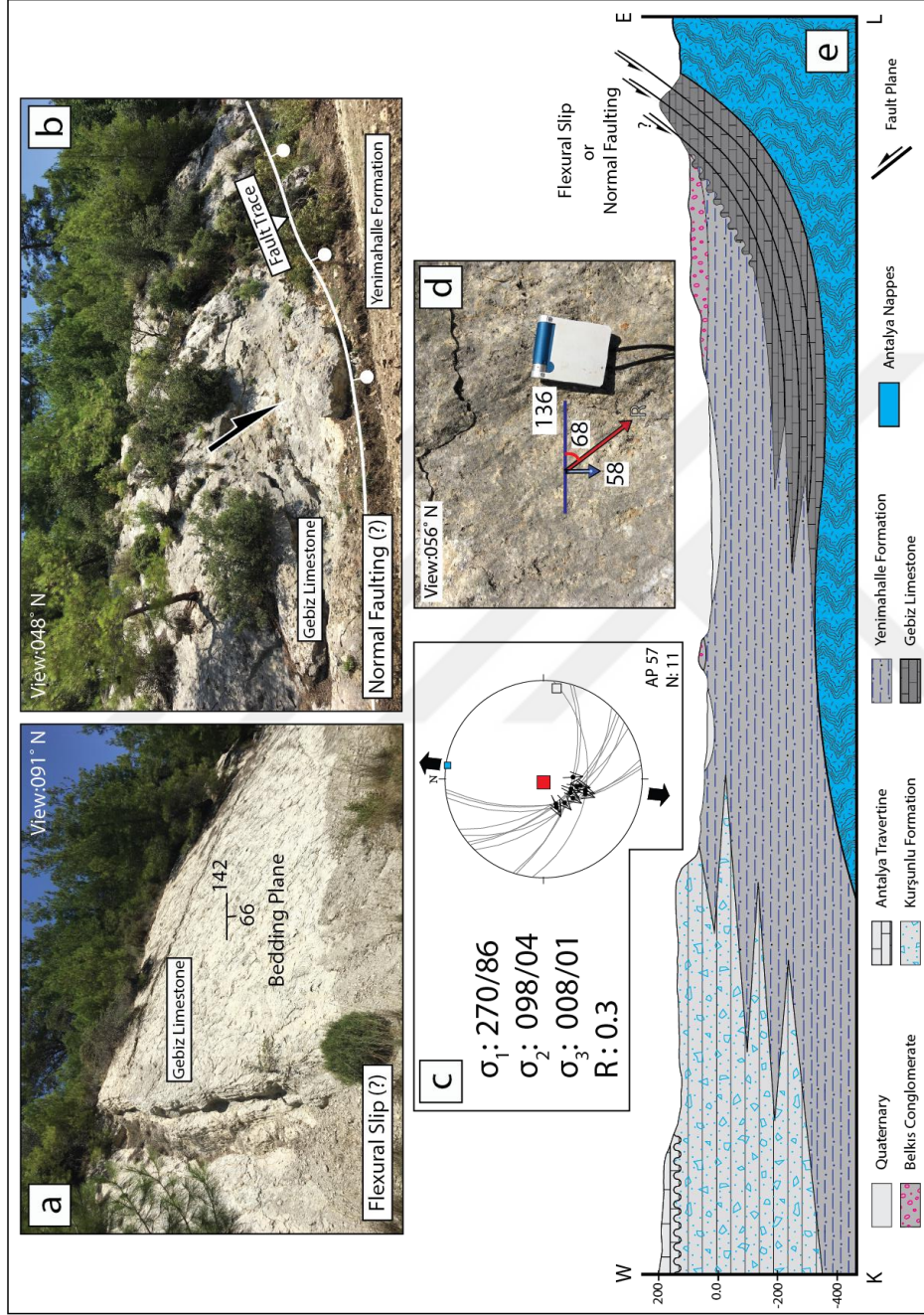
Figure 4. 11. (a) Field view indicates bedding orientation of the Gebiz Limestone in the southeastern part of the Aksu Basin, (b) Fault surface with slickenline and (c) constructed paleostress configuration based on the collected fault-slip data (equal area, lower hemisphere projection), (e) Cross-section (K-L) interprets the normal faults within the Gebiz Limestone (See the Figure 4.3 for the location of the cross-section line).
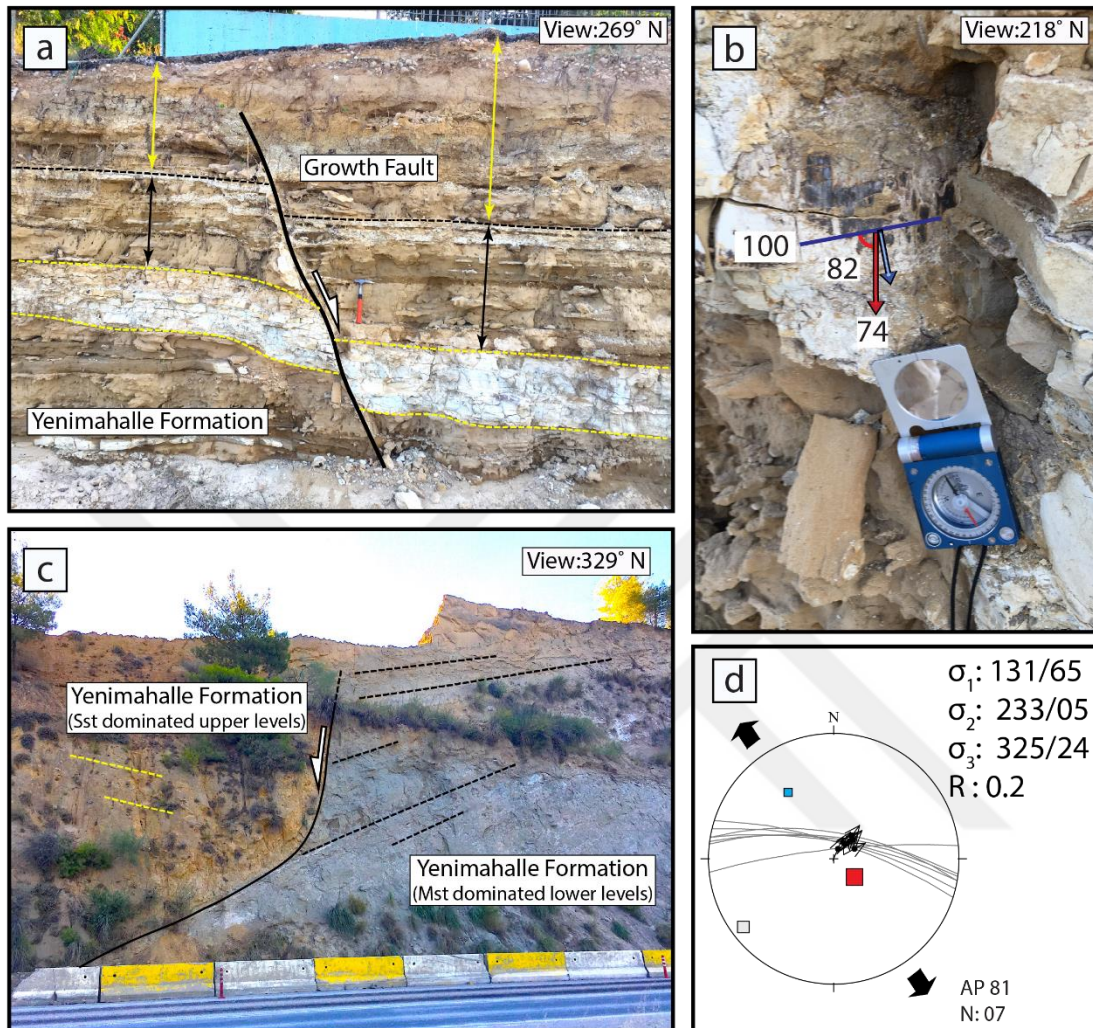
Figure 4. 12. a. Field view of the normal fault in the Yenimahalle Formations and in south of the Aksu Basin, b. Close-up view of the fault surfaces with slickenline (Site 81), c. Another normal fault with listric character in the Yenimahalle Formations, d. constructed paleostress configuration based on the collected fault-slip data (equal area, lower hemisphere projection).

102

4.2.2. Folds

Aksu Basin fill is characterized bywell-developed bedding planes and these beds display evidence for intense deformation. According to strike-dip measurements of the beds during the field study, a series of syncline and anticlines are interpreted and they indicated on the map that is given in (Figure 4.3).
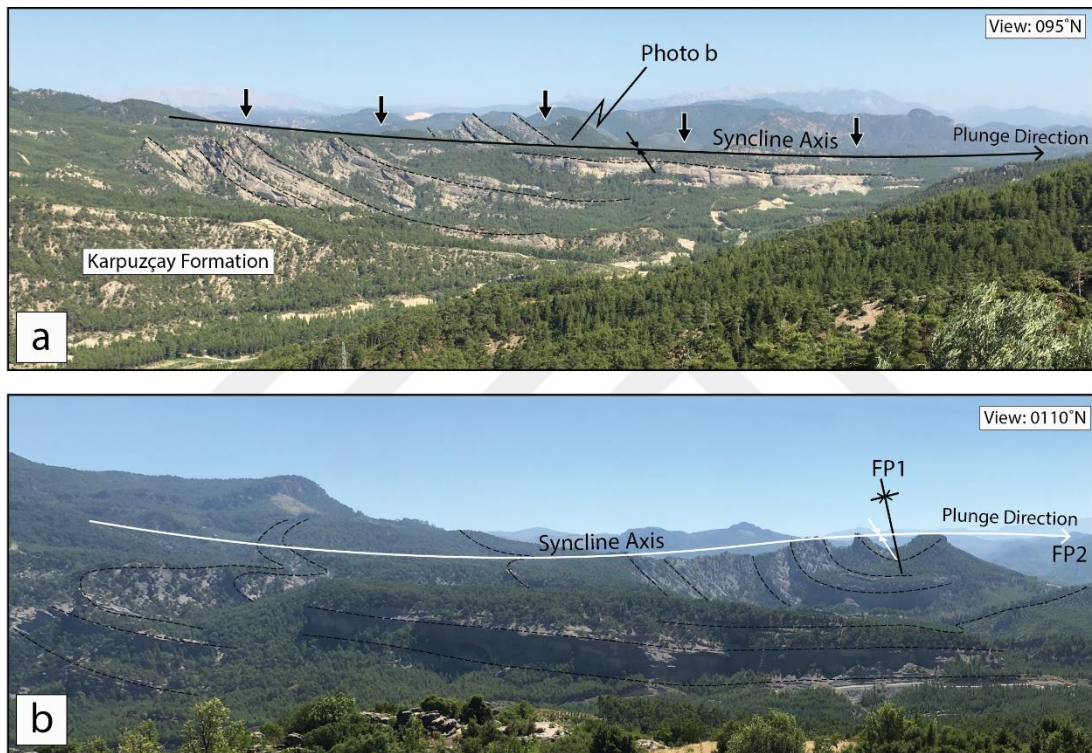
Figure 4. 13. a. Field view of the syncline which is located at the north of the Aksu Basin, close to the Kapıkaya Fault, b. Field view of the same syncline taken from the further south. Note that the syncline is double fold axes (dome like).

One of them is located in the north of the basin close to Kapıkaya Fault (Figure 4.13a). The strike-dip measurementsand V-rule observed in the satellite images (Google Earth) indicate that it is a doubly plunging syncline (Figure 14.13b). The long axis of the syncline is oriented in approximately N-S direction while the short is oriented approximately E-W direction. The syncline deforms the Kapruzçay Formation and Kapıkaya Conglomerate. The structure of the syncline may suggest that the infill of the

Aksu Basin is affected by two different stress regimes (FP1 and FP2 in Figure 3.13b) having perpendicular compressive stress axes to each other.

In the Karpuzçay Formation, the well-exposed small-scale folds are also observed (Figure 3.14). By using the strike and dip measurements, the attitude of the anticline axis is found N26W/82W with N28W/10 plunge. The interlimb angle of the fold is 101°, hence it is classified as an asymmetrical-open type fold.
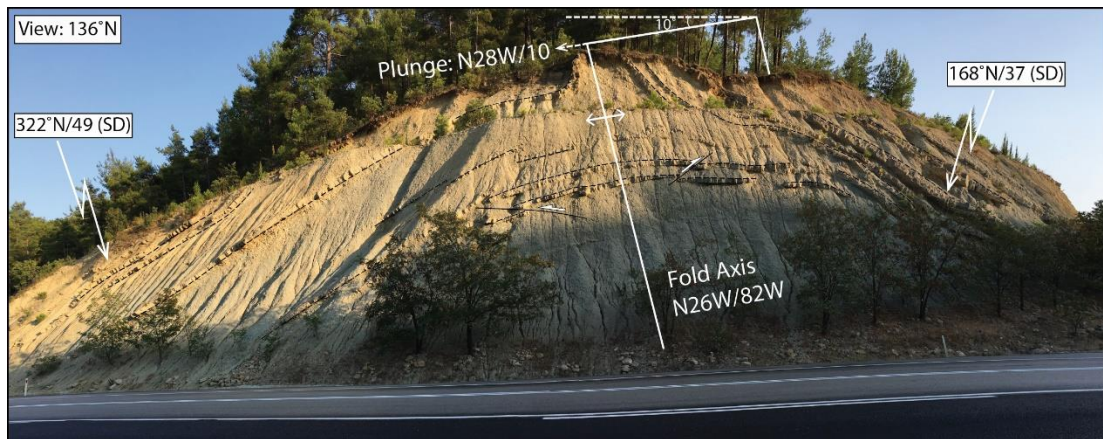
Figure 4. 14. A. Field view of the open type asymmetric anticline (with 101° interlimb angle) which is located at the center of the Aksu Basin, east of the Karacaören Dam Lake.

In general, based on the strike-dip measurements collected from the Aksu (including Kapıkaya and Karadağ Conglomerates) and Karpuzçay formations, several fold structures (series of anticlines and synclines) are observed and documented in this study (Figures 4.3, 4.13 and 4.14). The strikes of the fold axes are determined and a rose diagram is produced (Figures 4.3 and 4.15). The rose diagram indicates that the axes of the anticline and syncline display parallel-subparallel pattern with NNW-SSE direction, which may be interpreted as a major trend of folds axes.
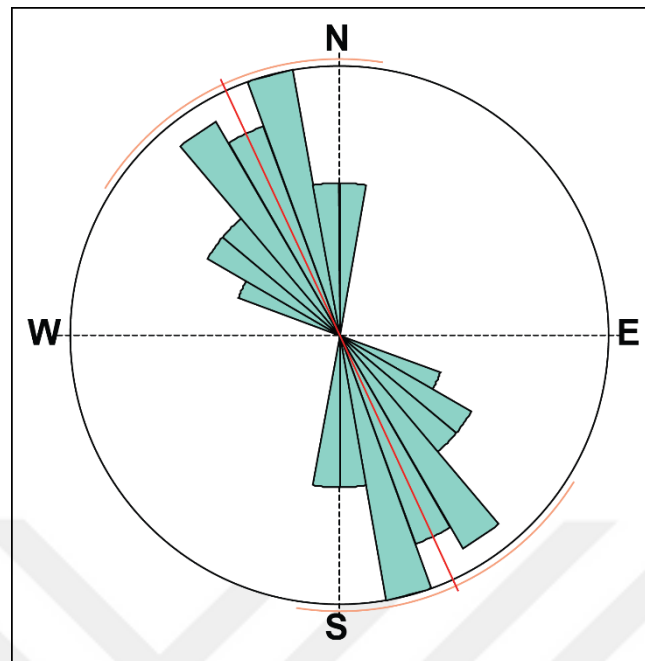
Figure 4. 15. Rose diagram is produced from the strike of the fold axes determined during the field study. The locations of these folds are indicated on the geological map given in Figure 4.3.

The limbs of folds are generally dip steeply with up to 90°. In order to perform overall fold analysis, poles to the bedding planes are plotted on the Schmidt lower hemisphere net (Figure 4.16). The average dip of the limbs are 42° (Limb 1) and 76° (Limb 2) whereas inter-limb angle is 62°. The overall fold axis is 328°N/70NE. Based on the stereographic plot, can be defined as asymmetric-tight fold.

The vergence direction can be specified from the asymmetry of the folds training in shear zone. The vergence is dominantly in the direction of thrusting took place. In that case, one limb is longer than the other. Based on this information, the vergence direction of the fold is determined from NE, which is consistent with the NNW-SSE oriented Aksu Thrust.
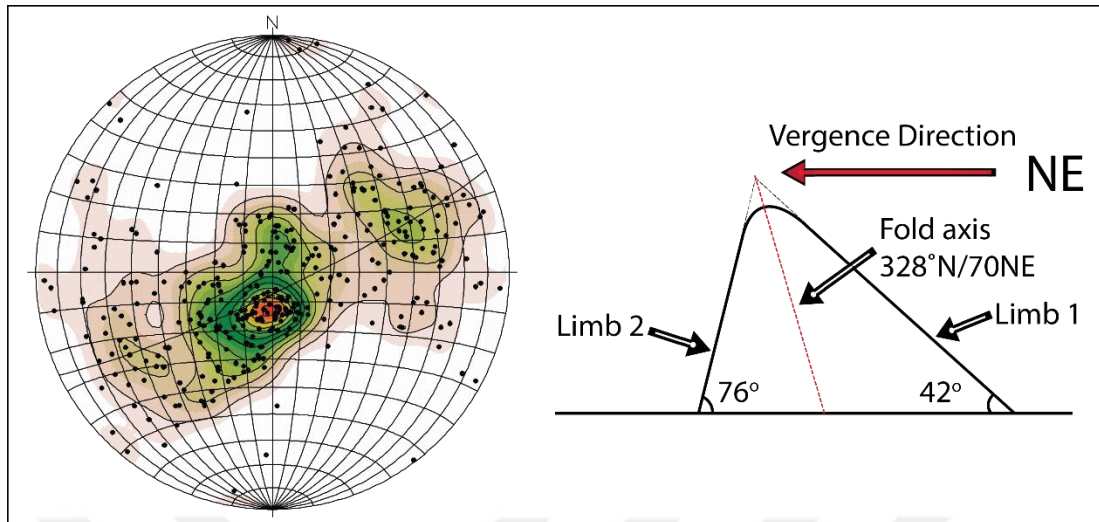
Figure 4. 16. Stereographic projection of the pole of the whole fold limbs (left) recorded in the Aksu Basin and graphical explanation of the stereographic plot (right).

5. DATA ANALYSIS

Addition to lithological and structural study, fault-slip data and Anisotropy of Magnetic Susceptibility (AMS) data were analyzed to clarify paleostress configuration during the Aksu Basin evolution.

5.1. Paleostress Analysis

A detailed kinematical analysis has been carried out using fault-slip data that were collected from mesoscopic faults in order to unravel stress conditions during the evolution of the Aksu Basin. The Gauss Stress Inversion method developed by Zalohar and Vrabec (2007) is applied to analyze fault-slip data. The T-Tecto software is used for reconstruction of the paleostress configurations. The detail information about this method is given in previous chapter (see Chapter 2, Section 2.2.2.3).

5.1.1 Data and Method

From 83 sites (Figure 5.1), 1175 fault-slip measurements including direction and sense of relative movements is collected (Figure 5.2a). Most of the paleostress data are from mesoscopic faults within the basin infill, and from faults juxtaposing Basement and basin deposits. A rose diagram is prepared from the strikes of the mesoscopic fault planes (Figure 5.2b) and shows clustering around NW-SE directions (~330°N), which is consistent with the general trend of the Aksu Fault. The dip amounts of fault- planes show a very broad range from 25° to 89° and the highest frequency lies between 70° and 80° (Figure 5.3a). Fault-slip data have also indicates that most of the faults in the measurement population have approximately 50° rake amount while amounts of the rake displays a very broad range from 10° to 89° (Figure 5.3b).

Inversion of the data collected from several sites are performed and 94 stress configurations are reconstructed. (Figure 5.4 and Table 5.1).
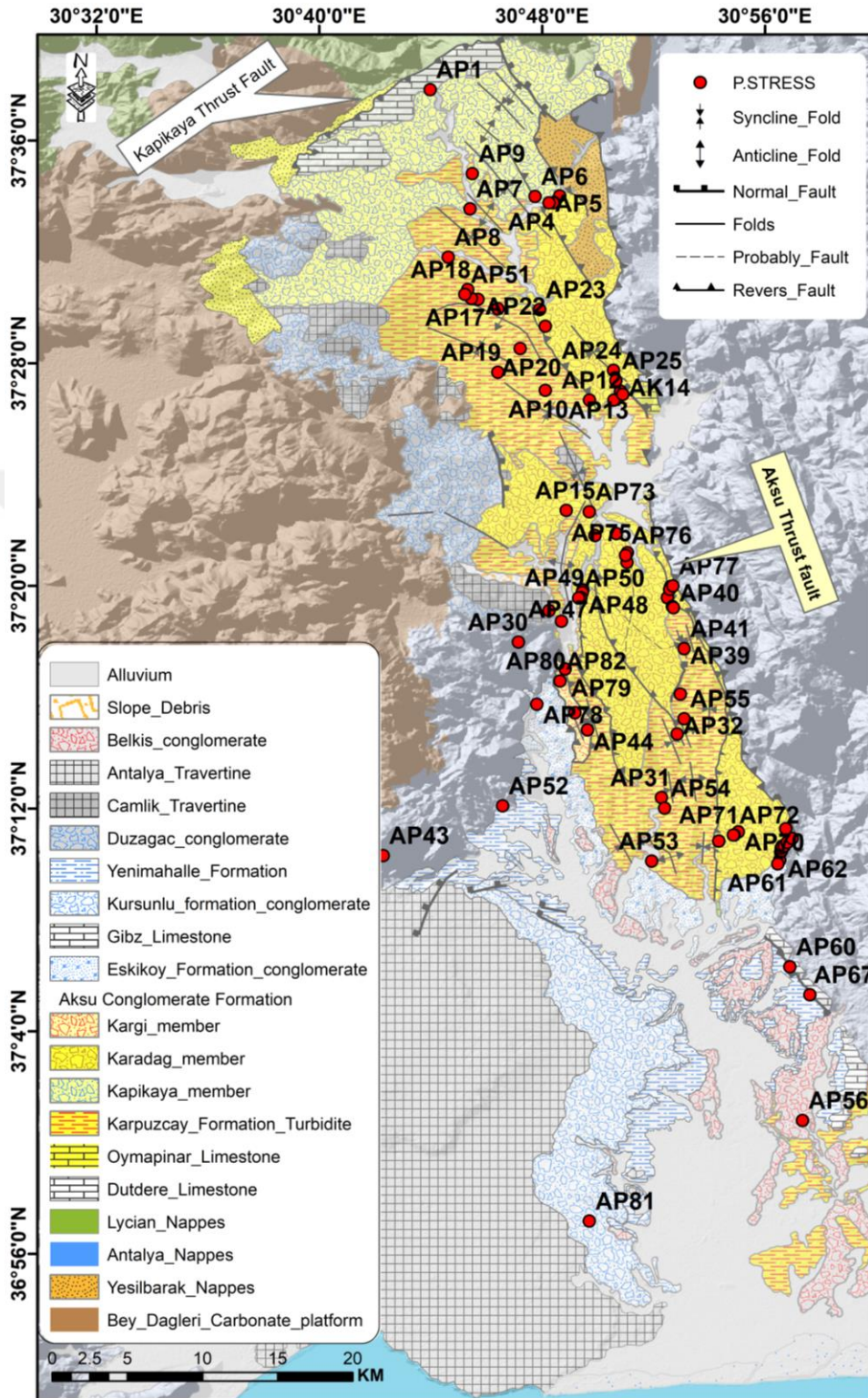
Figure 5. 1. Geological Map showing the location of paleostress sites (red circles) within the Aksu Basin (simplified from MTA 1/100.000 scale geological map series).

The Gauss stress inversion method (Zalohar and Vrabec, 2007) is also applied to analyze our fault-slip data. According to Zalohar (2007) approach, the best values obtained from the iversion method are: S=30°, Δ=60°, Ø1=60°, and Ø2=25°. Thus, 1027 fault-slip measurements are accepted while the program rejected 148 of them automatically. The rejected spurious data corresponds to 12.6 % of the whole data.
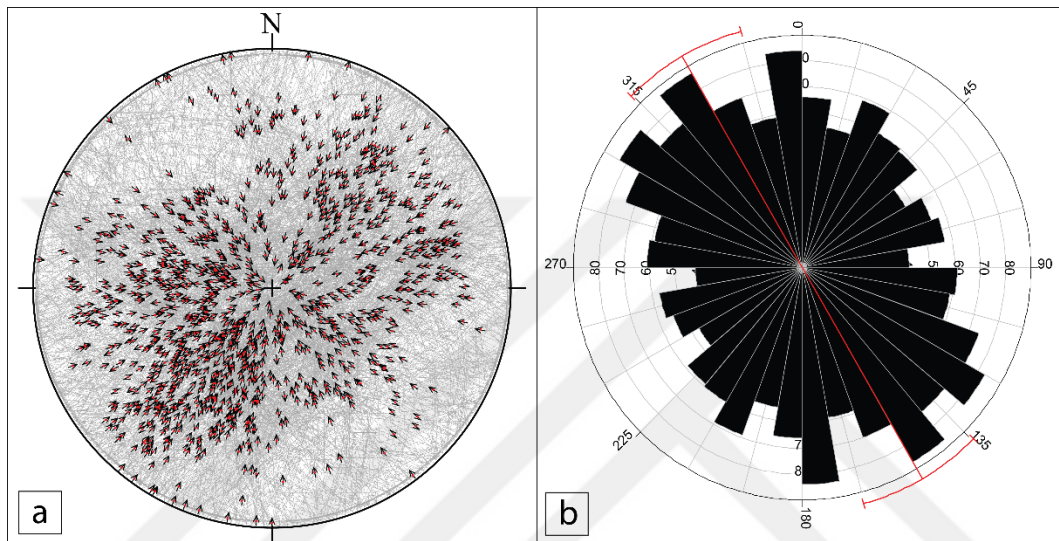
Figure 5. 2. a. Stereoplot showing all of the collected fault-slip data (N=1175), b. bi-directional rose diagram of fault strikes.
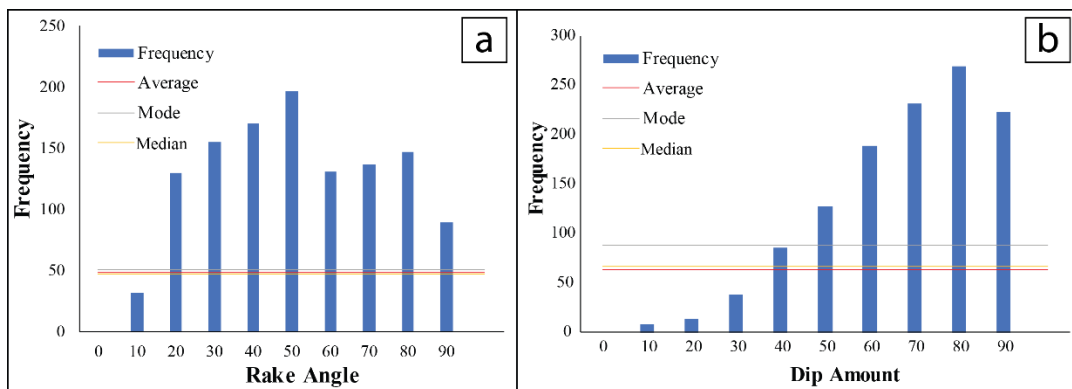
Figure 5. 3. a. Histogram showing the frequency distribution of rake (a) dip amount, b. of the whole fault-slip measurements.
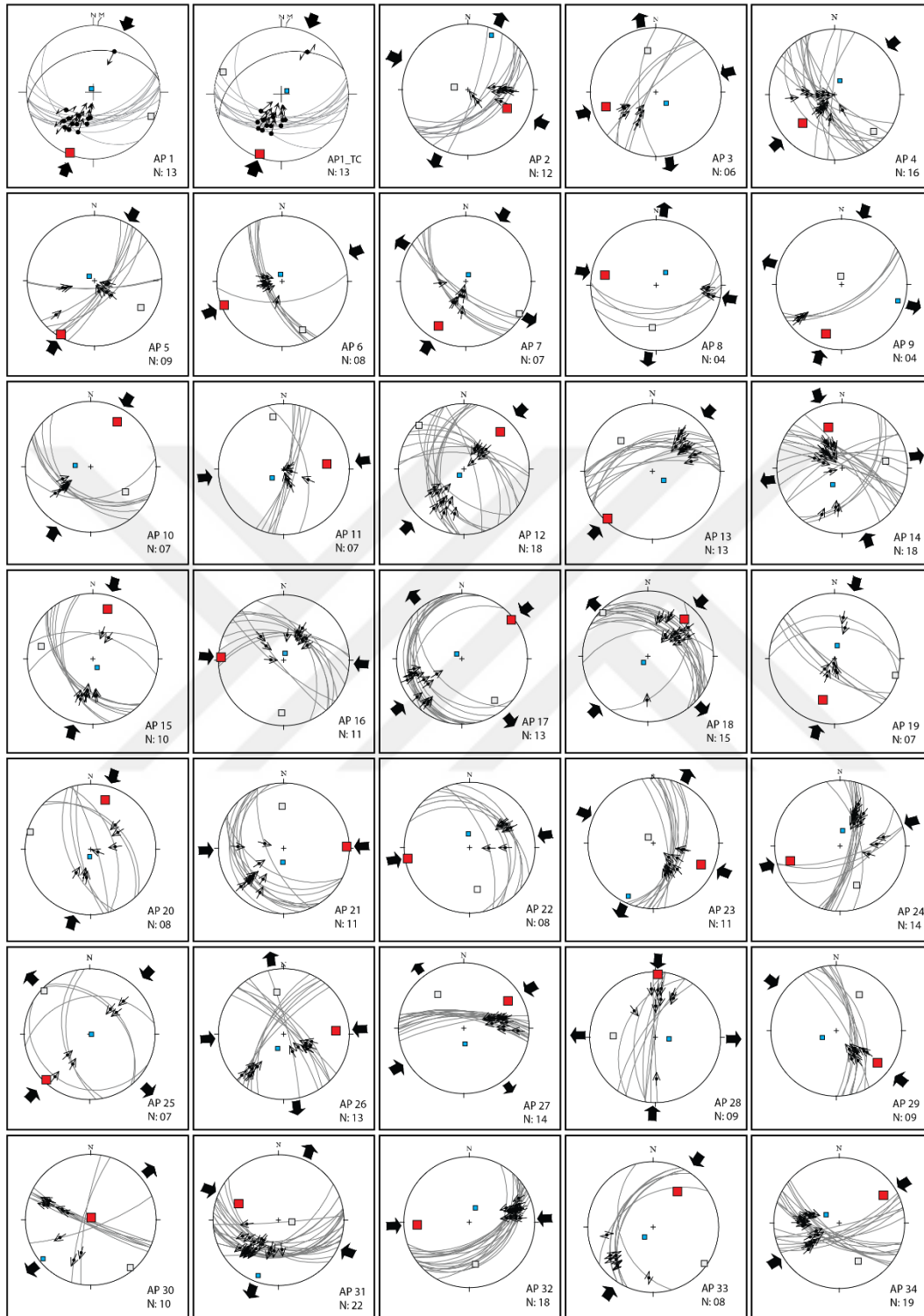
Figure 5. 4. The Stereographic plots of fault planes, slip-lines and constructed paleostress orientations on equal area lower hemisphere projection that measured from Aksu Basin.
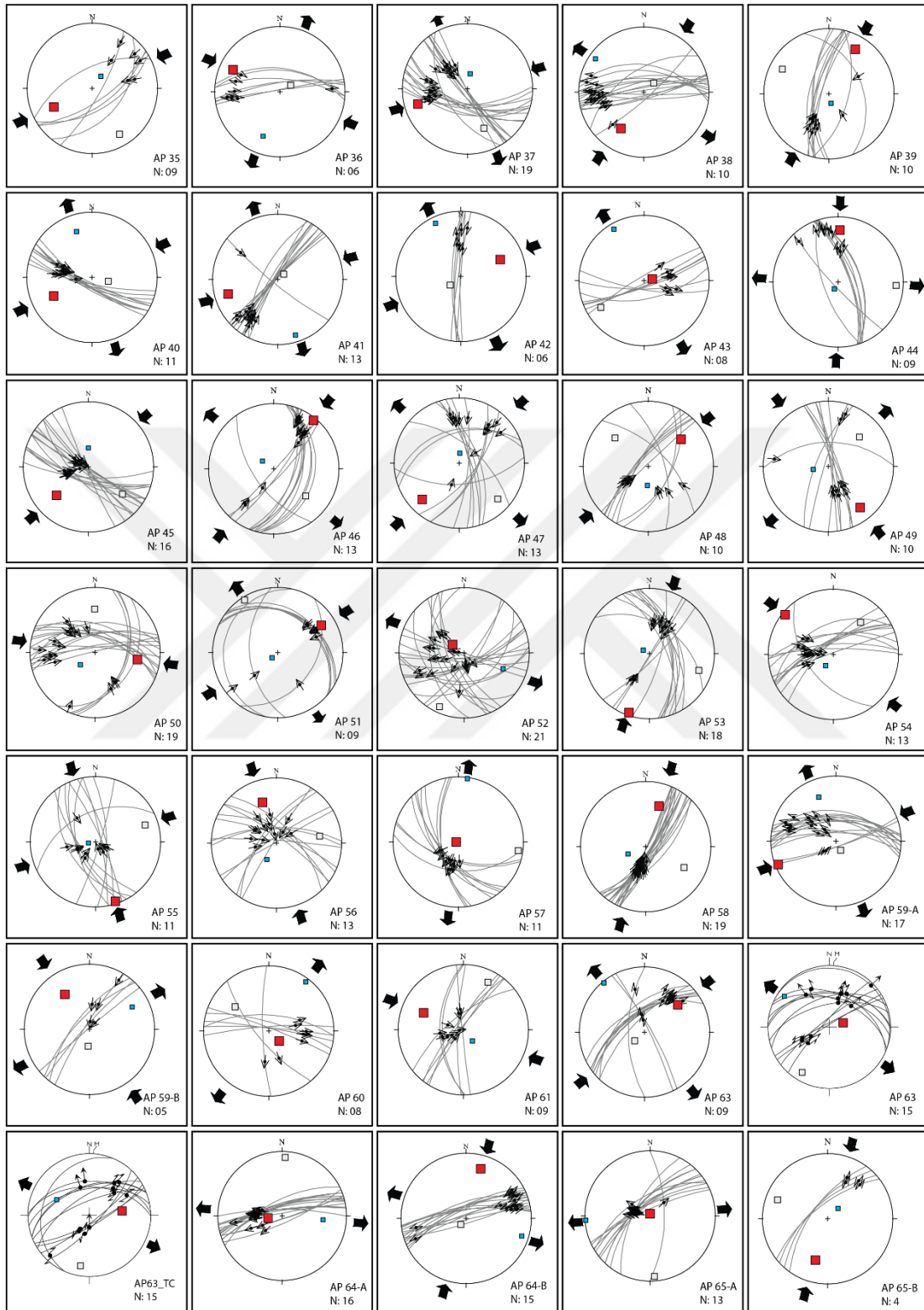
Figure 5.4. The Stereographic plots of fault planes, slip-lines and constructed paleostress orientations on equal area lower hemisphere projection that measured from Aksu Basin. (Continued)
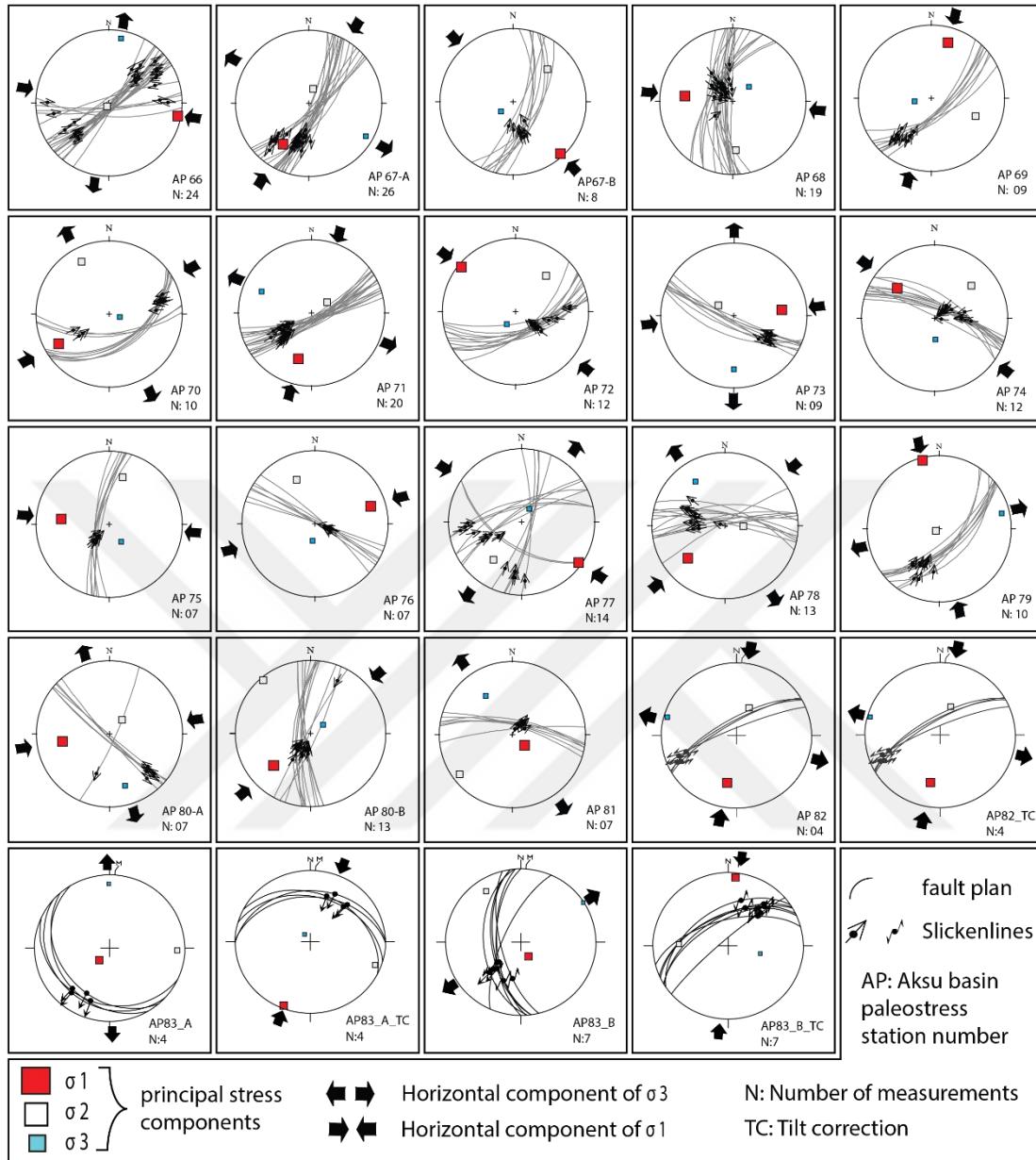
Figure 5.4. The Stereographic plots of fault planes, slip-lines and constructed paleostress orientations on equal area lower hemisphere projection that measured from Aksu Basin. (Continued)

Using the misfit criteria and separation procedure, the sites 59, 64, 65, 67, 80 and 83 produced two different paleostress configurations. The separated configurations are labeled as "B" and resultant stress configurations are depicted in Figure 3.28 and Table 4.1.

Table 5. 1. The Locations and paleostress orientations from the Aksu Basin. σ_1, σ_2, σ_3 major, intermediate, and minor principle stresses, D/P: direction/plunge, R (ϕ): stress ratio, Nc: number of measurements collected for each site Nu: number of measurements that accepted during analyzation and Ns: number spurious data.

Site	Long	Lat	σ1	σ2	σ3	R(φ)	Nc	Nu	Ns
AP1	30° 43' 57" E	37° 37' 46" N	202/04	112/03	342/85	0.3	13	13	0
AP1_TC	30° 43' 57" E	37° 37' 46" N	201/06	291/05	057/82	0.3	13	13	0
AP2	30° 48' 36" E	37° 33' 57" N	116/23	280/67	023/06	0.1	12	10	2
AP3	30° 48' 24" E	37° 33' 43" N	254/13	349/23	137/63	0.2	9	6	3
AP4	30° 48' 22" E	37° 33' 42" N	228/23	134/11	020/64	0.4	17	16	1
AP5	30° 48' 12" E	37° 33' 42" N	211/02	121/12	310/78	0.5	9	9	0
AP6	30° 47' 43" E	37° 33' 56" N	248/02	157/12	347/78	0.7	8	8	0
AP7	30° 45' 23" E	37° 33' 29" N	211/12	121/02	022/78	0.2	7	7	0
AP8	30° 44' 36" E	37° 31' 45" N	281/13	185/23	037/63	0.2	4	4	0
AP9	30° 45' 28" E	37° 34' 45" N	198/13	353/76	106/06	0.3	4	4	0
AP10	30° 48' 05" E	37° 26' 58" N	030/12	126/23	275/63	0.7	7	7	0
AP11	30° 49' 40" E	37° 26' 37" N	083/23	348/11	234/65	0.8	8	7	1
AP12	30° 50' 33" E	37° 26' 37" N	044/13	314/02	215/77	0.4	18	18	0
AP13	30° 50' 47" E	37° 26' 56" N	224/02	314/24	129/66	0.3	13	13	0
AP14	30° 50' 52" E	37° 26' 49" N	341/23	081/22	210/57	0.2	21	18	3
AP15	30° 48' 50" E	37° 22' 39" N	016/13	284/12	153/73	0.5	10	10	0
AP16	30° 45' 39" E	37° 30' 14" N	273/02	182/12	012/78	0.8	11	11	0
AP17	30° 45' 26" E	37° 30' 16" N	052/02	142/12	312/78	0.1	13	13	0
AP18	30° 45' 18" E	37° 30' 35" N	044/13	214/02	215/77	0.1	15	15	0
AP19	30° 46' 23" E	37° 27' 37" N	196/23	105/02	011/67	0.5	7	7	0
AP20	30° 47' 11" E	37° 28' 28" N	017/13	286/02	187/77	0.7	8	7	1
AP21	30° 46' 23" E	37° 29' 54" N	088/02	358/24	183/66	0.5	12	11	1
AP22	30° 48' 05" E	37° 29' 16" N	260/02	169/24	354/66	0.3	8	8	0
AP23	30° 47' 53" E	37° 29' 52" N	114/12	320/76	205/06	0.2	11	11	0
AP24	30° 50' 32" E	37° 27' 41" N	253/13	158/23	009/63	0.4	16	14	2
AP25	30° 50' 37" E	37° 27' 19" N	224/02	314/02	089/87	0.2	8	6	2
AP26	30° 49' 51" E	37° 21' 45" N	086/13	351/23	202/63	0.2	14	13	1
AP27	30° 51' 01" E	37° 20' 47" N	058/13	323/23	175/63	0.1	16	14	2
AP28	30° 52' 27" E	37° 19' 31" N	002/02	272/24	096/66	0.1	9	9	0
AP29	30° 48' 13" E	37° 19' 03" N	128/12	032/23	244/63	0.3	10	9	1
AP30	30° 47' 07" E	37° 17' 54" N	007/86	140/03	231/03	0.6	10	10	0
AP31	30° 52' 15" E	37° 12' 20" N	293/23	097/66	200/06	0.8	23	22	1
AP32	30° 52' 49" E	37° 14' 37" N	267/13	172/23	023/63	0.3	19	18	1
AP33	30° 52' 56" E	37° 16' 03" N	035/23	125/02	220/67	0.4	8	8	0
AP34	30° 52' 35" E	37° 19' 55" N	058/12	153/23	302/63	0.5	19	19	0
AP35	30° 52' 36" E	37° 19' 55" N	244/23	149/11	036/64	0.5	9	6	3
AP36	30° 52' 39" E	37° 19' 12" N	295/13	059/68	201/18	1.0	7	6	1
AP37	30° 52' 33" E	37° 19' 49" N	253/13	158/23	009/63	0.1	19	19	0
AP38	30° 52' 41" E	37° 19' 09" N	212/23	047/66	305/06	0.4	17	17	0
AP39	30° 53' 04" E	37° 17' 41" N	031/13	298/12	167/73	0.5	11	10	1
AP40	30° 52' 41" E	37° 19' 09" N	244/23	104/61	342/16	0.1	11	11	0
AP41	30° 53' 03" E	37° 17' 41" N	254/13	048/78	162/06	0.3	20	13	7
AP42	30° 54' 19" E	37° 10' 46" N	067/23	232/66	334/06	0.2	7	6	1
AP43	30° 42' 15" E	37° 10' 15" N	078/75	238/14	329/05	0.3	8	8	0
AP44	30° 49' 36" E	37° 14' 46" N	002/12	093/06	209/76	0..0	9	9	0
AP45	30° 49' 09" E	37° 15' 23" N	228/23	128/22	360/57	0.5	18	16	2

Table 5.1. The Locations and paleostress orientations from the Aksu Basin. σ_1, σ_2, σ_3 major, intermediate, and minor principle stresses, D/P: direction/plunge, R (ϕ): stress ratio, Nc: number of measurements collected for each site Nu: number of measurements that accepted during analyzation and Ns: number spurious data. (Continued)

Site	Long	Lat	σ_1	σ_2	σ_3	$R(\phi)$	Nc	Nu	Ns
AP46	30° 48' 40" E	37° 18' 40" N	039/02	130/24	305/66	0.1	14	13	1
AP47	30° 49' 26" E	37° 19' 47" N	226/13	133/12	001/73	0.2	23	13	10
AP48	30° 49' 25" E	37° 19' 42" N	050/23	311/22	182/57	0.9	10	10	0
AP49	30° 49' 22" E	37° 19' 31" N	142/12	047/63	258/63	0.2	17	10	7
AP50	30° 49' 17" E	37° 19' 30" N	099/23	359/22	231/57	0.5	22	19	3
AP51	30° 45' 11" E	37° 30' 24" N	058/13	328/02	228/77	0.1	9	9	0
AP52	30° 46' 33" E	37° 12' 02" N	305/65	204/05	112/24	0.1	21	21	0
AP53	30° 51' 54" E	37° 10' 03" N	199/02	109/12	298/78	0.4	18	13	5
AP54	30° 52' 22" E	37° 11' 57" N	309/02	040/24	215/66	0.5	15	13	2
AP55	30° 53' 04" E	37° 15' 10" N	162/02	071/12	261/78	0.9	15	11	4
AP56	30° 57' 19" E	37° 00' 44" N	341/23	081/22	210/57	0.3	16	13	3
AP57	30° 57' 35" E	37° 05' 15" N	270/86	098/04	008/01	0.3	13	11	2
AP58	30° 56' 30" E	37° 10' 05" N	018/23	118/22	247/57	0.9	25	19	6
AP59-A	30° 56' 32" E	37° 10' 22" N	248/02	151/72	339/18	0.6	18	15	3
AP59-B	30° 56' 32" E	37° 10' 22" N	325/23	184/61	062/17	0.2	7	5	2
AP60	30° 56' 52" E	37° 06' 15" N	133/65	306/25	037/03	0.6	10	8	2
AP61	30° 56' 26" E	37° 09' 57" N	293/23	027/11	141/65	0.4	16	9	7
AP62	30° 56' 34" E	37° 10' 25" N	051/23	228/67	320/01	0.0	17	13	4
AP63	30° 56' 33" E	37° 10' 31" N	072/70	211/15	304/12	0.4	15	15	0
AP63_TC	30° 56' 33" E	37° 10' 31" N	082/44	190/18	296/40	0.5	15	15	0
AP64-A	30° 56' 33" E	37° 10' 31" N	261/65	003/05	095/24	0.1	17	16	1
AP64-B	30° 56' 33" E	37° 10' 31" N	016/13	222/78	108/06	0.6	16	15	1
AP65-A	30° 56' 35" E	37° 10' 35" N	000/86	176/04	266/00	0.2	13	13	0
AP65-B	30° 56' 35" E	37° 10' 35" N	196/23	291/11	045/65	0.5	4	4	0
AP66	30° 56' 40" E	37° 10' 36" N	101/02	210/84	011/06	0.1	26	24	2
AP67-A	30° 56' 46" E	37° 10' 43" N	211/12	058/76	303/06	0.1	36	22	14
AP67-B	30° 56' 46" E	37° 10' 43" N	138/02	047/24	232/66	0.6	9	9	0
AP68	30° 56' 57" E	37° 10' 52" N	277/23	177/22	048/57	0.5	20	19	1
AP69	30° 56' 43" E	37° 11' 13" N	016/13	112/23	260/63	0.4	19	9	10
AP70	30° 55' 01" E	37° 11' 06" N	240/12	332/12	104/73	0.2	10	10	0
AP71	30° 54' 52" E	37° 10' 59" N	196/23	055/61	293/16	0.1	20	20	0
AP72	30° 54' 50" E	37° 10' 59" N	309/02	040/24	215/66	0.4	16	12	4
AP73	30° 49' 40" E	37° 22' 36" N	083/23	303/61	180/17	0.5	9	9	0
AP74	30° 50' 38" E	37° 21' 49" N	309/23	049/22	177/57	0.9	12	12	0
AP75	30° 51' 02" E	37° 21' 08" N	276/23	016/22	145/57	1.0	8	7	1
AP76	30° 50' 58" E	37° 21' 02" N	073/12	337/23	188/63	0.8	8	7	1
AP77	30° 52' 40" E	37° 19' 56" N	125/02	216/24	031/66	0.1	21	14	7
AP78	30° 47' 47" E	37° 15' 41" N	229/22	092/62	326/18	1.0	14	13	1
AP79	30° 48' 48" E	37° 16' 57" N	346/02	239/84	076/06	0.2	10	10	0
AP80-A	30° 48' 37" E	37° 16' 31" N	261/24	041/61	163/16	0.9	9	7	2
AP80-B	30° 48' 37" E	37° 16' 31" N	228/23	319/02	053/67	0.4	18	13	5
AP81	30° 49' 40" E	36° 57' 07" N	131/65	233/05	325/24	0.2	7	7	0
AP82	30° 48' 37" E	37° 16' 31" N	191/33	023/56	284/06	0.8	4	4	0
AP82_TC	30° 48' 37" E	37° 16' 31" N	192/34	021/56	284/04	0.8	4	4	0
AP83-A	30° 45' 23" E	37° 33' 29" N	359/13	092/11	221/73	0.7	4	4	0
AP83-A_TC	30° 45' 23" E	37° 33' 29" N	347/50	134/35	236/17	0.3	4	4	0
AP83-B	30° 45' 23" E	37° 33' 29" N	057/02	326/18	153/72	0.7	7	7	0
AP83-B_TC	30° 45' 23" E	37° 33' 29" N	105/55	273/35	007/06	0.7	7	7	0

5.1.2. Syn-sedimentary fault-slip data

One of the most problematic issues in the paleostress inversion studies is to date the constructed stress configuration (Kaymakçi, 2006). Dating of the stratigraphical horizons involved in faulting and the relationship between sedimentation and tectonics may help to solve this problem (Angelier, 1994). In this perspective, invaluable information for the dating of the constructed stress configurations is provided by syn-sedimentary structures (Figure 5.5a).
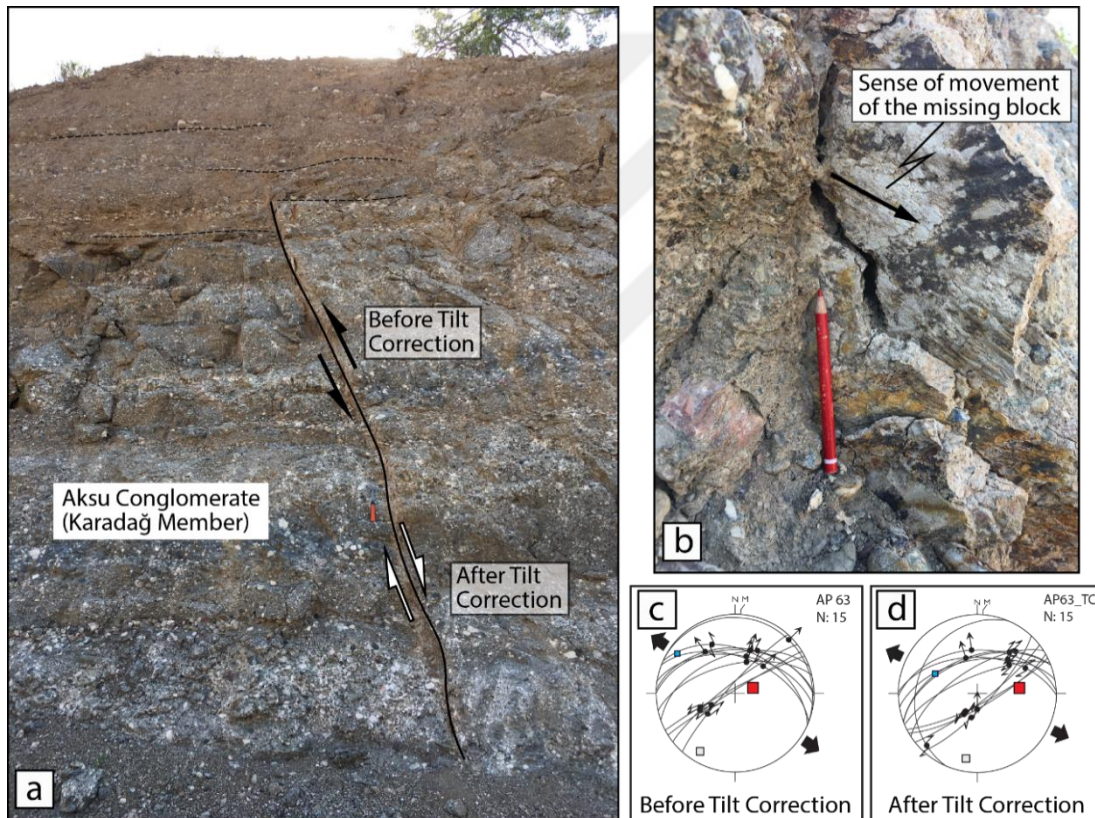
Figure 5. 5. a. Field views from a syn-sedimentary normal fault (Site 63) within the Karadağ Member of the Aksu Conglomerate, b. slickenside with slickenline indicate normal motion, c. reconstructed paleostress solution before, d. after tilt correction.

Syn-sedimentary faults were observed at sites (AP1, AP63, AP82, and AP83). From these sites, bedding altitudes are also measured to perform tilt correction. Pre- and

post-tilt resultant paleostress reconstructions of a syn-sedimentary normal fault within the Karadağ Conglomerate (Figure 5.5a) indicates a ~ESE-WNW extension.

Other syn-sedimentary faults are recorded (Site 83) within the Karpuzçay Formation (Figure 5.6a, b, and c). These faults seem to have a thrust fault character with low dip-angle (Figure 5.6a), However, after tilt correction, it is clear that these faults are syn-sedimentary normal faults.

Figure 5. 6. A, b. Syn-sedimentary normal faults (Site 83) within the Karpuzçay Formation, c) slickenside with slickenlines indicates normal motion, d, e. reconstructed paleostress solution before after tilt correction, respectively.

In Kapıkaya Conglomerate unit (Tortonien in age), site AP1 is recorded as syn-sedimentary fault (Figure 4.4 in Chapter 4). The reconstructed paleostress orientations show ~N-S compressional system, which corresponds to the strike of the Lycian Nappes.

Another syn-sedimentary fault in the Aksu Basin is observed in the relatively young sedimentary unit, namely Yenimahalle Formation (Figure 4.12a in Chapter 4). This

fault has nicely developed growth fault chacteristics and indicates NW-SE oriented extensional deformation.

5.2. Anisotropy of Magnetic Susceptibility (AMS) Analyses

In order to analyze the anisotropy of magnetic susceptibility (AMS), a total of ~490 oriented core samples of Middle/Late Miocene and Pliocene mudstone and fine sandstone units, from the 19 sites are collected (Table 5.2). The samples are analyzed at the Fort Hoofddijk Paleomagnetic Laboratory, Utrecht University, the Netherlands. The samples taken care from suitable locations to avoid secondary magnetization effects and lithological alterations onto the sedimentary rocks. The sampled locations (from AK1 to AK19) are shown in (Figure 5.7). The AMS specimens aremeasured with an automatic field variation (low field, 200 A/m) susceptometer using the Multi-Function Kappabridge MFK1-FA (AGICO-Brno, Czech Republic), equipped with an up-down mechanism and a rotator. The measurement sensitivity is 10^{-8} SI which is very critical for some sedimentary rocks (especially limestones) that exhibit very weak magnetic magnetization properties. Anisoft 4.2 data browser (Chadima and Jelink, 2009) is used for the display of AMS results and their density distributions by converting from specimen coordinates to geographic and tectonic coordinates (tilt corrected). The site mean AMS parameters are calculated according to Jelinek statistics (Jelinek, 1977; 1978) and tilt corrected results are given in (Table 5.2) and (Figure 5.8)
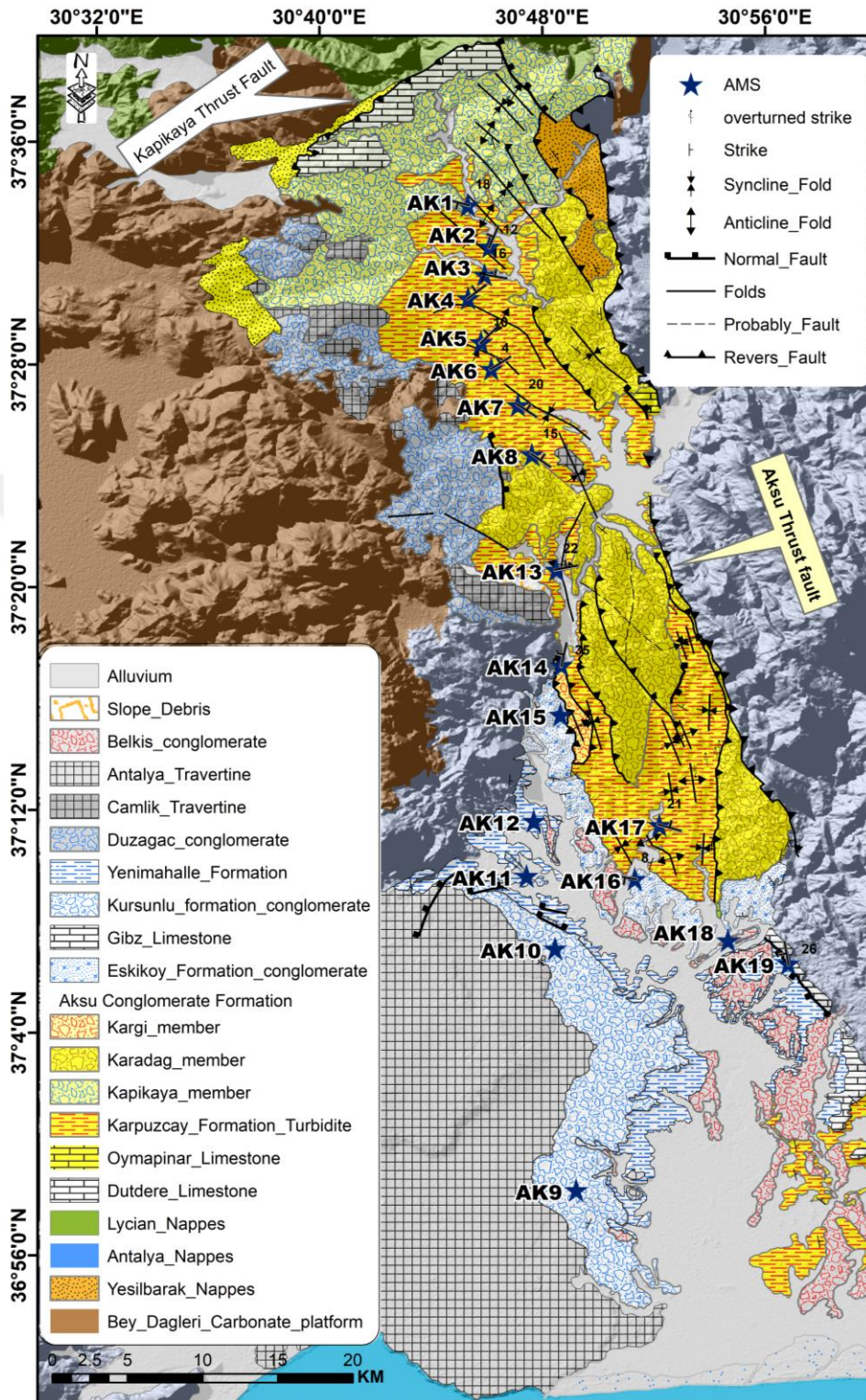
Figure 5. 7. Geological Map showing the location of 19 AMS sites (blue stars) within the Aksu Basin (simplified from MTA 1/100.000 scale geological map series).

5.2.1. Origin of anisotropy of magnetic susceptibility

To illustrate the rock magnetic mineral properties of all analyzed sites, mean susceptibility values (k_m) of all specimens collected from the Miocene and Pliocene sedimentary rocks are plotted (Figure 5.8 and Table 5.2). The k_m values show a rather wide range, from very low and even negative (-10, diamagnetism in few specimens) up to very high values of more than 6000×10^{-6} SI. In the Miocene results; there are two identical mean magnetic susceptibility clusters. The first grouped around $200\text{-}300 \times 10^{-6}$ (SI) and second one around $2000\text{-}3000 \times 10^{-6}$ (SI) that clearly higher than the first cluster (Figure 5.9a). Furthermore, the Flinn Diagram presents that the majority of the Miocene samples are oblate in AMS shape and only few of them are shows prolate in shape (Figure 5.9b, c). However, the Pliocene results present clearly low magnetic intensity and dominantly around 200×10^{-6} SI. When the Miocene and Pliocene samples are compared, it is clear that especially the Miocene specimens especially exhibit the highest susceptibilities and dominate the high susceptibility cluster. The k_m values show a wide range proving that the specimens include a varying composition and concentration of (ferro)magnetic minerals (Figure 5.9a).

The distributions of the susceptibility axes directions after tilt correction sites generally present a predominantly oblate shape (Figure 5.10a), which reflects the essentially sedimentary origin of the fabric (k_3 typically vertical and perpendicular to the bedding plane), but the clustering of the k_1 and k_2 axes reflect the type and magnitude of the tectonic deformation prevailing in the region (Figure 5.8). The mean foliation parameters (F) of the Miocene sites have some scatters in the range of $1.001 \leq F \leq 1.07$ ($F_{mean} = 1.027$). The range of site mean magnetic lineation (L) parameters of the Miocene sites, ranging between $1.00 \leq L \leq 1.008$ ($L_{mean} = 1.026$). Although Lmean is slightly higher than F_{mean}, it is clear from Figure 5.10b that the large majority of the foliation values is higher than the lineation values, reflecting the mainly oblate character of the distributions.

120

Table 5. 2. The anisotropy of magnetic susceptibility results (AMS) in Miocene to Pliocene sedimentary rocks at 19 sites.

Site	Lat. (N)	Long. (E)	N_{AMS}	Age	Bedding Azi/dip	$k_m*10^{-6}(SI)$	L	F	Pj	T	D/I (k_{max})	D/I (k_{min})	$e_1°$	$e_2°$	$e_3°$
AK9	36.9715	30.8199	32	Pliocene	000/00	9.01E-11	1.002	1.012	1.015	0.724	81.4/6.7	212.4/79.8	52.3	52.4	13.5
AK10	37.1161	30.8073	31	Pliocene	000/00	2.18E-10	1.007	1.01	1.017	0.209	127.4/12.4	237.3/57.1	28.6	38.9	36.4
AK11	37.1595	30.7902	29	Pliocene	000/00	1.40E-10	1.004	1.016	1.021	0.639	167.4/1.7	310.1/87.4	22.2	22.2	4.1
AK12	37.1925	30.7945	31	Pliocene	000/00	1.84E-10	1.005	1.019	1.025	0.587	147.8/2.5	339.7/87.4	12.2	12.2	5.9
AK18	37.121	30.9107	14	Pliocene	000/00	1.24E-10	1.003	1.01	1.013	0.542	351/7.6	202.5/81.1	21.6	21.4	10.1
AK1	37.5609	30.755	33	Miocene	101/18	2.42E-10	1.009	1.028	1.039	0.519	122.3/13.5	323.1/75.6	24.2	25	13
AK2	37.5364	30.768	39	Miocene	200/14	1.73E-09	1.013	1.043	1.059	0.537	345.4/16.1	128/70.1	18.9	22.7	14.9
AK3	37.5195	30.7651	41	Miocene	275/18	2.35E-09	1.014	1.027	1.043	0.306	353.5/36.7	218.4/43.6	11.4	12.2	10.3
AK4	37.5054	30.7552	35	Miocene	230/07	4.58E-10	1.02	1.022	1.042	0.047	318.1/12.2	179.2/74	7.3	9.7	8.1
AK5	37.4791	30.7629	28	Miocene	230/07	2.79E-09	1.029	1.023	1.053	-0.108	308/22.2	151.1/66.1	9	15.8	15.4
AK6	37.4631	30.7691	19	Miocene	235/04	2.12E-10	1.013	1.023	1.037	0.269	309/6.8	150.1/82.7	3.4	4.2	3.9
AK7	37.4414	30.785	24	Miocene	300/23	1.01E-09	1.024	1.01	1.035	-0.431	315.5/16.1	213.3/36.2	12.5	29.7	30.2
AK8	37.4119	30.7934	10	Miocene	300/16	1.98E-10	1.012	1.014	1.026	0.067	327.3/14.7	199.4/66.8	4.7	5	4.8
AK13	37.3429	30.8080	30	Miocene	256/21	1.91E-10	1.005	1.013	1.019	0.458	13.1/65.1	231.5/20	27.2	27.2	8.5
AK14	37.2857	30.8110	11	Miocene	190/36	5.53E-10	1.031	1.01	1.043	-0.518	340/26	111.9/53.8	5.7	15.9	16.1
AK15	37.2560	30.8104	10	Miocene	000/00	1.95E-09	1.014	1.01	1.025	-0.143	169.1/4.4	267.2/61.2	7.5	14.3	14.3
AK16	37.1577	30.8550	26	Miocene	098/08	1.02E-10	1.004	1.003	1.007	-0.175	358.9/16	222.9/68.3	39.5	39.9	31.4
AK17	37.1900	30.8697	36	Miocene	286/21	2.73E-09	1.017	1.034	1.053	0.316	312.9/16.2	188.1/63	28.8	30.4	19.4
AK19	37.1072	30.9468	14	Miocene	166/26	6.85E-11	1.006	1.009	1.016	0.179	308.5/11.7	60.3/60.8	11.6	22.1	22

N_{AMS}, number of studied samples at a site. k_m, site mean susceptibility in 10^{-6} SI. Magnetic lineation (L), magnetic foliation (F), corrected anisotropy degree (P'), and shape factor (T) according to Jelinek (1981). D and I are the *in-situ* site-mean declination and inclination, respectively, of the maximum susceptibility axis (k_{max}). $e_1°$, $e_2°$, $e_3°$ semi-angles of the 95% confidence ellipse around the declination of the k_{max}, k_{int}, k_{min}, respectively.
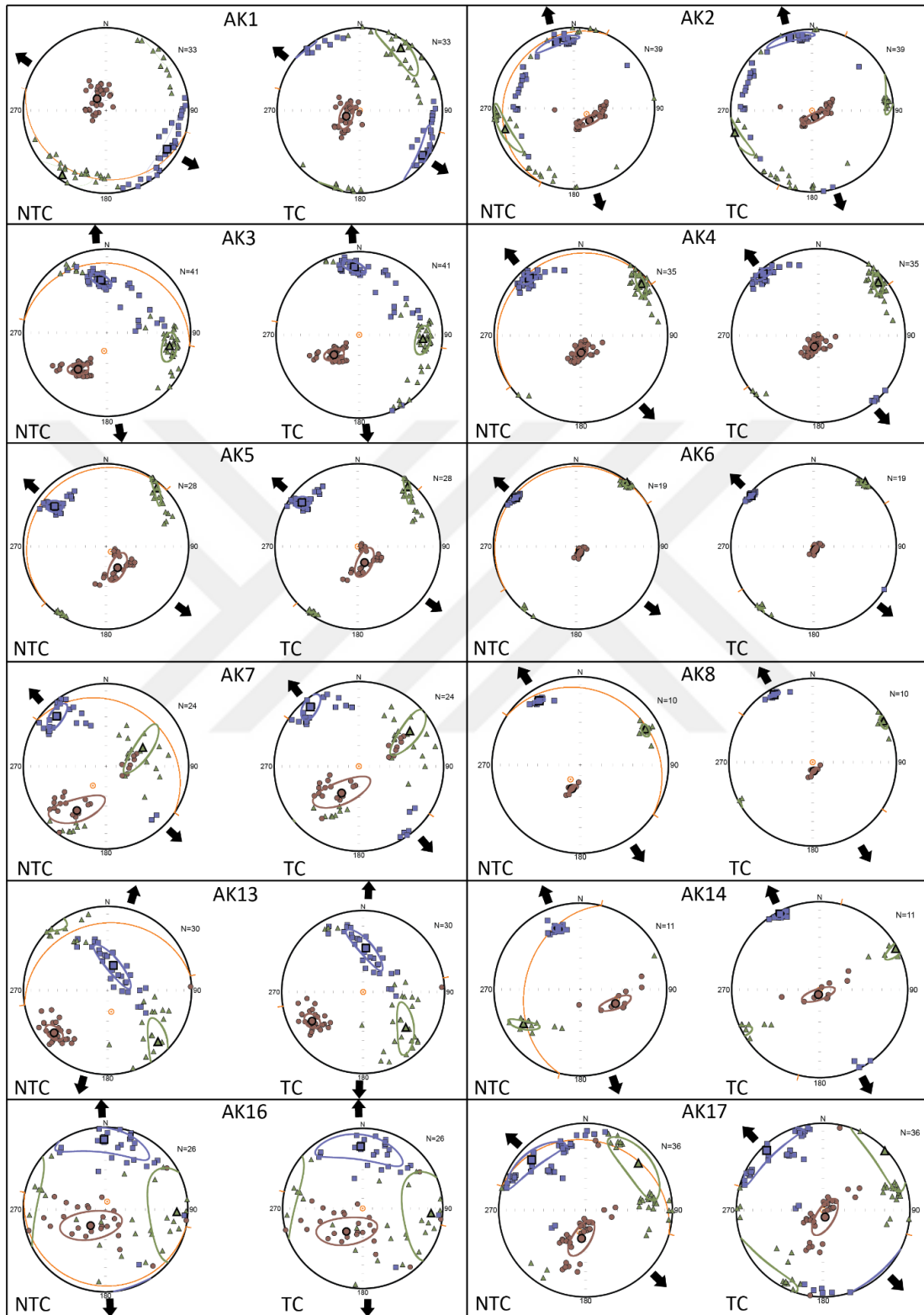
Figure 5. 8**.** The equal-area (lower-hemisphere) projection of the 19 AMS s site results before and after tilt correction. Black arrows indicate k_{max} mean direction.
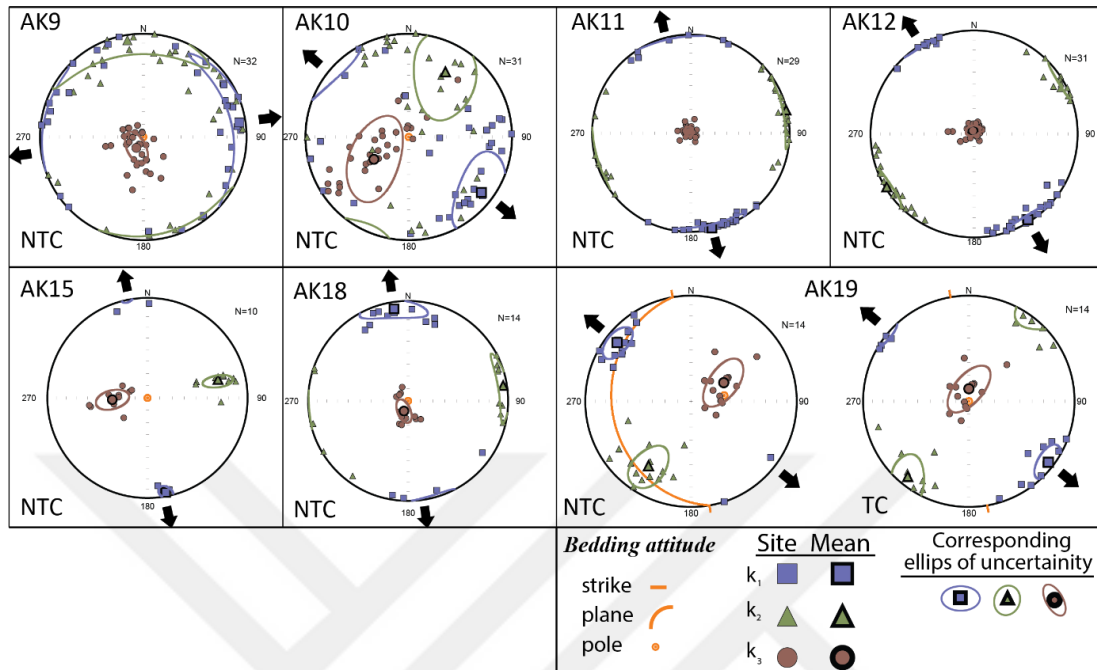
Figure 5.8. The equal-area (lower-hemisphere) projection of the 19 AMS s site results
before and after tilt correction. Black arrows indicate k_{max} mean direction.
(Continued)

The Pliocene sites present tighter cluster in both lineations and foliations results but slightly inclined to more oblate structure (foliated) than prolate shape (lineated) due to deformation which is probably sedimentary compaction (Figure 5.9b).

The corrected anisotropy degree Pj is relatively low in the Pliocene results with a dominant mean clustering around 1.02, although the results of the Miocene samples are significantly high (Pj mean:1.05) due to increased effect of the deformation. In general, the shape of the AMS ellipsoids is mostly moderately oblate (Figure 5.9c), but also negative T values (prolate) are also observed. We note that there is no evident correlation between T and Pj. Therefore, AMS results are not affected from the lithological variations or the temporal-spatial distribution of the sites, suggesting that AMS essentially determines the strain (Figure 5.9c).

According to the site means of corrected anisotropy versus shape parameter diagram (Figure 5.10a) of Miocene results; most of the sites represent oblate geometry except only five sites (AK16, AK15, AK14, AK7, AK5) which are close to neutral (T:0)

123

except the site AK14 gives prolate in shape. All the Pliocene sites give an oblate geometry and clearly faraway from the neutral axis. This indicates that the Pliocene sites are affected by deformation (Figure 5.7a).
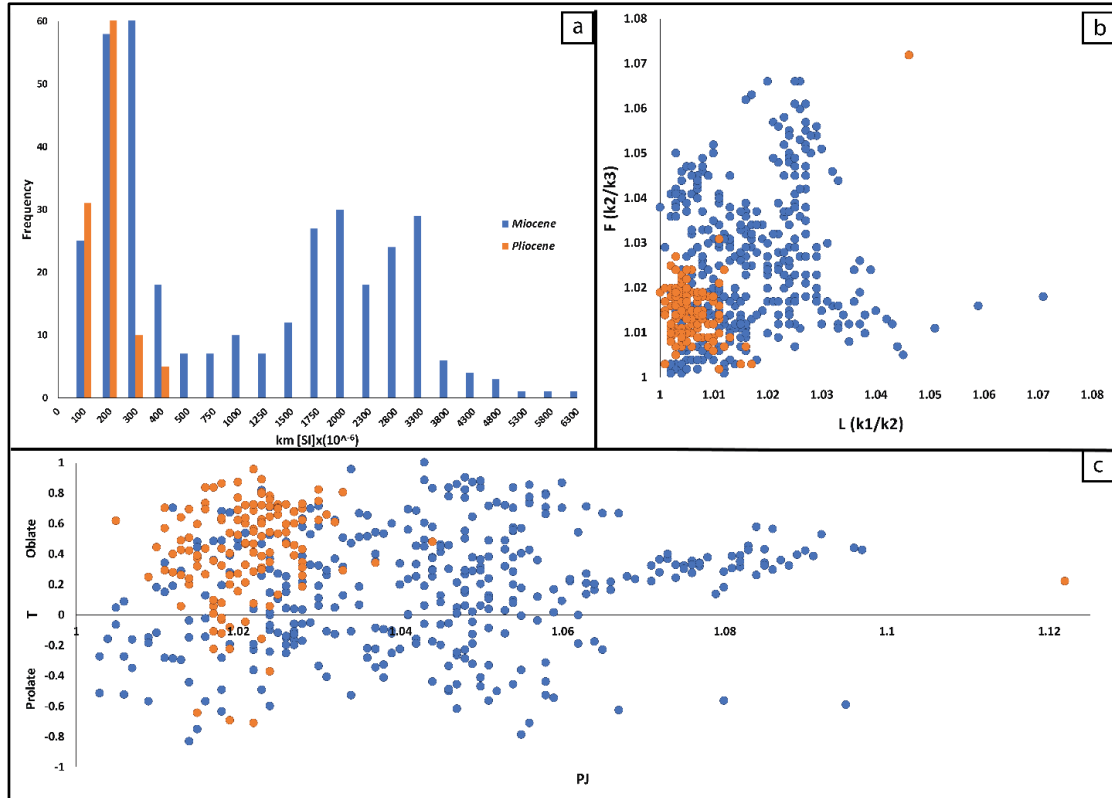
Figure 5. 9. Rock magnetic and Flinn and Jelinek diagrams of Miocene to Pliocene sites in the Aksu Basin. a. The mean susceptibility (km) versus frequency diagram, b. Flinn's diagram, and c. Jelinek diagram for Miocene to Pliocene sites in the area.

The Flinn diagrams of the site means have the similar results. Most of the Miocene sites (all Pliocene sites) show oblate geometry and few of them indicate neutral to prolate geometry (Figure 5.10b).
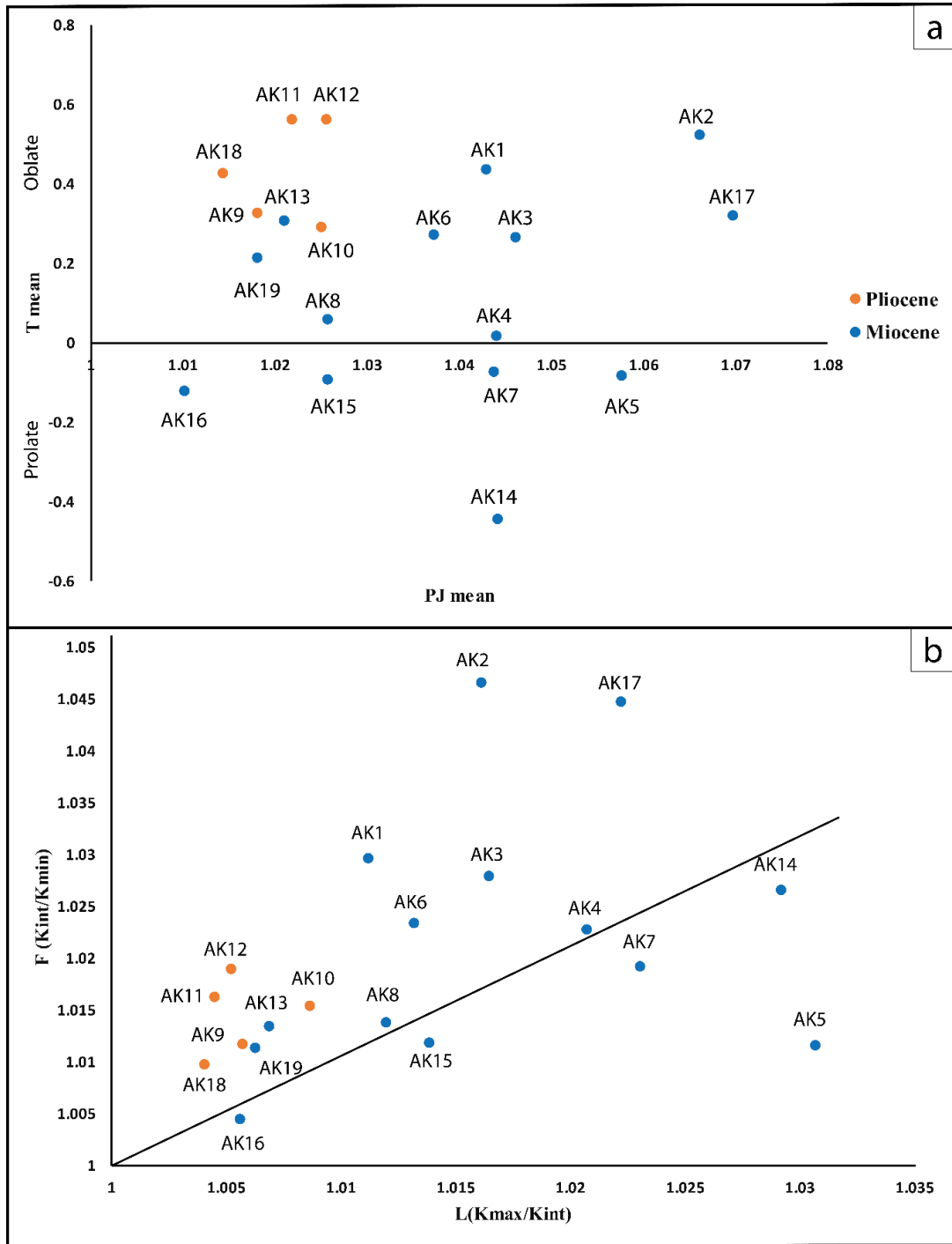
Figure 5. 10. Miocene to Pliocene site mean magnetic susceptibility plots of Jelinek (a), b. Flinn diagram results, respectively.

The equal area projections of the AMS ellipsoids from each of the 19 sampled sites before and after bedding plane correction are illustrated in Figure 5.8. Distributions of the maximum (k_{max}), intermediate (k_{int}), and minimum (k_{min}) susceptibility axes at the site level also exhibit a variable degree of clustering, from rather scattered (large confidence ellipses) to very well-defined clusters. Firstly, site based AMS results are compared with local deformation, secondly, location based AMS distributions are compared with deformation at the larger scale, and finally, we combined all AMS (location) data at the largest scale in the Aksu Basin, SW Anatolia.

5.2.1.1. Miocene AMS directions

For the Miocene sedimentary rocks, a total number of 356 samples from 14 different sites are analyzed in the Aksu Basin. The AMS directions of the Miocene sites (AK1, AK2, AK3, AK4, AK5, AK6, AK7, AK8, AK13, AK14, AK15, AK16, AK17 and AK19) are plotted on equal-area (lower hemisphere) projection and they clearly show a clustered geometry of (k_{min}, k_{int} and k_{max}). After tilt correction, the AMS directions generally stay in their positions and don't show any a big difference in the results (Figure 5.8).

There are two groups of maximum anisotropy of susceptibility direction in the Miocene results. In the first group shows approximately N to S k_{max} orientations in the sites AK3, AK13, AK15, and AK16. However, the rest of ten Miocene site results give an NW-SE orientation of the maximum susceptibility direction in the basin. The maximum susceptibility directions (k_{max}) in the most Miocene sites (AK1, AK2, AK7, AK8, AK13, AK14, AK17 and AK19) approximately parallel to local bedding planes while in some Miocene sites (AK3, AK4, AK5, AK6 and AK16) show the k_{max} orientations sub-perpendicular to the local bedding planes (Figure 5.8). According to the regional aspect; the k_{max} direction of some sites (AK1, AK2, AK3, AK4, AK5, AK6, AK7, AK8 and AK17) approximately give parallel to the local folding axis in the area (Figure 6.9). The k_{max} direction of the sites AK13, AK14 and AK15 orients parallel to the Aksu Fault plane (Kargı). The k_{max} of the site AK16 is parallel to the Aksu Thrust Fault, while k_{max} direction of AK19 is parallel to the Gebiz Normal Fault plane at the south-east

of the basin. Generally, k_{max} direction of the Miocene samples are changing between N-S and NW-SE direction and they are sub-parallel to parallel to the Aksu Thrust Fault.

5.2.1.2. Pliocene AMS directions

Total number of 137 samples from 5 sites are collected from the Pliocene sedimentary rocks (Table 5.2). The samples were collected from Pliocene sedimentary units (AK9, AK10, AK11 AK12 and AK18) are plotted on equal area (lower hemisphere) projection (Figure 5.8). Only two sites (AK9 and AK10) show slightly scattered in directions, they are disregarded for further analyses. The remained three sites (AK11, AK12 and AK18) make a cluster in three AMS directions and used to their directions in the statistics (Figure 5.8). All the Pliocene samples are collected from horizontal beddings (undeformed strata). The maximum susceptibility direction (kmax) of AK11 and AK12 are perpendicular to the local normal fault plane. The k_{max} of AK10 is directed NW-SE which is approximately parallel to those normal fault plane. The site AK18 gives approximately N-S k_{max} direction and orients perpendicular to the Aksu Fault Plane

Despite there are three Pliocene sites are remained, again two different k_{max} orientations can be classified. The AK11 and AK18 show an almost N to S k_{max} orientations but the site AK12 slightly switches to NW-SE orientations similar to Miocene results (Figure 5.8).

6. RESULTS AND DISCUSSIONS

This chapter integrates and synthesizes the information presented in the preceding sections. In this regard, stratigraphic and structural relationships together with light of paleostress and AMS data are integrated in local and regional context. In doing so, in addition to newly provided information previous studies are also incorporated extensively. Finally, the tectonic and paleogeographic settings of the Aksu Basin are discussed within the geodynamics of Eastern Mediterranean region.

6.1. Evaluation of the Paleostress and AMS Data

One of the most problematic issues in the paleostress inversion studies is about the interpretation of the constructed stress configuration. Dating of the stratigraphical horizons involved in faulting and the relationship between sedimentation and tectonics may help to overcome this problem. In this perspective, it is tried to construct paleostress stratigraphy, asexplained below in detail.

6.1.1. Interpretation of the Paleostress Data

The interpretations of reconstructed principal stress orientations help us to understand the stress regimes that are effective on the evolution of the Aksu Basin. In this point of view, the detailed data analyses are performed to understand the nature of the stress regime, and compatibility of the principal stress orientations with structural elements in the Aksu Basin. Figure 6.1 shows that σ_3 is generally oriented (sub-) vertically in most of the sites, whereas σ_1 and σ_2 are located (sub-)horizontal with well-clustered consistent directions. Such distribution is characteristics for tri-axial stress conditions. The dominant deformation that affected the Aksu Basin is obviously compressional, as indicated by the vertical σ_3, and this consistent with thrust activity along the major Aksu thrust in the basin. The ϕ ratio approaching zero value means that the σ_2 and σ_3 are very close to or equal in magnitudes while the σ_1 magnitudes are much

grater than that of σ_2. As seen in Figure 6.1d, the frequency distribution of ϕ ratio has peak value at 0.1, however, most of the data, in more than 60 sites ϕ values are less than 0.5. This means that the trans-pressional to pure compressional stress conditions is dominant in the region.
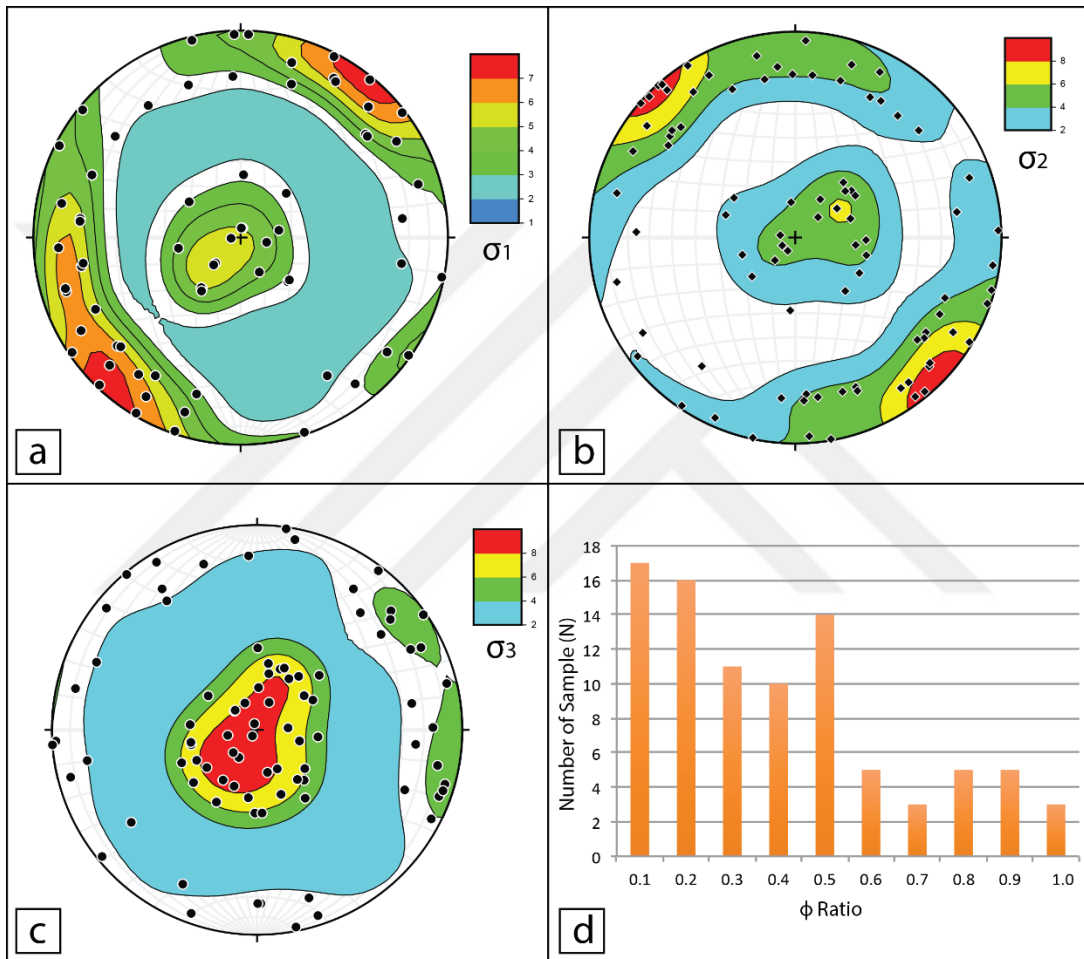
Figure 6. 1. Density diagrams for principal stress orientations, a. σ_1, b. σ_2, c. σ_3 and frequency distribution of the ϕ values. Notice that the σ_3 is dominantly sub-vertical while σ_2 and σ_3 orientations are sub-horizontal with well-developed directions.

In order to verify the compatibility of the reconstructed paleostress configurations relative to the structural component of the Aksu Basin, horizontal components of maximum (σ_1) or minimum (σ_3) principal stress plotted on the map given in Figure 6.2 (north of the basin) and Figure 6.3 (south of the basin).
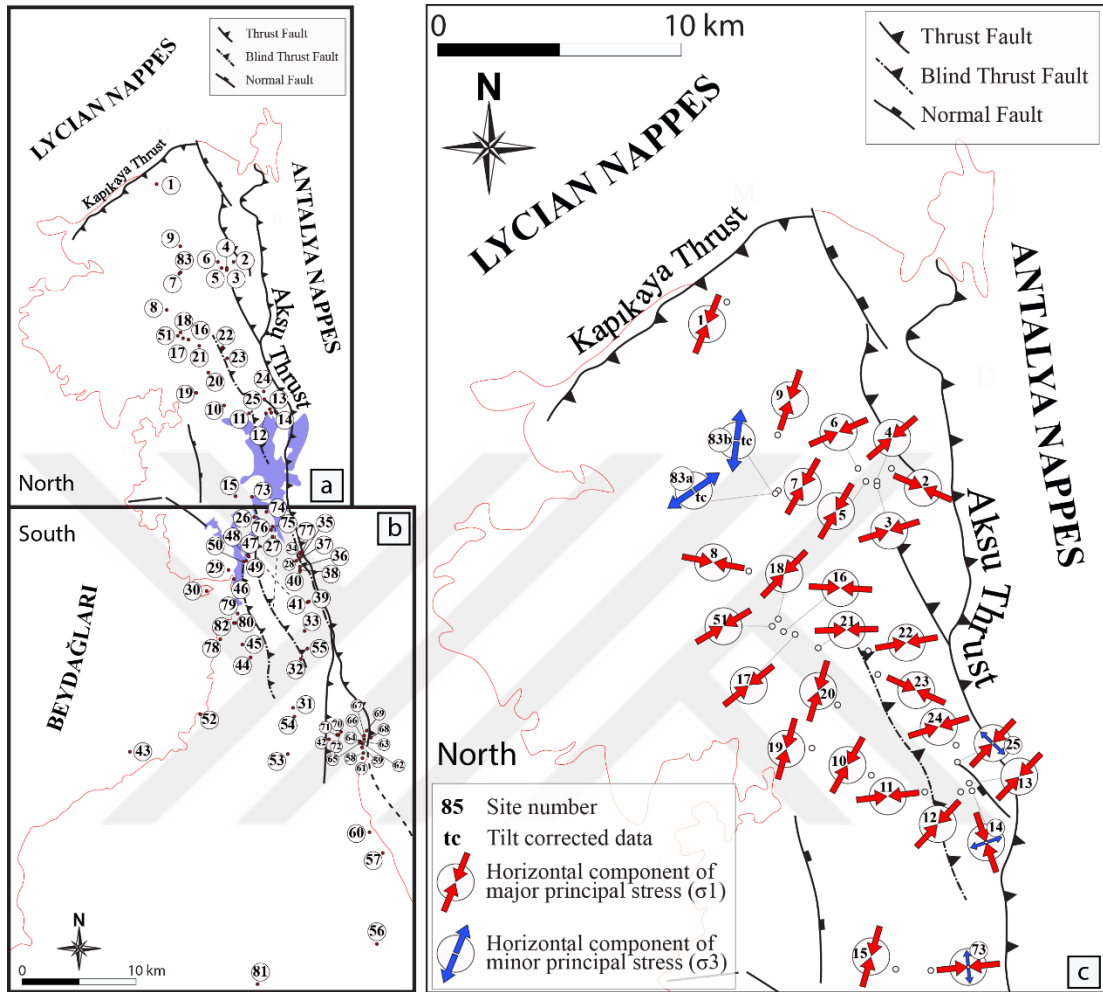
Figure 6. 2. a and b. Map indicates the site location of the Aksu Basin and major faults of the Aksu Basin, c. Spatial distribution of the horizontal component of the major (red) and minor (blue) principal stress (σ_1) in the northern part of the Aksu Basin.

In the Aksu Basin, there are recorded two major fault trends. The one is strikes in ENE-WSW direction and corresponds to the Kapıkaya Fault set. The second and the most prominent fault set is oriented in NNW-SSE direction, which corresponds to the Aksu Fault Zone. Apart from some normal fault solutions (sites 30, 43, 52, 57, 59, 63, 64a, 65, 81, and 83a) most of the σ_1 directions are (near-) orthogonal to these dominant trends of the major structures.

Figure 6. 3. A Spatial distribution of the horizontal component of the major (red) and minor (blue) principal stress (σ_1) in the southern part of the Aksu Basin (Figure 6.2a), b. Detailed view of the subset as indicated by black Rectangle in (a).

.

This pattern implies two directional compressional tectonic regimes, which may work simultaneously or at different times or may overlap (diachronous) within a certain time. The sites with strike-slip solutions are indications of transfer faults and/or stress permutations due to relaxation of local stress.

In addition to compressive stress, there are some locations (sites 30, 43, 52, 57, 60, 63, 64, 65, 81 and 83) with normal fault solutions, as not expected in compressional stress regimes. In this point of view, temporal changes of the paleostress configurations throughout the basin stratigraphy are very important to qualify the tectonic evolution of the basin (Kleinspehn et al., 1989; Koç et al., 2012).

In the paleostress stratigraphy, the basement rocks potentially contain the entire paleostress history during the basin subsidence, whereas basin strata record paleostress tensors that were coeval with sedimentation. Kleinspehn et al. (1989) reported that structures developed in the uppermost basin fill offer insight into only the youngest tectonism. It means that the younger tectonic event needs to be extracted from the older ones, and then it should successively be performed from younger to older. Therefore, the paleostress data is ordered according to the age of the rock from which they were collected (Figure 6.4).

The youngest, possibly still active extension direction in the Aksu Basin, is not reflected any major structure on the surface, indicated by paleostress site 81. The trend of the extension direction is determined as approximately NNE-SSW. At sites 57 and 60, maximum (σ_1) principal stresses are vertical and minimum (σ_3) principal stress are located at the horizontal plane, which indicates approximately N-NE extension direction. These data are collected within the Gebiz Limestone and its age is determined as Messinian to Early Pliocene (Poisson et al., 2003 and 2011). In the Karpuzçay Formation, only one site (site 31) are found, which may be related to the recent tectonic regime (Figure 6.5). Resolved principal paleostress axes are compatible with the data collected from the Gebiz Limestone and minimum (σ_3) principal stress is approximately N-S in direction. The extensional tectonic regime indicated above is possibly related to recent tectonic regime, which is possibly active after Early Pliocene (Figure 6.4).
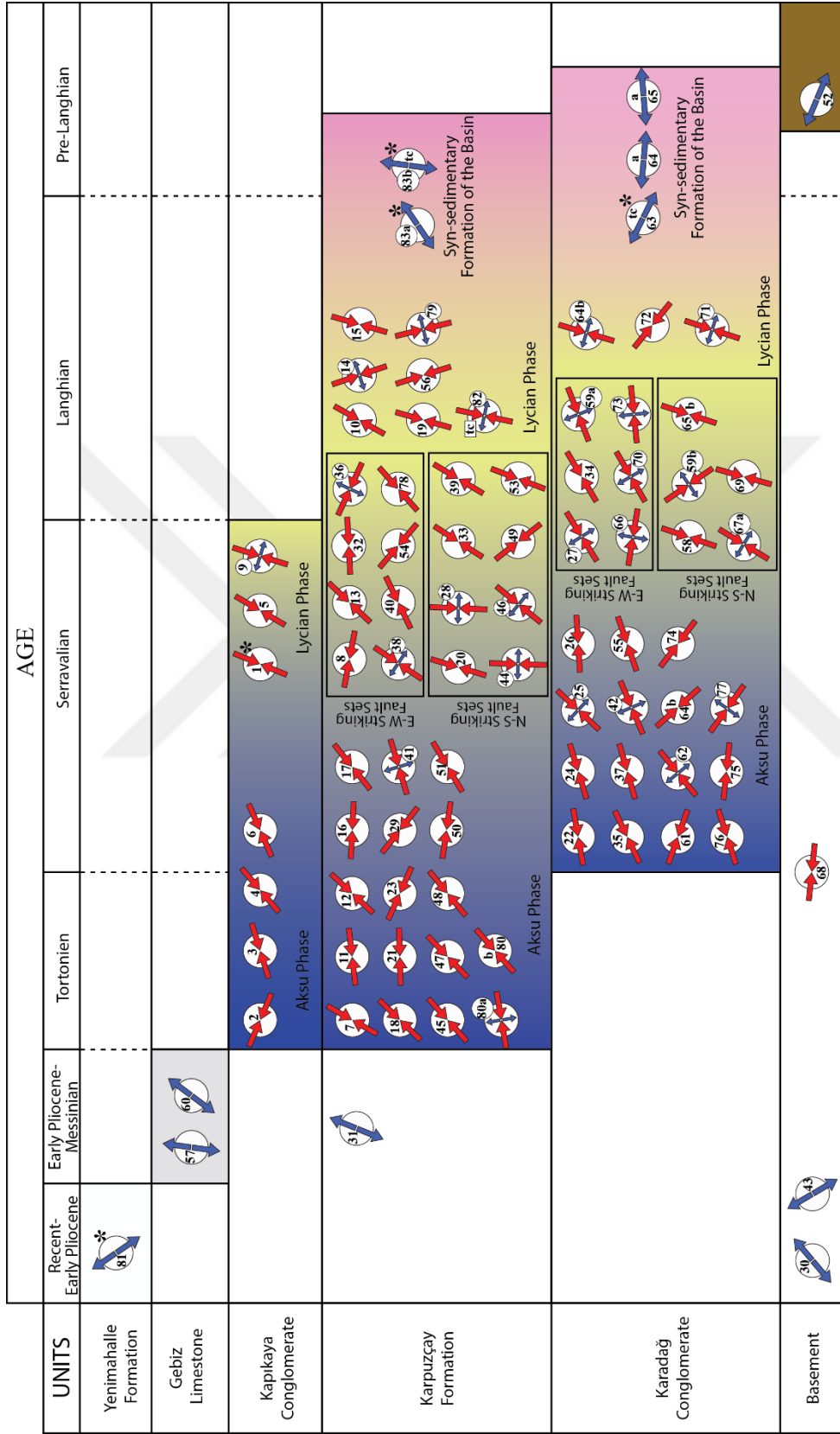
Figure 6. 4. a) Paleostress stratigraphy of the Aksu Basinfrom the Miocene to Recent. Arrows represent σ_1 (red) and σ_3 (blue) directions.

133

The paleostress stratigraphy also indicates that there is roughly E-W compressional tectonic regime. It has been defined as the "Aksu Phase" defined by (Poisson, 1977; Poisson et al., 2003; 2011). The compression direction is reflected by Aksu Thrust and the effect of this tectonic regime can be observed in Karadağ and Kapıkaya Conglomerates, Karpuzçay Formation and partly the Gebiz Limestone. The northern edge of the Gebiz limestone has more steep dip amount (more than 50°) than the southern edge (10-15°). The data sets given above and the previous sections enable us to constrain the timing of Aksu Fault activity. Based on the lithological, structural and paleostress stratigraphy data (Figure 6.4), the Gebiz Limestone is the youngest unit that is affected from the Aksu Thrust and tectonic regime was changed from compressional to the extensional after the Late Pliocene that is the youngest age for the Gebiz Limestone.
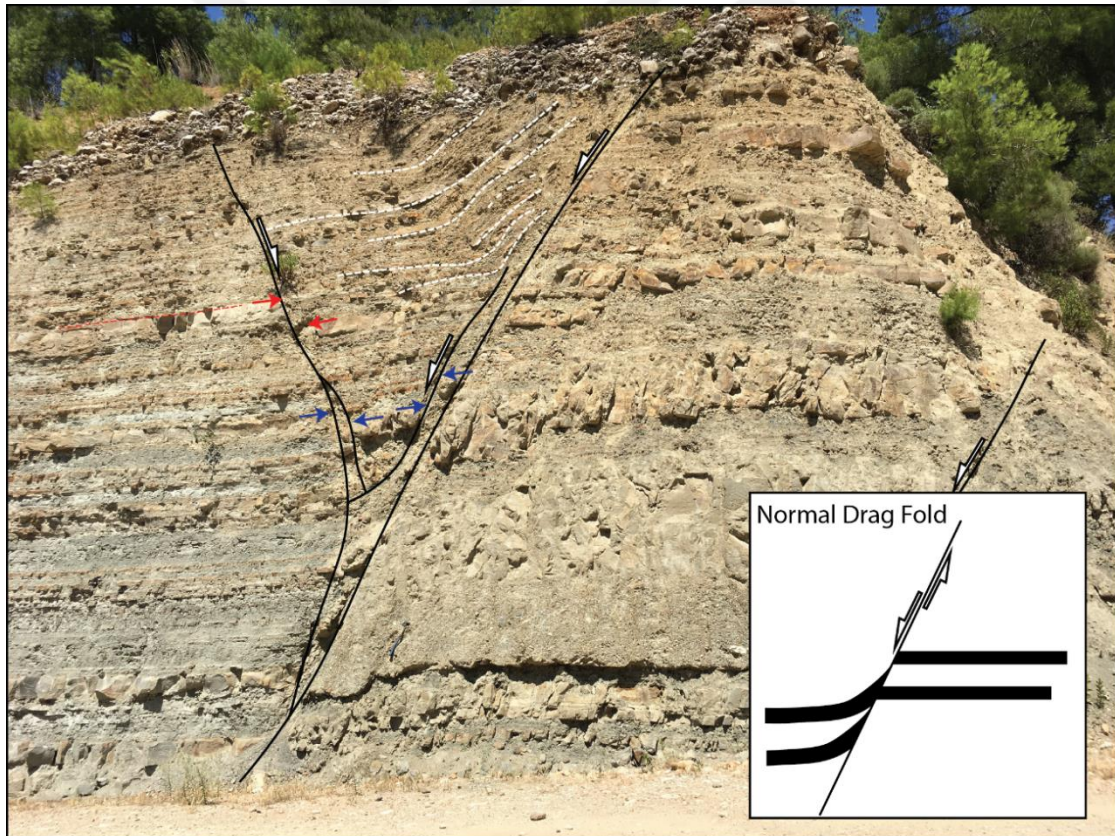
Figure 6. 5. Field view of the normal drag fold which is observed in the Karpuzçay formation. Data collected from this location is given in Site 31.

Kapıkaya Conglomerate also contains imprints of two different tectonic phases. First data set characterizes an E-W compressional stress regime and it is clearly defined as Aksu Phase (sites AP2, AP3, AP4 and AP6), the second data set is significantly different from the Aksu phase and indicates roughly N-S compressional stress (sites AP1, AP5 and AP9). Among these data AP1 is syn-sedimentary and gives the stress orientation during the sedimentation. This phase is possibly related to the Kapıkaya Fault which defines the emplacement of the Lycian Nappe units. Hayward (1984) suggested that the last emplacement of the Lycian Nappes prevailed until at the end of the Tortonian while Flecker et al. (2005) claimed that final emplacement of the Lycian Nappes occurred during or after Langhian times. In this study, the record of the roughly N-S compressional stress in the Kapıkaya Conglomerate may relate to pulses of the Lycian Nappes advance and associated nappe-stack geometry.

In the Karpuzçay Formation, four different stress orientations are recorded (Figure 6.4). These are 1) approximately N-S oriented recent stress orientation, 2) compressional stress with E-W direction (namely Aksu Phase), 3) roughly N-S compressional stress which is related to Lycian Nappe emplacement and 4) N-S and NE-SW oriented extensional stresses inferred from the syn-sedimentary fault (site 83) in the lower level of the Karpuzçay Formation.
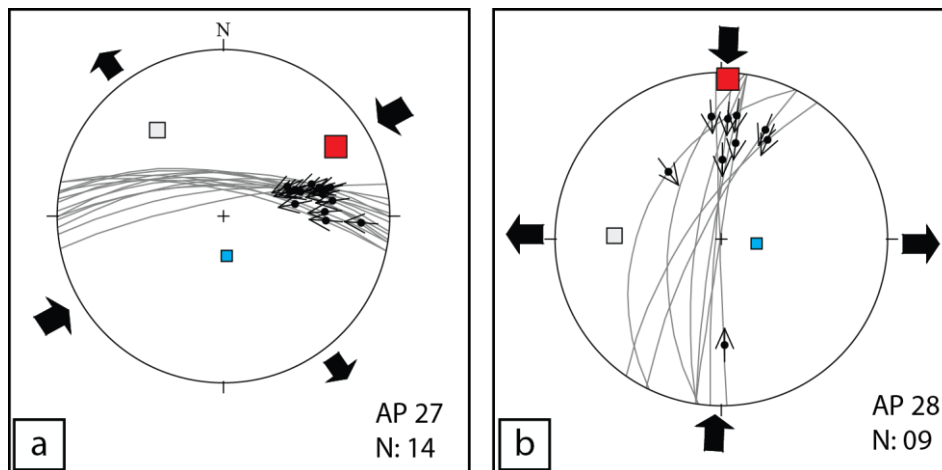
Figure 6. 6. Strikes of the faults and the principal stresses of corresponding stress regime may be not compatible with each other (maximum principal stress axes is E-W oriented).

Apart from these data sets, in some sites, we noticed that strikes of the faults and the principal stresses of corresponding stress regime are not compatible with each other for pure compressional stress regime. In Figure 6.6a, E-W striking faults are observed under roughly E-W compressional stress regime, they are part of the Aksu Fault. Mainly N-S oriented faults are expected under this stress condition. It is interesting to note that many are oriented E-W, nearly perpendicular to the strike of the east-bounding Aksu Fault. On the other hand, N-S striking faults are compatible with the Aksu Phase, but resolved stress condition does not fit this stress regime (Figure 6.6b). These solutions which are given in Figure 6.6 as an example may be interpreted in two different ways: 1) these faults may be inherited from the previous tectonic regime (Figure 6.7a) and they are therefore reactivated structures or 2) these faults may be transfer faults linking two thrusts (Figure 6.7b).
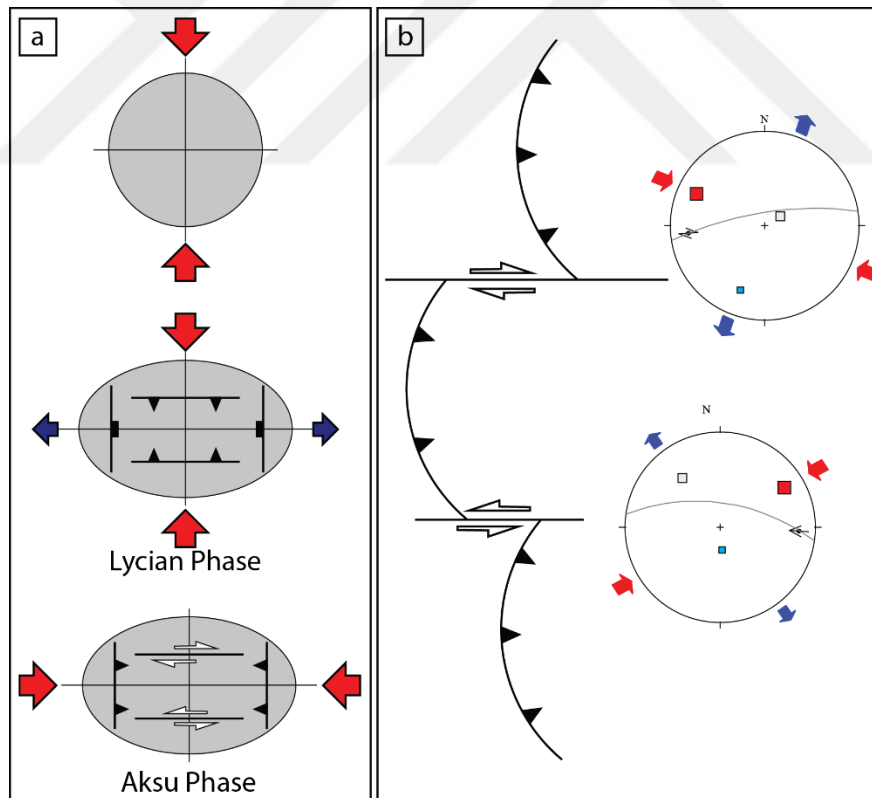
Figure 6. 7. a. Illustration indicates the movement of the faults which are inherited from the previous stress regime, b. transfer faults linking two thrust faults may also produce different paleostress solutions compared with the prevailed stress regime.

Similar resolved paleostress orientations are observed in the Karadağ Conglomerate (Figure 6.4). In addition to these stress configurations, NW-SE and roughly E-W oriented extensional stress configurations are also recorded from the superimposed slickenline sets (sites 63*, 64a and 65b) determined on the fault plane in the Karadağ Conglomerate. The slickenlines with ~45-50° rake -its solution gives E-W extension- cut by the ones with rake of ~15-20° – its solution refers to N-S compression- (Figure 5.4. This indicates the E-W extension is older than the N-S compression. Therefore, this E-W extension may be interpreted as the stress regime that results in the formation of the Aksu Basin during the Langhian time.

Kinematic studies performed in the Aksu Basin (Glover and Robertson, 1998a; Poisson et al., 2003; Üner et al. 2015) indicates at least three main deformation stages; 1) NW-SE compression associated with the emplacement of the Lycian Nappes (Hayward, 1984; Flecker et al., 1998), 2) NE-SW compression known as the Aksu Phase (Poisson, 1977; Poisson et al., 2003 and 2011) and 3) E-W or NE-SW extension which is the last tectonic phase is responsible from the opening of the Kovada Graben during Late Pliocene to Recent (Poisson et al., 2003 and 2011). Our results from the Aksu Basin further demonstrate that apart from the Lycian and Aksu phases there are some differences in tectonic phases throughout the basin history. These are; 1) E-W extension recorded in the older units including Karpuzçay, Karadağ and Basement unit are defined as the first phase and 2) N-S extension is defined as the last phase.

Within this compressional context, very few extensional features obviously relating to the formation of the Aksu Basin are apparent. In this study, E-W extension (Langhian) is defined as the first phase that is responsible for the formation of the Aksu Basin. Flecker (1995) also reported that NE-SW oriented normal faults, but the author claimed that it is not possible to be absolutely certain that these faults are Miocene in age. Dominant normal fault orientation is shown in Figure 6.8 and strikes ENE-WSW. These faults are Langhian in age and their genesis may be related to the onset of the basin formation.
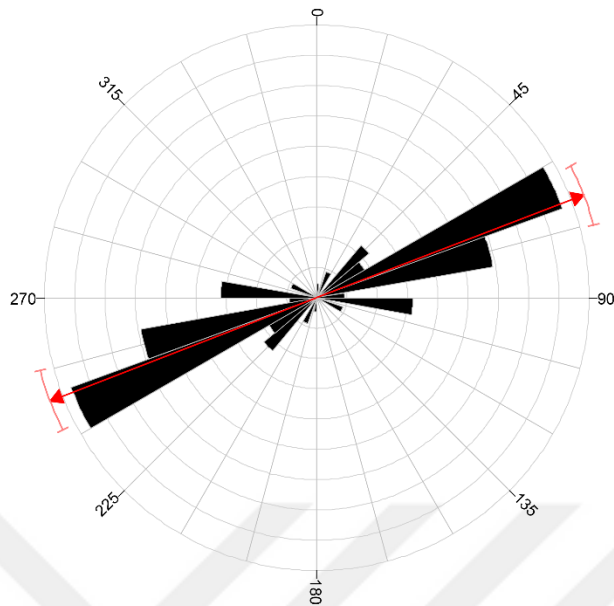
Figure 6. 8. A Rose diagram of the fault strikes that are collected in the Karadağ and Karpuzçay formations. The resolved stress orientation is E-W extension, which is responsible for the formation of the Aksu Basin.

Stress orientation of the Neotectonic period is extensional in character. The direction of extension in the Aksu Basin is ranges from NW to NE and change locally (Figure 6.3). Similar stress configuration is also reported in Isparta Angle and the surrounding regions (Koç et al., 2012, 2016; Koçyiğit and Özacar, 2003; Koçyiğit and Deveci, 2007). Especially data from the Miocene continental basins located in the center and eastern limb of the Isparta Angle indicates the multi-directional extension has likely being active since at least Middle Miocene (Koç et al., 2016). On the other hand, the recent extensional regime in the Aksu Basin has just started after Late Pliocene.

6.1.2. Interpretation of the AMS data

Analysis of the AMS is used to establish tectonic history in the deformed sediments of the Aksu Basin, since it may reflect the regional stress field (Tarling and Hrouda, 1993). It means that AMS can be used as an independent method helping to construct the paleostress stratigraphy and also to test the constructed paleostress stratigraphy.
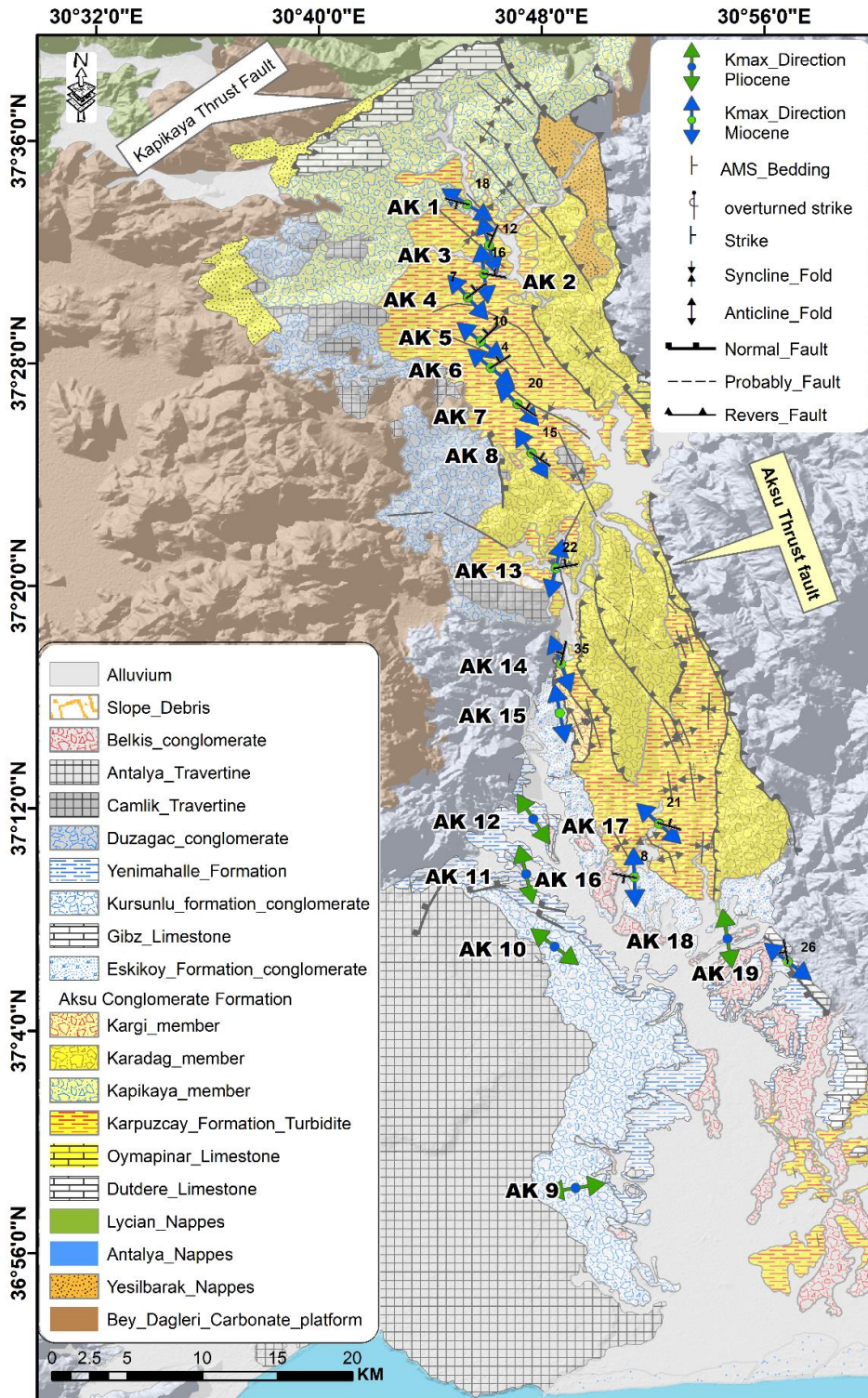
Figure 6. 9. Geological Map showing mean maximum susceptibility directions (arrows) in 19 sites within the Aksu Basin (simplified from MTA 1/100.000 scale geological map series).

.

The AMS analyses are conducted on samples from 19 sites in the sedimentary units (contains mudstone, siltstone and fine sandstone) of the Aksu Basin (Figure 6.9). Ages of the samples ranges from Miocene to Pliocene.

The AMS results generally show mainly oblate ellipsoid. Except for Pliocene samples (AK11, AK12, and AK18), the Kmin axes have slightly deviated from the pole of the bedding plane (Figure 6.10) and this suggests that the magnetic fabrics of the detrital sediments are shaped by tectonic deformation. Kmin axes of the AK11, AK12, and AK18 are close to the pole of the bedding plane, which means that they retain much of their original sedimentary fabric. Sites AK9 and AK10 show slightly scattered in directions (Figure 6.10) probably due to having diamagnetic susceptibilities or adverse magnetic properties and these sites are excluded them for further analyses.

The significant clustering of the K_{max} axes indicates that deformation has caused the K_{max} to align along the direction of maximum extension or perpendicular to maximum compression. In the Miocene samples, the mean AMS shapes are slightly prolate and the K_{min} axes are not all perpendicular to the bedding plane. This may imply a possible transitional fabric between weak and stronger deformation. The Miocene sedimentary rocks of the Aksu Basin reveals K_{max} axes ranging from N-S (sites AK3, AK13, AK15 and AK16) to NW-SE (sites AK1, AK2, AK4, AK5, AK6, AK7, AK8, AK14, AK17 and AK19) alignment, implying N-S to NW-SE extension or E-W to NE-SW compression (Figure 6.10). From north to the south, the K_{max} directions do not change geographically and they are (sub)parallel to the NNW-SSE oriented main Miocene thrusting direction (Figure 6.9).

In the Pliocene samples (AK11, AK12 and AK18), deformation related AMS patterns are marked by well-defined foliations coinciding with bedding poles and distinct magnetic lineation's with low error ellipsoids (Table 5.2, Figure 6.10). In these samples, the clear clustering of maximum anisotropy axes in the horizontal plane are identical and it suggests that deformation is weak and only Kmax is affected. This helpsto establish the sequence of the tectonic stresses that have been prevailed in the basin. In Pliocene samples, the mean orientations of the AMS lineation are approximately NNW direction.
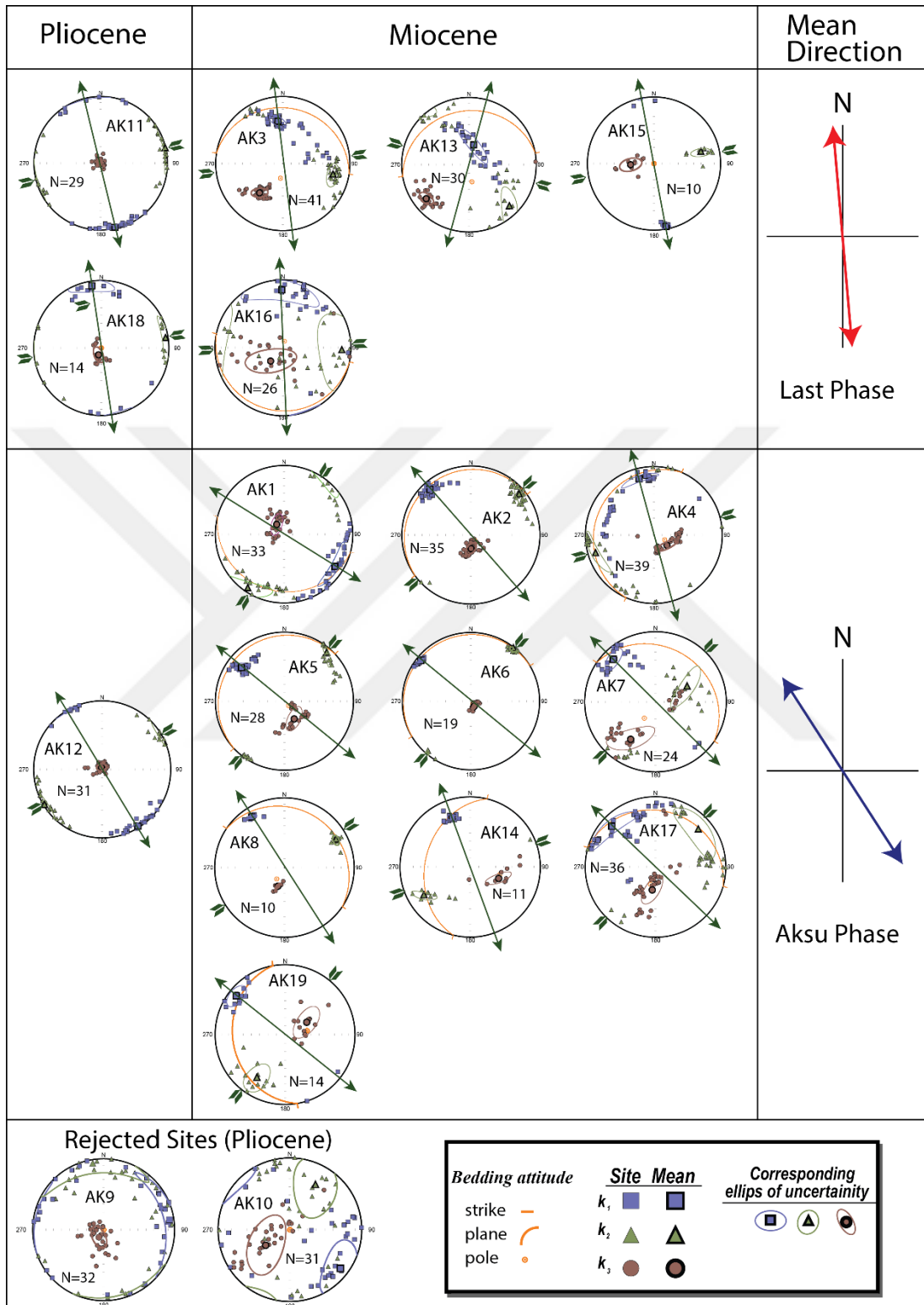
Figure 6. 10. AMS results of the Aksu Basin. Lower hemisphere, the equal-area projection of AMS principal axis and extension directions (kmax, k1) shows two identical ~N-S and NW-SE extension directions.

6.1.3. Comparison of Paleostress and AMS data

Anisotropy of magnetic susceptibility (AMS) results demonstrate that two dominant stretching direction are: 1) N-S oriented stretching in the Pliocene sediments and 2) NW-SE oriented stretching axes in the Miocene sediments.

In Pliocene sediments, AK11 and AK18 represent the N-S stretching direction. These samples clearly belong to the youngest and possibly still active extension direction in the Aksu Basin. On the other hand, site AK12 shows NE-SW oriented stretching direction, which resembles the Miocene samples in orientation. It is known that the Aksu Phase prevailed until the Early Pliocene and the result of the AK12 may reflect the effect of the Aksu Phase. In paleostress data, sites AP31 (Karpuzçay Formation), AP57, AP60 (Gebiz Limestone) and 81 (Yenimahalle Formation) represent recent phase. In Figure 6.11, the magnetic lineation directions (AMS) and stretching directions, which are calculated by adding 90° to the σ_1 direction, are compared and the graphical representation shows that the mean magnetic lineation orientation (162°N) and the mean strechthing direction (188°N) are close to each other. If the site AK12 excludes from the data, then the mean values of these two data sets are getting close to each other.

Distribution of the AMS patterns in the Miocene changes from N-S to NE-SW in the Aksu Basin. The magnetic fabric is mainly tectonic where magnetic lineations are parallel to the Aksu Thrust front (Figure 6.9). The changes in the orientation of the magnetic lineation are explained by thrust front geometry since the magnetic lineation is orient themselves according to the orientation of the thrust front. In sites AK5, AK6 and AK7, NW-SW oriented magnetic lineation and the orientation of the thrust front clearly has the same orientation (NW-SE). A similar pattern is also shown in sites AK14 and AK15 where nearly N-S oriented magnetic lineation is present. In paleostress data, this deformational phase corresponds to the Aksu Phase, which is the last and the most pervasive compressional phase in the Aksu Basin. The mean direction of the magnetic lineation for the Miocene samples are determined as 150°N while the stretching directions from the paleostress data, which just includes the kinematic data of the Aksu Phase, evaluated as 171°N. They are really reasonably close to each other. When we use whole paleostress data (including Aksu and Lycian phase) is considered for the graphical

representation, then the mean stretching direction is found as 161°N, which does not make a big difference since the Aksu Phase is extremely pervasive throughout the Aksu Basin.

AMS data are consistent with kinematic observations and provide independent support for the understanding of the deformation pattern in the Aksu Basin. Based on the AMS data, Recent and the Aksu Phase can be differentiated from the rest of the data. AMS data can therefore be evidently used help to construct the paleostress stratigraphy.
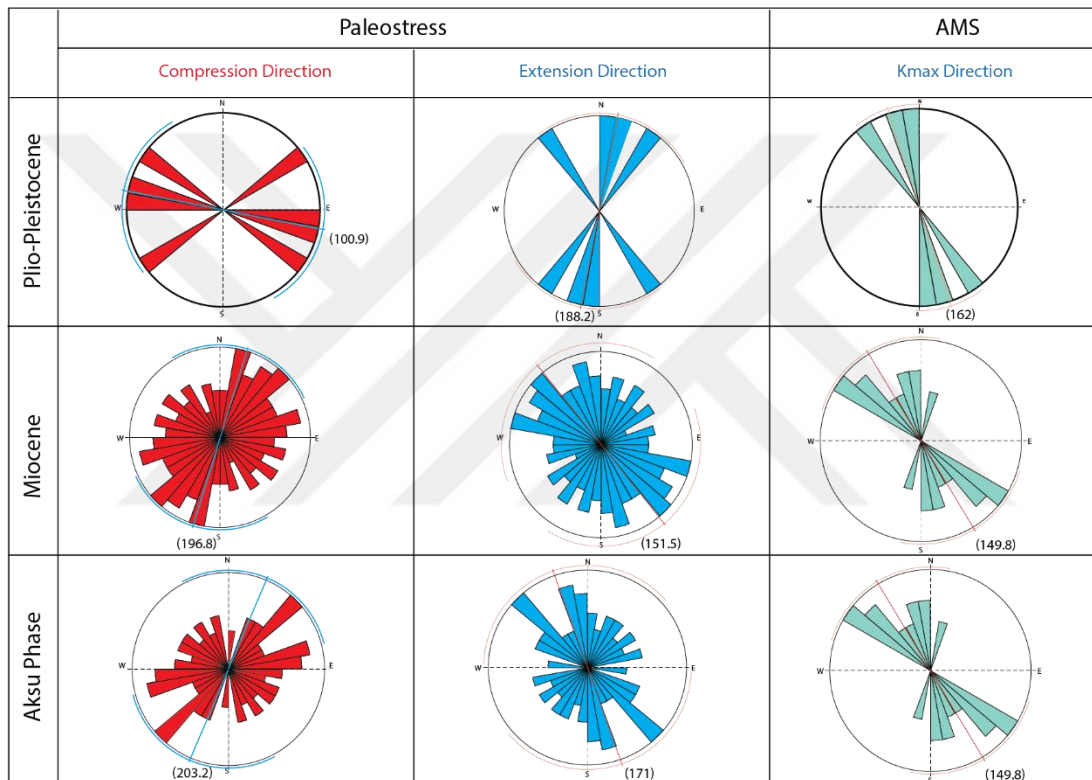
Figure 6. 11. Comparative table of the paleostress and AMS data.

6.2. Implications on Aksu Basin

The Aksu Basin developes unconformably on top of the Beydağları autochthonous and Antalya Nappes and the nappes have formed during subduction and collision in Late Cretaceous to perhaps Oligocene time (Şengör and Yılmaz, 1981; Collins and Robertson, 2003). The onset of the sedimentation in the basin is not known precisely, but must have occurred during or before Late Burdigalian, which is the oldest age we obtained from the

Oymapınar Limestone, which is the common lithostratigraphic unit in the whole Antalya Basin (including Aksu, Köprüçay and Manavgat basins).

The modern margin of the basin in the west and the north are actual paleomargins, but in the east, the Aksu Thrust controls the modern margin of the basin. Overall the basin-fill shows a coarsening upwards character, with the clearest depo-center represented by the fine-grained marine sediments of the Karpuzçay Formation. Additionally, most of the accommodation space was formed in the period towards the deposition Langihan to Serravalian Karpuzçay Formation. Based on the paleostress data in this study, the onset of the basin subsidence was likely roughly E-W-directed extension (or maybe multi-directional). Flecker (1995) claimed that the NNW-SSE extensional faulting event occurred in the Manavgat during Late Burdigalian-Langhian time, prior to the deposition of the Geceleme Formation. It is known that the Oymapınar Limestone is a common lithostratigraphic unit in whole Antalya Basin, and similar paleostress condition is likely valid during the onset of the basin formation. Similarly, Poisson et al., (2011) concluded that the N-S orientation of the Aksu Basin has resulted from pre-Neogene paleo-geographies and the deep-seated thrust faults constituted a zone of weakness for the future Neogene faulting. On the other hand, some researchers (Flecker, 1995; Flecker et al., 1998; Glover and Robertson, 1998) proposed that the NW-SE compression has occurred due to southeastern movement of the Lycian Nappes and this is interpreted as the as a first phase that controls the formation of the Aksu Basin. But, this model does not explain the syn-sedimentary faults in the Karpuzçay Formation and Karadağ Conglomerate.

The presence of thick coarse clastic deposits (Langhian-Serravalian for Karadağ Member and Serravallian-Tortonian for Kapıkaya Member) are common at the margin of the Aksu Basin and these conglomeratic sequences are interpreted as a fan-delta deposition. Among these conglomeratic units, in the Karadağ conglomerate has north-south linear geometry that it may represent the channel system of a fan-delta active throughout the Langhian-Serravalian from which finer-grained turbidity currents were also sourced, since it is not possible to differentiate the Aksu Conglomertaes from the turbidite succession (Karpuzçay Formation). The current (flow) directions were collected are mainly from NE to SW. This result is different from NE-SE direction as reported in

the literature (Flecker, 1995; Flecker et al., 1998; Üner et al., 2015). On the other hand, similar conglomeratic units with north-south linear geometry is also observed in the Köprüçay Basin which is just located at the east of the Aksu Basin. they may be interpreted as these conglomerates deposited in a single, unified delta front during the Langhian-Serravalian and if this hypothesis is working, then the current directions obtained during this study make sense. In the north of the Aksu Basin, another conglomeratic unit directly overlyn the basement rocks, which is the part of the Lycian Nappes. Conglomerates have roughly east-west linear geometry along the northern fault-controlled margin suggest that deposition of the Kapıkaya Conglomerate was fault (ENE-WSW) controlled and active throughout the Serravalian to Tortonian time.

Aksu Basin is likely developed as NNE-SSW oriented half-graben since the western margin of the Aksu Basin is largely unfaulted with sedimentary evidence suggesting passive contact between the Miocene sediments and Mesozoic Basement. However, the eastern margin of the Aksu Basin is well-defined by ~N-S striking fault traces which may be inherited from the pre-Neogene tectonic deformation and was then activated during Early Burdigalian-Langhian E-W extension. In other words, the subsidence that causes the formation of Aksu Basin may be related to reactivation of several inherited discrete thrust faults related to the emplacement of the Antalya Nappes. As expected in this context, the Aksu Basin is not a local basin with its own depocenter and faulted basin. A similar stratigraphy and basin geometry are reported for Köprüçay-Manavgat basins in the east of the study area (Flecker, 1995; Karabıyıkoğlu et al., 2000; Deynoux et al., 2005; Çiner et al., 2008). This further means that this subsidence must be in regional scale.

Available information indicates a considerable heterogeneity in northern and southern parts of the Aksu Basin in terms of stratigraphy, sedimentation, tectonics and basin evolution. Sedimentation in the northern part of Aksu Basin is different from the southern part in terms of lithology and tectonic activity. Except the Quaternary sediments, the age of the youngest unit in the north of Aksu Basin is Tortonian, which belongs to the Kapıkaya Conglomerate. On the other hand, the southern part contains Messinian to Pleistocene sediments. This may be associated with southernward migration of the depocenter of the Aksu Basin.

Results from the Aksu Basin further demonstrate that throughout the basin history, extension responsible for the onset of the basin formation has not remained active and but changed into a compressional tectonic regime (approximately N-S, Lycian Phase) during the Serravallian. One of the main basin bounding fault, namely Kapıkaya Fault, is a roughly E-W striking reverse fault that formed in response to the N-S compression. In the AMS data, the effect of this compressional stress (mainly E-W stretching) is not observed, this phase should therefore be the older than the Aksu Phase. Similar kinematic records are also reported by some other researchers (Flecker, 1995; Flecker et al., 1998), but they claimed this phase as the first tectonic phase in the Aksu Basin. Based on the syn-sedimentary faults in the lower levels of the Karpuzçay Formation, the onset of this compressional phase may be dated as Late Langhian-Early Serravallian (?). Upper age limit for the Lycian Phase is determined as Tortonian in this study, according the kinematic data are recorded in the Kapıkaya Conglomerate. The third tectonic phase in the Aksu Basin is related to the compressional tectonics with E-W orientation and is determined by N-S oriented Aksu Thrust. Magnetic lineations fabrics obtain from the AMS data are also used to differentiate this tectonic phase. Based on the stratigraphic, structural and the kinematic data, the time span for Aksu Phase is determined as Serravallian to Early Pliocene. In this context, the Lycian and the Aksu phases might have worked together from at some point duringSerravallian to Tortonian, thisis also supported by the paleostress stratigraphy data.

The neotectonic period is characterized by generally extensional tectonic activity. Kinematic and AMS data indicate roughly N-S oriented extension direction. Üner et al. (2015) described the orientation of the youngest tectonic phase in the Aksu Basin as NE-SW extension while Poisson et al. (2011) attributed the last tectonic phase to normal faulting during a N-S extension. Data supported by Poisson et al., (2011) is coincided with present data and suggest the current tectonic regime in the Aksu Basin is a N-S extension. This Recent extensional regime may be explained by the southward's rollback of the Cyprus slab.

The field observations presented in our study show that folds developed in the Karadağ Conglomerate and Karpuzçay Formation are characterized as asymmetric-tight folds with more than 60° interlimb angle. This type of folded structures only developed

under the compressional tectonic regime. The axes of the anticlines and synclines are a (sub)parallel with NNW-SSE direction, which is consistent with the orientation of the Aksu Thrust. The vergence direction of the fold (NE) also supports this information.

6.3. Regional Implications

The results of present studypoint out that an interesting discussion in terms of the cause of the E-W shortening in the heart of the Isparta Angle along the Aksu Thrust (Poisson, 1977; Poisson et al., 2003a and 2011) as well as offshore in the Antalya Bay (Hall et al., 2014), which has been active from Serravallian to Early Pliocene (Poisson et al., 2011). E-W extension and also the E-W shortening in the center of the Isparta Angle are interesting given the plate tectonic setting driving by N-S convergence of the Africa and Eurasia. Poisson et al. (2011) suggested that the Aksu Thrust is caused by the westward escape of the Anatolia along the North Anatolian Fault. This idea may be originated from the broadly similar age inferred for the collision (~12 Ma) between Arabia and Eurasia in eastern Anatolia (Şengör et al., 2003; Keskin, 2003 and Faccenna et al., 2014).

The data that is reported by Koç et al. (2016 and 2016b), however, cast doubt on the validity of this mechanism, since the E-W extension in the eastern part of the Isparta Angle indicates that E-W shortening to the west, in the Aksu Basin, cannot be caused by a push driven by the collision in the east. Similarly, the E-W Serravallian-Early Pliocene shortening in the Aksu Basin demonstrates that extension in the eastern part of the Isparta Angle cannot be driven by Aegean extension which is directed NNE-SSW (van Hinsbergen and Schmid 2012; Koç et al. 2016). Geological records suggesting that extension direction in the west Anatolia are currently N-S in the Middle Miocene, but rotated counterclockwise (Van Hinsbergen at al. 2010; Kaymakçi et al., 2018). This history of extension is synchronous with and occurs in the hanging wall of a top-to-the-southeast thrust that brings the Lycian Nappes over the Bey Dağları platform (Hayward 1984; van Hinsbergen et al. 2010a). This extension history is restricted to the Lycian nappes and did not affect the Bey Dağları foreland, or the Menderes hinterland. The final emplacement of the Lycian Nappes is accomplished by 15 Ma, i.e. predating most of the

history in our study area (Hayward, 1984). According to present paleostress stratigraphy data, the Lycian deformation should be accomplished by ~11 Ma, which is synchronuous extension in the Yalvaç, Altınapa and Ilgın continental Basin located at the eastern limb of the Isparta Angle.

The simultaneous activity of NW-SE and E–W shortening in the west and the center of the Isparta Angle, respectively, and E–W extension ~100 km, therefore, requires a dynamic explanation on the scale of the Isparta Angle. Van Hinsbergen et al. (2010a) explained the possible reason of the NW-SE shortening in the west (the Lycia Nappes over the Bey Dağları platform) is likely as a result of gravitational sliding accomplished by ~15 Ma. Flecker et al. (2005) suggested that southwards rollback of the Cyprus slab may be the possible cause of the extensional basin formation in the eastern limb of the Isparta Angle. Although this mechanism may explain N–S extension component that is found in the Yalvaç, Altınapa and Ilgın basins (Koç et al., 2012, 2016a and 2017), it is not very successful to explain the E–W component of the extension in these basins. The E–W shortening along the Aksu Thrust is discussed by Van Hinsbergen et al. (2010a, b) and the of strain partitioning of transpression along the Kırkkavak and Aksu Faults are proposed as a possible cause for this shortening. Although this mechanism may explain the shortening in the centre of the Isparta Angle, it is insufficient to explain the E–W extension along the eastern limb of the Isparta Angle (Koç et al., 2016a).

Fortunately, seismic tomographic images of the mantle below the Isparta Angle published by de Boorder et al. (1998) and later, in more detail, Biryol et al. (2011), as well as a study focused on earthquake hypocentres in the mantle below the study area (Kalyoncuoğlu et al. 2011) and subsequent oroclinal bending reflected by the vertical axis rotations in the Köprüçay and Manavgat basins (Koç et al., 2016b), have indicated that there are two separate slab segments below southern Turkey; 1) a northwards dipping slab below Cyprus and 2) N–S striking slab associated Benioff zone below the Isparta Angle and Antalya Bay, called as Antalya Slab (Koç et al., 2016a, 2016b). Along the prominent STEP fault (Govers and Wortel, 2005), the Antalya slab is disconnected from the Aegean slab (Biryol et al., 2011). Biryol et al. (2011) and Schildgen et al. (2012) suggested that the Antalya slab is a fragment of the Cyprus slab that for some reason rotated into a N–S orientation. On the other hand, Koç et al. (2016a) suggested that the Antalya slab formed

as a result of a separate, N–S striking subduction zone, that dips eastwards and until at least Pliocene time connected to the surface along the Aksu thrust and its offshore equivalents, with Bey Dağları in the lower plate, and the Taurides in the upper plate. This narrow slab fragment, experiencing westwards trench retreat, would create overriding plate extension consistent with the basin evolution documented in Koç et al. (2012, 2016a and 2017), as well as the oroclinal bending in the Köprüçay and Manavgat Basin (Koç et al. 2016b) and shortening in the Aksu Basin documented in this study.

The extension regime in the Aksu Basin is active today as shown by recent seismicity (Kalyancuoğlu et al., 2011 and Schildgen et al. 2012). The uplift history of southern Anatolia in latest Miocene and Pliocene time recently has received wide attention (Cosentino et al. 2012; Schildgen et al. 2012, 2014; Koç et al., 2012) and the driving mechanism of this uplift may have led to the extension regime in the Aksu Basin. Some researchers (Cosentino et al., 2012; Schildgen et al. 2012, 2014) suggested that the disconnection between the Aegean, Antalya, and Cyprus slab segments may have led to asthenospheric inflow and resulted dynamic topographic effects. We know from the seismic tomography images that the Antalya slab has no known connection to the surface. If the slab has entirely broken off, it must have done so recently so as to still generate a Benioff zone, and not generate a visible gap in the tomography (Koç et al., 2016b), therefore the Antalya slab has had an important contribution to the kinematic evolution of the Isparta Angle in Mio-Pliocene, and even modern times. This recent deformation may also have significantly contributed to the uplift history of the Taurides since the late Miocene.

7. CONCLUSIONS

In this study, we study stratigraphic, sedimantological and structural evolution of the Miocene Aksu Basin located at the southern center of the Isparta Angle using paleostress and AMS methods. This study represents the following conclusions:

I. Stratigraphical studies demonstrate that

   a. The Aksu Basin is developed unconformably on top of the Beydağları autochthonous and Antalya Nappes and the onset of the sedimentation in the basin is not known precisely, but must have occurred during or before Late Burdigalian.

   b. The presence of thick coarse clastic deposits (Langhian-Serravalian for Karadağ Member and Serravallian-Tortonian for Kapıkaya Member) are common at the margin of the Aksu Basin and these conglomeratic sequences has been interpreted as a fan-delta deposition.

   c. Overall sedimentation characteristics are coarsening upwards, with the clearest depo-center represented by the marine fine-grained Karpuzçay Formation. Additionally, most of the accommodation space was formed in the period towards the deposition of the Karpuzçay Formation, which according to biostratigraphic interpretations listed above is from Langihan to Serravalian.

   d. The northern part of the sedimentation in the Aksu Basin is different from the southern part in lithology. The youngest age in the north of Aksu basin is Tortonian while the southern part contains the sedimentation whose ages are ranging from the Messinian to Pleistocene. This may be associated with southernward migration of the depocenter of the Aksu Basin.

II. Structural studies demonstrate that

a. Our field observations show that the modern margin of the basin in the west and the north are the paleomargins, but in the east, the Aksu Thrust controls the modern margin of the basin.

b. Aksu Basin is likely developed as NNE-SSW oriented half-graben since the western margin of the Aksu Basin is largely unfaulted with sedimentary evidence suggesting passive contact between the Miocene sediments and Mesozoic Basement.

c. Our paleostress stratigraphy from the Aksu Basin demonstrates that throughout the basin history, ~E-W extension responsible for the onset of the basin formation. This ~E-W extension is defined as the first tectonic phase in the Aksu Basin.

d. The second phase is the compressional tectonic regime with approximately N-S oriented, which likely starts to be active in the Early Serravallian. This phase terminated in the Tortonian.

e. The third tectonic phase in the Aksu Basin is related to the compressional tectonics with E-W orientation and is determined by N-S oriented Aksu Thrust. Time span for Aksu phase was determined as from Serravallian to Early Pliocene.

f. The paleostress stratigraphy data supported that the Lycian and the Aksu phase have worked together from at some point of the Serravallian to Tortonian.

g. The youngest tectonic regime is characterized by generally extensional tectonic activity. Kinematic data and AMS data show roughly N-S oriented extension direction.

h. The field observations presented in our study show that folds developed in the Karadağ Conglomerate and Karpuzçay Formation are characterized as asymmetric-tight folds with more than 60° interlimb angle. The axes of the anticline and syncline are a (sub)parallel with NNW-SSE direction, which is consistent with the orientation of the Aksu Thrust.

III. Methodological approach demonstrate that

a. Our AMS data are consistent with kinematic (paleostress) data and provide independent support for the understanding of the deformation pattern. AMS data can be evidently used help to construct the paleostress stratigraphy.

IV. Regional implications

a. In Middle Miocene to Pliocene time, E–W shortening was accommodated along the Aksu Thrust, and offshore within the Bay of Antalya in the heart of the Isparta Angle, ~100 km to the west of the study area. The E–W extension in the Yalvac and Altınapa Basins renders a causal relationship of this shortening with westwards escape of Anatolia unlikely.

b. The Antalya slab formed as a result of a separate, N–S striking subduction zone, that dips eastwards and until at least Pliocene time connected to the surface along the Aksu thrust and its offshore equivalents, with Bey Dağları in the lower plate, and the Taurides in the upper plate. This narrow slab fragment, experiencing westwards trench retreat, would create overriding plate extension as well as the oroclinal bending in the Köprüçay and Manavgat and shortening in the Aksu Basin.

c. The Antalya slab has had an important contribution to the kinematic evolution of the Isparta Angle in Mio-Pliocene, and even modern times. This recent deformation may also have significantly contributed to the uplift and the recent extensional regime in the Aksu Basin.

REFERENCES

Akay, E., Uysal, S., Poisson, A., Cravatte, J., & Muller, C. (1985). Stratigraphy of the Antalya Neogene Basin: *Bulletin of the Geological Society of Turkey*, **v.** 28.

Akbulut, A. (1977). *Etude Géologique d'une Partie du Taurus Occidental au Sud d'Egridir (Turquie)* (Doctoral dissertation).

Aleksandrowski, P. (1985). Graphical determination of principal stress directions for slickenside lineation populations: an attempt to modify Arthaud's method. *Journal of Structural Geology*, **7**(1), 73-82.

Allmendinger, R. W., Gephart, J. W., & Marrett, R. A. (1989). Notes on fault slip analysis. *Geol. Soc. Am. Short Course*, **66**.

Altınlı, E. (1944). Etude stratigraphique de la région d'Antalya. *Rev. Fac. Sci. Univ. Istambul, BIX*, **3**, 227-38.

Altınlı, E. (1945). Etude tectonique de la région d'Antalya. *Revue de la Faculté des Sciences de l'Université d'Istanbul B*, **10**, 60-67.

Anchuela, Ó. P., Juan, A. P., & Imaz, A. G. (2010). Tectonic imprint in magnetic fabrics in foreland basins: a case study from the Ebro Basin, N Spain. *Tectonophysics*, **492**(1-4), 150-163.

Anderson, E. M. (1951). *The Dynamics of Faulting and Dyke Formation with Applications to Britain,* Hafner Pub. Co., Oliver and Boyd, London.

Angelier, J. (1979). Determination of the mean principal directions of stresses for a given fault population. *Tectonophysics*, **56**(3-4), T17-T26.

Angelier, J. (1984). Tectonic analysis of fault slip data sets. *Journal of Geophysical Research: Solid Earth*, **89**(B7), 5835-5848.

Angelier, J. (1989). From orientation to magnitudes in paleostress determinations using fault slip data. *Journal of Structural Geology*, **11**(1-2), 37-50.

Angelier, J. (1990). Inversion of field data in fault tectonics to obtain the regional stress—III. A new rapid direct inversion method by analytical means. *Geophysical Journal International,* **103**(2), 363-376.

Angelier, J. T., & Mechler, P. (1977). Sur une methode graphique de recherche des contraintes principales egalement utilisables en tectonique et en seismologie: la methode des diedres droits. *Bulletin de la Société Géologique de France*, **7**(6), 1309-1318.

Angelier, J., & Goguel, J. (1979). Sur une méthode simple de détermination des axes principaux des contraintes pour une population de failles. *CR Acad. Sci. Paris*, **288**, 307-310.

Angelier, J., & Hancock, P. L. (1994). *Paleostress Determinations*. Continental Deformation*s*, 53-100.

Angelier, S. (1975). Sur l'analyse de mesures recueillies dans des sites faillés: l'utilité d'une confrontation entre les méthodes dynamiques et cinématiques. *CR Acad. Sci*, **281,** 1805-1808.

Aral, İ. (1989). Geology of the Menderes Massif and the Lycian Nappes south of Denizli, western Taurides. *Mineral Res.Expl. Bull.,* **109**, 37-51

Arlegui-Crespo, L. E., & Simón-Gómez, J. L. (1998). Reliability of palaeostress analysis from fault striations in near multidirectional extension stress fields. Example from the Ebro Basin, Spain. *Journal of Structural Geology*, **20**(7), 827-840.

Armijo, R., Carey, E., & Cisternas, A. (1982). The inverse problem in microtectonics and the separation of tectonic phases. *Tectonophysics*, **82**(1-2), 145-160.

Arthaud, F. (1969). Méthode de détermination graphique des directions de raccourcissement, d'allongement et intermédiaire d'une population de failles. *Bulletin de la Société géologique de France*, **7**(5), 729-737.

Atkinson, B. K. (1977). The kinetics of ore deformation: Its illustration and analysis by means of deformation-mechanism maps. *Geologiska Föreningen i Stockholm Förhandlingar*, **99**(2), 186-197.

Averbuch, O., de Lamotte, D. F., & Kissel, C. (1992). Magnetic fabric as a structural indicator of the deformation path within a fold-thrust structure: a test case from the Corbières (NE Pyrenees, France). *Journal of Structural Geology*, **14**(4), 461-474.

Barka, A., & Reilinger, R. (1997). Active tectonics of the Eastern Mediterranean Region: Deduced from GPS, Neotectonic and Seismicity data. *ANNALI GEOFISICA, VOL. XL, N. 3.*

Barrier, E., & Vrielynck, B. (2008). MEBE atlas of paleotectonic maps of the Middle East. *Atlas of,* **14.**

Berk Biryol, C., Beck, S. L., Zandt, G., & Özacar, A. A. (2011). Segmented African lithosphere beneath the Anatolian region inferred from teleseismic P-wave tomography. *Geophysical Journal International*, **184**(3), 1037-1057.

Berk Biryol, C., Beck, S. L., Zandt, G., & Özacar, A. A. (2011). Segmented African lithosphere beneath the Anatolian region inferred from teleseismic P-wave tomography. *Geophysical Journal International*, **184**(3), 1037-1057.

Bizon, G., Biju-Duval, B., Letouzey, J., Monod, O., Poisson, A., Ozer, B., & Oztumer, E. (1974). Nouvelles précisions stratigraphiques concernat les bassins tertiaires du sud de la Turquie (Antalya, Mut, Adana). *Revue de l'Institut Français du Pétrole*, **29**(3), 305-326.

Blumenthal, M. (1951). Recherches geologiques dans le Taurus occidental dans l'arriere-pays d'Alanya: *Maden Tetkik Arama Enstitüsü Publications, no. D5*, **134**, 1955.

Blumenthal, M. (1963). Le systeme structural du Taurus sud-anatolien, In Livre a'memoire du Professeur P. Fallot. *Mem. Soc. Geol. Fr.*, **2,** 611-662.

Borradaile, G. J. (1982). Comparison of Archean structural styles in two belts of the Canadian Superior Province. *Precambrian Research*, **19**(2), 179-189.

Borradaile, G. J. (1988). Magnetic susceptibility, petrofabrics and strain. *Tectonophysics*, **156**(1-2), 1-20.

Borradaile, G. J., & Henry, B. (1997). Tectonic applications of magnetic susceptibility and its anisotropy. *Earth-Science Reviews*, **42**(1-2), 49-93.

Borradaile, G. J., & Jackson, M. (2004). Anisotropy of magnetic susceptibility (AMS): magnetic petrofabrics of deformed rocks. *Geological Society, London, Special Publications*, **238**(1), 299-360.

Borradaile, G. J., & Jackson, M. (2010). Structural geology, petrofabrics and magnetic fabrics (AMS, AARM, AIRM). *Journal of Structural Geology*, **32**(10), 1519-1551.

Borradaile, G. J., & Jackson, M. (2010). Structural geology, petrofabrics and magnetic fabrics (AMS, AARM, AIRM). *Journal of Structural Geology*, **32**(10), 1519-1551.

Borradaile, G. J., & Tarling, D. H. (1981). The influence of deformation mechanisms on magnetic fabrics in weakly deformed rocks. *Tectonophysics*, **77**(1-2), 151-168.

Borradaile, G., Mothersill, J., Tarling, D., & Alford, C. (1986). Sources of magnetic susceptibility in a slate. *Earth and Planetary Science Letters*, **76**(3-4), 336-340.

Bott, M. H. P. (1959). The mechanics of oblique slip faulting. *Geological Magazine*, **96**(2), 109-117.

Boulton, S. J., & Robertson, A. H. (2007). The Miocene of the Hatay area, S Turkey: Transition from the Arabian passive margin to an underfilled foreland basin related to closure of the Southern Neotethys Ocean. *Sedimentary Geology*, **198**(1-2), 93-124.

Brunn, J. H., Graciansky, P. C. D., Gutnic, M., Juteau, T., Lefevre, R., Marcoux, J., ... & Poisson, A. (1970). Structures majeures et corrélations stratigraphiques dans les Taurides occidentales. *Bulletin de la Societe Geologique de France*, **7**(3), 515-556.

Brunn, J.H., Graciansky, P.C. De, Gutnic, M., Juteau, T., Marcoux, T., Monod, O. & Poisson, A. (1971). Outline of the geology of the western Taurids. In: CAMPELL, A. (ed), *Geology and Istory of Turkey*, 225–255.

Burg, J. P. (2018). Script to Structural Geology. In *Lectures 651-3422-00L and 651-3422-00V*. ETH Zurich.Jelínek, V. (1977). *The Statistical Theory of Measuring Anisotropy of Magnetic Susceptibility of Rocks And Its Application* (pp. 1-88). Brno: Geofyzika.

Carey E., 1976. *Analyse Numérique d'un Modèle Mécanique Élémentaire Appliquéà l'Etude d'une Population de Failles: Calcul d'un Tenseur Moyen des Contraintes à partir des Stries de Glissement, thèse de 3e Cycle*, Université de Paris-Sud, 138pp.

Carey, E. (1974). Analyse theorique et rumerique d'un modele mecanique elementaire applique a l'etude d'une population de failles. *Comptes Rendus Hebdomadaires des Seances de l'Academie des Sciences, Serie D: Sciences Naturelles*, **279**(11), 891-894.

Celâl, A. M., & Yılmaz, Y. (1981). Tethyan evolution of Turkey: a plate tectonic approach. *Tectonophysics*, **75**(3-4), 181-241.

Chadima, M., & Jelinek, V. (2009). Anisoft 4.2: Anisotropy data browser for windows. *Agico Inc., Brno*.

Chaput, G., & Darkot, B. (1953). Sur le pliocene des environs dantalya (turquie). *Comptes Rendus Hebdomadaires des Seances de l Academie des Sciences*, **236**(23), 2259-2260.

Cifelli, F., Mattei, M., Chadima, M., Lenser, S., & Hirt, A. M. (2009). The magnetic fabric in "undeformed clays": AMS and neutron texture analyses from the Rif Chain (Morocco). *Tectonophysics*, **466**(1-2), 79-88.

Çiner, A., Karabiyikoğlu, M., & Monod, O. (2008). Late Cenozoic sedimentary evolution of the Antalya Basin, southern Turkey. *Turkish Journal of Earth Sciences*, **17**(1), 1-41.

Çiner, A., Köse, O., Sarikaya, M. A., Yıldırım, C., Candas, A., & Wilcken, K. M. (2018, December). Late Pleistocene Cosmogenic 36Cl Glacial Chronology of the Mount Karanfil, Central Taurus Range, Turkey. In *AGU Fall Meeting Abstracts*.

Clark, M., & Robertson, A. (2002). The role of the Early Tertiary Ulukisla Basin, southern Turkey, in suturing of the Mesozoic Tethys ocean. *Journal of the Geological Society*, **159**(6), 673-690.

Colby, B. R. (1963). *Fluvial Sediments: A Summary of Source, Transportation, Deposition, and Measurement of Sediment Discharge* (No. 1181). US Government Printing Office.

Collins, A. S., & Robertson, A. H. (1997). Lycian melange, southwestern Turkey: an emplaced Late Cretaceous accretionary complex. *Geology*, **25**(3), 255-258.

Collins, A. S., & Robertson, A. H. (1998). Processes of Late Cretaceous to Late Miocene episodic thrust-sheet translation in the Lycian Taurides, SW Turkey. *Journal of the Geological Society*, **155**(5), 759-772.

Collins, A. S., & Robertson, A. H. (2003). Kinematic evidence for Late Mesozoic–Miocene emplacement of the Lycian Allochthon over the western Anatolide belt, SW Turkey. *Geological Journal*, **38**(3-4), 295-310.

Collins, A. S., & Robertson, A. H. (2003). Kinematic evidence for Late Mesozoic–Miocene emplacement of the Lycian Allochthon over the western Anatolide belt, SW Turkey. *Geological Journal,* **38**(3-4), 295-310.

Collinson, D.W. (1983). *Methods in Paleomagnetism and Rock Magnetism*. Chapman and Hall. London, 500 pp.

Collombat, H., Rochette, P., & Vialon, P. (1995). Magnetic fabric as a strain indicator in unconsolidated sediments of the Chile Triple Junction area. In *Proceedings of the Ocean Drilling Program, Scientific Results* (Vol. 141, pp. 29-49). College Station, TX: Ocean Drilling Program.Commission for the geological map of the world.

Coulomb, C. A. (1776). An attempt to apply the rules of maxima and minima to several problems of stability related to architecture. *Mémoires de l'Académie Royale des Sciences*, **7,** 343-382.

Cox, A., & Doell, R. R. (1960). Review of paleomagnetism. *Geological Society of America Bulletin*, **71**(6), 645-768.

Daly, L. (1967). Possibilite dexistence dans les roches de plusieurs anisotropies magnetiques superposees-leur separation. *Comptes Rendus Hebdomadaires des Seances de l Academie des Sciences Serie b*, **264**(19), 1377.

De Boorder, H., Spakman, W., White, S. H., & Wortel, M. J. R. (1998). Late Cenozoic mineralization, orogenic collapse and slab detachment in the European Alpine Belt. Earth and Planetary *Science Letters,* **164**(3-4), 569-575.

De Lamotte, D. F., Souque, C., Grelaud, S., & Robion, P. (2002). Early record of tectonic magnetic fabric during inversion of a sedimentary basin Short review and examples from the Corbieres transfer zone (France). *Bulletin de la Société Géologique de France*, **173**(5), 461-469.

De Planhol, X. (1956). Contribution à l'étude géomorphologique du Taurus occidental et de ses plaines bordières. *Revue de Géographie Alpine*, **44**(4), 609-685.

Debacker, T. N., Hirt, A. M., Sintubin, M., & Robion, P. (2009). Differences between magnetic and mineral fabrics in low-grade, cleaved siliciclastic pelites: A case

study from the Anglo-Brabant Deformation Belt (Belgium). *Tectonophysics*, **466**(1-2), 32-46.

Delvaux, D., Moeys, R., Stapel, G., Petit, C., Levi, K., Miroshnichenko, A., ... & San'kov, V. (1997). Paleostress reconstructions and geodynamics of the Baikal region, Central Asia, Part 2. Cenozoic rifting. *Tectonophysics*, **282**(1-4), 1-38.

Deynoux, M., Çiner, A., Monod, O., Karabıyıkoglu, M., Manatschal, G., & Tuzcu, S. (2005). Facies architecture and depositional evolution of alluvial fan to fan-delta complexes in the tectonically active Miocene Köprüçay Basin, Isparta Angle, Turkey. *Sedimentary Geology*, **173**(1-4), 315-343.

Dilek, Y., Thy, P., Hacker, B., & Grundvig, S. (1999). Structure and petrology of Tauride ophiolites and mafic dike intrusions (Turkey): Implications for the Neotethyan ocean. *Geological Society of America Bulletin*, **111**(8), 1192-1216.

Dubey, A. K. (2014). Anisotropy of magnetic susceptibility. In *Understanding an Orogenic Belt* (pp. 17-34). Springer, Cham.

Dumont, J. F. (1976). *Etudes Géologiques Dans les Taurides Occidentales: les Formations Paléozoïques et Mésozoïques da la Coupole de Karacahisar (Province d'Isparta, Turquie)* (Doctoral dissertation).

Dumont, J. F., & Kerey, K. (1975). a. Basement geological study in the south of Egirdir lake. *Geology Bulletin of Turkey*, **18**(2), 169-174.

Dupoux, B. (1983). *Étude Comparée de la Tectonique Néogène des Bassins du Sud de Chypre et du Bassin d'Antalya (Turquie)* (Doctoral dissertation, éditeur inconnu).

Durand, B., Jolivet, L., Horvath, F., & Seranne, M. (Eds.). (1999). The Mediterranean basins: Tertiary extension within the Alpine orogen. *Geological Society of London.*

Eroskay, S. O. (1968). **Köprüçay-Beşkonak Rezervuarı Jeolojik İncelemesi. *EİEİ rapor, No: II-06-5, Ankara*.**

Etchecopar, A., Vasseur, G., & Daignieres, M. (1981). An inverse problem in microtectonics for the determination of stress tensors from fault striation analysis. *Journal of Structural Geology*, **3**(1), 51-65.

Evans, M. A., Lewchuk, M. T., & Elmore, R. D. (2003). Strain partitioning of deformation mechanisms in limestones: examining the relationship of strain and anisotropy of magnetic susceptibility (AMS). *Journal of Structural Geology*, **25**(9), 1525-1549.

Faccenna, C., Becker, T. W., Auer, L., Billi, A., Boschi, L., Brun, J. P., ... & Piromallo, C. (2014). Mantle dynamics in the Mediterranean. *Reviews of Geophysics,* **52**(3), 283-332.

Faccenna, C., Bellier, O., Martinod, J., Piromallo, C., & Regard, V. (2006). Slab detachment beneath eastern Anatolia: A possible cause for the formation of the North Anatolian fault. *Earth and Planetary Science Letters*, **242**(1-2), 85-97.

Flecker, R. (1995). *Miocene Basin Evolution of The Isparta Angle, Southern Turkey*. PhD thesis.

Flecker, R., Ellam, R. M., Müller, C., Poisson, A., Robertson, A. H. F., & Turner, J. (1998). Application of Sr isotope stratigraphy and sedimentary analysis to the origin and evolution of the Neogene basins in the Isparta Angle, southern Turkey. *Tectonophysics*, **298**(1-3), 83-101.

Flecker, R., Poisson, A., & Robertson, A. H. F. (2005). Facies and palaeogeographic evidence for the Miocene evolution of the Isparta Angle in its regional eastern Mediterranean context. *Sedimentary Geology*, **173**(1-4), 277-314.

Fry, N. (1992). A robust approach to the calculation of paleostress fields from fault plane data: discussion. *Journal of structural geology*, **14**(5), 635-637.

Fry, N. (1999). Striated faults: visual appreciation of their constraint on possible paleostress tensors. *Journal of Structural Geology*, **21**(1), 7-21.

Fry, N. (2001). Stress space: striated faults, deformation twins, and their constraints on paleostress. *Journal of Structural Geology*, **23**(1), 1-9.

Fuller, M. D. (1960). Anisotropy of susceptibility and the natural remanent magnetization of some Welsh slates. *Nature*, **186**(4727), 791.

Fuller, M.D. (1963). Magnetic anisotropy and paleomagnetism. *J. Geophys.Res. 68*, 293–309.

Gans, C. R., Beck, S. L., Zandt, G., Biryol, C. B., & Ozacar, A. A. (2009). Detecting the limit of slab break-off in central Turkey: new high-resolution Pn tomography results. *Geophysical Journal International,* **179**(3), 1566-1572.

Girdler, R. W. (1961). The measurement and computation of anisotropy of magnetic susceptibility of rocks. *Geophysical Journal International,* **5**(1), 34-44.

Glover, C. P., & Robertson, A. H. (1998a). Role of regional extension and uplift in the Plio-Pleistocene evolution of the Aksu Basin, SW Turkey. *Journal of the Geological Society,* **155**(2), 365-387.

Glover, C., & Robertson, A. (1998b). Neotectonic intersection of the Aegean and Cyprus tectonic arcs: extensional and strike-slip faulting in the Isparta Angle, SW Turkey. *Tectonophysics*, **298**(1-3), 103-132.

Glover, C., & Robertson, A. H. (2003). Origin of tufa (cool-water carbonate) and related terraces in the Antalya area, SW Turkey. *Geological Journal*, **38**(3-4), 329-358.

Gómez, J. S. (1986). Analysis of a gradual change in stress regime (example from the eastern Iberian Chain, Spain). *Tectonophysics*, **124**(1-2), 37-53.

Göncüoğlu, M. C. & Dirik, K., (1996). Neotectonic characteristics of central Anatolia. *International Geology Review*, **38**(9), 807-817.

Göncüoğlu, M. C., Dirik, K., & Kozlu, H. (1997). General characteristics of pre-Alpine and Alpine Terranes in Turkey: Explanatory notes to the terrane map of Turkey. In *Annales Geologique de Pays Hellenique* (Vol. 37, pp. 515-536).

Görür, N., Oktay, F. Y., Seymen, I., & Şengör, A. M. C. (1984). Palaeotectonic evolution of the Tuzgölü basin complex, Central Turkey: sedimentary record of a Neo-Tethyan closure. *Geological Society, London, Special Publications*, **17**(1), 467-482.

Govers, R., & Wortel, M. J. R. (2005). Lithosphere tearing at STEP faults: Response to edges of subduction zones. *Earth and Planetary Science Letters,* **236**(1-2), 505-523.

Graham, J. W. (1954). Magnetic susceptibility, an unexploited element of petrofabric. *Geological Society of American Bulletin*, *65*, 1257-1258.

Graham, J. W. (1996). Significance of magnetic anisotropy in Appalachian sedimentary rocks. *The Earth Beneath the Continents: A Volume of Geophysical Studies in Honor of Merle A. Tuve*, 627-648.

Granar, L. (1958). Magnetic measurements on Swedish varved sediments: Arkiv for Geofysik, v. 3. *Grew, ES and Manton, WI (1986) A new correlation of sapphirine granulites in the Indo-Antarctic metamorphic terrain: Late Proterozoic dates from the Eastern Ghats. Precambrian Res*, **33**, 123.

Gülyüz, E., Kaymakçi, N., Meijers, M. J., van Hinsbergen, D. J., Lefebvre, C., Vissers, R. L., ... & Peynircioğlu, A. A. (2012). Late Eocene evolution of the Çiçekdağı Basin (central Turkey): Syn-sedimentary compression during microcontinent–continent collision in central Anatolia. *Tectonophysics*, **602**, 286-299.

Gutnic, M. (1979). *Géologie des Taurides Occidentales (Turquie)* (No. 137). Société géologique de France.

Hall, J., Aksu, A. E., King, H., Gogacz, A., Yaltırak, C., & Çifçi, G. (2014). Miocene–Recent evolution of the western Antalya Basin and its linkage with the Isparta Angle, eastern Mediterranean. *Marine Geology*, **349**, 1-23.

Hamilton, N., & Rees, A. I. (1971). The anisotropy of magnetic susceptibility of the Franciscan rocks of the Diablo Range, Central California. *Geologische Rundschau*, **60**(3), 1103-1124.

Hancock, P. L. (1985). Brittle microtectonics: principles and practice. *Journal of structural geology*, **7**(3-4), 437-457.

Handin, J. (1969). On the Coulomb-Mohr failure criterion. *Journal of Geophysical Research*, **74**(22), 5343-5348.

Hayward, A. B. (1984). Miocene clastic sedimentation related to the emplacement of the Lycian Nappes and the Antalya Complex, SW Turkey. *Geological Society, London, Special Publications*, **17**(1), 287-300.

Heller, F. (1973). Magnetic anisotropy of granitic rocks of the Bergell massif (Switzerland). *Earth and Planetary Science Letters*, **20**(2), 180-188.

Henry, B. (1983). Interprétation quantitative de l'anisotropie de susceptibilité magnétique. *Tectonophysics*, **91**(1-2), 165-177.

Henry, B., & Daly, L. (1983). From qualitative to quantitative magnetic anisotropy analysis: the prospect of finite strain calibration. *Tectonophysics*, **98**(3-4), 327-336.

Hrouda, F. (1982). Magnetic anisotropy of rocks and its application in geology and geophysics. *Geophysical Surveys*, **5**(1), 37-82.

Hrouda, F. (2007). Magnetic susceptibility, anisotropy. *Encyclopedia of Geomagnetism and Paleomagnetism*, 546-560.

Hrouda, F., & Janák, F. (1976). The changes in shape of the magnetic susceptibility ellipsoid during progressive metamorphism and deformation. *Tectonophysics*, **34**(1-2), 135-148.

Hrouda, F., & Jelinek, V. (1990). Resolution of ferrimagnetic and paramagnetic anisotropies in rocks, using combined low-field and high-field measurements. *Geophysical Journal International*, **103**(1), 75-84.

Hüsing, S. K., Zachariasse, W. J., Van Hinsbergen, D. J., Krijgsman, W., Inceöz, M., Harzhauser, M., & Kroh, A. (2009). Oligocene–Miocene basin evolution in SE Anatolia, Turkey: constraints on the closure of the eastern Tethys gateway. *Geological Society, London, Special Publications*, **311**(1), 107-132.

Ising, G. (1942). *The magnetic propenies of varved clay*. Ark. Mat., Astron. Fys., 29A: 1-37.

Islamoglu, Y. (2001). The molluscan fauna and stratigraphy of Antalya Miocene basin (West-Central Taurids, SW Turkey)**. Bulletin of the Mineral Research and Exploration, 123**(124), 27-58.

Işler, F. I., Aksu, A. E., Hall, J., Calon, T. J., & Yaşar, D. (2005). Neogene development of the Antalya Basin, Eastern Mediterranean: An active forearc basin adjacent to an arc junction. *Marine Geology*, **221**(1-4), 299-330.

Jackson, M. (1991). Anisotropy of magnetic remanence: a brief review of mineralogical sources, physical origins, and geological applications, and comparison with susceptibility anisotropy. *Pure and Applied Geophysics*, *136*(1), 1-28.

Jaeger, J. C., & Cook, N. G. (1969). Fundamentals of rock mechanics, Methuen & Co**. Ltd., London, 513**.

Jelínek, V. (1977). *The Statistical Theory of Measuring Anisotropy of Magnetic Susceptibility of Rocks and its Application* (pp. 1-88). Brno: Geofyzika.

Jelinek, V. (1981). Characterization of the magnetic fabric of rocks**. Tectonophysics, 79**(3-4), T63-T67.

Jelínek, V., & Kropáček, V. (1978). Statistical processing of anisotropy of magnetic susceptibility measured on groups of specimens**. Studia Geophysica et Geodaetica, 22**(1), 50-62.

Jelínek, V., & Kropáček, V. (1978). Statistical processing of anisotropy of magnetic susceptibility measured on groups of specimens. *Studia Geophysica et Geodaetica*, **22**(1), 50-62.

Juteau, T. (1975). Les ophiolites des nappes d'Antalya (Taurides occidentales, Turquie): Univ**. Nancy, Sci. Terre, M• m. 2, 692**.

Karabıyıkoğlu, M., Çiner, A., Deynoux, M., Monod, O., Tuzcu, S., & Manatschal, G. (2004). Miocene tectonosedimentary evolution of the Late Cenozoic Antalya basin. *MTA-CNRS (France)-TÜBİTAK Co-Project*.

Karabıyıkoğlu, M., Çiner, A., Monod, O., Deynoux, M., Tuzcu, S., & Örçen, S. (2000). Tectonosedimentary evolution of the Miocene Manavgat Basin, western Taurides, Turkey. In *Tectonics and Magmatism in Turkey and the Surrounding Area* (Vol. 173, pp. 271-294). Geological Society, London, Special Publication.

Karabıyıkoğlu, M., Tuzcu, S., Çiner, A., Deynoux, M., Örçen, S., & Hakyemez, A. (2005). Facies and environmental setting of the Miocene coral reefs in the late-orogenic fill of the Antalya Basin, western Taurides, Turkey: implications for tectonic control and sea-level changes**. Sedimentary Geology, 173**(1-4), 345-371.

Kaymakçi, N. (2006). Kinematic development and paleostress analysis of the Denizli Basin (Western Turkey): implications of spatial variation of relative paleostress magnitudes and orientations**. Journal of Asian Earth Sciences, 27**(2), 207-222.

Kaymakçı, N., Langereis, C., Özkaptan, M., Özacar, A. A., Gülyüz, E., Uzel, B., & Sözbilir, H. (2018). Paleomagnetic evidence for upper plate response to a STEP fault, SW Anatolia. *Earth and Planetary Science Letters*, **498**, 101-115.

Kelling, G., Robertson, A., & Van Buchem, F. (2005). Cenozoic sedimentary basins of southern Turkey: an introduction. *Sedimentary Geology*, **1**(173), 1-13.

Kent, D. V., & Lowrie, W. (1975). On the magnetic susceptibility anisotropy of deep-sea sediment. *Earth and Planetary Science Letters*, **28**(1), 1-12.

Keskin, M. (2003). Magma generation by slab steepening and breakoff beneath a subduction-accretion complex: An alternative model for collision-related volcanism in Eastern Anatolia, Turkey. *Geophysical Research Letters*, **30**(24).

Khair, K., & Tsokas, G. N. (1999). Nature of the Levantine (eastern Mediterranean) crust from multiple-source Werner deconvolution of Bouguer gravity anomalies. *Journal of Geophysical Research: Solid Earth*, **104**(B11), 25469-25478.

Khan, M. A. (1962). The anisotropy of magnetic susceptibility of some igneous and metamorphic rocks. *Journal of Geophysical Research*, **67**(7), 2873-2885.

King, R. F. (1966). The magnetic fabric of some Irish granites. *Geological Journal*, **5**(1), 43-66.

Kissel, C., & Poisson, A. (1987). Étude paléomagnetique préliminaire des formations cénozoïques des Bey Daglari (Taurides occidentales, Turquie). *Comptes rendus de l'Académie des sciences. Série 2, Mécanique, Physique, Chimie, Sciences de l'univers, Sciences de la Terre*, **304**(8), 343-348.

Kissel, C., Averbuch, O., de Lamotte, D. F., Monod, O., & Allerton, S. (1993). First paleomagnetic evidence for a post-Eocene clockwise rotation of the Western Taurides thrust belt east of the Isparta reentrant (Southwestern Turkey). *Earth and Planetary Science Letters*, **117**(1-2), 1-14.

Kissel, C., Barrier, E., Laj, C., & Lee, T. Q. (1986). Magnetic fabric in "undeformed" marine clays from compressional zones. *Tectonics*, **5**(5), 769-781.

Kleinspehn, K. L., Pershing, J., & Teyssier, C. (1989). Paleostress stratigraphy: A new technique for analyzing tectonic control on sedimentary-basin subsidence. *Geology*, **17**(3), 253-256.

Koç, A., Kaymakçı, N., Van Hinsbergen, D. J., & Kuiper, K. F. (2017). Miocene tectonic history of the Central Tauride intramontane basins, and the paleogeographic evolution of the Central Anatolian Plateau. *Global and Planetary Change*, **158**, 83-102.

Koç, A., KaymakçıKaymakçı, N., Van Hinsbergen, D. J., & Vissers, R. L. (2016b). A Miocene onset of the modern extensional regime in the Isparta Angle: constraints from the Yalvaç Basin (southwest Turkey). *International Journal of Earth Sciences,* **105**(1), 369-398.

Koç, A., KaymakçıKaymakçı, N., van Hinsbergen, D. J., Kuiper, K. F., & Vissers, R. L. (2012). Tectono-Sedimentary evolution and geochronology of the Middle Miocene Altınapa Basin, and implications for the Late Cenozoic uplift history of the Taurides, southern Turkey. *Tectonophysics*, **532**, 134-155.

Koç, A., van Hinsbergen, D. J., Kaymakçı, N., & Langereis, C. G. (2016). Late Neogene oroclinal bending in the central Taurides: A record of terminal eastward subduction in southern Turkey?. *Earth and Planetary Science Letters*, **434**, 75-90.

Koçyiğit, A., & Deveci, Ş. (2007). A NS-trending active extensional structure, the Şuhut (Afyon) graben: commencement age of the extensional neotectonic period in the Isparta Angle, SW Turkey. *Turkish Journal of Earth Sciences,* **16**(4), 391-416.

Koçyiğit, A., & Özacar, A. A. (2003). Extensional neotectonic regime through the NE edge of the outer Isparta Angle, SW Turkey: new field and seismic data. *Turkish Journal of Earth Sciences*, **12**(1), 67-90.

Koşun, E. (2012). Facies characteristics and depositional environments of Quaternary tufa deposits, Antalya, SW Turkey. *Carbonates and evaporites*, **27**(3-4), 269-289.

Lamarche, G., & Rochette, P. (1987). La fabrique magnétique du flysch dauphinois (Alpes françaises): origine et application quantitative. *Geodinamica Acta*, **1**(2), 103-112.

Lanza, R., & Meloni, A. (2006). *The Earth's Magnetism* (Vol. 280). Springer-Verlag Berlin Heidelberg.

Larrasoaña, J. C., Pueyo, E. L., & Parés, J. M. (2004). An integrated AMS, structural, palaeo-and rock-magnetic study of Eocene marine marls from the Jaca-Pamplona basin (Pyrenees, N Spain); new insights into the timing of magnetic fabric acquisition in weakly deformed mudrocks. *Geological Society, London, Special Publications*, **238**(1), 127-143.

Lheureux, A. (1983). *Les Formations Silico-Détritiques Triasico-Liasiques de La Plate-Forme Carbonatée Taurique Au SO d'Akseki (Taurides Occidentales, Turquie)* (Doctoral dissertation).

Liesa, C. L., & Lisle, R. J. (2004). Reliability of methods to separate stress tensors from heterogeneous fault-slip data. *Journal of Structural Geology*, **26**(3), 559-572.

Lisle, R. J. (1987). Principal stress orientations from faults: an additional constraint. **In** *Annales Tectonicae* (Vol. 1, No. 2, pp. 155-158).

Lisle, R. J. (1988). ROMSA: a BASIC program for paleostress analysis using fault-striation data. *Computers & Geosciences*, **14**(2), 255-259.

Lowrie, W. (1989). Magnetic analysis of rock fabric. *Geophysics*, 698-706.

Marcoux, J. (1987). *Histoire et Topologie de la Neotethys: Contribution a Partir des Exemples de la Turquie et de L'himalaya-Tibet* (Doctoral dissertation, Paris 6).

McClusky, S., Balassanian, S., Barka, A., Demir, C., Ergintav, S., Georgiev, I., & Kastens, K. (2000). Global Positioning System constraints on plate kinematics and dynamics in the eastern Mediterranean and Caucasus. *Journal of Geophysical Research: Solid Earth*, **105**(B3), 5695-5719.

McKenzie, D. P. (1969). The relation between fault plane solutions for earthquakes and the directions of the principal stresses. *Bulletin of the Seismological Society of America*, **59**(2), 591-601.

Meijers, M. J., Kaymakçı, N., Van Hinsbergen, D. J., Langereis, C. G., Stephenson, R. A., & Hippolyte, J. C. (2010). Late Cretaceous to Paleocene oroclinal bending in the central Pontides (Turkey). *Tectonics*, **29**(4).

Mitra, G., & Marshak, S. (1988). Description of mesoscopic structures. *Basic Methods of Structural Geology. Prentice Hall, Englewood Cliffs, New Jersey*, 213-247.

Mochales, T., Pueyo, E. L., Casas, A. M., Barnolas, A., & Oliva-Urcia, B. (2010). Anisotropic magnetic susceptibility record of the kinematics of the Boltaña Anticline (Southern Pyrenees). *Geological Journal*, **45**(5-6), 562-581.

Monod, O., 1977, Recherches Geologiques dans le Taurus occidental au Sud de Beyşehir (Turquie): *These d'Etat Univ. Paris Sud (Orsay),* 442 s., yayımlanmamış.

Morris, A., & Robertson, A. H. F. (1993). Miocene remagnetisation of carbonate platform and Antalya Complex units within the Isparta Angle, SW Turkey. *Tectonophysics*, **220**(1-4), 243-266.

Nakamura, N., & Borradaile, G. J. (2004). Metamorphic control of magnetic susceptibility and magnetic fabrics: a 3-D projection. *Geological Society, London, Special Publications*, **238**(1), 61-68.

Nemcok, M. (1995). A stress inversion procedure for polyphase fault/slip data sets. *Journal of Structural Geology*, **17**(10), 1445-1453.

Nemcok, M., Kovác, D., & Lisle, R. J. (1999). A stress inversion procedure for polyphase calcite twin and fault/slip data sets. *Journal of Structural Geology*, **21**(6), 597-611.

Okay, A. I. (1986). *High-Pressure/low-Tempemture Metamorphic Rocks of Turkey*.

Okay, A. I. (1996). Paleo-and Neo-Tethyan events in northwest Turkey: geological and geochronological constraints. *Tectonics of Asia*, 420-441.

Okay, A. I., & Özgül, N. (1984). HP/LT metamorphism and the structure of the Alanya Massif, Southern Turkey: an allochthonous composite tectonic sheet. *Geological Society, London, Special Publications*, **17**(1), 429-439.

Okay, A. I., Zattin, M., & Cavazza, W. (2010). Apatite fission-track data for the Miocene Arabia-Eurasia collision. *Geology*, **38**(1), 35-38.

Oliva-Urcia, B., Larrasoaña, J. C., Pueyo, E. L., Gil, A., Mata, P., Parés, J. M., ... & Pueyo, O. (2009). Disentangling magnetic subfabrics and their link to deformation processes in cleaved sedimentary rocks from the Internal Sierras (west central Pyrenees, Spain). *Journal of Structural Geology*, **31**(2), 163-176.

Orife, T., & Lisle, R. J. (2003). Numerical processing of palaeostress results. *Journal of Structural Geology*, **25**(6), 949-957.

Orife, T., & Lisle, R. J. (2006). Assessing the statistical significance of palaeostress estimates: simulations using random fault-slips. *Journal of structural geology*, **28**(6), 952-956.

Owens, W. (1993). Magnetic fabric studies of samples from Hole 808C, Nankai Trough. In *Proc. ODP Sci. Res*. (Vol. 131, pp. 301-320).

Owens, W. H., & Bamford, D. (1976). A Discussion on natural strain and geological structure-Magnetic, seismic, and other anisotropic properties of rock fabrics. *Philosophical Transactions of the Royal Society of London. Series A, Mathematical and Physical Sciences*, **283**(1312), 55-68.

Özlü N. (1978). *Etude Ge´ologique, Mine´ralogique et Ge´ochimique des Bauxites d'Akseki Seydis¸ehir (Taurus occidental), Turquie*. Doctorat d'Etat thesis, Universite´ de Paris VI, France.

Papazachos, B. C., & Papaioannou, C. A. (1999). Lithospheric boundaries and plate motions in the Cyprus area. *Tectonophysics*, **308**(1-2), 193-204.

Parejas, E. (1943). Le substratum ancien du Taurus Occidental au Sud d'Afyon Karashissar (Anatolie). *CR Soc. Sc. Phys. Hist. Nat. Genève*, **60**, 110-114.

Parés, J. M. (2004). How deformed are weakly deformed mudrocks? Insights from magnetic anisotropy. *Geological Society, London, Special Publications*, **238**(1), 191-203.

Parés, J. M., & Dinarés-Turell, J. (1993). Magnetic fabric in two sedimentary rock-types from the southern Pyrenees. *Journal of Geomagnetism and Geoelectricity*, **45**(2), 193-205.

Parés, J. M., & Van Der Pluijm, B. A. (2002). Evaluating magnetic lineations (AMS) in deformed rocks. *Tectonophysics*, **350**(4), 283-298.

Parés, J. M., van der Pluijm, B. A., & Dinarès-Turell, J. (1999). Evolution of magnetic fabrics during incipient deformation of mudrocks (Pyrenees, northern Spain). *Tectonophysics*, **307**(1-2), 1-14.

Parlak, O., & Robertson, A. (2004). The ophiolite-related Mersin Melange, southern Turkey: its role in the tectonic–sedimentary setting of Tethys in the Eastern Mediterranean region. *Geological Magazine*, **141**(3), 257-286.

Parry, G. R. (1971). *The Magnetic Anisotropy of some Deformed Rocks* (Doctoral dissertation, University of Birmingham).

Penck W. (1918). *Die tektonische Grundzu¨ge Westkleinasiens. Eiszeitalter. Stuttgart. Planhol X de. 1958. De la Plaine Pmphylienne aux lacs pisidiens*. The`se Doctorat d'Etat, Universite´ de Paris Sorbonne, Maisonneuve, France.

Piper, J. D. A., Tatar, O., Gursoy, H., Kocbulut, F., & Mesci, B. L. (2006). Paleomagnetic analysis of neotectonic deformation in the Anatolian accretionary collage, Turkey. *Special Papers-Geological Society of America*, **409,** 417.

Poisson, A. (1977). Recherches géologiques dans les Taurides occidentales (Turquie), 795 p. *Doctorat d'état thesis, Université de Paris-Sud, Orsay, France*.

Poisson, A., & Dumont, J. F. (1979). Geologie des Taurides occidentales (Turquie) Mem. *Soc. Geol. Fr,* **137.**

Poisson, A., Akay, E., Dumont, J. F., & Uysal, S. (1984). The Isparta angle: a Mesozoic paleorift in the Western Taurides. *Geology of the Taurus Belt. Proceedings Mineral Research and Exploration Institute, Ankara*, 11-26.

Poisson, A., Orszag-Sperber, F., Kosun, E., Bassetti, M. A., Müller, C., Wernli, R., & Rouchy, J. M. (2011). The Late Cenozoic evolution of the Aksu basin (Isparta Angle; SW Turkey). New insights. *Bulletin de la Société Géologique de France*, **182**(2), 133-148.

Poisson, A., Wernli, R., Sağular, E. K., & Temiz, H. (2003a). New data concerning the age of the Aksu Thrust in the south of the Aksu valley, Isparta Angle (SW Turkey): consequences for the Antalya Basin and the Eastern Mediterranean. *Geological Journal*, **38**(3-4), 311-327.

Poisson, A., Yağmurlu, F., Bozcu, M., & Şentürk, M. (2003b). New insights on the tectonic setting and evolution around the apex of the Isparta Angle (SW Turkey). *Geological Journal*, **38**(3-4), 257-282.

Pourteau, A., Candan, O., & Oberhänsli, R. (2010). High-pressure metasediments in central Turkey: Constraints on the Neotethyan closure history. *Tectonics*, **29**(5).

Ramsay, J. G., & Huber, M. I. (1983). *The Techniques of Modern Structural Geology: Strain Analysis* (Vol. 1). Academic press.

Ranalli, G., & Yin, Z. M. (1990). Critical stress difference and orientation of faults in rocks with strength anisotropies: the two-dimensional case. *Journal of Structural Geology*, **12**(8), 1067-1071.

Rees, A. I. (1961). The effect of water currents on the magnetic remanence and anisotropy of susceptibility of some sediments. *Geophysical Journal International*, **5**(3), 235-251.

Rees, A. I. (1965). The use of anisotropy of magnetic susceptibility in the estimation of sedimentary fabric 1. *Sedimentology,* **4**(4), 257-271.

Robertson AHF. (1990). Tectonic evolution of Cyprus. In Ophiolites-Oceanic Crustal Analogues, Malpas J, Moores J, Panayiotou EM, Xenophontos C (eds). Proceedings of the Symposium 'Troodos 1987'. *Geological Survey: Cyprus*; 235–252.

Robertson, A. H. (1998). Mesozoic-Tertiary tectonic evolution of the easternmost Mediterranean area: integration of marine and land evidence. *Proceedings of the Ocean Drilling Program, Scientific Results, Vol. 160; Chapter 54*.

Robertson, A. H. (2000). Mesozoic-Tertiary tectonic-sedimentary evolution of a south Tethyan oceanic basin and its margins in southern Turkey. *Geological Society, London, Special Publications*, **173**(1), 97-138.

Robertson, A. H. F. (1994). Mesozoic–Tertiary sedimentary and tectonic evolution of Neotethyan carbonate platforms, margins and small ocean basins in the Antalya Complex of southwest Turkey. *Tectonic Controls and Signatures in Sedimentary Successions*, 415-465.

Robertson, A. H. F., & Dixon, J. E. (1984). Introduction: aspects of the geological evolution of the Eastern Mediterranean. *Geological Society, London, Special Publications*, **17**(1), 1-74.

Robertson, A. H. F., & Woodcock, N. H. (1982). Sedimentary history of the south-western segment of the Mesozoic-Tertiary Antalya continental margin, south-western Turkey. *Eclogae Geologicae Helvetiae*, **75**(3), 517-562.

Robertson, A. H. F., & Woodcock, N. H. (1984). The SW segment of the Antalya Complex, Turkey as a Mesozoic-Tertiary Tethyan continental margin. *Geological Society, London, Special Publications*, **17**(1), 251-271.

Robertson, A. H., & Mountrakis, D. (2006). Tectonic development of the Eastern Mediterranean region: an introduction. *Geological Society, London, Special Publications*, **260**(1), 1-9.

Robertson, A. H., & Ustaömer, T. (2009). Formation of the Late Palaeozoic Konya Complex and comparable units in southern Turkey by subduction–accretion processes: Implications for the tectonic development of Tethys in the Eastern Mediterranean region. *Tectonophysics*, **473**(1-2), 113-148.

Robertson, A. H., Ustaömer, T., Pickett, E. A., Collins, A. S., Andrew, T., & Dixon, J. E. (2004). Testing models of Late Palaeozoic–Early Mesozoic orogeny in Western Turkey: support for an evolving open-Tethys model. *Journal of the Geological Society*, **161**(3), 501-511.

Robion, P., Grelaud, S., & de Lamotte, D. F. (2007). Pre-folding magnetic fabrics in fold-and-thrust belts: Why the apparent internal deformation of the sedimentary rocks from the Minervois basin (NE—Pyrenees, France) is so high compared to the Potwar basin (SW—Himalaya, Pakistan)?. *Sedimentary Geology*, **196**(1-4), 181-200.

Rochette, P., & Fillion, G. (1988). Identification of multicomponent anisotropies in rocks using various field and temperature values in a cryogenic magnetometer. *Physics of the Earth and Planetary Interiors*, **51**(4), 379-386.

Rochette, P., & Vialon, P. (1984). Development of planar and linear fabrics in Dauphinois shales and slates (French Alps) studied by magnetic anisotropy and its mineralogical control. *Journal of Structural Geology*, **6**(1-2), 33-38.

Rocks, O. A. T. E. U. (1964). Chief Geologist of MTA (Mineral Research and Exploration Institute), Ankara. In *Méthodes de Prospection de la Chromite: Methods of Prespection for Chromite. Proceedings of an OECD Seminar on Modern Scientific Methods of Chromite Prospecting, Athens, 16th-30th April* **1963** (p. 79). Organisation de Coopération et de Developement Économiques.

Sagnotti, L., & Speranza, F. (1993). Magnetic fabric analysis of the Plio-Pleistocene clayey units of the Sant'Arcangelo Basin, southern Italy. *Physics of the Earth and Planetary Interiors*, **77**(3-4), 165-176.

Sagnotti, L., Speranza, F., Winkler, A., Mattei, M., & Funiciello, R. (1998). Magnetic fabric of clay sediments from the external northern Apennines (Italy). *Physics of the Earth and Planetary Interiors*, **105**(1-2), 73-93.

Sagnotti, L., Winkler, A., Montone, P., Di Bella, L., Florindo, F., Mariucci, M. T., ... & Frepoli, A. (1999). Magnetic anisotropy of Plio–Pleistocene sediments from the Adriatic margin of the northern Apennines (Italy): implications for the time–space evolution of the stress field. *Tectonophysics*, **311**(1-4), 139-153.

Saint-Bezar, B., Hebert, R. L., Aubourg, C., Robion, P., Swennen, R., & De Lamotte, D. F. (2002). Magnetic fabric and petrographic investigation of hematite-bearing sandstones within ramp-related folds: examples from the South Atlas Front (Morocco). *Journal of Structural Geology*, **24**(9), 1507-1520.

Sans, M., Vergés, J., Gomis, E., Parés, J. M., Schiattarella, M., Travé, A., ... & Doulcet, A. (2003). Layer parallel shortening in salt-detached folds: constraint on cross-section restoration. *Tectonophysics*, **372**(1-2), 85-104.

Sato, K., & Yamaji, A. (2006). Embedding stress difference in parameter space for stress tensor inversion. *Journal of Structural Geology*, **28**(6), 957-971.

Scheepers, P. J. J., & Langereis, C. G. (1994). Magnetic fabric of Pleistocene clays from the Tyrrhenian Arc; a magnetic lineation induced in the final stage of the middle Pleistocene compressive event. *Tectonics*, **13**(5), 1190-1200.

Schildgen, T. F., Cosentino, D., Caruso, A., Buchwaldt, R., Yıldırım, C., Bowring, S. A., ... & Strecker, M. R. (2012). Surface expression of eastern Mediterranean slab dynamics: Neogene topographic and structural evolution of the southwest margin of the Central Anatolian Plateau, Turkey. *Tectonics*, **31**(2).

Schmidt, V. A., Ellwood, B. B., Nagata, T., & Noltimier, H. C. (1988). The measurement of anisotropy of magnetic susceptibility using a cryogenic (SQUID) magnetometer and a comparison with results obtained from a torsion-fiber magnetometer. *Physics of the earth and planetary interiors*, **51**(4), 365-378.

Scriba, H., & Heller, F. (1978). Measurements of anisotropy of magnetic susceptibility using inductive magnetometers. *J. Geophys*, **44**, 341-352.

Şenel M, Gedik _I, Dalk_l_c¸ H, Serdaroğlu M, Bilgin AZ, Oğuz MF, Bo¨lu¨kbas¸_ AS, Koruc¸uM, O¨zgu¨l N. (1996). Isparta bu¨klu¨mu¨ dog˘usunda otokton ve allokton birimlerin stratigrafisi (Bat_ Toroslar) [Geology of autochthonous and allochthonous units (Western Taurides) at the east of Isparta Angle]. *General Directorate of Mineral Research and Exploration (MTA) Bulletin* 118: 111–160.

Şenel, M. (1997). *1:250 000 Scale Geological Maps of Turkey, No: 4, Isparta Sheet; N•3, Antalya Sheet.* Mineral Research and Exploration Institute of Turkey (MTA) Publication, Ankara.

Şenel, M., Dalkılıç, H., Gedik, İ., Serdaroğlu, M., Metin, S., Esentürk, K., & Özgül, N. (1998). Orta Toroslar'da Güzelsu koridoru ve kuzeyinin stratigrafisi, Türkiye. *Bulletin of Mineral Research and Exploration of Turkey,* **120**, 171-198.

Şenel. M., Dalkilic, H., Gedik, i., Serdaroglu, M., Bolukbasi, A.S., Metin, S., Esenturk, K., Bilgin, A.Z., Uguz, F., Korucu, M. ve Ozgul, N., (1992). 1:100,000 O¨lc¸ekli Tu¨rkiye Jeoloji Haritalari, Isparta J11 Paftasi [Geological Maps of Turkey at

1:100,000 Scale, Isparta J11 Sheet]. General Directorate of Mineral Research and Exploration (MTA) Publication No. 14.

Şengör, A. M. C., Özeren, S., Genç, T., & Zor, E. (2003). East Anatolian high plateau as a mantle-supported, north-south shortened domal structure. *Geophysical Research Letters*, **30**(24).

Shan, Y., Lin, G., Li, Z., & Zhao, C. (2006). Influence of measurement errors on stress estimated from single-phase fault/slip data. *Journal of structural geology*, **28**(6), 943-951.

Shan, Y., Suen, H., & Lin, G. (2003). Separation of polyphase fault/slip data: an objective-function algorithm based on hard division. *Journal of Structural Geology*, **25**(6), 829-840.

Simón-Gómez, J. L. (1998). Reliability of palaeostress analysis from fault striations in near multidirectional extension stress fields. Example from the Ebro Basin, Spain. *Journal of Structural Geology*, **20**(7), 827-840.

Soto, R., Larrasoaña, J. C., Arlegui, L. E., Beamud, E., Oliva-Urcia, B., & Simón, J. L. (2009). Reliability of magnetic fabric of weakly deformed mudrocks as a palaeostress indicator in compressive settings. *Journal of Structural Geology*, **31**(5), 512-522.

Souque, C., Robion, P., & de Lamotte, D. F. (2002). Cryptic magnetic fabric of tectonic origin revealed by heating of sedimentary samples from the Corbières, France. *Physics and Chemistry of the Earth, Parts A/B/C*, **27**(25-31), 1253-1262.

Stampfli, G. M., & Borel, G. D. (2002). A plate tectonic model for the Paleozoic and Mesozoic constrained by dynamic plate boundaries and restored synthetic oceanic isochrons. *Earth and Planetary Science Letters*, **196**(1-2), 17-33.

Stephenson, A., Sadikun, S. T., & Potter, D. K. (1986). A theoretical and experimental comparison of the anisotropies of magnetic susceptibility and remanence in rocks and minerals. *Geophysical Journal International*, **84**(1), 185-200.

Storetvedt, K. M. (1990). The Tethys Sea and the Alpine-Himalayan orogenic belt; mega-elements in a new global tectonic system. *Physics of the Earth and Planetary Interiors*, **62**(1-2), 141-184.

Suppe, J. (1985). *Principles of structural geology*. Prentice Hall.

Tarling, D., & Hrouda, F. (Eds.). (1993). *Magnetic Anisotropy of Rocks*. Springer Science & Business Media.

Tarling, D.H. (1983). *Paleomagnetism*. Chapman and Hall, London, 379 pp.

Topak, Y., Gul, M., & Yaman, S. (2009). Miocene lacustrine succession of the Hoyran Lake Basin, Isparta, southwest Turkey. *Acta Geologica Polonica*, **59**(2), 245-259.

Torsvik, T. H., & Cocks, L. R. M. (2009). The Lower Palaeozoic palaeogeographical evolution of the northeastern and eastern peri-Gondwanan margin from Turkey to New Zealand. *Geological Society, London, Special Publications*, **325**(1), 3-21.

Tuzcu S. & Karablylkoğ lu M. (2001). The palaentology, stratigraphy, facies and depositional environments of Miocene coral reefs at Western Taurus Belt. *Min. Res. Explor. Inst. of Turkey (MTA) Report,* No. 10438, 1—214.

Tuzcu, N. (1972). *Etude Minéralogique et Pétrographique de la Région de Baskisla dans le Taurus Occidental (Karaman, vilâyet de Konya, Turquie)* (No. 1). Université de Genève, Département de Minéralogie.

Üner, S., Özsayin, E., Dirik, R. K., Ciner, T. A., & Karabiyikoğlu, M. (2018). Reconstructing the sedimentary evolution of Miocene Aksu Basin based on fan delta development (eastern Mediterranean-Turkey) 2. *Delta, 2, 3.*

Üner, S., Özsayin, E., Kutluay, A., & Dirik, K. (2015). Polyphase tectonic evolution of the Aksu Basin, Isparta Angle (Southern Turkey). *Geologica Carpathica*, **66**(2), 157-169.

Uysal, S., Dumont, J. F., & Poisson, A. (1980). Western Taurus platforms. *Min. Res. Explor. Inst. of Turkey (MTA) Report*, (80), 1-13.

Van Hinsbergen, D. J. (2010). A key extensional metamorphic complex reviewed and restored: the Menderes Massif of western Turkey. *Earth-Science Reviews*, **102**(1-2), 60-76.

Van Hinsbergen, D. J. J., & Schmid, S. M. (2012). Map view restoration of Aegean–West Anatolian accretion and extension since the Eocene. *Tectonics* **31**, TC5005.

Van Hinsbergen, D. J., Dekkers, M. J., & Koc, A. (2010). Testing Miocene remagnetization of Bey Dağları: Timing and amount of Neogene rotations in SW Turkey. *Turkish Journal of Earth Sciences*, **19**(2), 123-156.

Van Hinsbergen, D. J., Dekkers, M. J., Bozkurt, E., & Koopman, M. (2010a). Exhumation with a twist: Paleomagnetic constraints on the evolution of the Menderes metamorphic core complex, western Turkey. *Tectonics*, **29**(3).

Vasiliev, I., Maţenco, L., & Krijgsman, W. (2009). The syn-and post-collisional evolution of the Romanian Carpathian foredeep: New constraints from anisotropy of magnetic susceptibility and paleostress analyses. *Tectonophysics*, **473**(3-4), 457-465.

Voigt, W., & Kinoshita, S. (1907). Bestimmung absoluter Werte von Magnetisierungszahlen, insbesondere für Kristalle. *Annalen der Physik*, **329**(13), 492-514.

Wallace, R. E. (1951). Geometry of shearing stress and relation to faulting. *The Journal of Geology*, **59**(2), 118-130.

Weil, A. B., & Yonkee, A. (2009). Anisotropy of magnetic susceptibility in weakly deformed red beds from the Wyoming salient, Sevier thrust belt: Relations to layer-parallel shortening and orogenic curvature. *Lithosphere*, **1**(4), 235-256.

Will, T. M., & Powell, R. (1991). A robust approach to the calculation of paleostress fields from fault plane data. *Journal of Structural Geology*, **13**(7), 813-821.

Winkler, A., Alfonsi, L., Florindo, F., Sagnotti, L., & Speranza, F. (1997). The magnetic anisotropy of rocks: principles, techniques and geodynamic applications in the Italian peninsula. *Annals of Geophysics*, **40**(3).

Yagmurlu, F., Savaslclin, Y., & Ergün, M. (1997). Relation of alkaline volcanism and active tectonism within the evolution of the Isparta Angle, SW Turkey. *The Journal of Geology*, **105**(6), 717-728.

Yamaji, A. (2000a). The multiple inverse method applied to meso-scale faults in mid-Quaternary fore-arc sediments near the triple trench junction off central Japan. *Journal of Structural Geology*, **22**(4), 429-440.

Yamaji, A. (2000b). The multiple inverse method: a new technique to separate stresses from heterogeneous fault-slip data. *Journal of Structural Geology*, **22**(4), 441-452.

Yamaji, A. (2003). Are the solutions of stress inversion correct? Visualization of their reliability and the separation of stresses from heterogeneous fault-slip data. *Journal of Structural Geology*, **25**(2), 241-252.

Yamaji, A., Otsubo, M., & Sato, K. (2006). Paleostress analysis using the Hough transform for separating stresses from heterogeneous fault-slip data. *Journal of Structural Geology*, **28**(6), 980-990.

Yılmaz, Y. (1993). New evidence and model on the evolution of the southeast Anatolian orogen. *Geological Society of America Bulletin*, **105**(2), 251-271.

Žalohar, J., & Vrabec, M. (2007). Paleostress analysis of heterogeneous fault-slip data: the Gauss method. *Journal of Structural Geology, * **29**(11), 1798-1810.

EXTENDED TURKISH SUMMARY (GENİŞLETİLMİŞ TÜRKÇE ÖZET)

1. GİRİŞ

Doğu Akdeniz bölgesindeki Alp-Himalaya orojenezi, Mesozoyik'ten başlayarak Senozoik ve günümüze kadar devam eden levha tektoniği çerçevesinde Tetis okyanusunun kapanması ve sonrasında Arap ve Afrika plakasının kuzeye doğru hareket ederek Avrasya plakası ile çarpışması ile kontrol edilen plaka tektoniği çerçevesinde oluşmuştur (Barrier ve Vrielynck, 2008; Şengör ve Yılmaz, 1981). Bu çarpışmalar sonucunda şekillenen Türkiye jeolojisi eski okyanusları konumlarını tanımlayan pek çok yitim zonlarından meydana gelmektedir (Şengör ve Yılmaz, 1981; Robertson ve Dixon, 1984; Okay, 1986; Yılmaz, 1993; Göncüoğlu vd., 1996, 1997, Okay ve Tüysüz, 1999, Robertson, 2002, Stampfli ve Borel, 2002, Robertson ve Ustaömer, 2004, Robertson vd., 2006, 2007, 2009; Oberhänsli vd., 2010; Pourteau vd., 2010). Bunlardan en önemlisi, kuzeyde, Erken Mesoziyik dönemden Avrasya plakasına ait olan Pontitler ile güneyde, Triyas'ta Gondwana'dan riftleşerek ayrılan Toros ve Anatolit platformunun Neotetis'in kuzey kolunun tamamen tükenmesi ve arkasından çarpışması sonucu oluşan İzmir-Ankara-Erzincan Kenet Zonu'dur (İAEKZ). Pontitler ve Toros platformu arasındaki bu çarpışma muhtemelen Geç Kretase'de başlamış ve Geç Eosen'de sona ermiştir (Okay ve Özgül, 1984; Meijers vd., 2010; van Hinsbergen vd., 2010, Gülyüz vd., 2012). İkinci dalma-batma zonu ise, İAEKZ'nun güneyinde Türkiye'nin orta kesiminde bulunan Toroslar ve Kırşehir Blokları arasında meydana gelmiştir (İç Toros Kenet Zonu, örneğin Görür vd., 1984; Dilek vd., 1999; Okay vd., 1996; Clark ve Robertson, 2002; Parlak ve Robertson, 2004; Pourteau vd., 2010). Bu okyanusal havza Geç Kretase ile Erken Senezoik dönemde yitime uğramış, bu yitim esnasında ise Güney Anadolu'da bulunan Toroslar kıvrım ve bindirme kuşağı meydana gelmiştir.

Neotetis'in güney kolu, bugün hala Torosların güneyinde Kıbrıs Yayı boyunca dalmaya devam etmektedir (Khair ve Tsokas, 1999; Papazachos ve Papaioannou, 1999; Biryol vd., 2011). Bu yayın doğuya doğru devamında ise, okyanusal kabuk tamamen

tükenerek, Orta Miyosen sonunda Bitlis Kenet Zonu boyunca Arap Plakası ile Anadolu plakasının çarpışması ile sonuçlanmıştır (Faccenna vd., 2006; Hüsing vd., 2009; Keskin, 2003; Okay vd., 2010; Şengör ve Yılmaz, 1981; Şengör vd., 2003). Torosların altında yüksek derinliklere ulaşan dalan plaka, devamlı ve kırılmamış bir dalma-batma zonuna işaret ederken, levha ayrılmaları (slab detachment) ve bu ayrılmalara bağlı diagonal yırtılmalar ve Orta Miyosen'den bu yana doğudan batıya doğru ilerleyen kıta-kıta çarpışması olarak kendini göstermektedir (Gans vd., 2009; Facenna vd., 2006; van Hinsbergen vd., 2010; Biryol vd., 2011).

Afrika ve Avrasya arasındaki uzun süredir devam eden ve halen devam etmekte olan yakınsamaya bağlı olarak meydana gelen yoğun deformasyonun sonucunda, yay şekilli karmaşık dalma-batma zonları oluşmuştur, bunlar batı Anadolu'da Ege Yayı olarak adlandırılırken, doğuda Kıbrıs yayı olarak tanımlanmaktadır. Bu iki yayın kesiştiği bölgede, Isparta Açısı (Blumenthal, 1963) olarak tanımlanan açısal şekilli morfolojik bir yapı oluşmuştur ve Antalya Körfezi'nin açıklarına kadar uzanmaktadır. Bu yapı aynı zamanda batı ve orta Torosları birbirinden ayırmaktadır. Isparta Açısı, Geç Kretase'den Miyosen'e kadar etkin olan sıkışmalı tektonik rejim altında gelişen birdirme ve nap sistemleri ile şekillendirilmiş Mesozoik birimlerden ve Ofiyolitlerden meydana gelmektedir. Isparta Açısı'nın batı kanadında yer alan en derin tektonostratigrafik birim, Üst Triyas'tan Eosen'e kadar olan zaman dilimine ait sığ deniz kireçtaşları, dolomitler ve neritik kireçtaşlarından oluşan Beydağları platformudur (Robertson ve Woodcock, 1982, 1984). KB'dan gelen Ofiyolit ve Mesozoik sediman karmaşığından oluşan Likya Napları, Beydağları üzerine tektonik olarak gelmektedir. Likya Napları'nın Beydağları üzerine doğru en son yerleşimi Erken Miyosen olarak belirlenmiştir (Hayward 1984; Okay 1989; Collins ve Robertson 1997, 1998, van; Hinsbergen 2010). Isparta Açısı'nın doğu kanadını ise kıvrımlı ve bindirmeli bir kuşak olan Toroslar oluşturmaktadır ve Beydağları platformunu GD'dan tektonik olarak üzerlemektedir. Bu bindirmeli sistem, Geç Kretase'den Neojen'e kadar sürekli veya aralıklı olarak meydana gelmiştir (Şengör ve Yılmaz, 1981; Hayward, 1984; Collins ve Robertson, 2003; Poisson vd., 2003; van Hinsbergen vd., 2010). Beydağları ve Toroslar arasında gelişen en genç bindirme zonunun yaşı Erken Miyosen olarak belirlenmiştir (Hayward, 1984).

Uzun ve yoğun bir deformasyon geçmişinin ardından, Orta Toroslar, Miyosen döneminde çok yönlü açılmalı bir rejimin etkisinde kalmaya başlamıştır (Koç vd., 2012, 2016 ve 2017). İlginç bir şekilde, bu açılma Isparta Açısı'nın ortasında K-G uzanımlı kıvrım ve bindirme zonlarının geliştiği D-B yönlü bir kısalma ile eşzamanlı olarak meydana gelmiştir (Dumont ve Kerey 1975; Glover ve Robertson 1998; Poisson vd., 2003; Deynoux vd., 2005; Flecker vd., 2005; Çiner vd., 2008; Schildgen vd., 2012a). Bu yapıların en iyi gözlemlendiği yerler Aksu, Köprüçay-Manavgat Havzaları (Antalya Havzası) olarak bilinen ve Torosların üzerinde uyumsuz (unconformity) olarak yerleşen Miyosen denizel havzalardır (Şekil 2). Isparta Açısı'nın merkezinde yer alan bindirme, aynı zamanda Aksu Havzası'nın doğu sınırını da oluşturmaktadır. Isparta Açısı'nın çekirdeğinde görülen bu bindirme, Antalya Körfezi'nin açıklarında görülen eşleği ile birlikte, bölgede görülen en genç sıkışmalı tektonik rejimin Pliyosen'e kadar (Poisson vd., 2003 ve 2011) ya da Kuvaterner'e kadar (Hall vd., 2014) bile gidebileceğini göstermektedir.

Miyosen döneminde olan E-W sıkışmalı tektonik rejim Isparta Açısı'nın merkezi ile sınırlıdır ve güney Anadolu'nun başka yerlerinde belirgin değildir. Bu durumda, burada meydana gelen tektonik rejim; 1) Eosen'de durmamış ve devam etmiştir ya da 2) belli bir süre durmuş sonrasında Orta Miyosen'den Pliyosen'e kadar yeniden aktive olduğunu söylemek mümkündür. Bu projede, Isparta Açısı'nın kalbinde yer alan, yoğun kıvrımlı ve bindirmeli Miyosen yaşlı denizel sedimanter dolguya sahip Aksu Havzası'na odaklanılmıştır (Şekil 3). Bu bağlamda, Aksu Havzası'nın yapısal, sedimantolojik ve kinematik karakteristiklerinin ortaya konulması, çalışma alanı ve çevresinde meydana gelen alışılmadık deformasyon desenlerinin oluşmasına neden olan manto ve kabuk süreçlerinin jeolojik olarak anlamlandırılması için çok önemlidir (Biryol vd., 2011; Koç vd., 2016b; Kaymakçı vd., 2018).

2. KAYNAK BİLDİRİŞLERİ

Bu tez ile ilgili önceki çalışmalar dört gruba ayrılmıştır. İlk grup bölgesel jeoloji ile ilgili çalışmaları içerirken, ikinci grup ise Aksu Havzasına dair jeolojik (sedimantolojik ve stratigrafik) çalışmaları içermektedir. Üçüncü ve dördüncü grup ise, bu çalışmada kullanılan metodolojiye odaklanır ve sırasıyla paleostress ve AMS ile ilgili önceki çalışmaları içermektedir. Bu gruplar aşağıda ayrıntılı olarak açıklanacaktır.

2.1 Bölgesel Çalışmalar

Bu derleme, Isparta Büklümü ve Antalya havzasını kapsayan çalışmalara odaklanmaktadır. Isparta Büklümü kavramı ilk olarak Penck (1918) tarafından ortaya atılmış ve bu çalışmada bölgedeki Burdur-Fethiye, Dinar, Kırkavak ve Beyşehir gibi ana tektonik hatlar irdelenerek, Paleojen stratigrafisi üzerine çalışılmıştır.

Isparta Büklümü'nü oluşturan ana stratigrafi serisi üzerine yoğunlaşan Parejas (1943), Paleozoik temel birimlerinin Mezozoik transgresif istiflerinden ayırt edilmesi ve yaşlandırılması konusunda çalışmıştır. Altınlı (1944, 1945) sırasıyla Beydağları'nın doğusundan batısına doğru gelişen Antalya ve Likya bindirme hatlarını tanımlamıştır.

Akdeniz kıyıları ile Burdur-Isparta göller bölgesi arasındaki bölgenin jeomorfolojik tanımı Planhol (1956, 1958) tarafından yapılmıştır ve bölgedeki en önemli jeolojik problemlerden biri olan Antalya havzasının oluşumu konusuna işaret etmiştir. Sonrasında bu konu, jeologlar arasında uzun süreli bir tartışmaya neden olmuştur.

Alandaki temel araştırma, Blumenthal (1963) tarafından ilk defa stratigrafik verilere dayandırılarak yapılan "Isparta Büklümü" sentezidir. Bu çalışmada, Isparta büklümünde yer alan farklı tektonik kuşaklar tanımlanmaya çalışılmıştır. Bunlar kuşaklar kabaca; 1) Beyşehir'den Dinar'a kadar uzanan ofiyolitik zonu, 2) Aksu bindirmesini oluşturan allokton karbonat dilimlerini içeren Serik-Isparta hattı, ve bu hattı takip eden 3) Elmalı-Burdur kuşağı ve 4) Antalya Naplarına ait şisto-radyolaritli formasyonlar olarak tanımlanmıştır.

Isparta bölgesi, 1964 yılında Brunn liderliğindeki Fransız bir grup tarafından, Isparta Büklümü'nün güney ve güney-batı kesimini içeren Korkuteli, Antalya ve Isparta arasında

kalan bölge (A. Poisson), bölgenin güney-doğu ve doğu tarafında yer alan Beyşehir ve Akseki arasında kalan bölge (O. Monod) ve Isparta büklümünün kuzeyini (M. Gutnic) kapsayan bölge haritalanmıştır. Bu öncü çalışmalardan sonra, Brunn vd. (1970; 1971) tarafından bölgede yapılan çalışmalar daha da detaylandırılmış ve bölgedeki ana yapısal unsurlar tanımlanmıştır. Örneğin; güneybatıda bulunan Beydağları birimi ile kuzeydoğuda yer alan Beyşehir-Akseki birimlerini içeren otokton karbonat platformu ile 3 farklı allokton nap sistemi (Likya, Antalya ve Hoyran-Beyşehir-Hadim napları) tanımlamaları yapılmıştır.

Özgül ve Arpat (1973) batı Toroslarda, Üst Triyas'tan Kuaterner'e kadar uzanan stratigrafik kesiti incelemişlerdir. Stratigrafik istif, Beydağları otokton birimi ve Antalya Napları olmak üzere iki farklı birime ayrılmıştır. Bu çalışmada ayrıca, Torosların yapısal unsurları da tanımlanmıştır.

Dumont (1976) ve Akbulut (1977) tarafından Isparta Büklümü'nün merkez kısmı çalışılmıştır. Isparta Büklümü'nün kuzeydoğu kesiminde bulunan Eğirdir Gölü'nün doğusu Dumont (1976) tarafından haritalanırken, Akbulut (1977) tarafından yapılan çalışma, Isparta Büklümü'nün, Aksu fazı olarak tanımlanan Geç Miyosen bindirme tektoniğinden önemli ölçüde etkilendiğini göstermiştir.

Isparta Büklümü, yetmişli yıllarda birçok Fransız ve Türk araştırmacı tarafından tez konusu olarak seçilmiştir (Fethiye bölgesi için: Juteau (1975); ofiyolitler için: Monod (1977); Poisson, (1977); Marcoux, (1987); Tuzcu, (1972) ve Özlü (1978)).

Yapılan bu tezin çalışmalarının yanı sıra, Dumont vd. (1980) ve Lheureux (1983) tarafından, Mesozoyik karbonat platformlarına odaklanan tematik projeler de yapılmıştır. Bu çalışmalar, Beydağları platformunun güney kısmından ve Isparta Açısı'nın kuzeydoğusundaki Anamas Dağı'ndan yeni sonuçlar elde edilmesini sağlamıştır.

Toroslar karbonat platformunun üzerine uyumsuz olarak yerleşen Antalya Neojen birimleri, bir çok araştırmacı tarafından çalışılmıştır (Dupoux (1983), Poisson vd. (1983), Akay vd. (1985), Akay ve Uysal (1985), yayınlanmamış MTA raporu). Bu çalışmalar, litoloji, biyostratigrafi ve yapısal unsurlara ait veriler olmak üzere çeşitli araştırma alanlarını bir araya getirmiştir. Manavgat, Köprüçay ve Aksu havzalarının ayrıntılı jeolojik haritaları (1: 100 000 ölçekli) bu çalışmalar kapsamında üretilmiştir. Bu çalışmaların ana sonuçları, Isparta Büklümü merkezinde Geç Miyosen'e kadar etkin olan Aksu fazı evresinin doğrulanması ve Antalya Napları'nın ilk yerleşme yaşının Oligosen öncesi olarak

belirlenmesidir (Poisson vd., 1984; Akay vd., 1985). Bununla birlikte, Poisson vd., (1984) Mesozoyik'ten Neogen'e kadar, Isparta Açısı için elde edilen tüm verileri içeren ilk modeli önermiştir.

Isparta açısının doğusunda bulunan birimlerden elde edilen radyolarya türleri Jurassic ve Cretaceous yaşlarını vermiş olması (Waldron, 1984a and 1984b) bu bölgenin birkaç okyanus havzası ile ayrılmış küçük karbonat platformlarının bir mozaiği olarak yorumlanmasına imkan vermiştir. Bu model daha önce Antalya'nın güneybatısı için önerilmiş (Robertson ve Woodcock, 1984) ve sonrasında bütün Isparta Büklümü'ne uyarlanmıştır (Robertson, 1993 ve 2000).

Flecker vd. (1995, 1998) ayrıntılı olarak Miyosen Antalya Havzası üzerinde çalışırken, sonrasında ise bu havzaya ait Plio-Quaternary birimler Glover (1995), Glover ve Robertson (1998a, 1998b; 2003) tarafından çalışmıştır. Robertson (1990; 1993; 1998; 2000), Antalya bölgesinin genel tektonik organizasyonu hakkındaki tartışmayı yenilemiş ve Isparta Açısı ölçeğinde sentezlemiştir.

Nihayet, doksanlı yılların sonlarına doğru 1:100.000 ölçekli düzenli jeolojik haritalar Maden Tetkik ve Arama Kurumu tarafından yayınlanmıştır (MTA, Ankara, Şenel, 1997). Fasiyes analizi ve paleoekoloji çalışmaları daha yakın zamanda tamamlanmıştır (Karabıyıkoğlu vd., 1997, 2000, 2005; Tuzcu ve Karabıyıkoğlu, 2001; Deynoux ve arkadaşları, 2005; İşler ve diğerleri, 2005; Çiner ve diğerleri, 2008; Poisson ve arkadaşları, 2011).

Isparta Büklümü'nü kapsayan bölgede, zaman içerisinde sayısız jeolojik kapsamlı çalışmalar yapılmış olsa da, aynı zamanda bazı jeofizik temelli çalışmalar da yapılmıştır. Bunlardan ilk olarak Kissel vd. (1993), Isparta Büklümü'nün doğu kanadında meydana gelen düşey eksenli dönme verilerinin varlığına dikkat çekmişlerdir. Bu çalışmada elde edilen paleomanyetik verilerin sonuçları, Isparta Büklümü'nün doğu kanadında Eosen'den bu yana 40°'lik saat yönünde düşey eksenli dönmenin meydana geldiğini göstermektedir. Bu öncü çalışmanın ardından yapılan çalışmalardan, Kissel ve Poisson (1987), Morris ve Robertson (1993), van Hinsbergen vd. (2010) Isparta Büklümü'nün batı kanadında 20-30°'lik saatin tersi yönünde bir dönmenin varlığına işaret etmişlerdir. Son dönemlerde ise, Koç vd. (2016b) Antalya Havzası'nda düşey eksenli rotasyonlar üzerinde çalışmışlardır. Bu çalışma göstermiştir ki, Köprüçay Havzası 20-30°'lik saat yönünde bir dönmeye maruz kalırken,

Manavgat Havzası saat yönünün tersi yönünde yaklaşık 25-35°'lik bir düşey eksenli dönmeye uğramıştır. Öte yandan Isparta Büklümü'nün merkezinde bulunan Aksu Havzası ise Orta Miyosen'den bu yana orijinal konumunu korumaktadır.

2.2 Aksu Havzası Üzerine Yapılan Çalışmalar

Aksu Havzası, Isparta Büklümü'nün merkezinde bulunan ve bölgenin tektonik yapısını anlamak için önemli bir havzadır. Bu nedenle, 1944'ten bu yana bu havza üzerinde birçok çalışma yapılmıştır.

Bu çalışmalardan ilki Altınlı (1944) tarafından yapılmıştır. Aksu Havzası'nın stratigrafisinin temel alındığı bu çalışmada, Aksu Havzası'nın güneyindeki Tortoniyen yaşlı Aksu konglomerası ve Pliyosen birimler tanımlanmıştır. Yapılan çalışmalar arasında, Aksu havza dolgusunun en genç konglomeratik birimi olan Belkis konglomerasının tanımlanması ve yaşlandırılması Blumenthal (1951) tarafından yapılmıştır. Benzer şekilde, havzanın güneyinde yer alan Pliyosen birimlerin yaşlandırılması yumuşakça ve foraminifer fosilleri kullanılarak yapılmış (Tintant, 1952 ve 1953; Chaput ve Darkot, 1953). Bu öncü çalışmalardan sonra, Antalya Havzası ve kısmen Aksu Havzası'nın litostratigrafik ve biyostratigrafik özellikleri üzerine yoğunlaşmışlardır (Akbulut, 1977; Poisson, 1977; Monod, 1977; Gutnic vd., 1979; Dumont, 1976; Poisson vd., 1983; 1984; 2003; Akay vd., 1985; Akay ve Uysal, 1985)

Akay vd. (1985), Aksu Havza'nın stratigrafisi üzerine çalışma yapmıştır. Bu çalışmada, Aksu konglomerası, Aksu formasyonunun bir üyesi olarak ayırt edilmiştir. Sonrasında ise birimin fosil içeriğine bağlı olarak Şenel vd., (1992 ve 1996) tarafından Serravaliye-Tortoniyen yaşı bu birim için önerilmiştir. Bu çalışmaya göre, Gebiz kireçtaşının yaşına bağlı olarak, Aksu Bindirmesinin yaşı, Tortoniyen sonrası, Messiniyen öncesi olarak benimsenmiştir.

Aksu Havzası üzerine yapılan çalışmalardan bir diğeri ise, Flecker vd. (1995 ve 1998) tarafından yapılmıştır ve Aksu Havzası, Köprüçay ve Manavgat Havzaları ile birlikte değerlendirilmeye çalışılmıştır. Bu çalışmada havzalarınnın oluşumunun, Likya Naplarının güneydoğuya doğru bindirmesi ile ilişkili olabileceği önerilmiştir. Buna bağlı olarak

Havzaların depolanma merkezlerinin gelişimi, Likya Naplarının önünde eğilmeye bağlı (flexural) olarak gelişen fayların kontrolünde oluşan ön havzalar olarak açıklanmıştır.

Aksu Havzası'nın Pliyosen-Pleyistosen evrimi ise Glover ve Robertson (1998) tarafından incelenmiştir. Bu çalışmada, Aksu Havzası için iki aşamalı bir evrimsel gelişim önerilmiştir: bunlar, 1) Geç Miyosen-Erken Pliyosen transtansiyonel sistem ile gelişen çökme ve 2) Geç Pliyosen-Erken Pleyistosen açılma ve marjin (kıyı) yükselmesidir.

Poisson vd. (2003), Aksu Bindirmesi'nin ile ilgili yeni veriler önermişlerdir. Aksu Havzası'nın güneyinde baskın litolojileri çalışarak, bu litolojilerin barındırdığı Erken-Geç Pliyosen döneme ait yumuşakçaları, foraminiferleri ve nanoplanktonları tanımlamışlardır. Bununla birlikte, bu birimlerin sıkıştırma rejimi etkisinde kaldığını ve litolojik dizilimde bindirme fayları etkisinde tekrarlanmaların varlığına dikkat çekmişlerdir.

Benzer şekilde, Aksu Havzası'nı içeren Antalya Havzası'nın Senozoik gelişimi Çiner vd. (2008) tarafından çalışılmıştır. Görece son dönem çalışmalarından olan bu makalede, Antalya Havzası'nı meydana getiren Aksu, Köprüçay ve Manavgat Havzalarının, sedimantolojik açıdan tezat oluşturabilecek nitelikte, kolluvial, resif seviyeli alluvial fan/fan delta, resifal sığ karbonat sahanlığı, fay kontrollü resifal eğim alanları ve kırıntılı açık deniz sahanlığı gibi farklı depolanma ortamları temsil eden fasiyes oluşumları ile karakterize sedimantasyon türlerinin varlığını göstermişlerdir.

Sonraki dönemlerde ise, Poisson vd. (2011) geç dönem Senozoyik evrimini incelediği çalışmasında, Aksu Havzası'nın oluşumunun, N-S uzalımlı bir yarı-graben olarak başladığını öne sürmüştür. Bu çalışmada aynı zamanda, Aksu Havzası'nın kuzey sınırının yükselmesine bağlı olarak, havzanın güneye doğru göçünün söz konusu olduğundan ve ayrıca Messiniyen zamanında Aksu Havzası'nın küçülerek doğuda Gebiz kireçtaşının sınırladığı dar bir koy halini aldığı belirtilmiştir. Zankliyen zamanından sonraki evre ise Aksu Havzası'nın batı yönlü Aksu sıkışma tektoniğinin etkisinde kaldığı dönem olarak ifade edilmiştir.

Tüm bu sedimantolojik çalışmalar yanında Üner vd. (2015 and 2017), Aksu Havzası'nın kısmen güney kesimini içeren çalışmasında, havzanın tektonizmasını çalışmıştır. Bu çalışmada, yeni kinematik ve sedimantolojik veri setleri sunularak, Aksu Havzası'nın oluşumundan bu yana, dört farklı tectonik rejimin varlığı öne sürülmüştür. Bu

tektonik fazların bir sonucu olarak, havzada gözlemlenen alüvyon fanlarının ve dört farklı fan delta oluşumunun gelişimi aşıklanmıştır.

Bu literatür derlemesi göstermiştir ki, Aksu Havzası'nın oluşumu, birimlerin yaşı ve tektonik fazlar hakkında araştırmacılar bir görüş birliği sağlayamamışlardır (Bizon vd., 1974; Poisson, 1977; Akay vd., 1985; Akay ve Uysal, 1985; Glover, 1995; Glover ve Robertson, 1998; Tuzcu ve Karabıyıkoğlu, 2001; Karabıyıkoğlu vd., 2005; Poisson vd., 2003; Poisson vd., 2011).

2.3 Paleogerilim Üzerine Yapılan Çalışmalar

Fay-kayma verilerinden kinematik analiz yöntemleri temel olarak grafiksel ve analitik araçlara dayalı iki gruba ayrılmaktadır. Her iki yöntemin ardında yatan ana fikir aynıdır ve ilk kez Wallace (1951) tarafından açıklanan gerilme ve kayma arasındaki teorik ilişkilere dayanır. Sonrasında, Bott (1959) fay düzlemlerinde yapılan ölçümlerden elde edilen maksimum kayma gerilmesinin, ana gerilme büyüklüklerinin ve yönlerinin matematiksel ilişkisini ortaya koymuştur.

Fay-kayma verileri kullanan paleostress analizinin en basit grafiksel yöntemi, fay düzlemlerinin, gözlemlenen kayma yönü ile Schmidt stereografik projeksiyonuna çizilmesidir. Bu yöntemin dezavantajı, yalnızca basit eşlenik fay setlerinde çalışıyor olmasıdır (Suppe, 1985; Marshak ve Mitra, 1988). Arthaud (1969), bölgesel deformasyon elipsoidi ve bölgesel gerilme elipsoidi ile fay popülasyonu arasında var olan doğrudan ilişki üzerine temel alan bir grafiksel yöntem geliştirmiştir. Bu yöntem için de ciddi bir sınırlama vardır ve yalnızca tek eksenli stres alanından kaynaklanan fay popülasyonlarına uygulanabilmesidir (Carey, 1976; Aleksandrowski, 1985). Aleksandrowski (1985), Arthaud'un yöntemini geliştirmiş ve üç eksenli stres koşullarında da uygulanabilir forma getirmiştir.

Dik Dihedra Metodu (The Right Dihedral Method), sismik dataların fay-düzlemi çözüm yönteminin, fay-kayma düzlemlerine uyarlanması ile elde edilen başka bir grafiksel yöntemdir (McKenzie, 1969; Angelier ve Mechler, 1977; Lisle, 1987 ve 1988). Kayma vektörünün (S) yöneliminin, gerilme oranı (Φ) değiştikçe nasıl değiştiğini göz önünde bulundurarak, σ1 ve σ3 yönelimlerinin saptanmasına bağlı yöntem ise Lisle (1987)

tarafından geliştirilmiştir. Bu yöntemler, asimetrik fay-kayma popülasyonları için tatmin edici sonuçlar verirken, eşlenik faylar gibi simetrik fay popülasyonları için iyi sonuçlar vermemiştir.

Ters çözüm problemi, farklı yönelimlere sahip bilinen fay-kayma verilerinin yönlerinin (doğrultu, eğim ve yatım) ve hareket yönünün kullanılarak stres tensörünün belirlenmesinden ibarettir. 1974'te, ilk defa Carey ve Brunier, ters çözüm problemini tanımlayan matematiği formüle etme ve çözme girişiminde bulundular. İki yıl sonra, Carey (1976), seçilen paleo-gerilim tensörü (σ) için, ölçülen fay-kayma verileri ile hesaplanan kayma gerilmesi yönleri arasındaki açısal sapmaları en aza indirmeye çalışan ilk paleo-gerilim analizi programını geliştirmiştir. Angelier (1975) de yaklaşık olarak aynı zamanda benzer bir yöntem geliştirdi. Bu öncül çalışmalardan sonra, Angelier (1979, 1984, 1989, 1994) tarafından çeşitli ardışık yöntemler geliştirilmiş ve bu analiz için ciddi matematiksel algoritmalar geliştirilmiştir (Armijo vd., 1982; Etchecopar vd., 1981; Will ve Powell, 1991; Nemcok ve Lisle, 1995; Nemcok vd., 1999; Arlegui-Crespo ve Simon-Gomez, 1998; Fry, 1999; 2001; Yamaji, 2000; Shan vd., 2003; Tobore ve Lisle, 2003; Liesa ve Lisle, 2004; Shan vd., 2006; Orife ve Lisle, 2006; Sato ve Yamaji, 2006 ve Žalohar ve Vrabec, 2007).

Bu yöntemler homojen fay-kayma sistemlerinin analizinde başarılı olmuştur, ancak heterojen veri kümeleriyle başa çıkmak için oldukça problematik bir strateji izlemektedirler (Yamaji, 2006; Katsushi ve Yamaji, 2006). Bu nedenle, hetorojen fay-kayma verilerini, farklı fay fazlarına ayıran sayısal algoritmalar önerilmiştir (Simon-Gomez, 1986; Fry, 1992; Nemcok ve Lisle, 1995; Nemcok ve diğerleri, 1999; Yamaji, 2003 ve Žalohar ve Vrabec, 2007). Böylece, fay-kayma verileri, ters çözüm yöntemi uygulanmadan önce homojen alt homojen gruplara ayrılmasına imkan vermektedir.

Haralohar ve Vrabec (2007), çalışmasında heterojen fay sistemlerinin, homojen alt kümelere ayrıştırılması için Gauss metodunu önermiştir. Metot, geleneksel ters fay çözümü temeline (the best-fit stress tensor) dayanmaktadır. Ancak, yöntemde tanımlanan nesne fonksiyonunun en aza indirgenmesi ya da en yükseğe çıkarılması ile uygulanmaktadır.

2.4 Manyetik Duyarlılık Anizotropisi (MDA) Üzerine Yapılan Çalışmalar

Manyetik duyarlılık anizotropisi (MDA) ile ilgili ilk çalışma ve teori Voight ve Kinoshita (1907) tarafından yapılmıştır. Bu öncü çalışmanın ardından, AMS teorisi Ising (1942) ve Graham (1954) tarafından petrofabrik bir işaret olarak kullanılmış ve ilk olarak jeolojiye uygulanmasını önerilmiştir. Bu yazarlar ilk olarak, kaya örneklerinde minerallerin tercih edilen yönelimini karakterize etmek için manyetik yöntemlerin kullanılabileceğini fark ettiler. Ising (1942), kil örnekleri üzerinde çalışmış ve manyetik duyarlılığın tabakalanma düzleminde, dikine oranla daha yüksek olduğunu göstermiştir. Graham (1954), manyetik duyarlılık anizotropisini (MDA) kayaçlarda kullanmıştır. O zamandan beri, MDA, doku gelişiminin nicel tahmini için kayaç bileşenlerinin mekansal ve geometrik biçiminin araştırmak amacı ile başarıyla kullanılmıştır.

Manyetik petro-fabrik üzerine yapılan çalışmalarda kilit noktalardan biri Fuller (1963) tarafından yapılmıştır. Fuller (1963)'ün çalışması, manyetik duyarlılık anizotropisinin kökeninin, kayaç içerisindeki minerallerin frekans dağılımından kaynaklı olduğunu göstermiştir. Bununla birlikte, ferromanyetik minerallerin mekânsal dağılımlarının da MDA üzerinde önemli etkisinin olduğu aynı çalışmada tanımlanmıştır. Bu çalışmadan sonra dikkat çekici bir gelişme de manyetik anizotropiye katkıda bulunan manyetik taşıyıcılar kavramıdır. Zaman içerisinde, hem ferromanyetizmanın hem de paramanyetizmanın toplam manyetik anizotropiye katkıda bulunduğu anlaşılmıştır (Daly, 1967; Parry, 1971; Owens ve Bamford, 1976; Henry, 1983; Henry ve Daly, 1983; Rochette ve Vialon, 1984; Borradaile vd., 1986; Lamarche ve Rochette, 1987; Borradaile, 1988).

AMS günümüzde, yerbilimlerinde çok çeşitli disiplinlerde kulllanılan vazgeçilmez bir yöntemdir. Bunlar arasında en yaygın uygulama alanına sahip sedimantolojik çalışmalarda, MDA yönteminin kullanılması Graham (1966)'tan sonra olmuştur. Bu çalışmada, MDA yöntemi deforme olmuş tortul kayalara uygulanmış ve yatay çökellerin oblate manyetik duyarlılık elipsoidine sahip olduğu kaydedilmiştir. Ayrıca, bu çalışmalardan elde edilen sonuçlar, Graham (1966)'nın kıvrımlı yapılarda manyetik doku gelişimi üzerine spekülasyon yapmasına neden olmuştur. Bu öncü çalışmadan sonra, sedimanter kayaçlarda yapılan MDA çalışmaları (Granar, 1958; Fuller, 1960 ve 1963; Rees, 1961; 1965; Hamilton ve Rees, 1971; Kent ve Lowrie, 1975), sedimanter kayaçların

depolanma sırasında ve yüksek dereceli deformasyon etkisinde magnetik doku kazandığını göstermiştir.

Sedimanter kayaçların yanı sıra, birçok araştırmacı MDA'yı volkanik veya magmatik araştırmalarda (Girdler, 1961; Khan, 1962; King, 1966; Heller, 1973) ve metamorfik kayaçlarda da (Atkinson, 1977; Borradaile ve ark., 1982; Hrouda, 1982) kullanmıştır.

Tensör istatistikleri, doku oryantasyon dağılımlarının karakterize edilmesi için gereklidir. Çok sayıda örnekten, ana eksenlerin (kMAX, kINT, kMIN) ortalama yönlerinin belirlenmesi karmaşıktır ve tensör-istatistiği yaklaşımı gerektirir. Jelinek (1978), tensör örneklerinin doğru istatistiksel tanımlamasının yapılmasında temel bir katkı sağlamıştır.

Scribaand Heller (1978) ve Schmidt vd. (1988) kayaç dokularının ayırt edilmesini amaçlayan bir yöntem önermişlerdir. Bir SQUID manyetometrede 100 µT radyal alan içerisinde numuneyi 45 derecelik adımlarla ve toplam 24 konum için birbirine dik üç eksenin her biri etrafında döndürerek anizotropi tensörlerinin belirlenebileceğini önerdiler.

Borradaile ve Tarling (1981) çalışmasında, çamurtaşlarından toplanan örneklerden elde edilen MDA verilerini inceleyerek, MDA elipsoidindeki kMAX eksenlerinin, her zaman gerilme elipsoidinin maksimum uzamasına paralel olmadığını göstermiştir.

Ramsay ve Huber (1983), AMS'nin, makro düzeyde bir deformasyon olmaksızın bile, tortul kayaçlarda tercihli tane yöneliminin varlığına işaret etmektedir.

Kissel vd. (1986) zayıf deforme olmuş kayaçlarda çalışmışlardır. Bu çalışmada, MDA yöntemi deforme olmamış gibi görülen kayaçlara uygulanarak, MDA yönteminin, çok zayıf da olsa deformasyona maruz kalan kayaçların, deformasyon derecesini nicel olarak göstermede çok uygun bir teknik olarak potansiyelini gösteren ilk çalışmadır. Çok daha güncel çalışmalar ise, MDA yönteminin hassasiyetinin avantajlarını, zayıf tektonik manyetik doku yönelimlerinin belirlenmesinde kullanmışlardır (Aubourg vd., 1991; Averbuch vd., 1992; Owens 1993; Parés ve Dinares 1993; Sagnotti ve Speranza 1993; Collombat vd., 1995; Parés vd., 1999; Sagnotti vd., 1999).

Rochette ve Fillion (1988) ilk olarak ters manyetik doku tanımlaması yapılmış ve iki nedensel model önerilmiştir: bunlardan ilki, Ferroan kalsit tanelerinin maksimum duyarlılığının c eksenine paralel olması iken, ikincisi ise, uzun yapılı tek domainlerin varlığı

şeklindedir. Ayrıca, Rochette ve Fillion (1988) hem ferromanyetik hem de paramanyetik kısımların duyarlılık anizotropisine olan katkıları yeni bir yöntem kullanarak belirlenmiştir.

Hrouda ve Jelinek (1990), ferromanyetik katkının doygunluk mıknatıslanmasının üzerinde iki farklı manyetik alanda ölçümü ile bileşen katkısının belirlenmesini sağlayacak matematiksel bir yöntem öne sürmüştür.

Hrouda ve Tarling (1993) çalışmalarında, MDA yönteminin temellerini sunmuşlar ve düşük/yüksek manyetik alan manyetik duyarlılık anizotropisini tanımlamışlardır. Aynı zamanda, düşük ya da yüksek manyetik alan yaklaşımını kayaç ve pekişmemiş sedimanlar üzerine uygulamışlardır.

Pares vd. (1999), baskı altındaki çamurtaşlarında MDA evriminin ileri aşamaları için yeni bir model önermiştir. Bu model, ilerleyen deformasyon altında bırakılan zayıf deforme olmuş çamurtaşlarının dört farklı manyetik doku gelişimini maruz kaldığını göstermiştir.

Bu çalışmadan sonra, birçok araştırmacı tarafından benzer kaya türleri üzerinde benzer çalışmalar yapılmıştır (Frizon de Lamotte vd., 2002; Saint-Bezar vd., 2002; Souqué vd., 2002; Sans vd., 2003; Larrasoaña vd., 2004; Parés, 2004; Robionetal., 2007; Cifellietal., 2009; Debacker vd., 2009; Olivaetal, 2009; Sotoetal, 2009; Weil ve Yonkee, 2009; Mochales vd, 2010; Pueyo- Anchuela vd., 2010).

MDA yönteminin teorik alt yapısını oluşturmak için sayısız çalışma yapılmış olmasına rağmen, jeolojik deformasyon evrimini anlamak için bazı jeolojik uygulama çalışmalarının da yapılmasına ihtiyaç duyulmuştur. Son dönemde, Vasiliev vd. (2009) bu çabanın iyi örneklerindendir. Bu çalışmada, araştırmacı çarpışma döneminde ve sonrasında Karpatlar'ın (Romanya) evrimini çalışmış ve Geç Miyosen-Pliyosen zaman aralığı için MDA verileri ile paleostress verilerini karşılaştırmıştır. Çalışmada, MDA verilerinin k_{MAX} değeri ve paleostress verilerinin kısalma yönünün birbiriyle uyumlu olduğunu göstermiştir.

3. MATERYAL VE YÖNTEM

Bu çalışmada, belirlenen hedeflere ulaşmak maksadı ile çeşitli jeolojik disiplinlerden elde edilen veri setleri bir araya getirilmiştir. Bu yöntemler, Paleostress inversiyonu ve Manyetik Duyarlılık Anizotropisi (MDA) çalışmaları olarak iki gruba ayırmak mümkündür.

Paleostress verilerinin analizinde T-Tecto Software (Zalohar ve Vrabec, 2007) kullanılarak paleostress inversiyon tekniği uygulanmıştır. Bununla birlikte, Manyetik Duyarlılık Anizotropisi (MDA), hata kayma verilerinden elde edilen gerilme yönlerini test etmek amacıyla bağımsız bir yöntem olarak kullanılmıştır.

3.1 Paleogerilim Analizi

Paleogerilim, geçmiş tektonik gerilimin kayaçlarda iz bırakması gerektiğini söyleyen ilkeye dayanarak, kayacı etkileyen ve geçmiş zamanda etkin olan gerilim yönlerinin bulunması anlamına gelmektedir (Hancock, P.L.1985). Paleostress analizi, mevcut jeolojik yapılara uygun ve bölgesel gerilim tensörü belirlemeye çalışan çeşitli yöntemleri ifade eder. Başlıca gerilme yönleri ve göreceli büyüklükler, fay popülasyonu, deprem odak mekanizması, eklem setleri, sokulum setleri, kalsit ikizlenmesi, mikro-yapısal özellikler, kıvrımlar, stylolitler ve bükülme bantlarından belirlenebilmektedir.

Paleo-gerilim analizi, üç temel gerilmenin σ_1, σ_2 ve σ_3'ün göreceli büyüklüklerini ve yönelimlerini fay popülasyonlarından ve kayma yönlerinden elde etmek üzerine oturtulmuş bir araştırma alanıdır (Angelier, 1990, 1994; Carey ve Burinier, 1974). Gerilme ve kayma arasındaki teorik ilişkiler, ilk kez Wallace (1951) tarafından tanımlanmıştır. Sonrasında ise Bott (1959) ana gerilme büyüklüklerinin ve yönlerinin fay düzleminde oluşan maksimum kayma gerilmesinin yönleriyle ilişkisini formüle etmiştir.

Bahsi geçen çalışmalardaki amaç, stres tensörünü belirlemek için fay-kayma verileri kullanmaktır; bu nedenle bahsi geçen yenilme mekanizmaları (failure mechanism) üzerine bazı hipotezler yapılmalıdır. Üç ana eşlenik fay tipinde (normal, ters ve doğrultu fayları) üç ana gerilim eksenlerinin yönelimlerini tahmin etmek için, Anderson (1951)'in faylanma

üzerine çalışması (Şekil 4a) ve Coulomb'un yenilme kriterleri (Coulomb, 1776; Handin, 1969) kullanılmıştır.

Paleostress analizinde bir başka prensip ise, kayma gerilmelerinin, fay düzlemlerinin oryantasyonu ve kayma yönü ile olan ilişkisinin belirlenmesidir (Wallace, 1951). Bir başka deyiş ile ana gerilme büyüklüklerinin ve yönlerinin, sonuçta ortaya çıkan maksimum kayma gerilmesinin yönü ile olan ilişkisinin belirlenmesidir (Bott, 1959).

Temel prensiplere dayanarak, fay-kayma verilerini analiz etmek ve yerel gerilim tensörünün bileşenlerini tahmin etmek için pek çok teknik kullanılmaktadır (P-T, Dik Dihedral ya da Ters Çözüm metodu). Bu çalışmada, ters çözüm yöntemi kullanılmıştır.

Aksu Havzası'ndaki deformasyon deseni, basitçe ~N-S Afrika-Avrasya yakınsaması çerçevesinde açıklanması pek mümkün değildir. Bu duruma ek olarak, büyük ölçekli fayların yakın çevresinde görülen lokal gerilim değişimlerine bağlı olarak farklı gerilim dağılımlarını görmek, bu karmaşık yapıyı bir kat daha arttırmaktadır. Bu nedenle havza dolgusu içinde ve havza sınırlarında gelişen orta ve büyük ölçekli faylardan elde edilen fay-kayma verileri kullanılarak temel gerilim eksenlerinin yönelimlerini ve görece büyüklerinin hesaplanması mümkündür (Angelier, 1979 ve 1994). Her deformasyon fazının zamanlamasını sınırlandırarak, Aksu Havzası'nın paleo-gerilim geçmişini paleostres inversiyon tekniklerini kullanarak ortaya koymak bu projenin amaçlarından biri olarak benimsenmiştir.

3.2 Manyetik Duyarlılık Anizotropisi

Manyetik Duyarlılığın Anizotropisi (MDA), bilinen sabit bir manyetik alan içinde bir kayacın manyetik mıknatıslanabilirlik mukavametinin ölçüm alınan yöne bağlı olarak farklılıklar göstermesi olarak tanımlanmaktadır. Dolayısı ile MDA analizi kayacı oluşturan minerallerin manyetik özelliklerinin (duyarlılığı) belirgin bir hakim yönde değişkenlik gösterip göstermediğini ifade etmektedir.

MDA tekniği, kayaç üzerinde herhangi bir deformasyon ibaresi olmasa bile hemen hemen her tür kayaca kullanabilmektedir ve kayacın petro-fiziksel yapısını veya mineral yönelimlerini araştırmak için tahribatsız, hızlı ve ucuz bir analiz yöntemidir. Yapılan çalışmalar (Hrouda ve Janak 1976, Borradile 1988, Averbuch ve diğ. 1992, Robion ve diğ.

2007, Borradile ve Jackson 2010), deforme olmuş bir kayacın maksimum manyetik anizotropi yönlerinin genellikle kayacı şekillendiren tektonik yapılar -kıvrımlar, faylar, foliasyon ve lineasyon- ile ilişkili olduğunu göstermiştir. Diğer yandan, MDA tekniği pek çok açıdan yenilik getirmesine rağmen, analiz sonuçları birden fazla faktörden etkilenebilmektedir. Örneğin, kayaç minerallerinin fiziksel farklılıkları, kristal yapısı, mineral kompozisyonu, tektonik ve metamorfik süreçler (çökelme esnasındaki veya magmanın akış yönü) düşünüldüğünde MDA yöntemi ile elde edilen sonuçlar doğrudan deformasyon göstergesi olarak alınmamalıdır (Borradile ve Henry, 1997); Borradile ve Jackson,2004).

Paleo-gerilim çalışmalarına ek olarak, son dönemlerde kullanılmaya başlayan Manyetik Duyarlılık Anizotropisi (MDA) üzerine yapılan çalışmalar, bu yöntemin hafif deforme olmuş sedimanter kayaçlarda tektonik geçmişin oluşturulmasında kullanılabildiğini göstermiştir (Tarling ve Hrouda, 1993). Paleo-gerilim göstergelerinin genellikle eksik olduğu genç, zayıf deforme olmuş tortul kayaçlarda, MDA analizi, özellikle yapısal çalışmalarla ve diğer kinematik gözlemlerle birleştirildiğinde, deformasyon geçmişini çıkarmak için kullanılabilmektedir. Başka bir deyişle, MDA analizi çalışma alanında etkin olan en son tektonik fazın belirlenmesinde kullanılabilmektedir. Şimdiye kadar Aksu Havzası'nı konu alan pek çok çalışma yapılmış (Flecker, 1995; Karabıyıkoğlu ve diğerleri, 2004 ve 2005; Kelling ve diğerleri, 2005; Çiner ve diğerleri, 2008; Uner ve diğerleri, 2015, Koç ve diğerleri 2016 ve 2017) olmasına rağmen MDA çalışması ilk defa bu proje kapsamında gerçekleştirilmiştir. Koç vd., (2016) Aksu Havzası'nın, Orta Miyosen'den (yani oluşumundan bu yana) orjinal konumunu koruduğunu raporlamışlardır. Dolayısıyla, MDA çalışması yapmak için iyi bir anahtar alandır. Bu çalışma kapsamında, Aksu Havzası'na ait sedimanter istiflerden (Orta Miyosen-Pliyosen) elde edilen ilk MDA sonuçları sunulacaktır. Bu çalışmada, Aksu Havzası'nın Orta Miyosen'den Pliyosen'e maruz kaldığı farklı tektonik fazların belirlenmesine çalışılmış ve MDA yöntemi ise paleo-gerilim çalışmalarında elde edilen sonuçları test etmek maksadı ile bağımsız bir yöntem olarak kullanılmıştır.

4. BULGULAR

Çalışma alanı olarak belirlenen Aksu Havzası, Güneybatı Anadolu'da yer alan Orta Torosların batı ucunda yerleşmiş K-G uzanımlı denizel bir havzadır. Çalışma alanı Bucak-Sütçüler-Antalya yerleşkeleri arasında, yaklaşık 200 km^2'lik bir alana sahiptir. Batıda Beydağları, doğuda Orta Toroslar olmak üzere iki önemli kıtasal bloğu birbirinden ayırmaktadır. Coğrafi koordinatları 37°40′02″K / 37°39′43″K kuzey enlemleri ile 30°59′55″D / 31°00′02″D doğu boylamları arasında yer almaktadır. Çalışma alanı ve çevresi, Maden Tetkik ve Arama Müdürlüğü (Ankara, Türkiye) tarafından hazırlanan 1:500.000 ölçekli Konya paftasında bulunmaktadır. Bununla birlikte, 1:100.000 ölçekli J11, K11 ve L11 paftaları da arazi çalışmalarında kullanılmıştır.

Bu tez kapsamında, Aksu Havzası'nın lithostratigrafik özellikleri tanımlanmaya çalışılmıştır. Yapılan arazi gözlemleri, havzanın sedimater dolgusunun delta ortamından denizel ortama geçişi tanımlayan kalın konglomera, kumtaşı, çamurtaşı ve yama resifleri ile karakterize edildiğini göstermiştir ve Aksu havzası yaşlıdan gence 10 temel litolojik birime ayrılmıştır. Bunlar; 1) Oymapınar Kireçtaşı, 2) Aksu Formasyonu (Karadağ ve Kapıkaya üyeleri), 3) Karpuzçay Formasyonu, 4) Gebiz Kireçtaşı, 5) Kurşunlu Formasyonu, 6) Yenimahalle Formasyonu 7) Eskiköy Formasyonu, 8) Belkıs Konglomerası, 9) Antalya Traverteni 10) Çamlık Traverteni ve 11) Belkıs Konglomerası olarak adlandırılmıştır.

Sedimantasyon açık gri- kirli beyaz renkli Oymapınar Kireçtaşı ile başlar. Sedimantasyon başlangıç yaşı ise, bu birimin yaşı olan Erken Miyosen (Late Burdigaliyen-Langiyen) olarak belirlenmiştir ve temel kayayı oluşturan Beydağları platformu, Alanya metamorfikleri, Antalya ve Likya napları üzerine uyumsuz olarak gelmektedir. Oymapınar kireçtaşı ile çalışma alanında geniş bir yayılım gösteren Aksu konglomerası (Karadağ üyesi, Langiyen-Seravaliyen) arasındaki dokanak ilişkisi uyumludur. İstif, üst kesimlere doğru, seçilimin ve derecelenmenin olmadığı, köşeli, tane ve/veya matrix destekli, blok boyutunda tane içeriğine sahip Aksu Konglomerasının alt seviyelerine karşılık gelen Karadağ üyesine dönüşmektedir. Fasiyes özellikleri bakımından alüvyal fan-fan delta kompleksi ortamını işaret etmekte olan birim, üst seviyelerde tane boyu incelerek düşeyde ve yatayda Karpuzçay formasyonuna (Langiyen-Tortoniyen) geçer. Karpuzçay formasyonu türbiditlerden oluşan

derin deniz ortamını temsil eden kalın bir istiften oluşmaktadır. Genel olarak istif laminalı paralel tabakalı çamurtaşları ile desimetre kalınlığında normal derecelenmeli, düz tabaka altı yapısı ve ara ara tabaka üstlerinde rıpıl marklar görülen kumtaşları ile karakterize edilmektedir. Kumtaşı seviyeleri, istifin üst kısımlarına doğru frekansı ve kalınlığı artmaktadır. İstif içerisinde syn-sedimanter ve post-sedimenter özellikte irili ufaklı slump ve kıvrım yapıları gözlenmektedir. Karpuzçay formasyonu, kuzeyde Aksu Formasyonuna ait Kapıkaya üyesi ile yine düşeyde ve yatayda geçişli özellik göstermektedir. Kapıkaya konglomera üyesi (Tortoniyen), Aksu havzasının kuzeyinde dağılım gösteren, masif, kalın (1-1.5 m), yerel olarak orta tabakalı, erozyonel tabanlı konglomeratik birimlerden oluşmaktadır. Konglomerayı meydana getiren kırıntılar köşeli ve kötü boylanma göstermektedir. Birim temelde tane desteklidir ancak, yer yer matrix destekli seviyeler de görülmektedir. Matrix destekli seviyelerde genel olarak matrix kum ve çamurdur. Daha düşük stratigrafik seviyelerde, birim içinde bazen kumtaşı, kiltaşı, silttaşı ve marl gibi seviyeler görülmektedir. Tane binik yapıları ve kanal depolanması gibi sedimanter yapılar bu seviyelerde seyrek de olsa gözlenebilmektedir. Bu tanımlamalara dayanarak, Kapıkaya konglomerası fan deltasına dönüşen alüvyal fan ortamı olarak yorumlanmıştır.

Havza'nın lithostratigrafik karakteri kuzeyden güneye doğru değişiklik göstermektedir. Kapıkaya Konglomerası havzanın kuzeyinde gözlemlenen en genç birimi temsil ederken, havzanın güneyi Late Miyosen-Pleyistosen yaşlı birimlere ev sahipliği yapmaktadır. Bu birimlerden en önemlisi, güneyde Karpuzçay formasyonu üzerine uyumsuz olarak yerleşen Erken Pliyosen yaşlı Gebiz kireçtaşıdır ve depolanma ortamı olarak resifal sığ karbonat sahanlığını temsil etmektedir. Havzanın güney kesiminde varlık gösteren diğer bir formasyon ise Eskiköy formasyonudur ve Gebiz kireçtaşının yataydaki eşleniği olarak kabul edilmektedir. Eskiköy formasyonu orta tabakalı, tabaka içi derecelenme gösteren, yarı yuvarlak/köşeli taneler içeren, tane destekli konglomeratik bir birimdir ve bu tanımlamalara göre depolanma ortamı alüvyal fan olarak belirlenmiştir. Aksu Havzası'nın güneyinde, havzanın iç kesimleride silttaşı, kiltaşı ve çamurtaşı karakterde olan Yenimahalle formasyonu, Eskiköy formasyonunun yataydaki uzantılısı olarak, havzanın depolanma merkezindeki karşılığı olarak yorumlanmıştır. Yenimahalle formasyonu, barındırdığı fosil içerine bağlı olarak Erken Pliyosen dönemde çökelmiş olan sığ denizel ortamı yansıtmaktadır. İstif üst seviyelerde ise dereceli olarak Kurşunlu formasyonuna

dönüşmektedir. Delta ortamını yansıtan bu formasyon ise konglomeratik karakterde ve üst Pliyosen yaşlıdır. Aksu Havzası'nı oluşturan tüm bu birimleri, havzanın belli yerlerinde yamalar şeklinde kendini gösteren traverten birimleri örtmektedir. Havza'nın kuzeyinde yer alan traverten birimleri Çamlık traverteni olarak ile anılırken, güneyde aynı yaşlı birimler Antalya traverteni olarak benimsenmiştir. Tüm bu istifin en tepesinde ise güncel bir birim olan ve alüvyal ortamı temsil eden Belkıs Konglomerası yer almaktadır.

Benzer şekilde, arazi çalışmaları sırasında Aksu Havzası'nı oluşturan jeolojik yapılar da detaylı bir şekilde çalışılmıştır. Buna göre, genel olarak havzadaki ana jeolojik unsurları, büyük ölçekli bindirme fay sistemleri, genellikle birkaç metreden fazla atım yaratmayan mezoskopik ölçekteki faylar ve kapalı (tight)-asimetrik kıvrım sistemleri olarak tanımlamak mümkündür. Bu yapıların büyük bir kısmı, uzaktan algılama teknikleri kullanılarak uydu görüntüleri kullanılarak haritalanmış ve arazi çalışmaları ile doğrulukları test edilmiştir. Tez çalışmasının bu kısmında çizgisellik analizi, fayların paternleri ve uzaktan algılama verilerine dayanan jeomorfolojik özellikler çalışılmış ve arazi gözlemleri ile yapısal unsurlar belirlenmiştir.

Morfolojik olarak, çalışma alanını şekillendiren ve Miyosen havza dolgusunu etkileyen iki farklı yapısal unsur belirlenmiştir. Bu yapısal unsurlardan ilki KDD-GBB doğrultuya sahip Kapıkaya Fayı olarak isimlendirilirken, diğeri ise kabaca K-G uzanımlıdır ve Aksu Fayı olarak tanımlanmıştır. Her iki fay da sıkışmalı bir tektonizmanın varlığını işaret eden bindirme faylarıdır. Bu bindirme faylarına ek olarak, arazi çalışmaları havzada etkin olan KB-GD doğrultulu, genellikle Pliyosen-Pleyistosen yaşlı normal fayların varlığını da göstermişlerdir.

Kapıkaya Bindirme Fayı (KBF) yaklaşık 15 km uzunluğunda KDD-GBB uzanımlı, Aksu Havzası'nı kuzeyden sınırlamaktadır. Miyosen yaşlı havza dolgusu (Kapıkaya konglomerası), yüksek açılı Kapıkaya Bindirme dilimini meydana getiren Likya Naplarına ait Jura-Kretase yaşlı kireçtaşı temeli üzerine aşmalı olarak gelişmiştir. Topografyadaki ani değişiklik Kapıkaya Bindirme Fayının varlığını morfolojik olarak desteklemektedir. Bunula birlikte, farklı litolojilerin yan yana gelmesi ve iyi gelişmiş fay düzlemleri Kapıkaya Bindirme Fayının tanımlanmasında ölçüt olarak kullanılmıştır. Fay-kayma verilerinin stereografik analizi, Kapıkaya fayının bir bindirme fayı olduğunu göstermektedir. Ters çözüm ile elde edilen asal gerilim eksenlerinin yönelimleri ve gerilim oranı (Φ) sırası

ile $\sigma_1=204°N/17°$, $\sigma_2=296°N/05°$, $\sigma_3=043°N/72°$ ve $\Phi=0.655$ olarak belirlenmiştir. En küçük asal gerilim yönü olan σ_3'ün düşeyde yer alması, sıkışmalı bir tektonik rejimi ifade ederken, gerilim oranı ise iyi gelişmiş üç eksenli gerilme koşullarını temsil eder.

Aksu Bindirme Fayı (ABF) ise yaklaşık 60 km uzunluğunda ve 50 km genişliğindedir. Yaklaşık K-G doğrultuya sahip olan Aksu Bindirmesi, havzanın doğu kenarında dik yükselen doğrusal bir dağ cephesi çeklinde morfolojik olarak kolayca tanımlanmaktadır. Aksu Bindirmesi tek bir fay olarak kendini göstermez ve havza kenarını karmaşık tektonik dilimler oluşturarak birkaç paralel fay düzlemi şeklinde sınırlandırmaktadır. Miyosen havza dolgusunu en belirgin şekilde etkileyen yapı olarak kendini göstermektedir. Kuzeyden güneye, Aksu Fayı'nın geometrisini ve özelliklerini anlamak için. Kuzeyden güneye, Aksu Fayı'nın geometrisini ve özelliklerini anlamak için çeşitli ölçülü kesitler üretilmiş ve fay hattı boyunca fay-kayma verileri toplanmıştır. Ters çözüm ile elde edilen asal gerilim eksenlerinin yönelimleri ve gerilim oranı (Φ) sırası ile $\sigma_1=044°N/13°$, $\sigma_2=314°N/02°$, $\sigma_3=215°N/77°$ ve $\Phi=0.4$ olarak örnek çözüm olarak sunulmuştur. Aynı şekilde, en küçük asal gerilim düşeyde yer almakta ve gerilim oranı ise iyi gelişmiş üç eksenli gerilme koşullarını temsil etmektedir.

Aksu Havzası'nı kontrol eden ana yapısal unsurlar genellikle sıkışma tektoniği etkisinde gelişen bindirme faylarıdır. Öte yandan, Aksu Havzası'nın güney kısmında, nispeten genç havza dolgusunu kesen küçük ölçekli normal faylar (en fazla 5 km uzunluğunda) gözlenmiştir. Yaklaşık D-B doğrultuya sahip bu normal fayların gelişimi, genişlemeli bir tektonik rejim varlığına kanıt olarak gösterilmektedir ve daha genç olan Yenimahalle ve Kurşunlu formasyonlarını etkilemesi nedeni ile yaşları Pliyosen olarak önerilmiştir. Bununla birlikte, Antalya-Isparta yolu üzerinde Yenimahalle formasyonu içerisinde iyi gelişmiş fay-kayma verileri içeren normal faydan alınan verilerin analizi sonucunda elde edilen asal gerilme eksenlerinin yönelimleri $\sigma_1=131°N/65°$, $\sigma_2=233°N/05°$ ve $\sigma_3=325°N/24°$ olarak bulunmuştur. En büyük asal gerilim ekseni olan σ_1'in düşeyde yerleşmiş olması, tektonik rejim koşullarının açılmalı (extensional) olduğunu göstermektedir. Stres oranı $\Phi=0.2$ olması, σ_2 ve σ_3 birbirine çok yakın olduğu koşulları radyal gerilim koşullarını ifade etmektedir.

Arazi çalışmaları esnasında alınan tabaka ölçümlerinden, Aksu Havzası'nın maruz kaldığı yoğun deformasyonun da göstergesi olarak yoğun asimetrik ve kapalı

kıvrımlanmaların var olduğu gözlenmiştir. Karpuzçay Formasyonu içerisinde gözlemlenen küçük ölçekli kıvrımlardan alınan ölçümler, kıvrım ekseninin K26B/82B yönlü olduğunu göstermiştir. Kıvrım kanatları arasındaki açı ise 101° olarak bulunmuştur. Bununla birlikte arazide belirlenen tüm kıvrımlara ait kıvrım eksenleri gül diyagramında gösterilmiş ve ortalama kıvrım ekseni doğrultusu KKB-GGD olarak belirlenmiştir. Bu yön ise Aksu Bindirmesinin doğrultusu ile paralellik göstermektedir.

Litolojik ve yapısal çalışmalara ek olarak, belirlenen hedeflere ulaşmak amacı ile fay-kayma verileri ile Manyetik Duyarlılık Anizotropisi (AMS) verileri toplanmıştır. Fay-kayma verilerinin analizinde T-Tecto Software (Zalohar ve Vrabec, 2007) kullanılarak paleogerilim inversiyon tekniği uygulanmıştır. Bununla birlikte, Manyetik Duyarlılık Anizotropisi (MDA) ait veriler Anisoft 4.2 programı kullanılarak analiz edilmiştir. Bu tez çalışmasında, MDA yöntemi paleogerilim inversiyonu ile elde edilen asal gerilim eksenlerini test etmek amacıyla bağımsız bir yöntem olarak kullanılmıştır.

Paleogerilim inversiyon çalışmalarında kullanılmak üzere, arazi çalışmaları esnasında çalışma alanından 83 istasyondan yön ve bağıl hareketleri içeren 1175 adet fay-kayma verisi toplanmıştır. Paleogerilim verilerinin çoğu havza dolgusu içerisinde gözlemlenen mesoskopik ölçekli faylardan ve havzayı sınırlayan büyük ölçekli faylardan derlenmiştir. Verilerin analizinde Gauss gerilim inversiyon yöntemi (Zalohar ve Vrabec, 2007) de uygulanmıştır. İversiyon yönteminde kullanılan parametreler, $S = 30°$, $\Delta = 60°$, $Ø1 = 60°$ ve $Ø2 = 25°$ olarak belirlenmiştir (Zalohar, 2007). Bu durumda, program 148 adet ölçümü otomatik olarak reddetmiş ve verilerin % 12,6'ı popülasyon dışı yanıltıcı data olarak kabul edilmiştir. Geçmişe ait ana gerilim yönelerinin bulunması ve yorumlanması, Aksu Havzasının oluşumu üzerinde etkili olan gerilim rejimlerini anlamamıza yardımcı olmaktadır. Bu bakış açısıyla, elde edilen ana stres yönlerinin Aksu Havzasındaki yapısal unsurlarla uyumluluğu test edilmiştir ve havzanın paleogerilim stratigrafisi oluşturulmuştur.

Fay-kayma verilerine ek olarak, 19 farklı istasyondan Miyosen ve Pliyosen çamurtaşı ve ince kumtaşı birimlerinden toplam 490 yönlü örnek toplanmıştır. Örnekler, Utrecht Üniversitesi, Fort Hoofddijk Paleomanyetik Laboratuvarı'nda çok fonksiyonlu Kappabridge MFK1-FA (AGICO-Brno, Çek Cumhuriyeti) kullanılarak otomatik alan değişimi (düşük alan, 200 A/m) ile ölçülmüştür. MDA verilerinin istasyon ortalamaları Jelinek istatistiklerine göre hesaplanmıştır (Jelinek, 1977; 1978). Bu tez çalışmasında, MDA

analizi, gerilim yönlerinin test edilmesinde kullanıldığı gibi aynı zamanda son dönem gerilim fazını yansıtması nedeni ile paleogerilim stratigrafisinin oluşturulmasında da kullanılmıştır.

5. TARTIŞMA VE SONUÇ

Bu tez çalışmasında üç tür sonuçlar elde edilmiştir. Bunlar; 1) çalışma alanına ilişkin jeolojik sonuçlar, 2) yöntemsel sonuçlar ve 3) bölgenin jeolojisine ilişkin sonuçlardır. Bunlar aşağıda özet olarak listelenmiştir:

I. Aksu Havzası'na ilişkin sonuçlar

   a. Aksu Havzası, Beydağları otoktonunun ve Antalya Napları'nın üzerinde uyumsuz bir şekilde gelişmiştir. Havzadaki sedimantasyonun başlangıcı kesin olarak bilinmemektedir, ancak Geç Burdigaliyen sırasında veya öncesinde oluşmuş olmalıdır.

   b. Kaba taneli klastiklerin varlığı (Karadağ Üyesi için Langhian-Serravalian ve Kapıkaya Üyesi için Serravallian-Tortonian) Aksu Havzası kenarında yaygın bir oluşumdur ve bu konglomeratik istifler bir fan-delta oluşumu olarak yorumlanmıştır.

   c. İnce tane kırıntılı özelliğe sahip olan Karpuzçay Formasyonu istifin üst seviyelerine doğru kabalaşmaktadır. Havzada depolanma için ihtiyaç duyulan alan Karpuzçay Formasyonunun depolanma zamanı olan Langiyen-Serravaliyen zamanına karşılık gelmektedir.

   d. Aksu Havzası'nın kuzeyindeki litoloji, güneyindekinden farklıdır. Aksu havzasının kuzeyindeki en genç birim Tortoniyen yaşı verirken, güney kısımda yer alan birimler ise Messiniyen'den Pleyistosen'e kadar sedimantasyon yaşları içermektedir. Bu durum, Aksu Havzası'nın depolanma merkezinin güneye doğru göç etmesi ile açıklanabilmektedir.

e. Saha gözlemlerimiz, Aksu Bindirmesi tarafından kontrol edilen batı havza sınırının modern bir sınır, kuzeydeki havza sınırının ise eski bir (paleo) havza sınırı olduğunu göstermektedir.

f. Aksu Havzası'nın batı kenarı, Miyosen çökelleri ile temel birimler arasında pasif dokanak ilişkisine sahiptir ve herhangi bir faylanma izine arazi gözlemlerinde rastlanmamıştır. Bu durum ise, muhtemelen Aksu Havzası'nın, eski süreksizlik hatlarının tekrar aktive olması bağlı, KKD-GGB yönelimli yarı graben olarak gelişmiş olabileceği fikrini doğurmaktadır.

g. Aksu Havzası'ndan toplanan fay-kayma verileri kullanılarak oluşturulan paleostress stratigrafisi, havza oluşumundan sorumlu olan E-W yönlü bir genişleme fazının (ilk faz) varlığını göstermektedir.

h. İkinci tektonik faz ise, muhtemelen Erken Serravaliyen'de aktif olan ve Tortoniyen'de sona eren, yaklaşık K-G yönelimli sıkışma tektonik rejimidir.

i. Aksu Havzası'ndaki üçüncü tektonik faz ise, D-B yönelimli sıkışma tektoniğidir. K-G yönelimli Aksu Bindirmesi ile belirlenen bu faz, Serravaliyen ile Erken Pliyosen arasındaki jeolojik zamanda etkin olmuştur.

j. Paleogerilim stratigrafisi verileri, Likya ve Aksu fazının, Serravaliyen'de bir noktadan Tortoniyen'e kadar birlikte çalıştıklarını göstermektedir.

k. Çalışma alanında etkin olan en genç tektonik rejim genişlemeli karakterdedir. Kinematik veriler ve MDA verileri, kabaca K-G yönlü bir uzatmanın varlığına işaret etmektedirler.

l. Tez çalışmasında sunulan saha gözlemleri, Karadağ Konglomerası ve Karpuzçay Formasyonu'nunda gelişmiş olan kıvrımların, yaklaşık 60°'lik kanat arası açısına sahip dar-asimetrik karakterde olduklarını göstermiştir. Yapılan analizler, Antiklinal ve senklinal eksenlerinin, Aksu Bindirmesinin sıkıştırma yönü olan KKB-GGD yönü ile paralel veya paralele yakın konumlandığını işaret etmektedir.

II. Yöntemsel sonuçlar

a. MDA verileri ile kinematik (paleogerilim) verileri birbirleri ile tutarlılık göstermektedir ve MDA verileri deformasyon modelinin anlaşılması için bağımsız destek sağlar. Bu çalışma, MDA verilerinin, paleostress stratigrafisindeki son fazın tespitinde ve buna bağlı sonraki fazların belirlenmesinde açıkça kullanılabileceğini göstermiştir.

III. Bölgesel sonuçlar

a. Isparta Büklümü'nün merkezinde ve Antalya Körfezi'nin iç kesimlerinde, Orta Miyosen'den, Pliyosen'e kadar etkin olan D-B yönlü bir kısalmanın varlığına işaret olarak gösterilen Aksu Bindirmesi'nin nedeni olarak öne sürülen Anadolu Lavhası'nın batıya kaçışı, çalışma alanının yaklaşık 100 km hemen doğusunda yer alan Yalvaç, Altınapa ve Ilgın havzalarında görülen açılma dikkate alındığında çok muhtemel bir neden olarak görülmemektedir.

b. Isparta Büklümü'nün kapsadığı alanda meydana gelen kabuksal hareketler, yaklaşık N-S uzanımlı ve doğuya doğru dalan bir levhanın varlığı ile açıklanmıştır. Sismik tomografi verileri ile varlığı öne sürülen ve Antalya Levhası olarak adlandırılan bu levhanın geriye doğru bükülmesi ile Köprüçay ve Manavgat havzalarında oroklinal bükülmeye neden olmanın yanı sıra ve Aksu Havzası'nda da kısalmaya neden olacağı düşünülmektedir.

c. Mio-Pliyosen'deki Isparta Biklümü'nün kinematik gelişimi ve hatta güncel kinematiğinin anlaşılmasında dalan Antalya Levhası modeli önemli bir katkı sağlamıştır. Bu model ile, Aksu Havzası'ndaki yükselmeyi ve son döneme ait açılmalı tektonik rejimi de anlamlandırmak mümkün olmaktadır.

CURRICULUM VITAE

Muhammad Harbi Wasoo was born in 1993 in Erbil (IRAQ). He completed primary, secondary and high school education in Erbil. He was educated at the Department of Geology in Salahaddin University (IRAQ) between 2012 - 2016. After graduation from this department, he started M.Sc. at Geological Engineering Program of Institute of Natural and Applied Sciences of Van Yuzuncu Yil University (TURKEY) in 2016.

UNIVERSITY OF VAN YUZUNCU YIL
THE ISTITUTE OF NATURAL AND APPLIED SCIENCES
THESIS ORIGINALITY REPORT

Date: 22/07/2019

Thesis Title: COMPARISON OF STRAIN ELLIPSOID SHAPE BASED ON THE RESULTS OF THE

MAGNETIC SUSCEPTIBILITY ANISOTROPY AND PALEOSTRESS METHODS: CASE STUDY OF

AKSU BASIN (SW TURKEY).

The title of the mentioned thesis, above having total 215.pages with cover page, introduction, main parts and conclusion, has been checked for originality by TURNITIN computer program on the date of 22.07.2019 and its detected similar rate was 18 % according to the following specified filtering

Originality report rules:

- Excluding the Cover page,
- Excluding the Thanks,
 -Excluding the Contents,
- Excluding the Symbols and Abbreviations,
- Excluding the Materials and Methods
- Excluding the Bibliography,
- Excluding the Citations,
- Excluding the publications obtained from the thesis,
- Excluding the text parts less than 7 words (Limit match size to 7 words)

I read the Thesis Originality Report Guidelines of Yuzuncu Yil University for Obtaining and Using Similarity Rate for the thesis, and I declare the accuracy of the information I have given above and my thesis does not contain any plagiarism; otherwise I accept legal responsibility for any dispute arising in situations which are likely to be detected.

Sincerely yours,

22.07.2019
MUHAMMAD WASOO

Name and Surname: MUHAMMAD WASOO

Student ID#: 169101115

Science: Geological Engineering.

Program: Master with thesis.

Statute: M. Sc. X   Ph.D. ☐

APPROVAL OF SUPERVISOR
SUITABLE

Asst. Prof. Ayten KOÇ

APPROVAL OF THE INSTITUTE
SUITABLE